Electrochemical Society

GLC Anodes Are CUSTOM MADE

for

Hooker Chemical Corporation

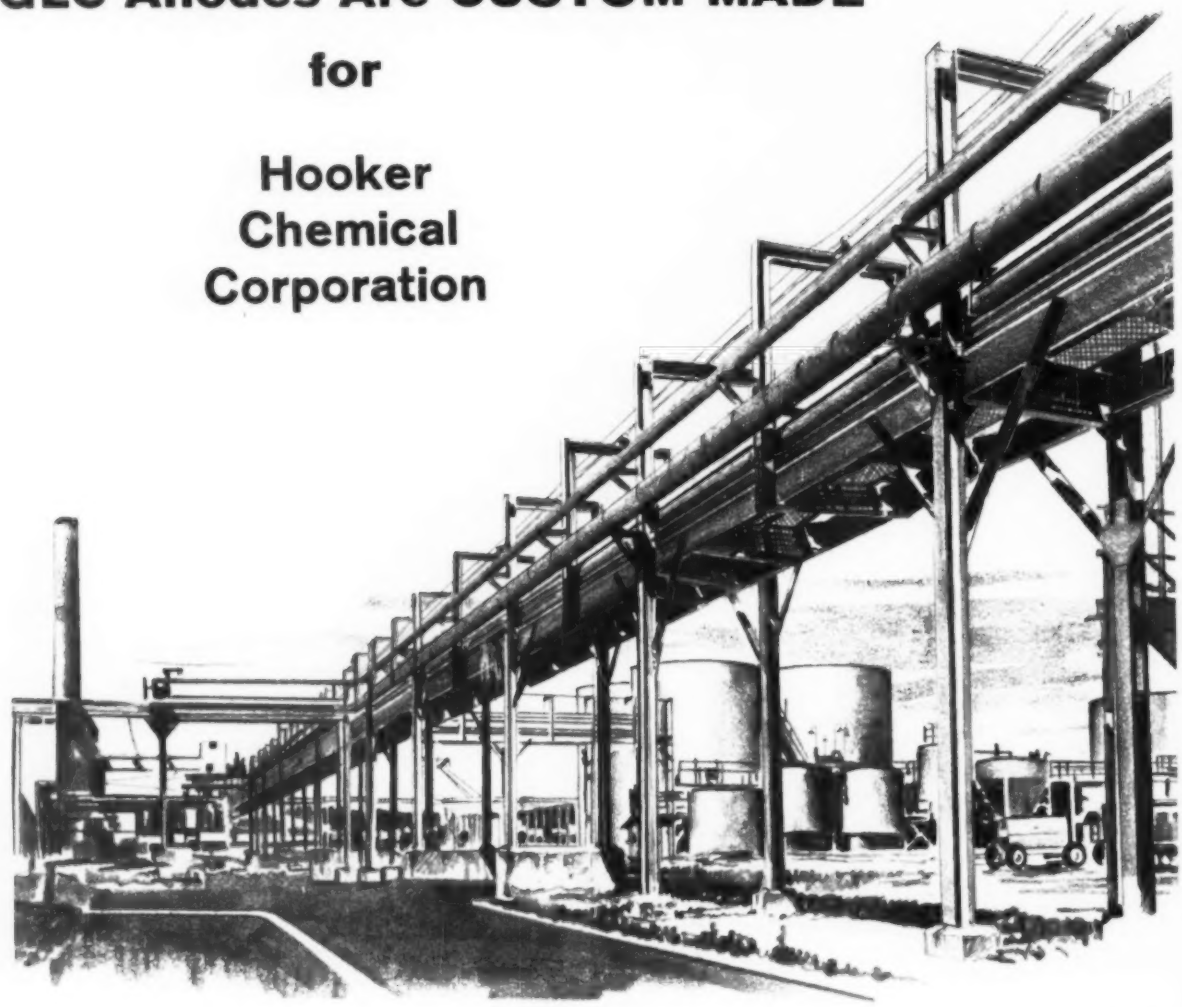

The Hooker Chlor-Alkali Plant at Montague, Mich.

Longer anode life, longer diaphragm life, reduced power consumption and reduced labor costs are the goals of the GLC program of technical exchanges between our engineers and those of our chlor-alkali customers.

GLC anodes now in use are achieving greater records of performance than ever before.

And as a result of our continuing technical exchange program, GLC customers can look forward to still better anode performance in the future.

Are your chlor-alkali operations experiencing the cost-saving advantages of GLC anodes, custom made to your special requirements?

PRODUCTS YOU CAN TRUST — GLC DIVISION — ELECTRODES

GREAT LAKES CARBON CORPORATION

18 EAST 48TH STREET, NEW YORK 17, N.Y. OFFICES IN PRINCIPAL CITIES

EDITORIAL STAFF

C. L. Faust, Chairman, Publication Committee

Cecil V. King, Editor

Norman Hackerman, Technical Editor

Ruth G. Sterns, Managing Editor

U. B. Thomas, News Editor

H. W. Salzberg, Book Review Editor

Natalie Michalski, Assistant Editor

DIVISIONAL EDITORS

W. C. Vosburgh, Battery

Milton Stern, Corrosion, I

R. T. Foley, Corrosion, II

T. D. Callinan, Electric Insulation

Seymour Senderoff, Electrodeposition

H. C. Froelich, Electronics, I

Ephraim Banks, Electronics, II

Ernest Paskell, Electronics—Semiconductors

Sherlock Swann, Jr., Electro-Organic, I

Stanley Wawzonek, Electro-Organic, II

John M. Blocher, Jr., Electrothermics and Metallurgy, I

J. H. Westbrook, Electrothermics and Metallurgy, II

N. J. Johnson, Industrial Electrolytic

C. W. Tobias, Theoretical Electrochemistry, I

A. J. deBethune, Theoretical Electrochemistry, II

ADVERTISING OFFICE

ECS

1860 Broadway, New York 23, N. Y.

ECS OFFICERS

R. A. Schaefer, President
Electric Storage Battery Co., Yardley, Pa.

Henry B. Linford, Vice-President
Columbia University, New York, N. Y.

F. L. LaQue, Vice-President
International Nickel Co., Inc., New York, N. Y.

W. J. Hamer, Vice-President
National Bureau of Standards, Washington, D. C.

Lyle I. Gilbertson, Treasurer
Air Reduction Co., Murray Hill, N. J.

I. E. Campbell, Secretary
National Steel Corp., Weirton, W. Va.

Robert K. Shannon, Executive Secretary
National Headquarters, The ECS, 1860 Broadway, New York 23, N. Y.

Manuscripts submitted to the Journal should be sent, in triplicate, to the Editorial Office at 1860 Broadway, New York 23, N. Y. They should conform to the revised Instructions to Authors, published on pp. 23C-24C of the January 1961 issue. Manuscripts so submitted become the property of The Electrochemical Society and may not be published elsewhere, in whole or in part, unless premission is requested of and granted by the Editor.

Inquiries re positive microfilm copies for volumes should be addressed to University Microfilms, Inc., 313 N. First St., Ann Arbor, Mich.

The Electrochemical Society does not maintain a supply of reprints of papers appearing in its Journal. A photoprint copy of any particular paper, however, may be obtained by corresponding directly with the Engineering Societies Library, 29 W. 39 St., New York 18, N. Y.

Journal of the Electrochemical Society

FEBRUARY 1961 **VOL. 108 • NO. 2**

CONTENTS

Editorial

A Story of Research 25C

Technical Papers

Passivity and Corrosion Resistance of Titanium and Its Alloys. *N. D. Tomashov, R. M. Altovsky, and G. P. Chernova* 113

Oxidation of Copper between 250° and 450°C and the Growth of CuO "Whiskers." *E. A. Gulbransen, T. P. Copan, and K. F. Andrew* 119

The Oxidation of Tin, III. The Mechanisms of Oxidation of Pure Tin and Their Dependence on Time and Oxgen Pressure. *W. E. Boggs* 124

The Oxidation and Corrosion of Zirconium and Its Alloys; The Mechanism of the Fission Fragment Induced Corrosion of Zircaloy-2. *B. Cox, K. Alcock, and F. W. Derrick* 129

The Effect of Surface Preparation on Oxide Films on Cr and Fe-Cr Alloys. *D. Caplan, A. Harvey, and M. Cohen* 134

Determination of the Thickness of Thin Porous Oxide Films on Aluminum. *M. S. Hunter and P. F. Towner* 139

The Effect of Dissolved Gases on the Electrical Conduction and Breakdown of Insulating Oil. *H. Tropper* 144

The Synthesis and Crystallography of Structurally Pure Cubic and Hexagonal Single Crystals of ZnS. *H. Samelson and V. A. Brophy* 150

Infrared Enhancement and Quenching of Photoconduction in Single Crystals of ZnS:Cu. *F. G. Ullman and J. J. Dropkin* 154

Some Optical Properties of Powder and Crystal Halophosphate Phosphors. *P. D. Johnson* 159

Study of Copper Precipitation Behavior in Silicon Single Crystals. *G. H. Schwuttke* 163

Radio-Frequency Carrier and Capacitive Coupling Procedures for Resisitivity and Lifetime Measurements on Silicon. *I. R. Weingarten and M. Rothberg* 167

Preparation of Uniform Resistivity n-Type Silicon by Nuclear Transmutation. *M. Tanenbaum and A. D. Mills* 171

Coatings for Columbium. *S. T. Wlodek* 177

A Study of Pore Structures on Anodized Aluminum. *T. A. Renshaw* 185

Galvanic Behavior in Fused Electrolytes, III. Potentials of Calcium, Magnesium, and Nickel in LiCl-KCl-K_2CrO_4 and NaCl-KCl-K_2CrO_4. *S. M. Selis and L. P. McGinnis* 191

Technical Notes

The Preparation of Fluorescent Germania. *J. F. Sarver and F. A. Hummel* 195

N- and P-Type Single Crystal Bismuth Telluride. *A. C. Yang and F. D. Shepherd* 197

A Chemical Treatment for Rendering Silicon-Doped Aluminum Solderable. *S. L. Matlow and H. J. Gould* 198

Brief Communication

Antimony-Rich Surface Layer on Diffused Germanium. *J. E. McNamara* 199

Feature Section

Science and Electrode Processes; Second William Blum Lecture. *S. Schuldiner* 29C

Current Affairs 32C-38C

Index (Vol. 107, 1960) ..... i-x

Published monthly by The Electrochemical Society, Inc., from Manchester, N. H., **Executive Offices, Editorial Office** and **Circulation Dept.,** and **Advertising Office** at 1860 Broadway, New York 23, N. Y., combining the JOURNAL and TRANSACTIONS OF THE ELECTROCHEMICAL SOCIETY. Statements and opinions given in articles and papers in the JOURNAL OF THE ELECTROCHEMICAL SOCIETY are those of the contributors, and The Electrochemical Society assumes no responsibility for them. Subscription to members as part of membership service; subscription to nonmembers $24.00. Single copies $1.70 to members, $2.25 to nonmembers.

Copyright 1961 by The Electrochemical Society, Inc.

Entered as second-class matter at the Post Office at Manchester, N. H., under the act of August 24, 1912.

Editorial

A Story of Research

MANY months ago, we told, on this page, the hypothetical story of how colleges might select their best future students by methods of prenatal testing, and suggested that the research corporation might assure itself of a capable future staff in similar fashion. John Hersey, in his novel "The Child Buyer," has found possibly a more promising scheme (also hypothetical, we trust). The book is highly recommended to every Vice-President in Charge of Research.

Our part of the story is somewhat as follows: a large corporation, with a 50-year "National Defense" Project, and liberal government financing, needs brains. It finds that it can buy children with IQ's approaching 200 and an intense interest in science, and condition them to its service. These children are of little use to their parents, are hated by their classmates, and in general are obnoxious to the community. In being made useful to the Project, they are first drastically brainwashed, by the use of drugs and special treatments. All memory is removed, without impairing future ability to learn and remember. Each "specimen" is then taught what he needs to know, and with no outside distractions this process is very rapid; in a few weeks he has mastered language, and has progressed from $1 + 1 = 2$ to study of the calculus. In the course of time, he is given harder and harder problems to solve, and his education proceeds until his IQ, estimated by special tests, may approach or even exceed 1000.

The subject is now pumped tremendous amounts of information which he will need for his lifework, and learns everything possible about the problems which he will be expected to solve. His capacity is unlimited, but the capacity of those who teach him is, so this period eventually comes to an end. At this point, the subject has not seen another being since his initiation and does not know that an outside world exists, except for his all-powerful but invisible Teacher. Now it is made impossible that any distracting influence may ever enter his future life, by methods which we shall skip. Henceforth he has nothing to do but think and communicate his thoughts to the Great Teacher, by the one simple method left to him, until eventually he has exhausted the possibilities in the store of information which was fed to him.

Actually, the above story is somewhat incidental to the book. Mr. Hersey needed a dramatic story on which to build a structure of satire. The book reports verbatim the proceedings and testimony of a legislative committee investigation into the alleged child-buying. No opportunity is lost to exploit the idiosyncrasies of the people concerned: the committee itself, and the Senator who has a little trouble with English (and ideas); the local school authorities, and the Principal who, in spite of the best intentions, cannot help giving evasive answers; the parents of the "specimen" concerned; the good-hearted and sympathetic teachers who become intrigued, after a while, with the idea of retiring with a little extra income. Perhaps the most honest and least venal character is the graduate of Boys Reform School, a lad with an unexceptional IQ who tries to be a real friend to his gifted buddy.

—CVK

how do you look at ANODES?

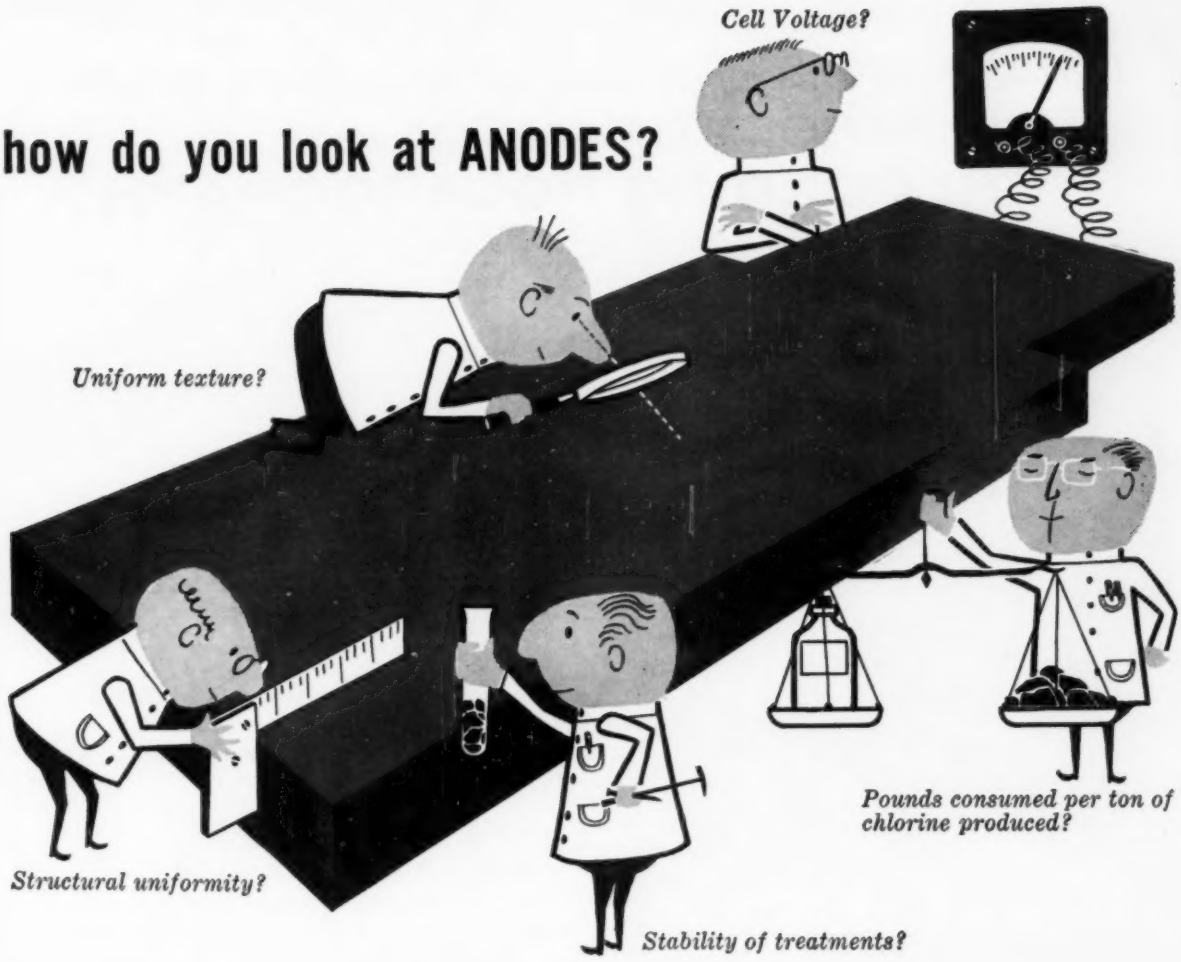

Judged by Cell Maintenance Costs Alone,

the highly stable impregnants used in Stackpole GraphAnode reduce diaphragm clogging to a bare minimum. The graphite is consumed slowly and evenly. Because GraphAnode anodes present uniform, low-porosity surfaces to the electrolyte, the graphite does not slough off to clog the diaphragm or to contaminate the cell.

Judged by Anode Cost and Performance,

Stackpole GraphAnode proves second to none whether you figure in terms of anode life, or in tons of chlorine produced per pound of graphite consumed. You get maximum anode life . . . and with the added advantage of low cell voltages. Stackpole engineers stand ready to offer a convincing demonstration on your equipment.

Stackpole Carbon Company, St. Marys, Pa.

STACKPOLE
GraphAnode®

ELECTROCHEMICAL ANODES FOR DIAPHRAGM, MERCURY, MANGANESE DIOXIDE, & SODIUM CHLORATE CELLS. OTHER TYPES FOR CATHODIC PICKLING, ALUMINUM ANODIZING, AND OTHER USES.

CATHODIC PROTECTION ANODES • FLUXING & DE-GASSING TUBES • SALT BATH RECTIFICATION RODS • ROCKET NOZZLES • RISER RODS • GRAPHITE BEARINGS & SEAL RINGS • ELECTRODES & HEATING ELEMENTS • WELDING CARBONS • VOLTAGE REGULATOR DISCS • "CERAMAGNET"® CERAMIC MAGNETS • ELECTRICAL CONTACTS • BRUSHES for all rotating electrical equipment • and many other carbon, graphite and electronic components.

The SARGENT Model XV
RECORDING POLAROGRAPH®

offers you—

- **FULL 10 INCH CHART**
- **1/10% ACCURACY OF MEASUREMENT**
- **TEN STANDARDIZED POLARIZING RANGES**

This new Sargent Polarograph gives you a large 250 mm (10 inches) chart and the highest accuracy and current sensitivity at the lowest price of any pen writing polarographic instrument on the market.

It offers you optimum specifications based on over twenty years of leadership in design, manufacture and service in this specialized field of analysis.

The polarographic method is capable of reproducibility to 1/10% and analytical accuracy to ½%. To make use of this facility, the instrument must be accurate to 1/10% and chart space must be provided for recording large steps to achieve measuring precision. We strongly advise against the purchase of any polarographic instrument using miniature (5 inch) charts and low gain balancing systems in the 1% order of precision.

This Model XV is adaptable to 10^{-4} M determinations with the S-29315 Micro Range Extender

Current Ranges:	19, from .003 to 1.0 μA/mm.
Current Sensitivity:	standard specifications, 10^{-4}μA/mm.
Polarizing Ranges, volts:	0 to −1; −1 to −2; −2 to −3; −3 to −4; +.5 to −5; 0 to −2; −2 to −4; +1 to −1; 0 to −3; +1.5 to −1.5.
Balancing Speed:	standard, 10 seconds; 1 second or 4 seconds optional.
Bridge Drive:	synchronous, continuous repeating, reversible; rotation time, 10 minutes.
Chart Scale:	current axis, 250 mm; voltage axis, 10 inches equals one bridge revolution.
Current Accuracy:	1/10%
Voltage Accuracy:	¼%
Chart Drive:	synchronous, 1 inch per minute standard; other speeds optional.
Writing Plate:	10½ x 12½ inches; angle of slope, 30°.
Standardization:	manual against internal cadmium sulfate standard cell for both current and voltage.
Damping:	RC, four stage.
Pen:	ball point; Leroy type optional.
Suppression:	zero displacement control, mercury cell powered, 6 times chart width, upscale or downscale.
Potentiometric Range:	2.5 millivolts, usable as general potentiometric recorder.
Finish:	case, enameled steel; panels, anodized aluminum; writing plate, polished stainless steel; knobs and dials, chromium plated and buffed.
Dimensions:	23 x 17 x 10.
Net Weight:	65 pounds.

Catalog number **S-29310** with accessories and supplies. . . . **$1585.00**

For complete information write for Sargent Bulletin P

®Registered Trade Mark (Pat. No. 2,931,964)

SARGENT SCIENTIFIC LABORATORY INSTRUMENTS • APPARATUS • SUPPLIES • CHEMICALS

E. H. SARGENT & CO., 4647 W. FOSTER, CHICAGO 30, ILLINOIS
DETROIT 4, MICH. • DALLAS 35, TEXAS • BIRMINGHAM 4, ALA. • SPRINGFIELD, N. J.

Passivity and Corrosion Resistance of Titanium and Its Alloys

N. D. Tomashov, R. M. Altovsky, and G. P. Chernova

Department of Metal Corrosion, Institute for Physical Chemistry, Academy of Sciences of U.S.S.R., Moscow, U.S.S.R.

ABSTRACT

A brief review is given of possible ways to increase corrosion resistance of titanium in acids proceeding from analysis of its electrochemical characteristics and passive state stability. Rational ways of alloying titanium for acid resistance are indicated. Experiments include titanium alloys with palladium, chromium, and molybdenum in solutions of sulfuric and hydrochloric acids. It is established that the greatest increase of corrosion resistance is obtained when titanium is alloyed with cathodic additions capable of shifting the corrosion potential of alloys in the noble direction (as, for instance, by palladium and other noble metals) and simultaneously by metals which increase the tendency of titanium to passivate or which diminish the degree of its thermodynamic instability (as is the case with chromium, molybdenum, zirconium, and possibly tungsten).

The present commercial titanium-base alloys are distinguished by their high corrosion resistance under natural conditions of exposure to the atmosphere, soil, marine and fresh water, and also to oxidizing acids. Particularly remarkable is the good resistance of Ti to solutions of inorganic and organic chlorides. However, in some chemical media, especially sulfuric and hydrochloric acid solutions, Ti and its alloys are not sufficiently resistant. Therefore much attention is devoted to the problem of increasing corrosion resistance of Ti in these media and to the development of Ti-base corrosion-resistant alloys.

This paper discusses the possibilities of increasing the stability of the passive state and the corrosion resistance of Ti in H_2SO_4 and HCl, i.e., in media where Ti may be either in an active or a passive state, depending on conditions.

Analysis of experimental results on the stability of Ti in the passive state, mainly by a potentiostatic polarization curve (1), makes it possible to outline the main avenues for increasing the corrosion resistance of Ti. Resistance of Ti may be increased by shifting its steady-state potential either in the negative (active) or in the positive (noble) direction. The potential may be made more active by external cathodic polarization (cathodic protection) or by introducing cathodic inhibitors into the corrosive medium, which increase hydrogen overvoltage. This general method of protection is most likely not sufficiently effective for Ti. As has been shown by our studies, the corrosion rate of Ti in solutions of H_2SO_4 or HCl may be diminished considerably by cathodic polarization; however, the required protective cathodic current is very high. Moreover, it should be borne in mind that intensive absorption of H_2 takes place during cathodic polarization which affects the mechanical properties of Ti.

Shifting the potential in the noble direction is much more efficient even in acids of a nonoxidizing nature. By such shift of potential the corrosion rate of Ti can be diminished several hundredfold. The Ti is then in the passive state.

This condition may be achieved in general by several methods:

(*a*) By anodic polarization through an external current (anodic protection). As has been shown already (2-4), Ti can be protected successfully from corrosion by a small anodic current in different aggressive chemical media (sulfuric, hydrochloric, formic, and oxalic acids).

(*b*) By contact with noble metals, for instance, Pt, Pd, and others (5), or by depositing on the metal surface a porous coating of a noble metal (6).

(*c*) By introducing into the corrosive medium cations of noble metals which are reduced and may be precipitated on the cathodic areas of local cells on the corroding metal, for instance, the ions of Pt^{4+}, Cu^{2+} (3, 7, 8).

(*d*) By additions to nonoxidizing acids (H_2SO_4 and HCl) of oxidizing anions (nitric, chromic acids), or some other oxidizers, for instance, Fe^{3+} (3, 7, 8).

(*e*) By appropriate alloying. Some new possibilities of a rational choice of alloying components for acid-resistant Ti-base alloys are discussed below.

Possibilities of Acid-Resistant Alloying of Ti

Among the structural commercial metals Ti is one of the most thermodynamically unstable, but simultaneously it is a most easily passivated metal. Proceeding from the general principles of corrosion-resistant alloying (9, 10), it follows that an increase in the chemical resistance of these systems is achieved most efficiently by further increase in the stability of the passive state. In 1949 (11) we established the possibility of increasing the corrosion resistance of iron and stainless steels by increasing the stability of the passive state through small alloy additions of metals with noble electrode potentials (Cu, Ag, Pd, Pt, and others). Subsequently (12-13), we proved that the resistance of stainless chromium and chromium-nickel steels in solutions of H_2SO_4

could be improved by alloying with small amounts (0.1-1%) of Pd or Pt. This type of alloying for increasing corrosion resistance of Ti-base alloys should be particularly promising considering the fact that Ti is passivated easily and that its passive state is stable even in the presence of Cl^- (2, 14).

Recent work by Stern and Wissenberg (5) has demonstrated experimentally the possibility of obtaining alloys which are passivated more easily and which are more corrosion resistant in H_2SO_4 and HCl by alloying Ti with small additions of Pt, Pd, Rh, Ru, Ir, Os, Re, Au. Our previous work, independently and approximately concurrently, also proved that when Ti is alloyed with a small amount of Pd or Pt (1-2%) its corrosion resistance in these acids improved greatly (1). These alloys had good corrosion resistance in H_2SO_4 up to 70% and in HCl up to 25% at 18°C. In more concentrated solutions, in more dilute solutions, at higher temperatures, the corrosion resistance of the alloys Ti with Pt or Pd was considerably better than for Ti alone but insufficient to recommend these alloys for commercial use under these conditions.

The present work was undertaken for the purpose of further improving the corrosion resistance of Ti alloyed with noble elements by introducing a third component. In our opinion these new components should be metals of the type Mo, Cr, Zr, Ta, and some others, which, like Ti, have a pronounced tendency to passivate but have a somewhat different shape of the anodic polarization curve.

A number of investigators have proved the beneficial influence of Mo, Ta, Zr, and other metals on the resistance of Ti to chemicals (15-18). Simultaneous alloying of Ti with small amounts of noble metals (Pt, Pd) in addition to a considerable amount of another easily passivated metal may result in more chemically resistant Ti-base alloys.

In the present studies, a binary alloy of Ti-Pd was taken as the base. Palladium is the most available of noble metals and increases the corrosion resistance of Ti even more than Pt (1). For alloying additions of easily passivated metals, Cr and Mo were used for the first series of experiments.

Commercially pure Ti (BTI), commercially pure Mo, and electrolytic Cr and Pd were used for preparing the following alloys by melting (weight percentage): Ti-unalloyed (remelted); Ti-0.1% Pd; Ti-2% Pd; Ti-15% Mo; Ti-15% Mo-0.1% Pd; Ti-15% Mo-2% Pd; Ti-15%Cr; Ti-15% Cr-0.1% Pd; Ti-15% Cr-2% Pd; Ti-5% Pd.

The technology of vacuum electrofurnace melting, treatment of the ingots, and preparation of samples was that ordinarily employed for the preparation of similar experimental alloys. Chromium content did not exceed the maximum amount for which the intermetallic compound of $TiCr_2$ appears in the structure (19, 20). Corrosion rates were determined by weight loss. Polarization curves were recorded using an electronic potentiostat (21).

Corrosion Resistance in H_2SO_4 *and* HCl

Results of corrosion tests of the alloys as a function of H_2SO_4 concentrations at the boiling temperature and also at 18°C are presented in Fig. 1 and 2. These show that alloying Ti even in small amounts (0.1%) of Pd increases the corrosion resistance considerably. For instance, a 0.1% Pd alloy in 40% H_2SO_4 at 18°C proved to be fivefold more resistant than unalloyed Ti. In boiling 10% H_2SO_4 the alloy resistance is practically 35 times greater. An alloy with 2% Pd is much more resistant than the 0.1% Pd alloy. In boiling 10% H_2SO_4 2% Pd alloy is 156 times more resistant than Ti. Further increase in the amount of Pd, up to 5%, does not increase corrosion resistance noticeably. At 18°C the 0.1% Pd alloy is resistant in up to 20% H_2SO_4, the 2% Pd alloy up to 60%, the 5% Pd alloy up to 70% H_2SO_4. In 80% H_2SO_4 the corrosion rate of Pd-Ti alloys is only 1.5-4.5 times less than the corrosion rate of unalloyed Ti, and the corrosion rate of alloys in 90% H_2SO_4 is practically the same as that of Ti.

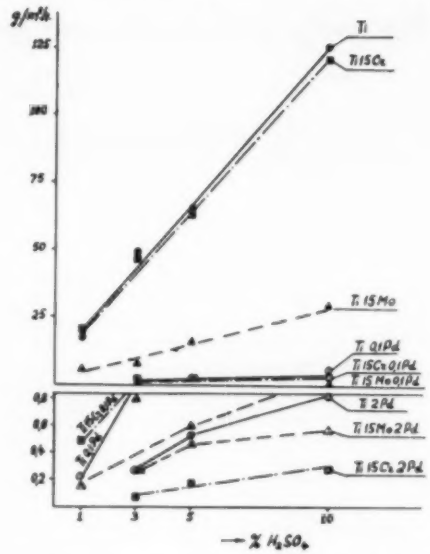

Fig. 1. Corrosion of Ti and its alloys in boiling H_2SO_4 solutions

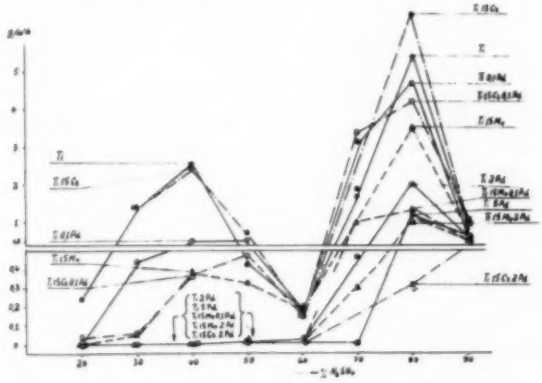

Fig. 2. Corrosion of Ti and its alloys in H_2SO_4 solutions, 18°C.

The 15% Mo alloy proved to be more resistant than Ti under all experimental conditions (2-4 times). The addition of 0.1% Pd to a Ti-Mo alloy increases the alloy resistance 2-3 times. Moreover, the resistance of this alloy is the same as that of

the 2% Pd alloy. Resistance of the Ti-Mo alloy increases but little with the addition of 2% Pd compared with the Ti-15% Mo alloy which contains 0.1% Pd.

The Ti-15% Cr alloy shows no advantage over pure Ti; in fact in some cases it is inferior. Introduction of 0.1% Pd to the Ti-15% Cr alloy gives some improvement. However, further addition of up to 2% Pd increases the resistance of the alloy considerably. This is particularly noticeable in dilute, boiling H_2SO_4 solutions. Here the corrosion rate of the Ti-15% Cr-2% Pd is less than 1/400 the corrosion rate of the binary alloy Ti-15% Cr, almost ¼ that of Ti-2% Pd, and approximately ½ that of the Ti-15% Mo-2% Pd alloy.

Results of corrosion tests of Ti and its alloys in HCl solutions at boiling temperature and at 18°C are presented in Fig. 3 and 4. Just as in the case of H_2SO_4, alloying Ti with Pd increases its resistance considerably.

Considerable reduction in the corrosion rate in HCl is achieved even by small additions of Pd. Thus, in 25% HCl at 18°C, the resistance of Ti-0.1% Pd is 12 times that of unalloyed Ti, while the resistance of an alloy containing 2% Pd is 300 times greater. Increase in Pd content up to 5% does not increase resistance in HCl up to 25%, whereas in solutions of higher concentration (30-35%) this addition entails a drop in corrosion resistance. This may be associated with a larger amount of eutectoid α Ti + $TiPd_3$ in the Ti-5% Pd than in the Ti-2% Pd. When 15% Mo is added to Ti, resistance increases considerably (approximately fivefold in 25% HCl).

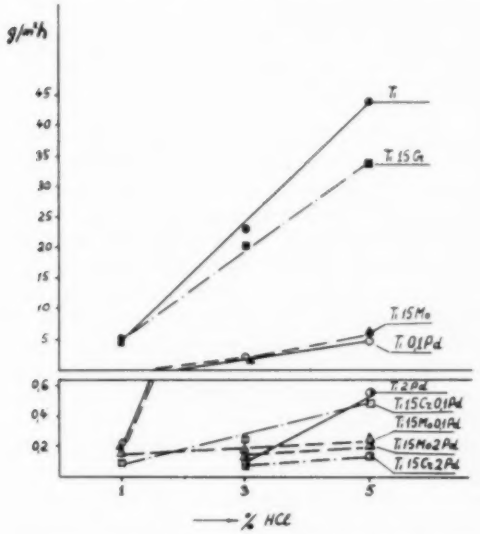

Fig. 3. Corrosion of Ti and its alloys in boiling HCl solutions

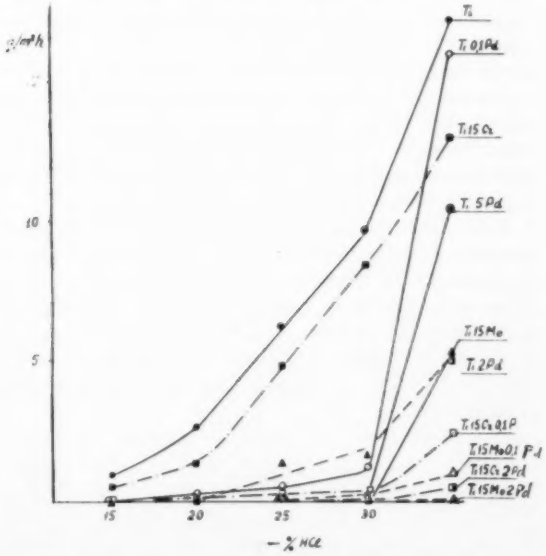

Fig. 4. Corrosion of Ti and its alloys in HCl solutions at 18°C

Electrochemical Studies

Electrochemical characteristics of the basic alloy components used in the present study are presented in Fig. 5. The anodic and cathodic curves are for 40% H_2SO_4 at 18°C.

The anodic polarization curve shows three characteristic points:

1. V_s-steady-state potential (when the external current is zero); the steady-state potentials for Cr and Ti proved to be rather similar.

2. The potential for passivation corresponds to the maximum current of the anodic dissolution of metal. At potentials which are more positive (more noble) that the passivation potential (V_p for Ti and V_p' for Cr, Fig. 5) the rate of anodic dissolution of metal diminishes.

3. The potential for complete passivation of the metal (V_{cp} for Ti and V_{cp}' for Cr) corresponds to minimum anodic current. At potentials which are more positive than the potential of complete passivation, the metal is in the passive state which is maintained by the external anodic polarization.

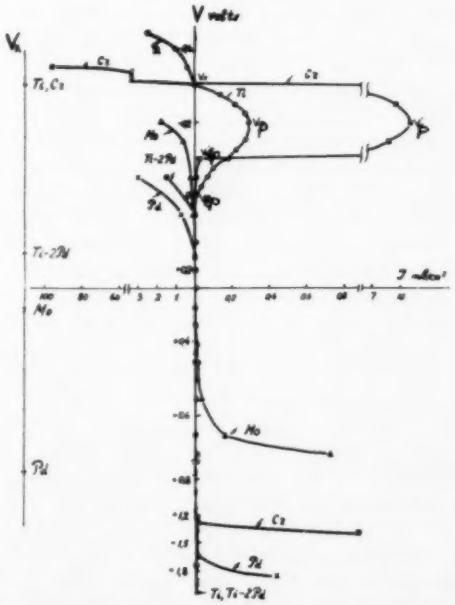

Fig. 5. Polarization curves of Ti, Cr, Mo, Pd, and the Ti-2% Pd alloy in 40% H_2SO_4 at 18°C. The (V_s) values of the steady-state potentials are shown on the left-hand side.

The difference in the anodic behavior of Ti and Cr is as follows: at very positive potentials the passive state of Ti is not destroyed, whereas for Cr a state of transpassivation sets in (22-24) under which it begins to dissolve in the form of hexavalent ions. The anodic current which corresponds to the potential of passivation (V_p') for Cr is considerably greater than that for Ti (V_p). The complete passivation potential for Cr (V_{cp}') is noticeably more negative (active) than for Ti (V_{cp}). The overvoltage of hydrogen on the surface of Cr is somewhat less than on that of Ti.

The anodic curve for Mo is of a somewhat different shape. Its steady-state potential in 40% H_2SO_4 is +0.3 v, *i.e.*, it is considerably more noble than the potential of complete passivation of Ti in this medium. The anodic dissolution of Mo is observed only when there is a considerable shifting of its potential in the positive direction. Comparison of weight losses and amount of electricity passed helped to determine, both here and in previous work (25), that the dissolution of Mo takes place to hexavalent ions. Molybdenum is a corrosion-resistant metal in H_2SO_4. Therefore dissolution of Mo in the form of ions of the highest valency under anodic polarization may be interpreted as a state of transpassivation. The overvoltage of hydrogen on Mo is considerably lower than on Ti or on Cr.

Palladium does not dissolve anodically in H_2SO_4. The increase in the anodic current at high positive potentials corresponds to oxygen evolution. The overvoltage of hydrogen on Pd is much lower than on Ti or Mo.

Polarization curves for Ti, Cr, Mo, and Pd in 30% HCl have similar shapes. The main differences from those presented in Fig. 5 which concern H_2SO_4 are as follows: Cr is not passivated in HCl even at high anodic current densities (50 ma/cm^2). The overvoltage of hydrogen on Ti in HCl is lower than on Cr. Unlike the H_2SO_4 system, Pd dissolves anodically in HCl.

Figure 5 also presents the polarization curve for the Ti-2% Pd alloys. The cathodic curve for this alloy is from 0.35 to 0.40 v more noble than the cathodic curve for Ti owing to a considerable decrease of hydrogen overvoltage because of the Pd in the alloy. The steady-state potential of the alloy, therefore, is in the range of potentials where Ti is completely passivated. This explains the corrosion resistance of the Ti-2% Pd alloy in H_2SO_4 up to 60%, and also in HCl up to 30%. The region of anodic dissolution is absent on the anodic curve for the alloy.

In order to interpret the increased chemical stability of ternary alloys Ti-Mo-Pd and Ti-Cr-Pd electrochemically, anodic polarization curves were obtained for Ti-Mo and Ti-Cr alloys by the potentiostatic method. These were compared with steady-state potentials for the alloys Ti-2% Pd, Ti-15% Mo-2% Pd, Ti-15% Cr-2% Pd. The results for 80% H_2SO_4 are presented in Fig. 6. Comparison of the anodic curves for Ti in 40% H_2SO_4 (Fig. 5) and in 80% H_2SO_4 (Fig. 6) shows that passivation of Ti is hindered in 80% H_2SO_4. This follows from the fact that the anodic current required for Ti passivation in 80% H_2SO_4 is much higher than in 40% H_2SO_4, and the potential for complete passivation is shifted greatly to the positive (noble) direction as against its position for 40% H_2SO_4. Therefore, alloying Ti with 2% Pd no longer yields such a marked increase in the corrosion resistance in 80% H_2SO_4 as was observed in 40% H_2SO_4. The steady-state potentials of the alloy are in the range where Ti is not fully passive. Therefore a rather large region of anodic dissolution (although somewhat smaller than for pure Ti) is observed during anodic polarization.

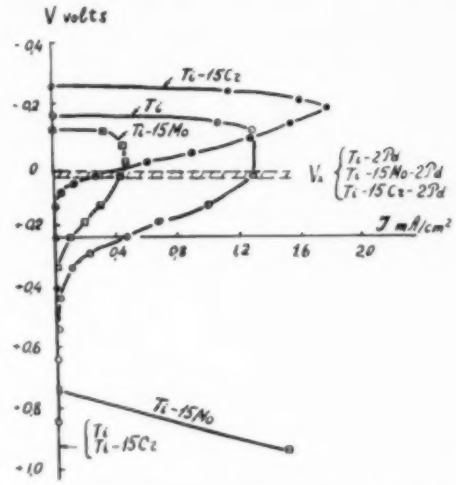

Fig. 6. Anodic polarization curves of Ti and alloys in 80% H_2SO_4 at 18°C. The horizontal dotted line indicates the region of the steady-state potentials of Ti-2% Pd, Ti-15% Mo-2% Pd, and Ti-15% Cr-2% Pd.

Previous work showed that alloying Ti with Pd does not have any direct influence on the anodic process of Ti ionization. With this basis, the corrosion rate of the alloy can be calculated provided the steady-state potential of the alloy and the curve of the anodic polarization of pure Ti under given conditions are known. Comparison of calculated and experimental data obtained by direct corrosion tests has shown good agreement (1). Therefore, the value of the corrosion rate of the ternary alloys Ti-Mo-Pd and Ti-Cr-Pd can be calculated graphically if we measure their steady-state potentials and determine the current density for anodic dissolution of Ti-Mo alloy and Ti-Cr alloy at the same potential.

As noted in the discussion of Fig. 5, a much bigger anodic current is required for anodic passivation of Cr than for Ti. Therefore, alloying Ti with Cr results in an increase of anodic current required for passivation of the alloy, *i.e.*, the ability of the alloy to dissolve anodically increases. In keeping with this, the Ti-15% Cr alloy is less resistant than the unalloyed Ti.

As indicated earlier, Mo does not dissolve at the same potential which suffices for the active anodic dissolution of Ti. Anodic dissolution of an alloy of Ti with Mo is considerably smaller than that of Ti. This has also been noted in a previous paper (18). This explains the higher resistance of the Ti-15%

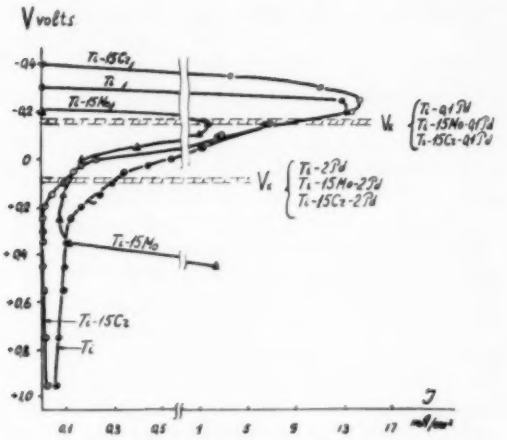

Fig. 7. Anodic polarization curves of Ti and alloys in boiling 10% H_2SO_4. The diagram shows the region of steady-state potentials of Ti-2% Pd, Ti-15% Mo-2% Pd, and Ti-15% Cr-2% Pd, and the range of steady-state potentials of the alloys Ti-0.1% Pd, Ti-15% Mo-0.1% Pd, and Ti-15% Cr-0.1% Pd.

Mo alloy over Ti. At high positive potentials the Ti-15% Mo alloy, unlike Ti, acquires the ability to dissolve anodically (transpassivation). Behavior of the alloy in this range of potentials is determined by that of pure Mo (Fig. 5). The steady-state potentials of the alloys Ti-15% Mo-2% Pd, Ti-15% Cr-2% Pd, and Ti-2% Pd, have nearly similar values, as is shown in Fig. 6. At this potential the current for anodic dissolution of Ti-15% Mo and Ti-Cr alloys, owing to the shifting of the complete passivation potential to the negative (active) side, relative to Ti, is considerably less than the current for anodic dissolution of Ti. Moreover, the current for Ti-15% Cr alloy dissolution is even less than the current for Ti-15% Mo alloy dissolution. In keeping with this, the corrosion resistance of Ti-15% Cr-2% Pd and Ti-15% Mo-2% Pd is much higher than the resistance of the binary alloy Ti-2% Pd.

Figure 7 shows anodic curves for Ti and the alloys Ti-15% Mo and Ti-15% Cr in boiling 10% H_2SO_4. In this case the complete passivation potentials of Ti and of the alloys practically do not differ one from another. However, the anodic current for dissolution of alloys in the passive state, particularly for the Ti-15% Cr alloy, is considerably less than the current for Ti. In the range of steady-state potentials of the alloys Ti-15% Cr-2% Pd, Ti-15% Mo-2% Pd, and Ti-2% Pd (see Fig. 7) the anodic dissolution current of the Ti-15% Cr alloy is less than that of the Ti-15% Mo alloy and that of the latter is less than that of Ti. Alloys of Ti-15% Cr-2% Pd, Ti-15% Mo-2% Pd, and Ti-2% Pd stand in the same order as regards corrosion resistance.

A similar explanation may be offered for the higher corrosion resistance of Ti-15% Mo-0.1% Pd compared to Ti-15% Cr-0.1% Pd and Ti-0.1% Pd in boiling 10% H_2SO_4 if the currents for anodic dissolution of Ti-15% Cr, Ti-15% Mo, and unalloyed Ti at the steady-state potentials are compared (Fig. 7).

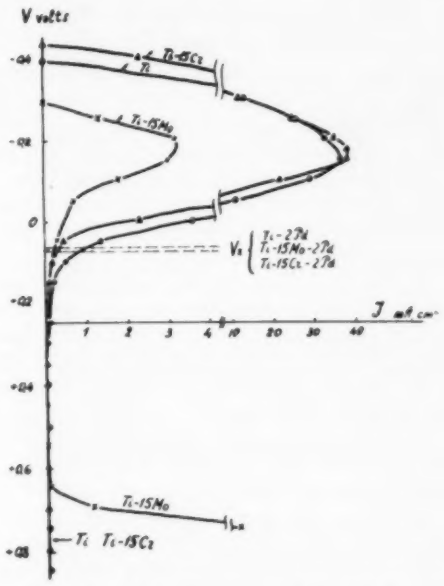

Fig. 8. Anodic polarization curves of Ti and alloys in 35% HCl at 18°C. The diagram shows the region of steady-state potentials of Ti-2% Pd, Ti-15% Mo-2% Pd, and Ti-15% Cr-2% Pd.

Figure 8 presents the anodic curves for Ti and for Ti-15% Mo and Ti-15% Cr in 35% HCl at 18°C. In this case, at a potential possessed by all these alloys and Ti-2% Pd, the anodic current density for the first is less than that for the second while that of the last is less than that of Ti. These data agree with the results of corrosion tests (Fig. 4) which prove that in 35% HCl, Ti-15% Mo-2% Pd is more resistant than Ti-15% Cr-2% Pd which, in turn, is more resistant than Ti-2% Pd.

Thus the results of corrosion tests agree fully with the results of electrochemical measurements. This is confirmation of the electrochemical mechanism of corrosion of Ti alloys and of the suggested rational approach to improving their corrosion resistance by creating conditions for more complete passivation. The beneficial influence of Mo or Cr on corrosion resistance of Ti-Pd alloys is explained by the fact that both these elements decrease the current for anodic dissolution of Ti or that of its alloy with Pd, close to the steady-state potentials of these alloys. For Cr alloys this is achieved because Cr has a more negative potential of the complete passivation than Ti. In the case of the Mo alloy it is due mainly to considerable decrease of the ability of the Ti-Mo alloy to dissolve anodically. The positive influence of additional alloying of Ti-Cr or Ti-Mo with Pd does not change the nature of the passivation noticeably, but shifts the steady-state potential in the positive (noble) direction considerably. This is why the steady-state potentials of Ti-Cr or Ti-Mo alloyed with Pd are in the range of values where the currents for anodic dissolution are much less than those for unalloyed Ti. Analysis of polarization curves helps to indicate rational ways of developing corrosion-resistant alloys and, in particular, the acid-resistant alloys based on Ti.

Basic Principle of Developing Ti-Base Corrosion-Resistant Alloys

As has been indicated in previous papers (26-27), the corrosion of Ti in H_2SO_4 and HCl proceeds with anodic control predominate. In keeping with the previously elaborated principles (9, 10), the greatest resistance of Ti should be expected when it is alloyed with elements that diminish anodic activity. There are three ways of reducing the anodic activity of Ti:

1. By cathodic alloying, i.e., by using alloying elements capable of causing a shift of the steady-state potential of the alloy in the positive (noble) direction; by diminishing the overvoltage of the cathodic reaction to such values that the dissolution of Ti decreased considerably.

2. By using alloying elements which diminish the ability of Ti to dissolve anodically by reducing the thermodynamic instability of the alloy.

3. By using alloying elements which increase passivity. Titanium possesses a great tendency to passivate (10), but it is possible by appropriate alloying to intensify this tendency still further.

Elements of the first group include noble metals: Pt, Pd (1, 9-13) and also, as has been shown by experiments conducted by Stern and Wissenberg, Ru, Rd, Ir, and Os (5).

The second group includes Ni which, as shown by others (15), increases corrosion resistance. Also in this group are Mo and W which are thermodynamically more stable than Ti. Besides reducing the thermodynamic instability of Ti these metals can also increase its passivity.

In the third group are such elements as Zr, Ta, Cr, and possibly Mo. As seen in Fig. 5, Cr, at potentials close to that for complete passivation of Ti, has a lower anodic dissolution rate, i.e., it is in a more stable passive state under these potentials and in a similar way changes the onset of the passive state of the Ti-Cr alloys (see Fig. 6-8).

An increase in the corrosion resistance of Ti by cathodic alloying is a promising approach since this method requires only small additions of alloying elements.

In order to achieve high corrosion resistance by alloying with a metal which is thermodynamically more stable or which is more easily passivated, it is necessary to add a considerable amount of the alloying component. For instance, according to Rudiger and Fischer (17), alloys of Ti with Mo acquire high corrosion resistance only when the Mo content is brought up to 20-30%.

As shown by the present investigation, in order to achieve further improvement in the corrosion resistance of binary alloys of Ti-noble element, it is expedient also to add a third component (and perhaps introduce an even more complicated alloying pattern). The third alloying component should either shift the complete passivation potential of the alloy to the more negative region (*e.g.*, Cr) or considerably diminish the anodic dissolution current in the proximity of the steady-state corrosion potential of the alloy (*e.g.*, Mo), or influence the electrochemical behavior of Ti along these two avenues simultaneously.

Conclusions

1. Alloying Ti with Pd considerably increases corrosion resistance in H_2SO_4 and HCl. A substantial lowering of the corrosion rate is observed even when Ti is alloyed with a small amount of Pd (0.1%). A higher Pd content (>2%) is deemed inexpedient.

2. Electrochemical investigations show that the increase in corrosion resistance when Ti is alloyed with Pd takes place owing to a shift of the steady-state potential of the alloy by a decrease in hydrogen overvoltage to the region of values where Ti is either partially or completely passive.

3. Alloying Ti with Mo increases resistance via a considerable inhibition of the anodic dissolution reaction of the alloy. This takes place due both to an increase in passivation of the alloy and, apparently, to some increase in thermodynamic stability.

4. As a rule alloying Ti with Cr only does not add to its corrosion resistance while, in some cases, it even diminishes it since in H_2SO_4 and HCl, at a potential corresponding to the steady-state potential of Ti, Cr possesses a lesser tendency to passivate than does Ti.

5. Ternary alloys Ti-Pd-Mo and Ti-Pd-Cr have high resistance in H_2SO_4 and HCl. This is associated with a considerable shifting of the steady-state corrosion potentials of these alloys in the noble direction due to the influence of alloying with Pd and to a concurrent reduction of the anodic dissolution current in the proximity of the steady-state potential by alloying with Cr or Mo.

Acknowledgment

A. D. Arteyev participated in the fulfillment of the experimental part of the research.

Manuscript received Sept. 2, 1960.

Any discussion of this paper will appear in a Discussion Section to be published in the December 1961 JOURNAL.

REFERENCES

1. N. D. Tomashov, G. P. Chernova, and R. M. Altovsky, *Z. Phys. Chem.*, **214**, 312 (1960).
2. N. D. Tomashov, R. M. Altovsky, and A. G. Arakelov, *Doklady of Ac. of Sc.*, **121**, [No. 5] (1958).
3. N. D. Tomashov, R. M. Altovsky, and A. G. Arakelov, "Anodic Protection of Titanium in Sulfuric and Hydrochloric Acids," Published by the branch of the USSR Institute of Scientific and Technical Information, subject No. 13, No. M-59-239/26.
4. J. B. Cotton, *Chem. & Ind.*, **1958**, No. 3, 69.
5. M. Stern and H. Wissenberg, *This Journal*, **106**, 759 (1959).
6. G. P. Chernova and R. M. Altovsky, *Doklady of Ac. of Sc.*, **110**, No. 6, 1030, 1956.
7. J. R. Cobb and H. H. Uhlig, *This Journal*, **99**, **13**, (1952).
8. D. Schlein and J. S. Smatko, *ibid.*, **99**, 417 (1952).
9. N. D. Tomashov, *Uspekhi Khim.*, **24**, No. 4 (1955); *Corrosion*, **14**, 229 (1958).
10. N. D. Tomashov, "Theory of Corrosion and Metal Protection," published by the Academy of Sciences, Moscow (1959).
11. N. D. Tomashov and G. P. Sinelshchikova. (Chernova), and M. A. Vedeneyva, *J. Phys. Chem.*, **23**. No. 3 (1949).

12. N. D. Tomashov and G. P. Chernova, *Doklady of Ac. of Sc.*, **89**, No. 1 (1953).
13. N. D. Tomashov and G. P. Chernova. Problems of Corrosion and Metal Protection. Proceedings of the 5th USSR Conference on Corrosion and Metal Protection, published by Academy of Sciences (1956).
14. N. D. Tomashov, G. P. Chernova, R. M. Altovsky, and G. K. Blinchevsky, Zavodskaya Laboratoriya, No. 3 (1958).
15. V. V. Andreyeva, G. P. Danilova, and J. M. Lipkes, "Hard Corrosion Resistant Titanium Alloys," Published by the branch of the USSR Institute of Scientific and Technical Information, series 19, No. T-56-452/9, 1956.
16. Nishimura and Hiramatsu. *J. Japan. Inst. Metals*, **21**, No. 7 (1957).
17. O. Rudiger and W. R. Fischer, *Z. Elecktrochem.*, **62**, No. 6-7 (1958).
18. V. V. Andreyeva and V. I. Kazarin, *Doklady of Ac. of Sc.*, **128**, No. 4 (1959).
19. R. J. Van Thyne, H. B. Kessler, and M. Hansen, *Trans. Am. Soc. Metals*, **44**, 974 (1952).
20. V. N. Yeremenko, "Titanium and Its Alloys," Pub.-lished by the Ukrainian Academy of Sciences, Kiev (1955).
21. M. N. Fokin and A. L. Vinogradov, Published by the USSR Institute of Scientific and Technical Information, No. II-59-12-1, 1959, Subject 39.
22. M. M. Kurtepov and G. V. Akimov, *Doklady of the Ac. of Sc.*, **87**, No. 1 (1952).
23. V. P. Batrakov and G. V. Akimov, *ibid.*, **89**, No. 2, 321 (1953).
24. N. D. Tomashov and G. P. Chernova, *ibid.*, **98**, No. 3 (1954).
25. G. Masing and G. Roth, *Werkstoffe u. Korrosion 3*, No. 5-6 (1952).
26. N. D. Tomashov, R. M. Altovsky and V. B. Vladimirov, Corrosion and Protection of Structural Materials, collection of papers published by the Mashgiz Publishing House, Moscow (1961).
27. N. D. Tomashov, R. M. Altovsky, A. V. Prosvirin, and R. D. Shamgunova, Corrosion and Protection of Structural Materials, collection of papers published by the Mashgiz Publishing House, Moscow (1961).

Oxidation of Copper between 250° and 450°C and the Growth of CuO "Whiskers"

E. A. Gulbransen, T. P. Copan, and K. F. Andrew

Research Laboratories, Westinghouse Electric Corporation, Pittsburgh, Pennsylvania

ABSTRACT

Thin oxide whiskers have been found to grow on copper by a number of investigators. The relation of these growths to the mechanism of oxidation and to changes in the kinetics of oxidation remains to be established. To answer these questions a study was made of the oxidation of copper using the vacuum microbalance method to determine the kinetics of reaction, x-ray and electron diffraction methods for study of the oxide crystal structures, and a high resolution electron microscope to determine the size and surface density of the oxide whiskers.

The results show that the oxidation of copper follows the cubic rate law between 250° and 450°C. Small embryonic whiskers are formed at 250°C and 6 hr of reaction. A surface density of $10^8/cm^2$ of long thin oxide whiskers was found at 450°C after 6 hr of oxidation. Less than 1% of the oxygen reacting with the metal at 450°C resulted in the growth of oxide whiskers. We conclude on the basis of the cubic rate law plots and analyses of the whiskers size and density that the formation of oxide whiskers, although of great interest as a natural phenomena, had no appreciable effect on the kinetics of the oxidation process.

The purpose of this paper is to report on a study of the growth of oxide whiskers on copper and their relationship to the kinetics and mechanism of oxidation. The growth of fine oxide whiskers on copper has been observed by Pfefferkorn (1-3), Cowley (4), Takagi (5), and by Morita, Usio, and Seiyama (6). Since all theories of oxidation assume the growth of a uniform oxide film, the growth of oxide whiskers may influence the kinetics and mechanism of oxidation.

Fischmeister and Drott (7) in a study of the Ag-H_2S system related the growth forms of the reaction product to the kinetics of reaction. A sudden increase in the reaction rate was accompanied by the appearance of needles perpendicular to the surface.

Hauffe (8) has suggested that oxide needles may grow on top of thick layers of oxide. Diffusion through a simple oxide film was suggested to be the rate-controlling step. This cannot be true under all conditions since Pfefferkorn (3) has reported oxide whiskers to form on copper after reacting for 5 sec in air at 400°C under conditions where a very thin purple tarnish film was formed.

Studies on the initial stages of oxidation of copper by Gronlund and Bénard (9) and by Harris, Ball, and Gwathmey (10) have shown that for certain conditions the initial oxide film is discontinuous.

A comprehensive review of the earlier oxidation studies of copper was given by Tylecote (11) in 1950 while Gulbransen and McMillan (12) reviewed the crystal structural aspects of the oxidation process in 1952. The work of Matyas (13, 14) is of particular interest from the kinetic point of view. Be-

tween 300° and 550°C the oxidation of copper followed the parabolic rate law. Cu_2O was formed below 250°C while, between 300° and 600°C, Cu_2O and CuO were formed. Diffusion of copper ions through the lattice was proposed. In an electron diffraction study Gulbransen and McMillan (12) showed that the cuprous ion was mobile in the Cu_2O lattice between 300° and 500°C.

Young, Cathcart, and Gwathmey (15) studied the rates of oxidation of several faces of single crystals of copper using a polarizing spectrometer at temperatures between 70° and 178°C. Large differences were observed between faces. Lawless and Gwathmey (16) studied the structure of oxide films on different faces of a single crystal of copper. Cu_2O was the major oxide formed between 170° and 450°C with CuO forming above a certain minimum thickness. Orientation relationships were presented. Tylecote (17) has studied the composition of copper oxide films by reduction in hydrogen and nitrogen.

Sample Preparation and Method

The method in brief was to oxidize strip specimens of copper in the vacuum microbalance reaction system (18, 19) under controlled conditions of time, temperature, and pressure. Measurements were made in a semicontinuous manner on the weight gain as a function of time. By means of x-ray diffraction and electron diffraction analyses crystal structure studies were made of the oxide films stripped from the metal electrochemically. Crystal habit studies were made on the edge of small half-disk samples using the electron microscope.

Samples for rate studies were 0.0125 cm thick strips 1.35 cm wide and 1.98 cm long OFHC copper. Specimens weighed about 0.6801 g. Table I shows the spectrographic analyses. Small half-disks of metal 0.0125 cm thick and 3 mm in diameter were reacted along with the large specimens for electron microscope and electron diffraction studies.

All samples were abraded under purified kerosene through 4/0 polishing paper and cleaned (20).

The electron microscope was a 100 kv RCA EMU-3-D with the new electron diffraction adapter. A modified Guinier-Hägg focussing x-ray diffraction camera (21-23) was used. The radiation was NiK_α.

Results

Kinetics.—Oxidation curves are shown in Fig. 1. A pressure of 7.6 cm of Hg was used for all experiments. The weight gain is in $\mu g/cm^2$, the time in minutes. A rapid initial rate of oxidation was found. As the oxide film increased in thickness the rate of oxidation decreased. This suggests that a protective oxide film was formed. No evidence was seen in Fig. 1 for a change in mechanism of oxidation over the time and temperature conditions studied.

Table I. Spectroscopic analysis of copper sheet

Element	ppm
Al	0.2
Ni	1
Si	9
Ag	2
Ca	0.3
Cr	10
Fe	15
Mg	3
Mn	11
Pb	0.5
Sn	1

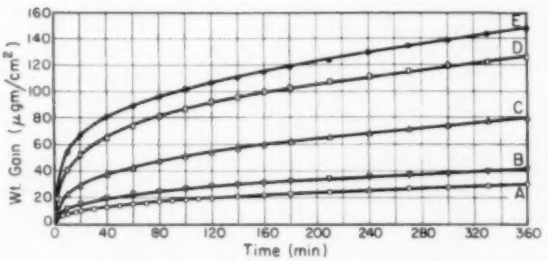

Fig. 1. Effect of temperature on oxidation of copper, 7.6 cm of Hg of O_2; A, 250°; B, 300°; C, 350°; D, 400°; E. 450°C.

Reproducibility of the oxidation curves was ± 20%. This poor reproducibility may be due to the complex nature of the reaction, since two oxides are formed, and to the fact that loss of adhesion may be occurring on a micro scale. The oxide scale spalled from the metal on cooling for several of the experiments.

Although Matyas (13) found the parabolic rate law to fit the data we have found the cubic rate law to give a better empirical correlation. The cubic rate law states $W = At^{1/3} + C$ (24). Here W is the weight gain, t is the time, and A and C are constants.

Figure 2 shows a plot of W *vs.* $t^{1/3}$ for the 250°C experiment. A straight line was observed for oxidation times of 2-240 min. The cubic rate law was found to fit all of the rate law data empirically except for the first several minutes of reaction. We conclude from Fig. 1 and 2 that the mechanism of oxidation does not change appreciably over the time course of the experiments.

A plot of the cubic rate law constants A *vs.* $1/T$ gives a heat of activation of 18,300 ± 2,000 cal/g mole. The slight difference in agreement with the values reported in literature might be attributed to the poor reproducibility of our oxidation curves and the fact that the conditions for reaction were not identical to those used by the other investigators.

Formation of oxide whiskers.—Electron micrographs were taken of the straight edges of the ox-

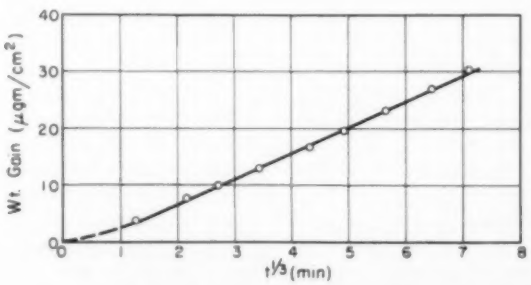

Fig. 2. Oxidation of copper, 250°C, cubic plot, 7.6 cm of Hg of O_2, abraded through 4/0.

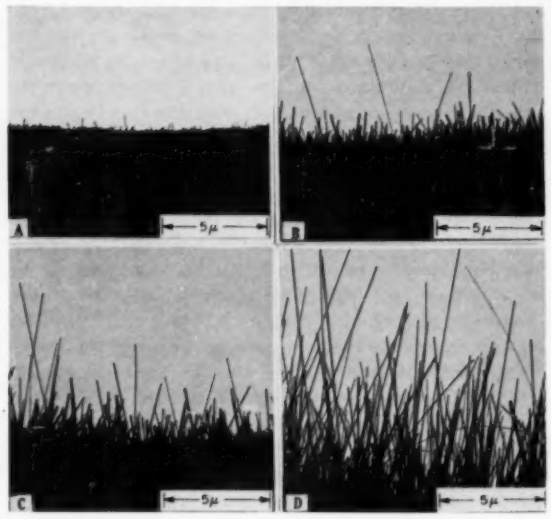

Fig. 3. Growth of oxide whiskers on pure copper, 7.6 cm of Hg pressure O_2, 6-hr experiments; A, 250°; B, 300°; C, 325°; D, 350°C. Magnification 6000X before reduction for publication.

idized half-disk samples using 100 kv electrons. These were reacted under the same conditions as the strip specimens. Figure 3A shows small embryonic oxide whiskers to form at 250°C. The whiskers were about 1500Å in diameter and from 1000Å to 7500Å high. Higher magnification electron micrographs show a structure in the whiskers. Figure 4 shows the outer sheath to be about 1500Å in size. However, a denser core about 150Å in diameter was found in the center. The light band or outer sheath surrounding the central core of the whisker is the result of contamination within the electron microscope. Contamination is inherent in vacuum systems

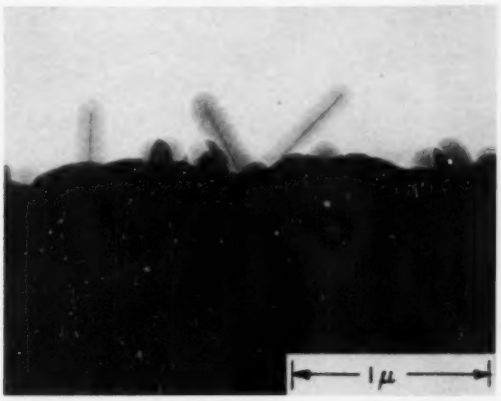

Fig. 4. Oxide whiskers on pure copper, 250°C, 7.6 cm of Hg oxygen pressure, 6-hr experiment. Magnification 30,000X.

where pump oils and rubber gaskets are utilized. The deposition is particularly noticeable after a specimen has been exposed to the electron beam for some length of time. When a very short exposure time is used, the whiskers appear to be free of the contaminant.

We estimate the surface density of these whiskers formed at 250°C to be 5 x 10^6/cm². This estimate is subject to error since the surface of the half-disk is not smooth. Some of the small whiskers may be concealed by surface irregularities. From the diameter of the core of the oxide whisker, the surface density, and a surface roughness ratio of 1 we estimate the fraction of surface area involved in whisker formation to be about 8 x 10^{-4}%. The weight of oxygen associated with these growths is less than 0.002 μg/cm². This compares to a weight gain of 30.2 μg/cm² found in the oxidation experiment. We conclude that the formation of oxide whiskers at 250°C

Table II. Electron microscope examination of oxide films on pure copper

Temp, °C	Oxide thickness, μg/cm²	Whisker growth	Size and distribution	A	Density
250	30.2	Local-small	Diameter*	1500	
			Avg. length	2000	5×10^6
			Max. length	7500	
300	42.5	General	Diameter	1300	
			Avg. length	8000	8×10^6
			Max. length	60000	
325	58.7	General	Diameter	500-1300	
			Avg. length	8000	8×10^6
			Max. length	60000	
350	80.6	General-heavy	Diameter	500-1300	
			Avg. length	40,000	1×10^7
			Max. length	140,000	
375	98.3	General-heavy	Diameter	500-1500	
			Avg. length	25,000	1×10^7
			Max. length	130,000	
400	126	Dense-heavy	Diameter	500-1300	
			Avg. length	45,000	5×10^7
			Max. length	200,000	
425	162.5	Dense-heavy	Diameter	500-1300	
			Avg. length	66,600	1.0×10^8
			Max. length	233,100	
450	148	Dense-heavy	Diameter	500-1300	
			Avg. length	150,000	1.0×10^8
			Max. length	250,000	
			Also a few heavy whiskers		

* Diameter includes contamination.

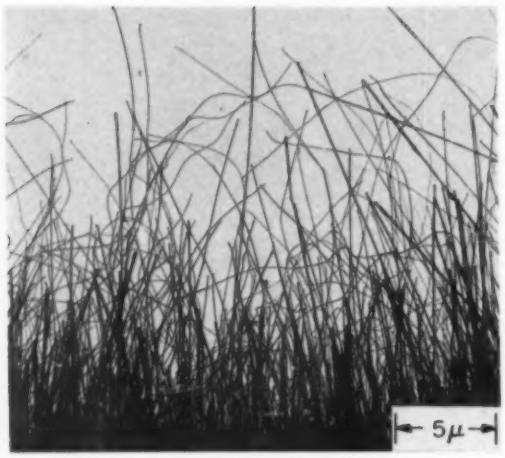

Fig. 5. Oxide whiskers on pure copper, 450°C, 7.6 cm of Hg of O_2, 6-hr experiment. Magnification 3000X.

has no effect on the kinetics of the oxidation reaction.

Figure 3B, C, and D shows electron micrographs of the oxide whiskers formed after 6 hr oxidation runs at 300°, 325°, and 350°C. Although the extent of oxidation changes from 30.2 $\mu g/cm^2$ at 250°C to 80.6 $\mu g/cm^2$ for the 350°C experiment the number and lengths of the oxide whiskers has increased greatly. These data are summarized in Table II.

Electron diffraction transmission studies were made of the oxide whiskers. CuO was the only crystal structure observed. These studies are summarized in Table III.

Figure 5 shows an electron micrograph of the oxide whisker growths formed after a 6-hr oxidation at 450°C. Two sizes of oxide growths are observed, small whiskers about 500Å in diameter and larger whiskers about 1300Å-1500Å in diameter. The smaller whiskers grow to much longer lengths than the thicker whiskers as seen in Fig. 5. These results are summarized in Table II.

High magnification electron micrographs show all of the oxide whiskers formed between 300° and 500°C to have a central core of about 150-200Å. This suggests that the oxide whisker diameters are nearly independent of temperature. Takagi (5) has observed some dependence of whisker diameter on temperature for iron above 600°C. Assuming a surface density of 10^5 and a diameter of 200Å we estimate the fraction of surface involved in whisker formation to be 3×10^{-3}% for the 450°C experiment.

We can calculate for the 450°C experiment the weight of oxygen in the oxide whiskers and compare this with the total weight of oxygen reacted with the copper. We assume a surface roughness ratio of unity in evaluating the number of oxide whiskers and a density of 6.45 for CuO. Using a diameter of 200Å and an average length of 150,000Å we calculate the weight of oxygen in the whiskers to be about 0.8 $\mu g/cm^2$. This is to be compared with a total pickup of oxygen of 148 $\mu g/cm^2$. In these calculations we have neglected the shorter but heavier whiskers. These occur with a surface density of less than 5% of the finer whiskers and are less than half of the length of the finer whiskers.

We conclude that less than 1% of the oxygen reacted at 450°C for 6 hr results in whisker formation. Under these conditions no appreciable effect should be noticed on the weight gain-time curves. No effect was observed in our studies.

Composition and crystal structure studies.—Table II shows a summary of the results. The x-ray diffraction studies were made on specimens of oxide stripped electrochemically from the oxidized surface. A Guinier-Hägg focussing camera was used which enables one to study the thin oxide films by transmission. No absorption corrections are necessary since the thin film is used directly. Cu_2O was found to be the main oxide at 250°C and a mixture of CuO + Cu_2O at 425°C. Electron diffraction studies showed the outer layer of the oxidized surface to be CuO while electron diffraction studies of the oxide whiskers showed CuO. We conclude that Cu_2O is formed next to the metal with CuO being formed in the outer layer and in the oxide whiskers.

Conclusions

Kinetic studies were made on OFHC copper over the temperature range 250°-450°C. Smooth weight gain *vs.* time curves were found with the rate of reaction decreasing as the oxide film thickened. The cubic rate law was fitted to the data for the time range of 2-360 min of reaction. No change with time of the rate law constants was observed.

X-ray and electron diffraction analyses were made of the film, and electron microscope studies were made of the size and surface density of the

Table III. Composition of oxide films and oxide whiskers formed on copper, 6-hr experiments, 7.6 cm of Hg of O_2

Temp, °C	Wt. gain, $\mu g/cm^2$	Oxide film color	Composition		
			Film, x-ray diff. (trans.)	Film, E.D. (reflection)	Whiskers, E.D. (trans.)
250	30.2	Black	Cu_2O + S.A.* CuO	CuO + tr.** Cu_2O	
300	41.1	Black		CuO	
325	58.7	Black	CuO + tr. Cu_2O	CuO	
350	80.6	Black		CuO	CuO
375	91.1	Black	CuO + Cu_2O		
400	126.0	Black			CuO
425	115†	Black	CuO + Cu_2O		CuO

* S.A., small amount.
** tr., trace.
† Spalled on cooling.

oxide whiskers. The whiskers were found to be CuO while the crystal structure of the oxide film was Cu_2O at 250°C and mixtures of Cu_2O and CuO at the higher temperatures. Electron microscope studies showed embryonic oxide whiskers to form after 6 hr of reaction at 250°C. The whiskers have a thin core of CuO about 150Å in diameter and a thicker sheath of contamination. The contamination is observed only by high voltage and high resolution electron microscopy.

An analysis of the rate law plots and of the whiskers suggests that the growth of oxide whiskers at 450°C has not influenced the kinetics of oxidation or the mechanism of oxidation.

Manuscript received May 26, 1960; revised manuscript received Sept 30, 1960. This paper was prepared for delivery before the Houston Meeting, Oct. 9-13, 1960.

Any discussion of this paper will appear in a Discussion Section to be published in the December 1961 JOURNAL.

REFERENCES

1. Von G. Pfefferkorn, *Naturwiss.*, **40**, 551 (1953).
2. Von G. Pfefferkorn, *Z. Metallkunde*, **46**, 204 (1955).
3. Von G. Pfefferkorn, *Z. Wiss. Mikroskopie*, **62**, 109 (1954).
4. J. M. Cowley, *This Journal*, **101**, 277 (1954).
5. R. Takagi, *J. Phys. Soc. Japan*, **12**, [11], 1212 (1957).
6. T. Morita, S. Usio, and T. Seiyama, *Oyo Butsuri*, **25**, 70, (1956). (In Japanese) [C.A., **50**, 16604c (1956)].
7. H. Fischmeister and J. Drott, *Acta Met.*, **7**, 777 (1959).
8. K. Hauffe, "Oxydation von Metallen und Metallegierungen," p. 70, Springer-Verlag, Berlin (1956).
9. F. Gronlund and J. Bérnard, *Compt. rend.*, **240**, 624 (1955).
10. W. W. Harris, F. L. Ball, and A. T. Gwathmey, *Acta Met.*, **5**, 574 (1957).
11. R. F. Tylecote, *J. Inst. Metals*, **78**, 259 (1950).
12. E. A. Gulbransen and W. R. McMillan, *This Journal*, **99**, 393 (1952).
13. M. Matyas, *Czechoslov. J. Phys.*, **5**, 214 (1955).
14. M. Matyas, *ibid.*, **4**, 174 (1954).
15. F. W. Young, Jr., J. V. Cathcart, and A. T. Gwathmey, *Acta Met.*, **4**, 145 (1956).
16. K. R. Lawless and A. T. Gwathmey, *ibid.*, **4**, 153 (1956).
17. R. F. Tylecote, *Metallurgia*, **53**, 191 (1956).
18. E. A. Gulbransen, *Trans. Electrochem. Soc.*, **81**, 187 (1942).
19. E. A. Gulbransen, *Rev. Sci. Instr.*, **15**, 201 (1944).
20. K. F. Andrew, T. P. Copan, E. A. Gulbransen, Westinghouse Research Report 6-94602-1-R8, April, 1958.
21. A. Guinier, *Ann. Phys.*, **12**, 161 (1939).
22. A. Guinier, "X-ray Crystallographic Technology," Hilger and Watts Ltd., London (1952).
23. R. J. Ruka and K. F. Andrew, Westinghouse Research Report 6-40807-11-R3, May, 1959.
24. Karl Hauffe, "Oxydation von Metallen und Metallegierungen," p. 160, Springer-Verlag, Berlin (1956).

Correction

In the paper by Milton Stern and A. C. Makrides "Inhibition of Metal Dissolution by Ferric Sulfate" [107, 877-883 (1960)] in the November 1960 *Journal* there are two typographical errors. In Table I on page 881, the third column heading should read $k \cdot 10^3$ (cm/sec); in Table II on page 882, the value of k should be $k = 6.4 \cdot 10^{-3}$ cm/sec.

The Oxidation of Tin

III. The Mechanisms of Oxidation of Pure Tin and Their Dependence on Time and Oxygen Pressure

William E. Boggs

Applied Research Laboratory, United States Steel Corporation, Monroeville, Pennsylvania

ABSTRACT

The rate curves obtained for the oxidation of pure tin at oxygen pressures of 1 mm Hg and above are sigmoid-shaped. The initial stage, in which the oxidation rate increases, is explained by nucleation and lateral growth of the oxide. Kinetic data fit an equation derived by Evans for the nucleation and lateral growth of an oxide film. Subsequently, the rate becomes logarithmic, and in this region cavities that act as diffusion barriers develop in the oxide film. The existence of cavities at the metal-oxide interface has been revealed by electron microscopy, and mechanisms for their formation and growth are presented. An activation energy is derived that is assumed to be associated with the diffusion of tin ions through the oxide film in areas between the cavities. Thus, the mechanism operating in the region of logarithmic growth is not simple. Basically, it consists of the diffusion of tin ions through the dense regions of the film according to a parabolic or cubic relationship. It is complicated, however, by the formation and growth in the oxide film of cavities that progressively reduce the area available for the passage of tin ions through the film, as suggested by Evans. The net effect of these concurrent processes on the kinetics of oxidation is the observed logarithmic rate. For still longer times of oxidation, the thick oxide film may or may not rupture, which results in an erratic rate of oxidation.

At oxygen pressures of less than 1 mm Hg, the oxidation rate increases continuously with time over the period investigated, and the dissociation of oxygen appears to be rate controlling, at least initially. The oxide film formed at these low oxygen pressures consists of fine dendritic crystals, rather than the large single-crystal platelets formed at higher pressures. The dendritic nature of the films indicates that the amount of oxygen available for oxide formation is depleted by the reaction faster than it is replaced from the atmosphere in the reaction vessel.

The two previous papers in this series discussed the influence of temperature and pressure on the kinetics of the oxidation of pure tin foil (1), and the microstructure and mode of growth of the oxide films as revealed by the electron microscope (2). The major portion of the data obtained above an oxygen pressure of 1 mm Hg has been shown to fit a direct logarithmic rate law of the type $w = k \log (at + 1)$, whereas at pressures below 1 mm, the rate of oxidation increases continuously with time (1). At the same time, the oxide film develops as relatively large platelets at the higher pressures and as fine dendrites at the low pressures (2).

The crystalline oxide has been shown to spread laterally over the tin surface from growth centers and grain boundaries, with an increasing oxidation rate in the initial stages of oxidation at the higher pressures. The structure of the growth centers changes with pressure, but the number remains approximately the same, $2 \times 10^6/cm^2$. At the higher oxygen pressures, the rate of oxidation becomes logarithmic, after laterally spreading oxide platelets begin to impinge on each other. At the lower pressures (at least during the time period of this investigation), the rate never becomes logarithmic, and the dendritic structure observed here is apparently nonprotective. The initial rate-determining process, at pressures less than 1 mm, is believed to be the dissociation of molecular oxygen.

Since the direct logarithmic rate law is observed frequently for the oxidation of many metals at relatively low temperatures (3), it is not surprising that the oxidation of tin should conform to this rate law at temperatures below the melting point of tin. Unfortunately, a logarithmic plot of experimental data is not very sensitive, and almost any process that tends to approach a limiting value will obey some sort of a logarithmic law (4). Several explanations for logarithmic behavior have been proposed in the literature (3, 5-8). It appears likely that many of these mechanisms are valid in certain systems, but that there is no single universal mechanism which gives rise to logarithmic behavior in all metal-oxidation systems. The worker must, therefore, select the explanation that best fits his experimental data and seek independent confirmation of his conclusions. In the present investigation, the electron microscope proved to be a powerful tool for obtaining the necessary independent data.

The explanations for logarithmic oxidation rates may be divided roughly into two groups: (*a*) the electrical theories proposed by Mott (6), Uhlig (5), and Engell, Hauffe, and Ilschner (8), and (*b*) the mechanical or geometrical theories proposed by Evans (9).

Theoretical Considerations

Region of Increasing Oxide-Growth Rate

As was shown in the first paper (1), the rate of oxidation is initially low, increases to a maximum, and then begins to decrease as it enters a period of logarithmic behavior. The initial sigmoid curl has been shown to be associated with the nucleation and lateral growth of the oxide crystals. Evans (10) has suggested that the data from this region of nucleation and lateral growth should fit the equation

$$dw/dt = k^* [1\text{-exp } (-kt^n)]$$

where n is 2 if the nuclei all appear simultaneously at time $t = 0$, and n is 3 if the nuclei keep appearing sporadically in time and space. It is reasonable to assume that all nucleation sites are present in the metal surface at the start of oxidation. This hypothesis is supported by the fact that the number of oxide growth centers observed by means of the electron microscope remained approximately the same, 2 x 10^6/cm^2, regardless of the oxidizing conditions: time, temperature, and oxygen pressure.

A rough fit of the data for the oxidation of tin at three temperatures, 180°, 190°, and 200°C, has been obtained, with the assumption that $n = 2$. The constant k appears to be essentially independent of temperature, at least in the 20° interval tested, although it includes the elements of nucleation density and radial growth velocity (10), Table I. However, the proportionality constant k^* shows a definite temperature dependence. It is necessary to obtain additional experimental data from a wider temperature range before attempting a rigorous interpretation of the kinetics of the nucleation and lateral growth of stannous oxide.

Table I. Rate data and calculation of constants in Evans' equation for nucleation and lateral growth

dw/dt μg/cm²/min	Temp, °C	Time, min	Weight, μg	k	k^*, μg/cm²/min
0.00085	180	20	0.086	0.0015	0.0019
0.00090		30	0.094		0.0012
0.00100		40	0.104		0.0011
0.00105		50	0.113		0.0011
0.00110		60	0.124		0.0011
0.00125		70	0.136		0.0013
0.00150		80	0.149		0.0015
0.00190		90	0.165		0.0019
					0.0014 Average
0.00210	190	20	0.076	0.0011	0.0058
0.00315		30	0.103		0.0049
0.00380		40	0.139		0.0046
0.00470		50	0.181		0.0050
0.00570		60	0.234		0.0058
					0.0052 Average
0.0039	200	20	0.160	0.0013	0.0096
0.0059		30	0.211		0.0085
0.0073		40	0.275		0.0083
0.0092		50	0.358		0.0096
					0.0090 Average

Since the number of etch pits found on a sample of the tin foil, electropolished and annealed in the same manner as the oxidized specimens, is also about 2 x 10^6/cm^2, it is suggested that oxide growth centers are associated with dislocations in the metal.

In view of experimental observations accumulated during the course of this study, the following mechanism is postulated for the nucleation and lateral growth of the stannous oxide film toward complete coverage.

It appears that a certain energy is required for the nucleation of crystalline oxide. Evidently, oxide growth centers may occur at dislocations. As tin ions diffuse from the dislocations into the oxide growth centers, these growth centers grow laterally and vertically, but as the distance from the center of the dislocation increases, the rate of growth appears to decrease. When the growth centers reach a certain maximum size, their growth is essentially halted. By this time, certain of the growth centers have begun to sprout the laterally spreading oxide platelets that grow to impingement. It is not known why the laterally spreading platelets do not grow from all of the growth centers. Perhaps future experimental observations will clarify the mechanism of the formation and growth of the oxide nuclei, growth centers, and platelets.

Region of Logarithmic Behavior

It was shown in the second paper (2) that cavities develop at the oxide-metal interface during the period of logarithmic behavior. These cavities increase in size as the oxidation time increases, until after 1000 min at 220°C and 10 mm oxygen, for instance, the area of contact between the metal and the oxide is reduced by as much as one-third.

The concept of the formation of cavities at the oxide-metal interface has been used by Evans (9) in the derivation of one version of the direct logarithmic rate law. An interpretation of this derivation is given in the Appendix. The basic assumptions are that (*a*) formation of cavities at the oxide-metal interface interferes with the movement of cations from the metal into the oxide; (*b*) where no cavities exist, the movement of ions conforms to a simple diffusion mechanism; and (*c*) lateral diffusion of cations in the skin of oxide bridging the cavities does not change the oxidation rate significantly. Thus, the oxidation rate must be proportional to the area of the oxide-metal interface not covered by cavities and to the velocity with which the cations move through the oxide film to the oxide-oxygen interface.

The kinetic and microstructural evidence obtained during this investigation tend to support these assumptions. It has been shown that the area of contact between the oxide and the metal decreases with time and that, simultaneously, the oxidation rate decreases with time and conforms to the direct logarithmic rate law. The cavities have nearly ver-

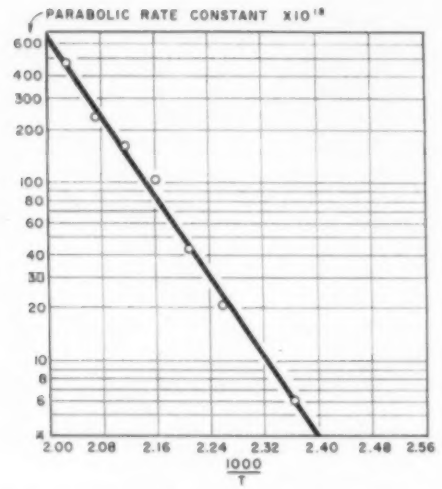

Fig. 1. Arrhenius plot of parabolic rate constants calculated from logarithmic rate data for the oxidation of tin from 150° to 220°C.

tical walls and the skin covering them appears to be very thin; this suggests that lateral diffusion in the oxide skin is not important in the oxidation process.

The movement of tin ions through the oxide film would be expected to conform to one of the simple rate laws, that is, the parabolic rate law ($w^2 = k_p t$) or the cubic rate law ($w^3 = k_c t$), where w is the weight of the oxide at time t, and k_p and k_c are the parabolic and cubic rate constants, respectively. Either of these rate laws can be fitted into the derivation of the logarithmic rate law given in the Appendix. The parabolic or cubic rate constants for different temperatures can be calculated by using the experimental data from the region of logarithmic behavior. An activation energy of 26 kcal/mole is obtained from the temperature dependence of either of these sets of rate constants, Fig. 1. In this treatment, no means was found for distinguishing between these two rate laws.

Thus, it appears that the movement of tin ions through the α-SnO crystal lattice in the regions between the cavities is governed by a chemical (11) or electrical potential gradient (6, 8, 12) or combination of the two, but that no distinction can be made between the two in the explanation of logarithmic oxidation behavior proposed by Evans. The formation of the cavities, with the resulting decrease in the number of tin ions moving through the film, appears to be the more important process in causing the observed logarithmic behavior.

Possible reasons for cavity formation.—There are several possible explanations for the formation of cavities at the oxide-metal interface. Evans has suggested that cationic vacancies moving to the interface may coalesce to form the cavities (9). If α-SnO is a p-type semiconductor with cation vacancies, such as FeO and Cu_2O, the semiconductor model and interface equilibrium equations could be written as follows (13-15).

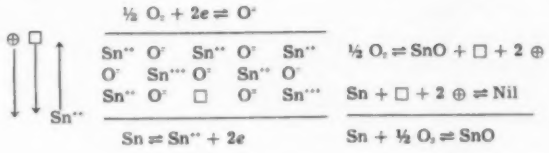

where □ is a cation vacancy, ⊕ is a positive hole, and Nil represents a stoichiometric crystal. In this model, oxygen reacts with tin at the oxygen interface and removes two electrons from tin^{++} ions; thus two positive holes and a tin-cation vacancy are formed. A tin ion can jump from a lower atom layer into a vacancy. This leaves a vacancy in its place, and as the process continues, the vacancy eventually reaches the oxide-metal interface. Electrons exchange positions with positive holes in somewhat the same manner. It is usually assumed that ions are not free to move in a solid by simple thermal diffusion at temperatures below the Tammann temperature (16). If this is correct, and since ion movement is involved, the ions in the stannous oxide must move under the influence of the electrical field set up by the dissociation of oxygen at the outer surface and the ionization of tin at the oxide-metal interface (12). A tin atom at the oxide-metal interface can fill a cation vacancy in the oxide lattice, and the electrons produced can change two positive holes to normal cations. This produces a stoichiometric crystal and leaves a vacancy at the oxide-metal interface. The cation vacancy may now remain at the metal-oxide interface, pass into the metal and become annihilated at a dislocation, or pass through the metal (if sheet or foil) and join a cavity on the far side (9). Vacancies remaining at the interface may collect to form cavities.

The considerations of Dravnieks and McDonald (17) extend this type of mechanism for the growth of voids to include n-type, metal-excess semiconductors. According to these investigators, when a metal ion moves into the oxide, a hole is left in the metal. Thus, as metal ions move into the oxide lattice, an empty space of unicellular thickness (a space 1-tin-atom-diameter high) is formed at the interface. The Maxwell-Boltzmann distribution law requires that such a space degenerate into cavities and points of contact between the oxide and the metal. As the oxidation process proceeds, the unicellular spaces will develop into cavities of microscopic dimensions.

With either type of semiconductor oxide, the cavity will contain a gas phase consisting of vapor of the metal and the oxide, and oxygen at the dissociation pressure of the oxide. This pressure is so low, at the temperatures of these experiments, that it would not support any appreciable reaction rate at the base of the cavities, and thus it can be ignored.

The arguments of Vermilyea (18) that the metal moves into the oxide lattice only from lattice steps at the oxide-metal interface tend to oppose this mechanism. According to these arguments, the vacancies produced at the interface are destroyed by the motion of the step along the surface. Since the

formation of cavities is observed during the oxidation of tin to very low temperatures (150°C), it must be that tin ions and vacancies are more mobile in the oxide lattice than is commonly believed, or that the atoms can jump into the tin-oxide lattice from positions other than lattice steps, once a complete oxide film has been formed. Otherwise, alternative mechanisms for the formation of voids must be proposed.

It is difficult to picture a mechanism by which voids could be produced and grow at the oxide-metal interface in a system in which oxygen anions rather than tin cations were the diffusing species, such as in an n-type anion-deficit semiconductor (anion vacancies). The vacancies would be produced at the oxide-metal interface and move outward to the oxide-gas interface. Furthermore, enough oxygen should diffuse into any cavities of the shape demonstrated in this work to support an appreciable rate of oxidation at the base of the cavities.

Other possible mechanisms for the formation of the observed cavities include some sort of plastic flow on the part of the oxide in relief of stress, and the coalescence of vacancies, the source of which is the metal base itself (19). In view of the softness of tin as compared to the hardness of its oxide, it appears that the tin would be more likely to flow under stress than would the oxide. On the other hand, the condensation of vacancies from the metal itself appears to be an attractive alternative hypothesis. The experiments were conducted in a temperature range in which vacancies should be free to move in the tin lattice but not so easily in the oxide. Also, qualitatively at least, it appears that the cavities comprise a volume greater than can be accounted for by the coalescence of vacancies produced by the defect reaction proposed above. It may be that more than one mechanism is operating to produce the observed cavities.

Semiconductor Classification of α-SnO.—Experimental evidence tends to support the hypothesis that α-SnO is a p-type cation-deficit semiconductor. The rate of oxidation is sensitive to oxygen pressure (1). Wagner (11) has shown from theoretical consideration that the rate of growth of an n-type excess interstitial metal oxide, such as ZnO, is practically independent of external oxygen pressure, whereas the rate of growth of a p-type metal-deficit oxide such as FeO should be pressure sensitive. Furthermore, the electrical conductivity of a p-type oxide should increase with increasing oxygen pressure whereas the electrical conductivity of an n-type oxide should decrease. The electrical conductivity of α-SnO increases with increasing oxygen pressure, Fig. 2. Finally, the addition of a minor constituent of proper ionic radius and of higher valence than the major metallic constituent should increase the rate of oxidation if the oxide is a p-type cation-deficit semiconductor (9, 13). And, in fact, the addition of 0.05 at. % bismuth to the tin appears to increase the rate of oxidation, Fig. 3.

Region of Erratic Oxidation Rate

It is to be expected that as the oxide film grows the oxide skin bridging the cavities should eventually become so strained that it would fracture, thereby admitting oxygen to react directly with the metal at the base of the voids, thus causing an increase in oxidation rate (20). Figure 3 of the first paper (1) represents the data obtained when samples of tin were oxidized at 10 mm oxygen pressure and 220°C long times. After 1000 minutes, there is in some instances an increase in rate, and the resulting oxide film shown in Fig. 18 of the second paper (2) contains fewer voids and appears to be fragmented.

It is believed that fracture of the very thin film-covering of the voids allowed oxide to form in the holes. This further increased the stress on the film and caused it to break up. Both the fracture of the skin over the cavities and the subsequent breaking of the oxide crystals caused an increase in the rate of oxidation.

Oxidation at Low Oxygen Pressure

Evidence was presented in a previous paper (1) that the dissociation of oxygen is rate controlling at oxygen pressures less than about 1 mm Hg, and that the microstructure of the oxide film formed at these

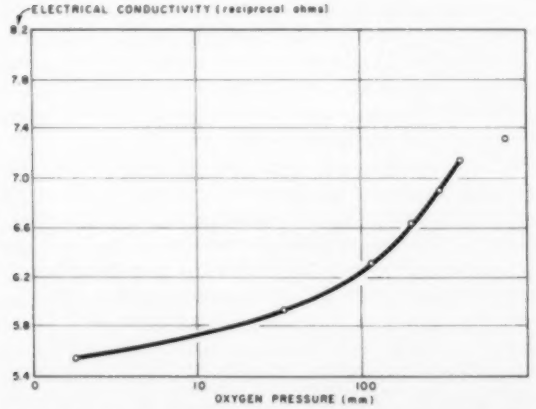

Fig. 2. Effect of external oxygen pressure on the electrical conductivity of stannous oxide film.

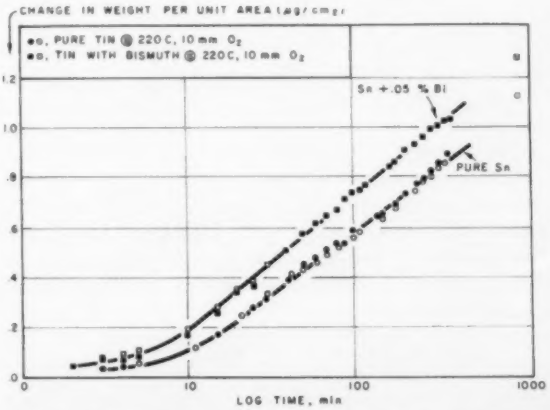

Fig. 3. Comparison of the oxidation of pure tin with the oxidation of a tin and 0.05% bismuth alloy.

lower oxygen pressures is radically different from that of the oxide film formed at pressures above 1 mm. The film formed at the lower pressures consists mainly of fine dendrites or filaments, whereas much larger single-crystal platelets form at the higher oxygen pressures.

These observations make possible a partial characterization of the film that may be present initially on the tin surface. It is possible to change the concentration of oxygen in this film by changing the external oxygen pressure.

To explain the dendritic oxide growth, it seems reasonable to assume an initial surface film of variable oxygen concentration, such as an incomplete layer of oxygen adsorbed or chemisorbed on the tin surface, or a mobile film consisting of tin ions and oxygen ions, but having no fixed chemical composition. The crystalline oxide nucleates at preferred sites such as grain boundaries and dislocations and then grows outward from the sites of nucleation. The area between adjacent oxide filaments becomes depleted of oxygen as the oxygen in the surface film is incorporated into the crystal lattice of the oxide filaments; therefore, the major growth of the oxide crystallites must be outward laterally into the areas richer in oxygen. As the external oxygen pressure is raised, the initial film approaches oxygen saturation, and the oxide eventually appears as platelets rather than as filaments or dendrites.

The oxide growth centers observed in films grown at low pressures are also different from those formed in oxygen at 1 mm and above. In the low-pressure region (10^{-2} mm) they assume shell-like shapes suggestive of spiral growth, and there is apparently no critical size such as is observed at the higher pressures. The low-pressure growth centers are polycrystalline and the high-pressure ones consist of one or a small number of much larger crystals. This probably explains why the low-pressure growth centers do not have a critical size. The number of these growth centers per unit area was of the same order of magnitude, $2 \times 10^6/cm^2$, as the number formed at higher pressures; this is again suggestive of association with dislocations in the metal substrate.

Summary

Rate curves for the oxidation of tin at oxygen pressures of 1 mm Hg and above are sigmoid-shaped. The rate of oxidation is initially low, increases to a maximum, and then decreases. After relatively long times, the data become erratic and the oxidation rate may increase. The "foot" of the sigmoid curve, the period of increasing rate, is caused by the nucleation and lateral growth of oxide crystals over the surface of the tin. The kinetic data obtained during this period of increasing rate can be made to fit the equation

$$dw/dt = k^* [1-\exp(-kt^n)]$$

where n is assumed to be 2, since all nucleation sites are believed to be present on the metal surface at the start of oxidation.

After the coverage of the metal by a compact crystalline oxide film is essentially complete, cavities begin to appear at the oxide-metal interface. These grow and coalesce as the thickness of the oxide film increases. As these cavities grow, they constitute a progressively more extensive barrier to the diffusion of ions through the oxide film; this causes the reaction rate to decrease more rapidly than would be expected in a normal diffusion process. The interplay between the decrease in the speed with which the ions move through the film as it thickens and the decrease in the number of ions caused by the lessening of the area of oxide in contact with the metal causes the observed logarithmic behavior. For the oxidation of tin, the direct logarithmic rate law

$$w = (1/2\,k_1) \ln (k_1^2 \rho^2 k_p t)$$

or

$$w = (1/3\,k_1) \ln (k_1^3 \rho^3 k_c t)$$

may be considered to be a deviation from the classical parabolic or cubic rate laws. An activation energy of 26 kcal/mole for the diffusion of tin ions through the SnO film has been derived by using a mathematical treatment based on these assumptions.

The most attractive explanation of the formation of the voids at the oxide-metal interface is that vacancies produced by the incorporation of oxygen into the stannous oxide crystal lattice at the gas-oxide interface diffuse to the oxide-metal interface and coalesce. Some experimental evidence on this point indicates that α-SnO is a p-type, cation-deficit semiconductor, such as would be required for the operation of the proposed mechanism of cavity formation.

At oxygen pressures of less than about 1 mm, the rate of oxidation increases continuously with time, and the dissociation of molecular oxygen, at least initially, appears to be rate controlling. The oxide films formed at these low oxygen pressures consist of fine dendritic crystals rather than the large, single-crystal platelets formed at the higher pressures. The dendritic nature of the films formed at low pressures, coupled with the observation that dissociation of molecular oxygen may be rate controlling, indicates that the oxygen at the surface of the metal is depleted by reaction with the tin faster than it is replaced from the gas phase. Thus, it is suggested that any film initially present on the metal surface consists either of a nonstoichiometric, mobile film of oxygen ions and tin ions, or of an incomplete monolayer of chemisorbed oxygen.

The concentration of oxygen in such a film obviously would be sensitive to the external oxygen pressure. Over the entire range of oxygen pressures, certain characteristic oxide structures are initially observed that serve as growth centers from which larger crystalline platelets develop to form the continuous oxide film. Inasmuch as the number of these growth centers is of the same order of magnitude as the number of etch pits developed in electropolished and vacuum-annealed tin samples, it is suggested that these growth centers are associated with dislocations in the metal substrate.

Acknowledgments

The author wishes to thank Dr. Waldo Rall for his interpretation of Evans' Logarithmic Rate Law, given in the Appendix, and Professor W. W. Smeltzer for his constructive criticism and helpful suggestions during the course of this study.

Manuscript received May 11, 1960. This paper was prepared for delivery before the Houston Meeting, Oct. 9-13, 1960.

Any discussion of this paper will appear in a Discussion Section to be published in the December 1961 JOURNAL.

REFERENCES

1. W. E. Boggs, G. E. Pellissier, and R. H. Kachik, *This Journal*, **108**, 00 (1961).
2. W. E. Boggs and P. S. Trozzo, *ibid.*, **108**, 00 (1961).
3. P. T. Landsberg, *J. Chem. Phys.*, **23**, 1079 (1955).
4. O. Kubaschewski and B. E. Hopkins, "Oxidation of Metals and Alloys," Butterworths Scientific Publication, London (1953).
5. H. H. Uhlig, *Acta Met.*, **4**, 541 (1956).
6. N. Cabrera and N. F. Mott, *Repts. Progr. Phys.*, **12**, 163 (1949).
7. C. Luner, *J. Metals*, **11**, 71 (1959).
8. H. J. Engell, K. Hauffe, and B. Ilschner, *Z. Elektrochem.*, **58**, 478 (1954).
9. U. R. Evans, *Rev. Pure Appl. Chem.* (Melbourne), **5**, 1 (1955); See also, U. R. Evans, "The Corrosion and Oxidation of Metals," pp. 836-837, St. Martin's Press, New York (1960).
10. U. R. Evans, *Trans. Faraday Soc.*, **51**, 365 (1945).
11. C. Wagner, Seminar on Atom Movements, *Amer. Soc. Met.*, p. 153 (1951).
12. T. P. Hoar and L. E. Price, *Trans. Faraday Soc.*, **34**, 867 (1938).
13. K. Hauffe, *Progr. Metal Phys.*, **4**, 71 (1953).
14. K. Hauffe, "Reaktionen in und an Festen Stoffen," Springer-Verlag, Berlin (1955).
15. K. Hauffe, "Oxydation von Metallen," Springer-Verlag, Berlin (1956).
16. A. L. G. Rees, "Chemistry of the Defect Solid State," John Wiley & Sons, Inc., New York (1954).
17. A. Dravniks and H. J. McDonald, *J. (and Trans.) Electrochem. Soc.*, **94**, 139 (1948).
18. D. A. Vermilyea, *Acta Met.*, **5**, 492 (1957).
19. P. E. Doherty and R. S. Davis, *ibid.*, **7**, 118 (1959).
20. J. V. Cathcart, J. J. Campbell, and G. P. Smith, *This Journal*, **105**, 442 (1958).

APPENDIX

Evans' Derivation of the Logarithmic Rate Law

The growth of cavities at the oxide-metal interface reduces the available area of contact between the oxide and the metal to α times its original amount ($\alpha < 1$), so that

$$dw/dt = \rho\, dy/dt$$

becomes

$$dw/dt = \alpha\rho\, dy/dt$$

where dw/dt is the rate of change in weight of the total oxide film, dy/dt represents the thickening rate of the film at places where no cavities have been formed, α represents the fraction of area not covered by cavities, and ρ is the density of the oxide in the absence of cavities. The chance that a vacancy may be retained at the interface is presumably proportional to the number of sites available, so that

$$-d\,\alpha = k_1\,\alpha\, dw$$

$$\ln \alpha = k_1 w + k_2$$

$$\alpha = \exp(-k_1 w + k_2) = \exp(-k_1 w)\exp(k_2) = k_3 \exp(-k_1 w)$$

but when $w = 0$, since none of the area is yet covered by cavities, for α to equal one k_3 must equal one, therefore

$$\alpha = \exp(-k_1 w)$$

Assuming that the rate of change of y falls off according to a single rate law such as the parabolic law where k_p is the parabolic rate constant from the expression

$$y^2 = k_p t$$
$$y = (k_p)^{1/2} t^{1/2}$$
$$dy/dt = (k_p)^{1/2}/2t^{1/2}$$
$$dw/dt = [\rho \exp(-k_1 w)]\,[(k_p)^{1/2}/2t^{1/2}]$$
$$\exp(k_1 w)\,dw = \tfrac{1}{2}\rho (k_p)^{1/2}\, dt/t^{1/2}$$
$$\exp(k_1 w)/k_1 = \rho (k_p)^{1/2} t^{1/2} + k_4$$
$$k_1 w = \ln(k_1 \rho k_p^{1/2} t^{1/2} + k_1 k_4)$$
$$w = (1/k_1) \ln\{[(k_1 \rho k_p^{1/2})^2 t]^{1/2} + k_1 k_4\}$$
$$w = \frac{1}{2} k_1 \ln[k_1^2 \rho^2 k_p t + (k_1 k_4)^{1/2}]$$

Thus we have the standard logarithmic formulation

$$w = K \ln(at + b)$$

where $K = \frac{1}{2} k_1$, $a = k_1^2 \rho^2 k_p$, and $b = (k_1 k_4)^{1/2}$

In the logarithmic oxidation of tin, since $t = 0$ when $w = 0$, therefore $b = 1$.

The Oxidation and Corrosion of Zirconium and Its Alloys

VI. The Mechanism of the Fission Fragment Induced Corrosion of Zircaloy-2

B. Cox, K. Alcock, and F. W. Derrick

United Kingdom Atomic Energy Authority, Atomic Energy Research Establishment, Harwell, Didcot, Berkshire, England

ABSTRACT

The results of investigations of the corrosion of zircaloy-2 in high-temperature uranyl sulphate solutions under irradiation are reported. The kinetics of corrosion under these conditions are compared with the kinetics of corrosion in water and aqueous solutions out-of-pile, and with the aid of electron microscopy a mechanism for the irradiation enhanced corrosion is offered.

Zirconium alloys are, at present, the most suitable corrosion resistant neutron transparent materials available for structural use in atomic reactors where pressurized water is employed as coolant and moderator. Zircaloy-2, an alloy developed in the U.S.A. for this purpose, has been used widely for fuel element cladding in this type of reactor, and its corrosion resistance, and that of other zirconium alloys, has been examined extensively in the absence of irradiation (1). Data on the effect of mixed neutron

and gamma irradiation in high-temperature water and aqueous solutions are scanty but serve to indicate that under these conditions, there is no significant change in the uniform corrosion of zircaloy-2 (2-4).

In one proposed version of the Homogeneous Aqueous Reactor a circulating uranyl sulfate solution provides fuel, moderator, and coolant. The most economic form of this system employs two zones, an inner zone in which fissile material is consumed, and an outer zone in which fissile material is produced by the irradiation of thorium in the form of a thoria slurry. The vessel separating these two zones is required to have a low neutron absorption, and a high corrosion resistance to fissioning uranyl sulfate solution on one side and to thoria slurry on the other. Elimination of possible materials of construction for one or other of these reasons reduces the choice to a zirconium alloy. Since zircaloy-2 is the alloy for which most fabrication and corrosion experience is available under related conditions the choice of material for investigation has fallen primarily on this alloy.

Experimental data on zircaloy-2 obtained under irradiation in fissile solutions have indicated that the corrosion resistance of this alloy is seriously impaired in the presence of fissioning uranium atoms, and an extensive search for an alloy able to withstand these conditions has been made (5, 6).

As a result of experience with autoclave and loop experiments at ORNL it has been found that the corrosion under irradiation with fission fragments is linear with time. Jenks has expressed the dependence of the corrosion rate on the fission power density in the form

$$C.R. = A.PD(1 - e^{-B/c.u.^{1.5}})$$

where A and B are constants. An equation of this form can be derived theoretically by making certain assumptions about the course of the corrosion reaction (7). However these assumptions are descriptive in nature and do not invoke any specific mechanism for the oxide failure which leads to the linear corrosion kinetics. There are several possible mechanisms by which this film failure could occur and all lead to a dependence on power density of the form experienced. Among these possibilities are:

1. An increase in the solution rate of the oxide as a result of the presence of defects in it. The ZrO_2 being reprecipitated as a nonprotective film owing to the nonisothermal conditions.
2. An irradiation induced phase transformation in the oxide (8) leading to mechanical failure of the film.
3. A "breakaway" type of reaction similar to that found in the absence of irradiation but with "breakaway" accelerated by the presence of radiation.

Of these possible explanations the second seems unlikely to occur with sufficient rapidity (9, 10) under the conditions found here, and should it occur there is no evidence that it would result in failure of the oxide. Jenks favors the first explanation, despite the absence of any positive evidence for increased solubility or reactivity of ZrO_2 under irradiation. Direct attempts to measure any effect of irradiation on solubility have failed so far to show any significant change (11). The only evidence for the third possibility is a short induction period observed during oxygen pressure measurements; this occurs immediately after the commencement of irradiation and lasts for a short but unspecified period (7). The mechanism by which the breakaway reaction takes place out-of-pile is still far from clear in the case of zircaloy-2, although several explanations have been offered (1, 12).

Thus while being in a position to describe the observed dependence on power density, there is as yet no positive evidence on the actual mechanism of the irradiation induced corrosion of zirconium alloys. Following experiments at very low power densities and subsequent observation of corroded specimens with an electron microscope it is now possible to offer such an explanation.

Experimental

Experiments have been carried out in a 4 in. diameter vertical hole in the BEPO Reactor at Harwell, using titanium autoclave equipment to ensure maximum cleanliness of the specimens. Details of the autoclaves and the arrangement of the experimental rig were given in an earlier report (13). Full details of the experimental procedures and equipment for unloading and opening the experiments will be published later (14). The experiments were carried out using 0.08M K_2SO_4/0.02M H_2SO_4/0.005M $CuSO_4$ solutions; these were "spiked" with the required amount of U^{235} as uranyl sulfate. It was found that uranium loss from solutions of this type was less than from solutions containing 0.08M uranyl sulfate but with the same concentration of U^{235}; thus deposition of uranium on the specimen surfaces was kept to a minimum. It is important to minimize this where observation with an electron microscope is contemplated. Some experiments also were carried out in fully enriched 0.08M uranyl sulfate solutions to provide a measure of the corrosion at power densities high enough to provide a readily measurable rate (0.5 watt/ml). This enabled an estimate to be made of the level of uranium required in the "spiked" solutions. An oxygen overpressure of approximately 200 psi (cold) was present in all experiments.

Specimens of zircaloy-2 from billet Z303 and I.C.I. titanium 130 have been used to date and an analysis of the former has been given previously (13). Specimens were disks 0.500 in. in diameter x 0.050 in. thick with a 9/64 in. center hole; they were mounted on the central thermocouple well of the autoclave, separated by titanium spacers and retained at the bottom by a titanium nut. Thus the specimens were in contact only with titanium or the solution in the autoclave.

Specimens were used either in the machined condition or after abrading to 3/0 emery followed by attack-polishing (15). No significant differences between the two types of specimen were found, and the

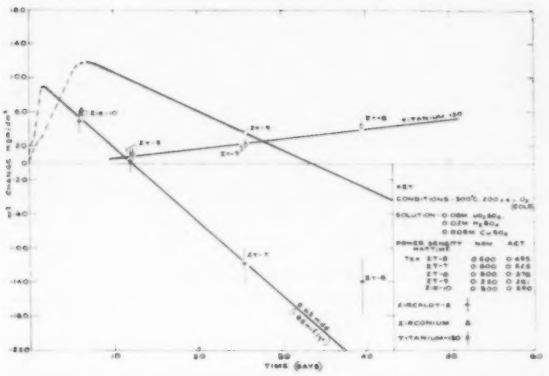

Fig. 1. Results of TE 4 irradiations at "high" power density

results are presented, therefore, as the mean of all specimens in a particular experiment. Replicas were prepared by a two stage formvar-carbon process and were shadowed with gold-palladium alloy at about 30°. Replication was by hand after sufficient cooling time had elapsed to permit handling for the short time required. The replicas were examined using a Phillips EM100 electron microscope.

Results

The results of the "high" (up to 0.5 watt/ml) power density runs are plotted in Fig. 1. The specimens from these runs had a tan color and despite the weight losses still appeared to be carrying a fairly heavy oxide film. Drying of the specimens did not result in spalling of this film as reported from ORNL(7), and immersion in various aqueous and nonaqueous solvents agitated ultrasonically did not dislodge a measurable quantity of film. Hence for the purposes of calculating corrosion rates in these experiments it is assumed that the residual oxide thickness remains approximately constant. The results calculated in this way are liable to considerable error, but, nevertheless, they differ by a factor of less than two from those expected from the ORNL data.

The low power density experiments were started at 0.0125 watt/ml (0.5 g/l U^{235}) and experiments have been carried out at this level and at 0.025, 0.0375, and 0.075 watt/ml (1.0, 1.5, and 3.0 g/l U^{235}, respectively); results are shown in Fig. 2. The variations in the actual power density at which the experiments operated are due largely to seasonal variations in the operating power of BEPO, and to flux depressions due to adjacent experiments. It is apparent from these results that the initial corrosion rate has an exponent less than 0.5 and that subsequently a "breakaway" type of reaction takes place at a weight gain of approximately 25 mg/dm². Thus the kinetics of the radiation induced corrosion of zircaloy-2 are formally similar to the out-of-pile corrosion kinetics, although the exponent of the pre-breakaway rate law is not identical with that out-of-pile. The low weight gains after three days in run Z-26 remain unexplained.

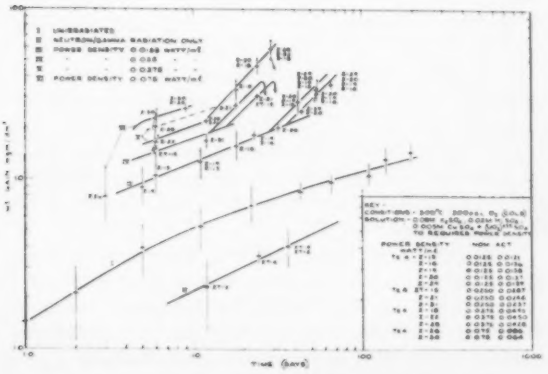

Fig. 2. Irradiation corrosion of zircaloy-2 at 300°C

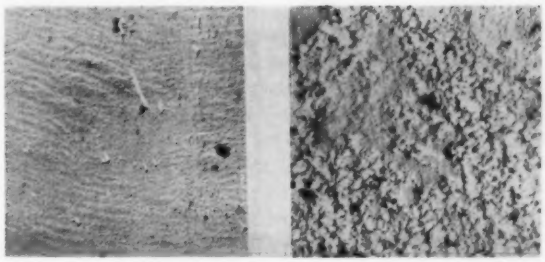

Fig. 3. Oxide film on zircaloy-2 after corrosion at low power density: (a) (left) before breakaway; slight ridging of the oxide film can be observed; magnification 8000X before reduction for publication; (b) (right) after breakaway; cracking of the oxide occurring but without any evidence of spalling; magnification 15000X before reduction for publication.

The electron microscope study of the oxide films showed that during the initial period the surface was virtually featureless. The grain boundaries were not visible, but an unusual ridging effect was noticed (Fig. 3a); this has not been observed in the absence of irradiation. Subsequently at the breakaway point the surface structure becomes very confused (Fig. 3b) and fine cracking or pores extending into the film were observed over the whole surface. These observations were difficult to interpret monocularly, but stereo electron micrographs were of considerable help in elucidating the topography of the surface. Finally spalling of the oxide occurred over wide areas (Fig. 4); the boundaries or cracks bordering these areas, however, do not appear to be grain boundaries.

Discussion

The kinetics of the irradiation induced corrosion of zircaloy-2 appear to be formally analogous with those found out-of-pile. The exponent of the rate law under irradiation is ~0.40, whereas, in the absence

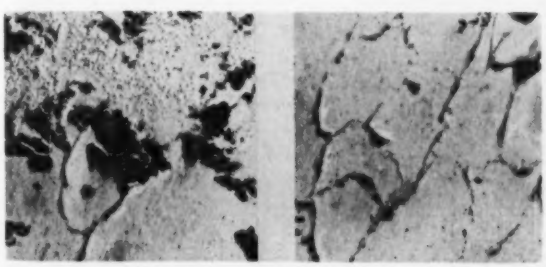

Fig. 4. Spalling of the oxide film after breakaway during corrosion at low power density. The pattern of cracks remaining does not appear to coincide with the grain structure.

of radiation, a steady decrease in exponent from about 0.6 to about 0.25 is observed. U.S. data give exponents of 0.26-0.38 at long periods (1). The suggestion that the unirradiated behavior of zircaloy-2 can be described in terms of the sum of two logarithmic rate laws has been made in an earlier report (12), and it would appear that under irradiation the same growth laws operate but that the balance between the two methods of film growth differs. The first of these two logarithmic rates is ascribed to the growth of a uniform thin oxide film by transport of the active species through the film under the influence of the electric field set up in it (16). Irradiation would be expected to modify the density of space charge in the oxide and hence alter the rate of this initial reaction although an equilibrium density probably would be reached and therefore, while the rate may be higher, the rate law still would remain logarithmic. Since the rate law is dependent also on the distribution of space charge (16), however, significant differences may occur. No closer estimate of this initial film growth rate can be made at present since irradiation times short enough to enable observation of interference color films would require a change in technique.

The second logarithmic rate law is thought to be due to diffusion along easy paths in the oxide such as grain boundaries and regions of inhomogeneity. Fission fragment tracks would act as such easy diffusion paths and a large increase in the rate of film growth by this mechanism would be expected. Although about 40% of irradiation damage in zirconium metal anneals at 300°C (17), in zirconia the neutron damage, which results in an irradiation induced phase transformation (8), does not anneal out below 800°C. Hence the number of fission fragment tracks in the oxide (which provide easy diffusion paths) would not be expected to reach equilibrium under our experimental conditions. While there will be some annealing of old fission fragment tracks and some blocking of tracks by the formation of fresh oxide at the metal/oxide interface, it would be expected that the number of diffusion paths through the oxide would increase with time. The logarithmic law, which describes the leakage rate along easy diffusion paths in the absence of irradiation, assumes that, on average, the number of paths available remains constant with time, and that blocking of existing paths and formation of fresh ones is a random process. In the irradiated material, where the number of paths increases with time, the rate law will not be logarithmic, but will lie between a logarithmic and a linear rate law. The actual rate law will be determined by the proportion of the damage which anneals out. The effect of this change in the second term in the film growth equation will be an over-all rate law, the exponent of which does not fall off as rapidly under irradiation as it does in the absence of irradiation. This is in accord with observations which give an exponent for the initial film growth law of ~0.40.

In view of the additional factor resulting from the effect of fission fragment tracks, the over-all growth law under irradiation can probably be described as the sum of three terms instead of the two used to describe the unirradiated case. These are:

A. The thin film growth law (logarithmic): growth rate controlled by the electric field set up in the oxide and by the distribution of space charge. Under irradiation the distribution of space charge will be affected not only by fission fragment but by β and γ radiation. In view of the absence of any significant effect on the corrosion rate of radiation other than with fission fragments, the rate of growth according to this law is not expected to differ much under irradiation from that in the absence of irradiation.

B. Diffusion along grain boundaries, etc. (logarithmic): by ignoring the effect of fission fragment tracks this growth law remains virtually unchanged under irradiation.

C. Diffusion along fission fragment tracks (between logarithmic and linear): the actual rate law will be determined by the degree of annealing which takes place and a law close to parabolic seems quite likely. The rate of oxidation by this process would not increase linearly with power density, since the proportion of tracks annealing would be a function of the degree of damage in the oxide.

It has been noted previously that, during corrosion in the absence of irradiation, the post-breakaway corrosion rate is not independently variable but can be estimated roughly by assuming that the corrosion rate is linear from the start and passes through the breakaway point (12). The same relationship is probably followed under irradiation, and the observed linear corrosion rate under these conditions will be determined by the time taken to reach the breakaway weight gain, and hence by the kinetics of the initial reaction. Breakaway of zircaloy-2 is thought to occur (out-of-pile) when the stresses set up in the oxide by nonuniform film growth (via inhomogeneous regions, grain boundaries, etc., in the oxide) become great enough to cause mechanical failure (12). Under fission fragment irradiation a very large number of similar paths will be provided, and it is not surprising, therefore, that the cracking is on a much smaller scale under these conditions (Fig. 5a). The ridges on the oxide film prior to breakaway may be an early manifestation of this nonuniform growth.

The visual resemblance between the mode of failure of the oxide film on zircaloy-2 under fission fragment irradiation and that of the oxide on some batches of niobium under the same chemical conditions in the absence of irradiation (Fig. 5) is very striking. This suggests that further examination of niobium and its alloys would be profitable both from the point of view of elucidating the breakaway process, and also with a view to possible substitutes for zirconium alloys for operation under these stringent conditions.

The mechanism proposed for the irradiation induced corrosion of zirconium alloys goes some way to explaining the fact that little difference has been observed at ORNL between a wide variety of zirconium alloys (6). Any zirconium alloy which shows normal out-of-pile corrosion kinetics and whose ini-

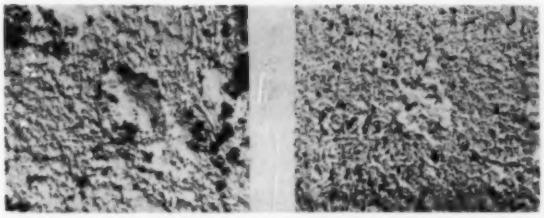

Fig. 5. Similarity between oxide failure on zircaloy-2 and niobium; (a) (left) breakaway of the oxide on zircaloy-2 after corrosion at low power density; magnification 15,000X before reduction for publication; (b) (right) surface of the oxide film on niobium after breakaway out-of-pile; magnification 10,000X before reduction for publication.

tial film growth rate does not differ widely from that of zircaloy-2 would be expected to show roughly the same corrosion rate under irradiation. Thus unalloyed zirconium has been found to have approximately the same corrosion rate under irradiation as zircaloy-2 (6) and unalloyed carbon melted zirconium specimens showed the same corrosion rate as zircaloy-2 in experiment TE4-Zir-10 (Fig. 3). In the absence of irradiation breakaway of this latter material occurs very rapidly (18); however, we have shown that, despite this early failure of the oxide on both carbon-melted and arc-melted zirconium, the initial film growth rate differs little from that for zircaloy-2 (18, 19). Out-of-pile the differences between these materials and zircaloy-2 are due to differences in the mechanism of film breakdown. Under irradiation the effect of fission fragment tracks on the breakaway reaction will override these differences and, since the initial film growth rates of each material will be affected to roughly the same extent under these conditions, the time to breakaway and the measured post-breakaway corrosion rates of unalloyed zirconium and zircaloy-2 will be very similar.

Considered in the light of this proposed mechanism the possibilities of improving zirconium alloy corrosion resistance under irradiation by alloying do not appear to be good, since alloys with very much lower initial film growth rates seem to be a remote possibility. However, the most hopeful approach will probably be via completely different alloying systems, perhaps based on niobium or zirconium-titanium alloys, where the film growth and failure mechanisms may differ considerably from those of zircaloy-2. ORNL data indicate that niobium shows considerably lower corrosion rates than zircaloy-2 at the same power density, although this effect is masked by large amounts of uranium absorbed in the oxide film on niobium. The dependence of titanium corrosion on power density differs markedly from that of zirconium alloys, and corrosion rates are much lower at equivalent power densities. However the necessity for neutron economy severely restricts the possible use of titanium either alone or in alloys.

Conclusions

Experimental evidence shows that the irradiation induced corrosion of zircaloy-2 follows a course similar to that of unirradiated corrosion. An initial period of nonlinear corrosion terminates in breakdown of the oxide film and the subsequent corrosion rate is linear. To account for this behavior the mechanism proposed for the initial corrosion of zircaloy-2 in the absence of irradiation (12) is modified by the addition of a further term which allows for the transport of reactive species through the oxide via fission fragment tracks. This third term in the oxidation equation is not logarithmic in nature, since at 300°C annealing of the damage in the oxide is not expected to result in an equilibrium density of tracks prior to breakaway. The addition of the third term results in an over-all exponent for the initial film growth law of 0.40. The failure of the oxide film under irradiation, while basically due to the same mechanism as failure out-of-pile, is on a much smaller scale and bears a striking visual resemblance to the failure of oxide films on some batches of niobium under the same chemical conditions in the absence of radiation. Thus the linear oxidation, which has been observed in previous work on the irradiation corrosion of zirconium alloys, is equivalent to the post-breakaway corrosion out-of-pile. In the light of this proposed mechanism for irradiation corrosion the absence of any significant differences in the corrosion resistance of different zirconium alloys under irradiation is understandable.

Acknowledgments

The authors would like to acknowledge the assistance of Mrs. B. C. Jenkins in the preparation of replicas and the assistance of BEPO Pile Operations staff during the course of these experiments. Discussions with, and the interest of Mr. J. A. Coiley and Dr. J. K. Dawson are appreciated greatly.

Manuscript received Oct. 22, 1959.

Any discussion of this paper will appear in a Discussion Section to be published in the December 1961 JOURNAL.

REFERENCES

1. B. Lustman and F. Kerze, "Metallurgy of Zirconium," McGraw Hill Book Co., New York (1955).
2. B. Cox and K. Alcock, A.E.R.E. C/M 353.
3. G. E. Galonian, KAPL-M-GEG-4.
4. F. H. Krenz, G. J. Biefer, and N. A. Graham, p. 194, 2nd Int. Conf. on the Peaceful Uses of Atomic Eng., Geneva (1958).
5. G. H. Jenks, Effect of Radiation on Corrosion, TID 7540.
6. G. H. Jenks, *et al.*, HRP Quarterly Progress Reports, ORNL No.: 1943, 2004, 2057, 2096, 2148, 2222, 2272, 2331, 2379, 2432.
7. G. H. Jenks, ORNL-CF-57-9-11.
8. M. C. Wittels and F. A. Sherrill, *J. Appl. Phys.*, **27**, 643 (1956).
9. J. K. Dawson, B. Cox, R. Murdoch, and R. G. Sowden, 2nd Int. Conf. Geneva, p/46.
10. J. Adam and B. Cox, *J. Nucl. Energy* (1959) in the press, (A.E.R.E.-M-415).
11. K. Alcock and B. Cox, (PE VIII) AERE R-3114.
12. B. Cox (Pt V) A.E.R.E. R-2931.
13. B. Cox and K. Alcock, (Pt I), A.E.R.E. C/R 2826.
14. B. Cox, K. Alcock, and F. W. Derrick, To be published.
15. J. G. Purchas, D. R. Harries, and H. Cobb, *Brit. Welding J.*, 1957, Sept. 412.
16. H. H. Uhlig, Acta Met., **4**, 541 (1956).
17. R. S. Kemper and W. S. Kelley, *A.S.T.M. Proc.*, **56**, 823 (1956).
18. B. Cox, (Pt. II), A.E.R.E.-R-2873.
19. B. Cox, (Pt. III), A.E.R.E.-R-2874.

The Effect of Surface Preparation on Oxide Films on Cr and Fe-Cr Alloys

D. Caplan, Alma Harvey, and M. Cohen

Division of Applied Chemistry, National Research Council, Ottawa, Canada

ABSTRACT

The high-temperature oxidation rate of Fe-26 Cr alloys proved highly sensitive to the method of surface preparation. An attempt to deduce the nature of the thin oxide films left by the various treatments was made using electrochemical measurements. Electron microscopy and diffraction and parallel experiments with Cr and Fe were carried out for purposes of clarification. Films formed under strongly oxidizing conditions including electropolishing yielded a cathodic reduction curve having an anomalous sharp minimum. It is proposed that such films are nonstoichiometric oxide containing considerable high valency chromium ion and having a high reduction potential and hydrogen discharge potential. The latter is lowered when at a high enough overpotential the chromium at the surface is reduced to a lower valence.

Numerous publications have referred to the marked effect that surface preparation may have on rates of film growth on metals. In a previous study, where such an effect was observed during oxidation of commercial stainless steels, discussion of some of the factors involved was presented (1). The object of the present work was to determine the nature of the thin films left on Fe-Cr alloy surfaces by various treatments and thus explain the large differences in oxidation kinetics they produced; also, to decide on a preferred method of surface preparation. These objectives were partly achieved.

A proper surface for corrosion studies of alloys should have a low roughness factor and be representative of the bulk composition, that is, not enriched either in impurities or in one of the alloying constituents. Recognizing that with the Cr-Fe some initial oxide film is unavoidable, it would appear that the proper preparation is that which gives the least interference with the subsequent scaling process. Abrasion, the method most often used, results in a cold-worked distorted surface layer containing embedded oxide and abrasive which is certainly unrepresentative of the bulk properties of the alloy. Etching of this surface to remove the worked layer leaves a rough surface which may also be enriched in the more noble metal, in this case Cr, by preferential dissolution or redeposition. Possible alternative methods such as cathodic reduction, ion bombardment, and thermal treatment in vacuum, hydrogen, or inert gas are liable, for alloys at least, to the same faults and to preferential oxidation or volatilization in addition. Electropolishing eliminates many of the deficiencies of the abraded surface, but the oxide film left, particularly on polycrystalline specimens, is nonuniform over the specimen, probably because of variations in both current density and the anolyte layer during electropolishing. The best surface preparation might then be a combination of electropolishing and etching, removing the electropolishing film by an acid etch too mild to cause roughening or preferential attack.

This paper reports an investigation of the nature of films left by various treatments on Cr and Fe-Cr alloys using electron diffraction and microscopy, microchemical analysis and electrochemical techniques. The latter had proven valuable in investigating thicker films (2, 3) and were applied here in the hope that, in combination with the others, characterization of the oxide films would be possible.

Experimental

The specimen materials were high-purity vacuum-melted Fe and Fe-Cr alloys, and U.S. Bureau of Mines chromium sheet. Compositions are shown in Table I.

The electrolyte for electropolishing the specimens was glacial acetic-70% perchloric acid (20:1). The bath was cooled to 16°C and polishing was done in 10-sec bursts to avoid overheating. A total thickness of about 10 μ of metal was removed.

Oxidation runs were made in a vertical tube furnace in flowing dried oxygen. Weight gain-time curves were obtained by a recording balance.

Table I. Analysis of specimen materials

	Fe	Cr	Si	C	Mn	Ni	Al	O	H	N
Fe	bal.	0.002	0.002	0.010	0.002		<0.002	0.10	0.004	0.001
Fe-11 Cr	bal.	11.2			<0.003		<0.002			
Fe-16 Cr	bal.	16.2	0.005	0.009	0.003			0.02		
Fe-26 Cr	bal.	25.5	0.02	0.015	0.003	0.02	0.017	0.025	0.0002	0.001
Fe-26 Cr-0.5 Si	bal.	26.2	0.55	0.025	0.004	0.02	<0.002	0.02	0.0002	0.001
Cr		bal.	<0.001				<0.002			

Cathodic reduction experiments were carried out with sheet specimens of 12 cm^2 area prepared with the various surface treatments. The change in potential measured against a reference electrode was recorded continuously while a constant current of 17 $\mu a/cm^2$ was applied to the specimen as cathode. Carefully deoxygenated borate-HCl buffer at pH 7.6 was used as electrolyte in an apparatus very similar to one previously described (2).

In a second type of electrochemical experiment conditions were much the same except that acid etchants served as electrolyte and no external current was applied.

The surfaces produced by the different pretreatments were examined by reflection electron diffraction and electron microscopy, using a preshadowed carbon replica from a primary plastic replica for the latter. The examination was repeated after cathodic reduction and etching to see if changes in the oxide film could be detected. The spectrophotometric procedures used to analyze the solutions for Fe and Cr could determine quantities down to 0.5 μg with an error of 0.2 μg for Fe and 0.3 μg for Cr.

Results

Oxidation curves of the first 4 hr for an Fe-26 Cr alloy are shown at two temperatures in Fig. 1 and 2. Specimens which had been electropolished only showed the greatest amount of oxidation as well as discontinuities in the oxidation rate. Least oxidation and smooth curves were obtained with specimens given a mild etch (as little as 1 $\mu g/cm^2$ of metal removed) after electropolishing. Abraded, abraded and etched, or as-machined specimens gave intermediate rates.

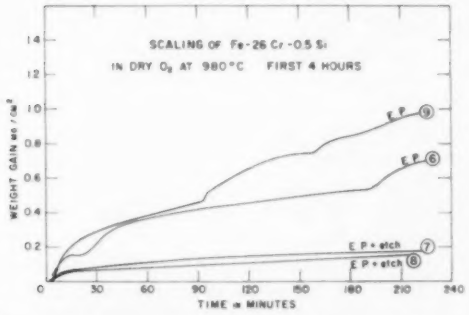

Fig. 1. Oxidation of Fe-26 Cr-0.5 Si alloy in flowing dry oxygen at 980°C. Electropolished in perchloric-acetic; etched in 5% HF.

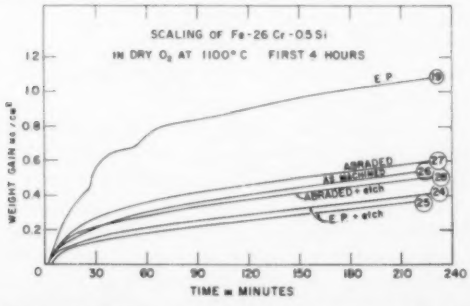

Fig. 2. Oxidation of Fe-26 Cr-0.5 Si alloy in flowing dry oxygen at 1100°C.

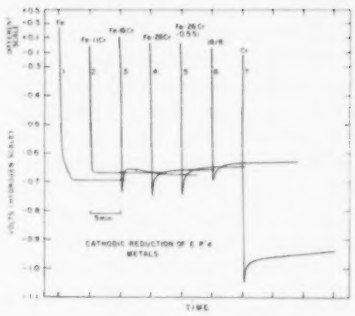

Fig. 3. Cathodic reduction of iron, chromium, 18 Cr-8 Ni stainless steel and four Fe-Cr alloys after electropolishing; 5-min time interval between electropolishing and cathodic reduction.

The potential-time curves obtained during the cathodic reduction of a variety of electropolished metals are shown in Fig. 3. Iron and Fe-11 Cr gave the smooth type of curve which on the basis of previous experience (2) would be expected from a very thin film of reducible oxide, but at higher Cr contents, curves 3-7, a sharp minimum was obtained. No difference in cathodic reduction behavior was observed between the Fe-26 Cr and Fe-26 Cr-0.5 Si alloys, which is of interest in view of the major part that silicon has been shown to play in passive films (4). Electropolished Cr gave a curve of the same form but with minimum and steady potentials more negative by about 300 mv. An 18/8 commercial alloy was included, curve 6, to demonstrate that the sharp minimum occurred generally with stainless alloys.

With other surface preparations a notably different cathodic reduction curve was obtained, as illustrated in Fig. 4. Etching immediately after electropolishing yielded cathodic reduction curve 4 lacking the minimum of curve 1. An extremely mild etch, such as 1% HF for 4 sec, was effective even though less than 1$\mu g/cm^2$ of metal was removed. A preliminary cathodic reduction, removing only 0.2 $\mu g/cm^2$, had the same effect (curve 6). The steady potential was more negative after these treatments than after electropolishing, probably because the surface became enriched in Cr. Heat tinting experiments showed quite minor color differ-

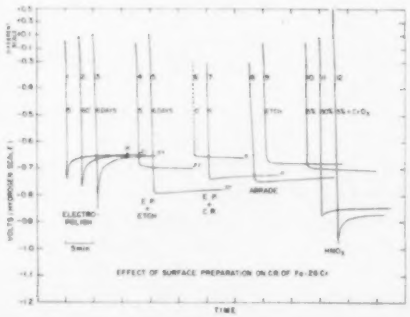

Fig. 4. Cathodic reduction of Fe-26 Cr alloy after various surface preparations. Number at end of each curve is amount of iron, in $\mu g/cm^2$ of specimen, found in cathodic reduction electrolyte.

ences between etched and cathodically reduced specimens, demonstrating that either treatment destroys the high propensity for rapid scaling of the electropolished surface which forms a thicker gray film under the same heat tinting conditions. A nitric-dichromate treatment of the type used commercially to passivate stainless steel for exposure to solutions (30 min in 5% HNO_3-0.5% $K_2Cr_2O_7$ at 60°) also can produce a sharp minimum, curve 12, but in contrast to electropolishing this preparation did not lead to rapid initial scaling. However, it is significant that, although the cathodic reduction curves are of similar shape, the overpotentials are much higher (curve 12 *vs.* 1). The heat tint color obtained was close to that after etching or cathodic reduction.

Also evident in Fig. 4 is that the immersion potential was more positive and the minimum more negative the larger the time of air exposure between electropolishing and cathodic reduction (curves 1-3). The same trend appeared after an etch or preliminary cathodic reduction (curves 4-7). These may be associated with a decrease in porosity and increase in thickness of the oxide film with longer air exposure. Consistent with this is that the amount of Fe found in the electrolyte at the end of the cathodic reduction experiments, noted on the curves in $\mu g/cm^2$ of specimen, also increased with the time interval. No analysis of the electrolyte after cathodic reduction ever showed Cr. When chromic ion was deliberately added to the electrolyte in advance then the same amount was found as had been added, showing that there was no redeposition from chromium ion in solution.

Parallel behavior was exhibited in the cathodic reduction of Cr, as seen in Fig. 5. Immersion, minimum and steady potentials all are lower than with Fe-26 Cr. A sharp minimum was obtained after electropolishing (curves 1 and 2) and not after etching (curve 3) or a preliminary cathodic reduction (curves 4 and 5). Again, the minimum was more negative the longer the time of air exposure before cathodic reduction. The sharp minimum type of curve can also be produced by dry oxidation of etched Cr: curves 6 and 7 show the result after heating in oxygen at 320° and 700°C. Presumably the shift to more negative potentials with increasing temperature of oxidation is due to an increased *IR* drop across films of greater thickness; the film thicknesses were 100-200Å and 3500Å after the 320° and 700° oxidations, respectively. Curve 8 shows that after a preliminary cathodic reduction these thicker films, as with the thin electropolishing film, do not give a sharp minimum.

The potential/time curves during etching in acid have the same form as those of cathodic reduction in 7.6 pH buffer. In Fig. 6, electropolished Cr immersed in HCl (curve 1) and electropolished Fe-26 Cr alloy in H_2SO_4 (curve 2) or HF (curves 3 and 4) all showed sharp minima. As in cathodic reduction, longer air exposure led to a deeper minimum, and if the electropolished specimen was given a preliminary etch, no minimum was observed.

The persistence of passivity, i.e., the time interval before the potential swung rapidly negative, varied widely with etchant and alloy and in Fig. 6 was 2.8, 2.4, 0.05, and 0.2 min for curves 1-4. But in addition it varied with minor changes in pretreatment as indicated by the difference between curves 3 and 4 and more clearly by the cathodic reduction curves in Fig. 7. The sharp minimum after electropolishing (curve 1, Fig. 7) was eliminated by an immediate 5-sec etch (curve 2) and not by an immediate 2-sec etch (curve 3). However, if after electropolishing the specimen was exposed to air for an appreciable time, even a 10-sec etch was inadequate (curve 4). The deeper minimum of curves 3 and 4 relative to curve 1 may be

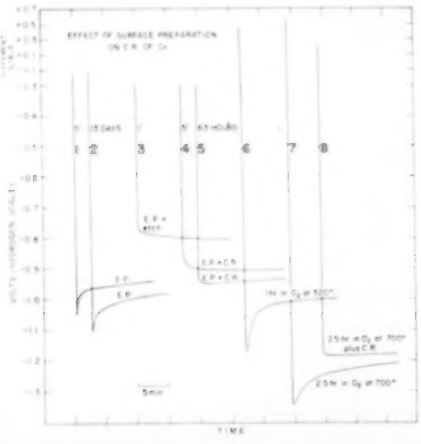

Fig. 5. Cathodic reduction of Cr after various surface preparations.

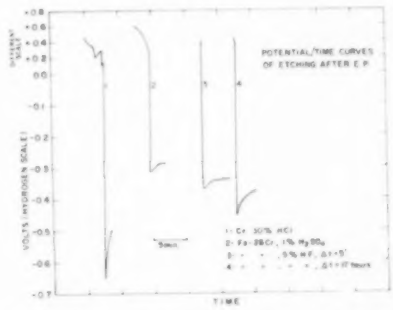

Fig. 6. Potential/time curves during acid etching of electropolished Cr and Fe-26 Cr alloy. Δt is the time of air exposure between electropolishing and etching.

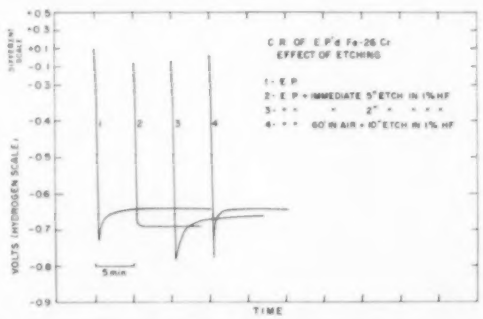

Fig. 7. Cathodic reduction of Fe-26 Cr alloy showing the influence of etching time and time interval before etching on the effectiveness of the etch.

the result of the removal by the inadequate etching treatment, as demonstrated by analysis of the etchant, of a small amount of iron oxide from the surface (0.4 μg Fe/cm^2).

Examination of the surfaces by reflection electron diffraction and electron microscopy proved disappointing. No significant change in surface topography was observed in electron photomicrographs before and after cathodic reduction, nor was any difference observed between the oxide films left by electropolishing and electropolishing plus a minimum etch. In spite of precautions taken to minimize perturbations to the electron beam from magnetic interaction and charging effects, electron diffraction yielded patterns of highly diffuse haloes only. The normal ring broadening due to the small crystallite size in these oxide films is intensified by the large refraction effect associated with the smooth surfaces produced by electropolishing (5). It may be, in view of the absence of proper haloes, that passive films on Cr alloys are more poorly crystalline than oxide films on metals such as Fe or Cu, but this has not yet been established.

Discussion

The most striking difference in initial oxidation behavior of Fe-26 Cr is between specimens which were electropolished and etched and those that were electropolished only. In both cases the oxide film present after the surface treatment is only about 20Å thick. It is surprising that a film this thin can so greatly modify the initial oxidation rate at temperatures even as high as 1100°C. The films also behave very differently electrochemically: the electropolished specimens show a sharp potential minimum during cathodic reduction or etching, whereas the etched surfaces do not. The following discussion is an attempt to characterize the two types of film from the electrochemical data.

As can be seen in Fig. 3 a sharp minimum in the cathodic reduction curve after electropolishing is obtained only at some alloy composition above 11% Cr. The depth of the minimum is increased by air exposure after electropolishing or by inadequate etching plus air exposure. A similar type of curve can also be obtained without anodic current by the use of a strong aqueous oxidizing agent, such as hot 50% HNO_3 or hot nitric-dichromate solution (Fig. 4). With pure Cr a minimum also is produced (Fig. 5) after heating in oxygen at various temperatures. (With Fe-26 Cr after the same dry oxidation treatment a different type of cathodic reduction curve is obtained due to the presence of a high-Fe as well as a high-Cr oxide. This is to be reported at a later date.) It would appear, therefore, that two prerequisites for the sharp minimum are a high enough Cr content and formation of the oxide under strong oxidizing conditions.

Sharp minimum cathodic reduction curve.—As just observed, the sharp minimum which occurs with alloys of more than 11% Cr appears only after a surface preparation involving strong oxidizing conditions. Inasmuch as the solution conditions are always the same, the phenomenon must be associated with some difference in film composition which leads to a different cathodic process. The process most consistent with the experimental observations is the reduction of an abnormally high valent oxide formed under the strong oxidizing conditions to the more normal Cr oxide, still insoluble, having a lower hydrogen discharge potential. Reduction to Cr metal would explain the nonappearance of Cr ion in the electrolyte equally well, but is improbable since some of the minimum potentials are still more positive than Cr deposition potentials (6). Alternative cathodic processes which, by initiating abruptly at the minimum potential, conceivably could generate the observed type of cathodic reduction curve –metal plating, a decrease in electrical resistance of the film, a decrease in the hydrogen discharge potential, or hydride formation (7)–seem untenable for one reason or another.

It is reasonable to expect that Cr oxide formed under the various strongly oxidizing conditions would be highly cation deficient and contain a corresponding number of cations of higher valence, Cr^{4+} or Cr^{6+}. The cathodic reaction then might be written:

$$Cr^{3+}_{2-2x}\,Cr^{6+}_{x}\,\square_x\,O_3 + 3\,xe + \frac{3x}{2}\,H_2O = \frac{2-x}{2}\,Cr_2O_3 + 3x\,OH^-$$

where $\square_x$ represents the concentration of cation vacancies in the surface of the oxide. To account for the minimum it is necessary to infer that the hydrogen overvoltage is large on the highly imperfect oxide but lower on the reduced surface oxide. It follows that the potential difference between the minimum and steady potential depends on the Cr^{6+} concentration at the surface, *i.e.*, on the oxidizing intensity of the treatment. This difference was 60 mv rather than 150 mv after heating Cr in tank argon containing a small O_2 impurity instead of in pure oxygen; and only 30 mv after treating Fe-26 Cr alloy in 50% HNO_3 (Fig. 4, curve 11) which apparently is only mildly oxidizing. The actual potential value has a less specific meaning since it includes an *IR* drop which varies with film resistance or thickness. Hence in Fig. 5 curves 1, 2, 6, and 7 are displaced progressively toward negative potentials because of the progressively thicker oxide. A second factor decreasing potentials with air exposure of thin films (curves 1 and 2, 4 and 5) can be the shrinking or sealing of film pores.

Oxidation rate.—If, as suggested above, the oxide formed in electropolishing is cation deficient and polyvalent, it can be expected to be a poor diffusion barrier and lead to high oxidation rates, as was observed. On the contrary, the more nearly stoichiometric films formed in room temperature air after etching or by cathodic reduction and subsequent air exposure of the electropolished surface would have lower cationic conductivity and a lower scaling rate. That this is the actual reason for the rate difference is not established; also involved might be moisture content, Cr/Fe ratio, impurities, recrystallization, or some other characteristic of the oxide film. A possibility that surface overheating could account for the difference in rate was rejected by experiments

in which the surface temperature was followed by thermocouples welded to the specimens (8).

Hydrogen discharge.—The mode of hydrogen discharge during the cathodic polarization varies with different pretreatments. With preparations yielding the sharp minimum type of curve, hydrogen bubbles appear shortly after the minimum. After etching or preliminary cathodic reduction hydrogen bubbles are less numerous or absent. In fact, if the experiment is prolonged, hydrogen blisters erupt in the metal. With chromium, where the hydrogen discharge potential is more negative, both bubbles and blisters are produced after electropolishing. On the other hand, with the thicker oxide put on Cr in elevated temperature oxidation, hydrogen bubbles soon appear even after a preliminary cathodic treatment (curve 8, Fig. 5). The significance of these observations has not been determined. It appears that both electrons and protons act as current carriers through the film (9). Which predominates, *i.e.*, whether bubbles or blisters form, may depend on hydrogen overvoltage, electrode potential, oxide defect structure, film thickness, and some undefined property of the surface affecting the catalytic step in the hydrogen discharge reaction.

Etching.—Self-corrosion during etching leads to much the same type of curves as cathodic reduction and presumably similar considerations apply, with the corrosion current serving in place of the impressed current. But a further important point, as seen from Fig. 6, is the variation in etching that can occur with alloys capable of developing surface passivity. By continuously observing the specimen potential while in the etchant, a minimum etch could be obtained reproducibly by etching for a fixed time after the specimen became active.

Specimen preparation.—On the basis of these considerations, the specimen preparation adopted for future scaling experiments was to electropolish to remove contamination and worked metal left by abrading, anneal in argon at 1100° for structural stability, again electropolish to remove surface modifications introduced by the anneal, and finally etch lightly to remove the oxide film left by electropolishing, using a standard minimum etch.

To summarize, the scaling rate of Fe-Cr alloys can be greatly modified by methods of surface preparation, and the films on these various surfaces also show different electrochemical behavior. The sharp minimum type of cathodic reduction curve, exhibited by Cr alloys after strongly oxidizing treatments, is believed to be associated with conversion of the surface of the chromium oxide film to a lower valence state. The rapid dry oxidation rate after electropolishing may be explained by this supravalent, cation-deficient oxide film. More specific characterization of the surface oxides was unsuccessful, largely due to the failure of reflection electron diffraction to yield usable patterns. Recent examination of oxide overgrowths on electropolished iron has shown that satisfactory patterns can be obtained if single crystal specimens are used (10). It is hoped that experiments of the same type can be made when single crystals of Cr and Fe-Cr alloys are obtained.

Conclusions

1. The oxide film left on Fe-Cr alloys by electropolishing leads to a markedly higher initial reaction rate in high-temperature oxidation than other surface preparations.

2. Cathodic reduction after electropolishing and other strongly oxidizing treatments yields a curve with an anomalous sharp minimum which is interpreted as due to a surface oxide of high reduction overvoltage and even higher hydrogen overvoltage. It is suggested that Cr^{6+} in a nonstoichiometric Cr_2O_3 film is cathodically reduced to Cr^{3+} with a corresponding decrease in cation vacancy concentration.

3. The same anomalous peak occurs in the potential/time curve during acid etching of electropolished Cr alloys.

4. Surface preparations for alloys exhibiting passivity are sensitive to the time intervals between operations. Standardization of the procedure is required.

5. A preferred surface preparation for corrosion studies is a combination of electropolishing and a minimum etch. For standardization of the etch, it is necessary to observe the specimen potential continuously during etching.

Manuscript received July 11, 1960; revised manuscript received Oct. 4, 1960. This paper was prepared for delivery before the Columbus Meeting, Oct. 18-22, 1959.

Any discussion of this paper will appear in a Discussion Section to be published in the December 1961 JOURNAL.

REFERENCES

1. D. Caplan and M. Cohen, *Corrosion*, **15**, 141t (1959).
2. H. C. Oswin and M. Cohen, *This Journal*, **104**, 9 (1957).
3. K. H. Buob, A. F. Beck, and M. Cohen, *ibid.*, **105**, 74 (1958).
4. T. N. Rhodin, *Corrosion*, **12**, 123t (1956).
5. P. B. Sewell, C. D. Stockbridge, and M. Cohen, *Can. J. Chem.*, **37**, 1813 (1959).
6. W. M. Latimer, "Oxidation Potentials," p. 248, Prentice Hall, New York (1952).
7. W. H. Smith, *This Journal*, **103**, 51 (1956).
8. D. Caplan, *ibid.*, **107**, 359 (1960).
9. J. E. Draley and W. E. Ruther, *ibid.*, **104**, 329 (1957).
10. P. B. Sewell, C. D. Stockbridge, and M. Cohen, To be communicated (presented at E.C.S. Columbus Meeting, 1959).

Determination of the Thickness of Thin Porous Oxide Films on Aluminum

M. S. Hunter and P. F. Towner

Alcoa Research Laboratories, Aluminum Company of America, New Kensington, Pennsylvania

ABSTRACT

A method is described for measuring the thickness of thin porous oxide films on aluminum, employing the grazing angle interference colors characteristic of thin transparent films. In conjunction with oxide film step gauges formed under precisely controlled conditions, measurements to about 7Å are possible. Application of the method for measuring film growth in various solutions and in the evaluation of the characteristics of barrier-type electrolytes is also demonstrated.

Practically all oxide films on aluminum are considered to consist of two layers, regardless of whether they are formed naturally or by thermal or anodic treatments. One of these, the barrier layer, is almost always extremely thin, seldom exceeding a few millionths of an inch in thickness. The other, generally described as the porous layer, may have a wide range of thicknesses from a few Angstroms, in the case of natural films formed under dry conditions, to as much as 2-5 mils in the case of certain anodically formed films. The thickness of these individual layers is very important in determining the characteristics and behavior of the oxide coatings. This paper describes a simple but effective method for measuring the thickness of the porous portion of thin oxide films which are difficult or impossible to measure by other means. This method, in conjunction with the barrier thickness measurement method already described in the literature (1), can be used to completely delineate such films.

Nature and Source of the Porous Layer

The description of the barrier and porous regions as layers is actually misleading, because they are not separate and distinct layers in the sense that they can be separated or that a definite line of demarcation exists between them. These zones or regions are separate and distinct, however, in the sense that they exhibit different characteristics. In particular, the barrier oxide layer is capable of electrolytic rectification, whereas the so-called porous layer offers practically no opposition to current flow in either direction. It is this difference in electrical behavior that is used directly in the measurement of the thickness of the barrier layer and indirectly in the measurement of the thickness of the porous layer.

The manner of formation of the porous layer is different depending on whether the coating is formed anodically or by natural and thermal means. In the case of natural or thermal films, a mechanism for the formation of the porous layer has been proposed (2). According to this mechanism, the outer surface of the aluminum combines with oxygen or moisture in the air to form a layer of aluminum oxide. This layer initially is of the barrier type and has a thickness that is a function of temperature. If the environment has the ability to react with the barrier layer, some of the oxide will be converted to a so-called porous type and the thickness of barrier oxide will be reduced. Since there is a tendency for the barrier layer to reach a certain limiting thickness for any given temperature, the barrier will be replenished continuously as long as any conversion to porous oxide takes place. As this process continues, the barrier portion of the coating generally tends to remain at a constant thickness, and the simultaneous formation and conversion of the barrier results in an increase in the thickness of the porous region. This region is porous in the sense that it is electronically conducting, but it is very doubtful that its structure is characterized by discrete pores.

In the case of oxide films formed anodically, a different mechanism has been proposed to account for the formation of the porous layer (3). When voltage is first applied, a layer of compact barrier oxide begins to form on the surface. If the electrolyte does not react with this barrier oxide, the barrier film will reach a limiting thickness of 14Å times the applied voltage and no porous layer will be formed. If the electrolyte does exert solvent action on the oxide, however, this solvent action will tend to reduce the thickness of the barrier oxide. When this occurs, the cell attempts to restore the barrier layer to the limiting thickness corresponding to the applied voltage. This results in simultaneous formation and solution of oxide and the eventual development of a compact array of oxide cells, each containing a tubular pore. During this process, a balance is established such that the barrier layer attains a constant value and continued coating formation results only in an increase in the thickness of the porous layer. With this type of coating, the outer region is truly porous since it contains a multitude of minute pores which can be observed with the electron microscope.

Measurement of Porous Films

The most satisfactory method of measuring the porous portion of oxide films depends on the total

thickness of the film. If the film is thicker than about 4000Å, the thickness of the entire film may be measured with a light microscope, the thickness of barrier oxide may be measured by the electrical method described previously (1), and the thickness of the porous portion may then be determined by subtraction. In this case, the accuracy of the measurement is governed by the accuracy of microscopic measurement and, since the coatings are comparatively thick, the relative error is generally small.

In the case of coatings having a total thickness less than about 4000Å but greater than about 500Å, the coatings themselves will have distinct interference colors which may be translated to thickness by comparison with step gauges (4) or from interference color charts. Alternately, the total thickness of film may be determined through the use of interferometry as described by Tolansky (5) and others. Once the total thickness of the coating is determined by either of these methods, the thickness of the porous layer may be determined by subtracting the thickness of the barrier. These methods have considerable precision and fairly accurate determinations may be made.

In measuring the thickness of films less than about 500Å, considerably greater difficulty is encountered. Films in this range do not exhibit interference colors, and the errors of interferometry lead to an appreciably greater percentage error as film thickness decreases. It is still possible to estimate the thickness of the entire film using the interferometry method, but highly specialized equipment is required for reasonably accurate results. It is with films below about 500Å in thickness that the method to be described is most useful.

Measurement Method.—The method to be described for measuring the porous portion of very thin oxide films on aluminum is an interference color method, similar in certain respects to the methods used by Blodgett and Langmuir (6), Blodgett (7), and by Langmuir, Schaefer, and Wrinch (8) for measuring thin deposited films. The method makes use of the fact that films of a given thickness have a characteristic interference color and the fact that it is possible to produce precisely controlled oxide films by anodic oxidation. The actual interference color observed with a thin film depends on the manner of viewing, the characteristics of the light source, and the optical properties and structure of the film.

The measurement is accomplished by stripping the film from a portion of the specimen, applying an appropriate barrier-type oxide film to the entire specimen, and comparing the interference colors of the stripped and unstripped regions. In the region that has been stripped, film thickness will be a function of the voltage used to apply the coating, and an interference color characteristic of this film thickness will be observed. In the region that has not been stripped, the anodic coating operation will increase the thickness of the barrier portion of the pre-existing film to the same thickness as that in the region that had been stripped. If any porous film

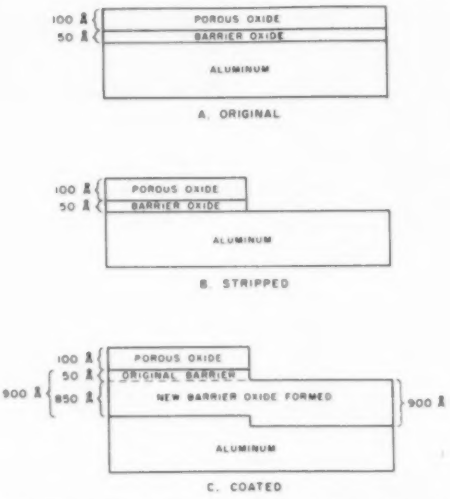

Fig. 1. Shows condition of specimen at three stages in film measurement.

exists in this region, the total film thickness will differ from that on the other region by the thickness of the porous portion of the pre-existing film, and an interference color, characteristic of the total thickness, will be visible. The difference in color, which represents the thickness of the porous portion of the film, may be translated to film thickness by comparison with appropriate interference color standards, the preparation of which is described later.

The detail of the method and its manner of operation can be understood more thoroughly by referring to Fig. 1, which illustrates the use of the method for a film 150Å in thickness, consisting of a 50Å barrier layer and a 100Å porous layer. Such a film is too thin to exhibit an interference color of its own. A cross section of such a coating with the barrier and porous portions indicated is shown at A. Half of the sample is immersed in a boiling solution containing 20 g CrO_3 and 35 cc of concentrated H_3PO_4 (85%) per liter of solution. This solution effectively removes the oxide film but does not attack the aluminum. The condition of the sample at this stage is shown at B, where the oxide film remains on one-half of the specimen with the other half essentially oxide free.

After the film has been removed from half the specimen, the entire sample is immersed in an electrolyte capable of forming an essentially barrier-type film, and voltage is applied. An electrolyte that has been used successfully consists of a 3% $C_4H_6O_6$ solution adjusted with NH_4OH to a pH of 5.5. When voltage is applied, barrier-type oxide forms to a thickness equivalent to the applied voltage over the entire specimen, as indicated at C in Fig. 1. In the stripped region, the entire 900Å of barrier oxide is formed in the coating operation. In the region which still has the original film, the barrier-type oxide is increased in thickness to the same value (900Å). In this region, however, the barrier now consists of the 50Å barrier portion of the original film and 850Å of barrier oxide formed during the coating step. On the stripped region, the total film thickness

is the 900Å of newly formed barrier oxide. The unstripped region has the same thickness of barrier oxide and, in addition, the 100Å of porous oxide that was present initially. Thus the total film thickness on the two regions differs by an amount equal to the thickness of the porous portion of the initial film.

It is also possible to use this method to advantage with somewhat thicker films, such as those which show a characteristic interference color. In this case, a similar procedure is used except that the specimen is divided into three regions instead of two. A region at one end of the specimen is stripped, and this region and the adjoining region are coated as described above. In the stripped region, the interference color will correspond to the thickness of film applied anodically. The central region, which was not stripped but was coated, will have a color equivalent to a somewhat greater thickness of oxide. The difference between these two colors represents the thickness of the porous layer, as in the case of thin films. In the region which has been neither stripped nor coated, the color will represent the over-all thickness of the initial film. Measurement can be made of the thickness of the barrier layer in this region. This thickness subtracted from the over-all thickness of the film will represent the thickness of the porous portion of the film. This value will constitute a check on the one determined by the difference between the colors of the two coated regions.

In forming the barrier-type film on the test specimen voltage is applied to increase the thickness of the barrier portion of the film and to bring the over-all thickness of the film into the range where interference colors are observed. While measurements can be made using any region of the interference spectrum, best results are obtained in the region of color from red-violet through blue to blue-green, because it is in this range that the interference colors change most rapidly with changes in film thickness. Consequently, it is best to select a voltage which produces on the stripped portion of the specimen a film having a red-violet interference color. When this is done, the final film thickness on the unstripped region will lie in the violet, blue, or blue-green regions or beyond, and the difference in color will be in the most sensitive range. A potential of 64 v produces a film having the desired red-violet interference color on the stripped region.

The time of coating should be sufficient to permit practically complete film formation and should be controlled. With the tartrate electrolyte described, a time of 12 min has proven to be optimum.

Conversion of the color differences to film thickness values can be made by comparison with carefully prepared oxide film step gauges. Such gauges should be made with great care with particular attention to the precise voltage and coating time used in the formation of the various oxide steps. Difficulty from this source may be avoided by using the same electrolyte and the same coating time for applying the barrier-type film in the measurement method as are used for making the comparison step gauge. With appropriate precautions, accurate step gauges having 7Å (0.5 v) steps can be made. Color differences corresponding to thickness differences of this order are about the least that can be detected visually.

Measurements of porous-film thickness may also be made by any instrument capable of accurately measuring the wave length of the interference colors or the difference between two such colors. A reflectance spectroscopic method for this purpose has recently been developed, using the same principle described here (9).

In measuring comparatively thick films by this method, it must be kept in mind that, as the films increase in thickness, the interference colors progress through one order of interference after another. The first color observed is yellow, followed by red, violet, blue, green, and then yellow again. The first order yellow corresponds to a film thickness of about 500Å, whereas second order yellow is observed with films about 1300Å thick. Thus, the interference order of the color observed must also be determined.

A simple method has been found for differentiating between the first four interference orders. This is simply to view the colors at grazing incidence by polarized light through a polaroid filter. If the color is in the first interference order, it will be observed when the plane of polarization of the filter is perpendicular to the plane of incidence, but will disappear when the plane of polarization is parallel to the plane of incidence. With second order colors, the reverse will be apparent, the color being observed when the plane of polarization is parallel and vanishing when it is perpendicular to the plane of incidence. With third order colors, the color with the plane of polarization perpendicular to the plane of incidence will be the same as that of a first order film but, with the plane of polarization parallel, the complementary color will be evident. With fourth order colors, the situation again reverses, for the color is seen when the plane of polarization is parallel, and the complementary color is seen when it is perpendicular to the plane of incidence.

As mentioned previously, the particular interference color observed with a given thickness of film depends on several factors. One of these is the manner in which the film is observed. The most satisfactory method of viewing the interference colors of thin oxide films on aluminum is at a large angle (grazing incidence) against a white background. The larger the angle used, the more intense are the colors. In addition, it has been found convenient to view the interference colors through a piece of polaroid film because this also intensifies the colors.

The light source for viewing interference colors also has a bearing on the particular color observed. It has been found that the most satisfactory light source is daylight or white light from a frosted light bulb or from fluorescent lights. For best results the light should be reflected from a white surface, across the specimen to the eye. In the present method, which uses comparison with standard samples, the method of viewing and the light source are eliminated as sources of error by viewing both the standard and the unknown in the same manner with the same type of lighting.

The optical properties and structure of the oxide films also have a bearing on the interference color observed. In particular, the color is a function of the index of refraction of the film. Since the indices of refraction of all types of thin oxide films on aluminum are similar (1.58-1.65), little error is involved even if the effect of refractive index is ignored. The effect of index of refraction may be nullified, however, by the use of oxide films on aluminum for the comparison standards.

In the course of this work, it has been observed that certain film porosity can introduce an error into the measurement. This has been found to be the case with porous films of the type made in electrolytes that have appreciable solvent action on the oxide and those that develop films having a comparatively large amount of porosity. The effect of porosity is to change the effective index of refraction because the film is not solid oxide but consists of a certain percentage of oxide and a certain percentage of air. It should be possible, however, to calculate the effective index of refraction from per cent porosity data, if it is known for the particular coating, and thence to apply a correction for porosity. This might be done by calculating the per cent porosity from cell and pore dimensions and the solvent action rate of the forming electrolyte. The effective refractive index could then be calculated from the ratio of the volume of the pores and the volume of compact oxide.

Applications

Since its development, this method for measuring thin porous-type films has received considerable usage in a variety of applications. Among these has been the measurement of thin films formed in various solutions. Two examples will serve to show the usefulness of the method for work of this type.

One interesting investigation was concerned with the development of alpha monohydrate films on aluminum by boiling in water. As shown by Fig. 2, which shows film formation on high-purity (99.99%) aluminum in boiling distilled water after a chemical polish, such treatment led to the rapid development of film along what appears to be a two-part curve. It is believed that the comparatively slow rate at the start of boiling is associated with the necessity of destroying or converting the pre-existing film on the aluminum. Once this film was disposed of, which required about 25 sec, film developed rapidly and in the expected manner. Similar behavior was encountered during the hydration of anodically formed films by boiling in water (10). In this case, it was demonstrated that the two-part curve represented the hydration of the anodic film until it was completely converted to alpha monohydrate, followed by monohydrate formation by reaction of water with the underlying metal.

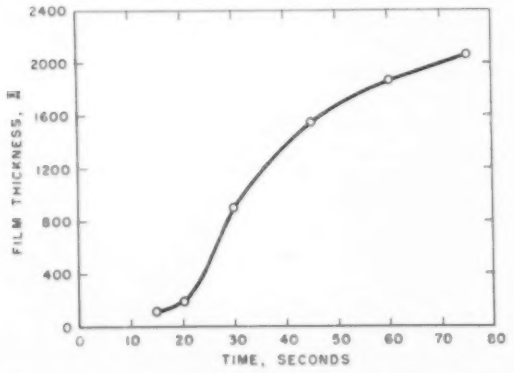

Fig. 2. Development of α monohydrate film on high-purity aluminum in boiling distilled water after chemical polish.

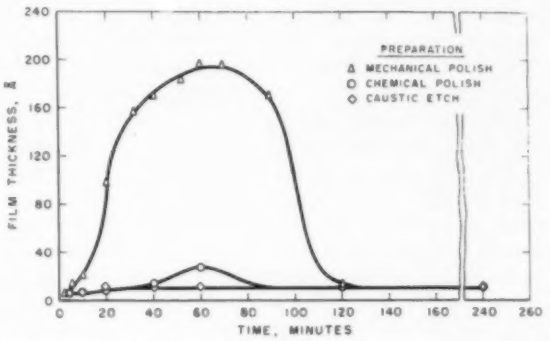

Fig. 3. Film growth on high-purity aluminum in concentrated nitric acid.

Another investigation was concerned with film formation in concentrated nitric acid at room temperature, a treatment which produces a very thin, stable film on aluminum. In this work, a mechanical treatment and two types of chemical treatments were used for surface preparation. As shown by Fig. 3, film thickness progressed through a maximum before reaching a low steady value. It is evident also that the type of preparation had little effect on the final film thickness but had a pronounced effect on the manner in which the final thickness was reached. It is believed that the changes in film thickness are related to the type of film present on the metal and that the pre-existing films had to undergo some change before the ultimate stable film could be formed. In the case of the two types of chemical surface preparation, the films were evidently such that only little readjustment was required. On the other hand, considerable readjustment was necessary in the case of the mechanically polished sample, in the course of which a comparatively thick intermediate film was created. The changes in film thickness after mechanical polishing in these experiments are in general agreement with those observed by Tronstad and Hoverstad (11), who followed the same phenomenon by measurements of optical constants.

A third interesting application of the film measurement method was in an investigation of the characteristics of several barrier-type electrolytes. When aluminum is made anode in such an electrolyte, current flow diminishes to a low, constant value which is considered to be leakage. At this point, it is assumed that the film is completely formed and has a thickness proportional to the applied voltage.

Investigation of several common barrier-type electrolytes, however, has shown that the final steady current is more than just leakage and that the film

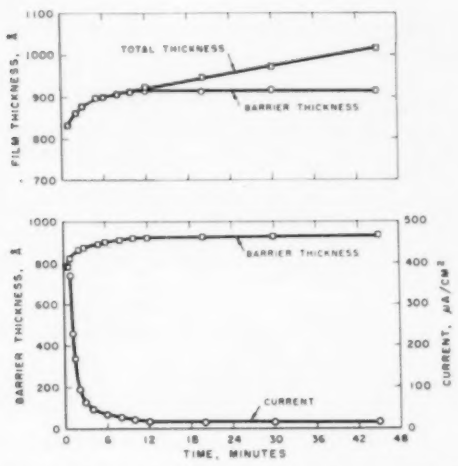

Fig. 4. Film growth in ammonium tartrate electrolyte

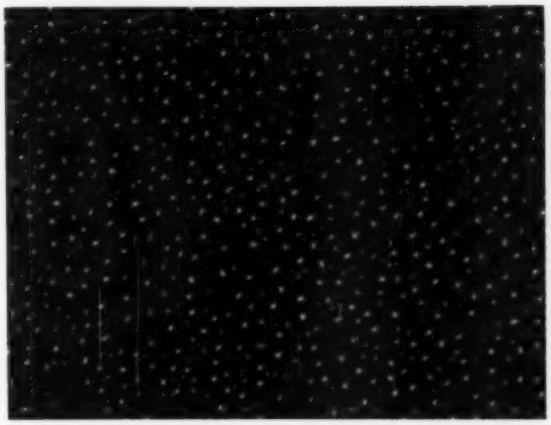

Fig. 5. Shows pore structure developed by 15-hr formation at 40 v in ammonium tartrate electrolyte. Magnification: 30,000X.

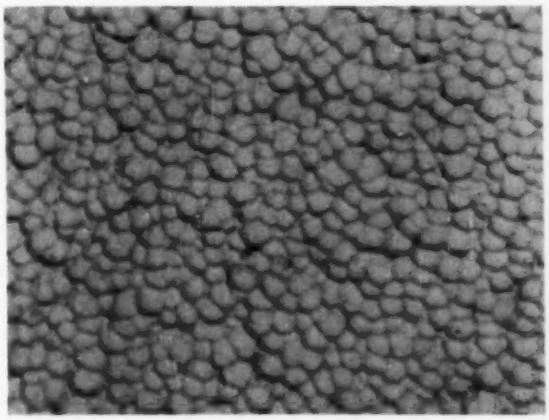

Fig. 6. Shows metal surface underlying coating formed 15 hr at 40 v in ammonium tartrate electrolyte. This cell base pattern is characteristic of porous type coatings. Magnification: 30,000X.

actually continues to grow by the formation of porous oxide. For instance, film formation on high-purity aluminum in an ammonium tartrate solution yielded the current and film thickness values shown in Fig. 4. During the first 12 min of coating time, barrier thickness increased in inverse proportion to current flow, after which both values remained substantially constant. When the formation operation was continued, however, the total film thickness increased gradually by virtue of the formation of porous-type oxide. The formation of porous oxide proceeded linearly with time, which is reasonable since the amount of oxide formed is a function of time, when current density is constant.

Since barrier thickness remained constant while the porous film thickness was increasing, additional barrier-type oxide was being formed to replenish that converted to porous oxide. This, in turn, would require passage of a certain current. Comparison of the current going to the formation of new oxide and the total current to the cell showed that only about half of the current could actually be considered as leakage since approximately half of the current flowing was involved in oxide formation.

Further proof of the formation of porous-type oxide in this electrolyte was obtained by electron microscopy. When a 40-v potential was applied to high-purity aluminum as anode for 15 hr and the film was removed and examined by electron transmission, the structure seen in Fig. 5 was observed. The light spots represent the pores in the film where the electron beam had to penetrate only the barrier layer. When the film was removed completely and the surface of the underlying metal was examined, the cell base pattern seen in Fig. 6 was evident. This and the pore pattern seen in Fig. 5 are characteristic of porous-type oxide coatings in which the pore structure is developed by virtue of solvent action of the electrolyte on the oxide (3).

In exploring the characteristics of various electrolytes with respect to their ability to form truly barrier-type films, the perfect electrolyte has not yet been found. The ammonium tartrate electrolyte is among the best, as are dilute chromic acid solutions and the boric acid electrolytes used extensively for high voltage work. No solution has been found, however, which does not exert some solvent action on the oxide and thus lead to the formation of porous film.

The fact that most electrolytes exert some solvent action on the oxide and thus lead to the formation of porous-type oxide is highly significant in the use of the porous film measurement described in this paper. Because of this situation, it is essential that the formation conditions used with a sample be the same as those used in the preparation of any step gauges employed. When the same electrolyte is used, the optimum time is a balance between complete film formation for the voltage used and creation of porous-type oxide as a result of solvent action.

Conclusion

The method for measuring the thickness of porous-type films is comparatively simple, but with moderate precautions is capable of considerable accuracy. While features such as per cent porosity and refractive index appear to have an effect on the values obtained and, consequently, might seem to re-

strict the utility of the method, it should be possible to calculate the effect of such factors and thus adapt the method for universal application. Until the details of such corrections can be established, the method can be used successfully provided the nature of the comparison step gauges is similar to that of the film being measured. This method should have considerable utility in dealing with thin films not only on aluminum but also on any other materials which develop similar types of films.

Acknowledgment

The authors gratefully acknowledge the assistance of F. Keller, under whose direction this work was conducted, and of D. L. Robinson, who made the electron micrographs.

Manuscript received March 9, 1960; revised manuscript received Oct. 3, 1960. This paper was prepared for delivery before the Chicago Meeting, May 1-5, 1960.

Any discussion of this paper will appear in a Discussion Section to be published in the December 1961 JOURNAL.

REFERENCES

1. M. S. Hunter and P. Fowle, *This Journal*, **101**, 481 (1954).
2. M. S. Hunter and P. Fowle, *ibid.*, **103**, 482 (1956).
3. F. Keller, M. S. Hunter, and D. L. Robinson, *ibid.*, **100**, 411 (1953).
4. D. A. Vermilyea, *Acta Met.*, **1**, 282 (1953).
5. S. Tolansky, "Multiple-Beam Interferometry," Oxford University Press, London (1948).
6. K. B. Blodgett and I. Langmuir, *Phys. Rev.*, **51**, 964 (1937).
7. K. B. Blodgett, *J. Phys. Chem.*, **41**, 975 (1937).
8. I. Langmuir, V. J. Schaefer, and D. M. Wrinch, *Science*, **85**, 76 (1937).
9. In preparation for publication.
10. M. S. Hunter and P. F. Towner, *Proc. Electroplaters Soc.* (1959).
11. L. Tronstad and T. Hoverstad, *Trans. Faraday Soc.*, **30**, 361 (1934).

The Effect of Dissolved Gases on the Electrical Conduction and Breakdown of Insulating Oil

H. Tropper

Department of Electrical Engineering, Queen Mary College, University of London, London, England

ABSTRACT

An experimental study has been made of the effect of dissolved air on the electrical conduction and breakdown of insulating oil. It was found that the breakdown of degassed oil is preceded by an appreciable conduction current which is accompanied by fluorescence of the highly stressed oil. It was shown that both the conduction current and the breakdown voltage, particularly the latter, are affected by the residual oxygen dissolved in the oil. Other observations are concerned with the change in breakdown voltage when the air content of the oil is increased up to its saturation value at atmospheric pressure.

The purpose of the paper is to present a résumé of some of the more important results of recent experiments on the effect of dissolved gases on the electrical conduction and strength of insulating oils. Work on this topic is still in progress, and results reported here were obtained by a number of workers using different test apparatus and testing techniques.[1] They have, therefore, to a great extent been confirmed independently.

Experimental

Although the test apparatus used differed in design, they consisted in all cases of glass systems which completely sealed the oil from the atmosphere during the tests. The excess pressure required for the filtration of the oil and for spraying it into the degassing or mixing chamber was obtained by mechanical means, such as a bellows pump or small rotary oil pump. In this way the undesirable procedure of admitting a small amount of air into the system was avoided, and thus a better control over the impurities in the oil was achieved. Samples of varying air content were prepared by introducing carefully dried and filtered air into the degassing chamber at the required equilibrium pressure and spraying degassed oil into this chamber. This operation could be carried out independently of the filtration of the oil, and it was therefore possible to prepare test samples of oil of different air content which had been filtered previously with different grades of filters. As a rule sintered glass filters of porosity No. 4, having a pore diameter of 5-15μ, and of porosity No. 5, of pore diameter less than 1μ, were used during the experiments. For the sake of brevity, oil filtered with these filters will be referred to in the following as No. 4 and No. 5 filtered oil, respectively.

In one of the investigations the oil was purified by molecular distillation. This was done at pressures from 0.01 to 1 mm Hg and at temperatures from 50° to 180°C.

In all cases a small-scale testing technique was adopted with the spacing between spherical electrodes varying from 25 to 150μ. The tests were made with direct voltages, and damage to the electrodes and oil contamination was kept to a minimum by

[1] The properties of insulating oils are studied in the laboratory by a small team under the supervision of the author. Most of the results contained in the paper were obtained by Khambanonda (1), but use also has been made of the work of M. Darveniza, C. H. Gosling, and W. P. Jayasekara. Mentioned also are some observations made by A. M. Sletten on hexane.

by-passing the discharge current using a hydrogen thyratron which shorted the test cell 0.5μ sec after breakdown.

All results quoted were obtained with normal commercial transformer oil complying with the B.S.148:51 and of 28 centistokes viscosity at 21°C. It was of Peruvian origin and consisted of 53.7% C contained in paraffinic components, 37.8% C in napthenic, and 8.5% C in aromatic components. The average molecular weight was 310 and the density 0.88. The vapor pressure at 0°C was 10^{-4} mm Hg. Test samples prepared from this oil, which contained air at a partial pressure of approximately 0.02 mm Hg, here are referred to as degassed oil.

During breakdown measurements a conditioning process was observed, that is to say, with fresh electrodes successive voltage applications gave either increasing (conditioning up) or decreasing (conditioning down) breakdown values, and only after a certain number of discharges had passed through the gap were steady conditions obtained. The breakdown values quoted are those measured after conditioning had taken place. The study of the conditioning process is important and may throw valuable light on the breakdown mechanism; some results relating to this effect are given below.

Results

The breakdown strength of degassed oil was high and it increased when finer filters were used for the oil filtration. No significant difference in the breakdown values was found for electrodes made of copper, chromium, aluminum, and steel but there was a marked increase of some 40% for electrodes of stainless steel. For example, for spherical stainless steel electrodes of ½ in. (12.7 mm) diameter and a gap setting of 89μ the breakdown strength of degassed No. 4 filtered oil was 980 kv/cm and the strength increased to approximately 1220 kv/cm when a No 5. filter was used. Still higher values were obtained with finer filters or when the oil was purified by molecular distillation.

The electrical breakdown of oil of such high dielectric strength is characterized by three distinctive features: (*a*) breakdown is always preceded by a pronounced conduction current; (*b*) during this current flow light is emitted from the highly stressed region of the oil; and (*c*) the breakdown strength is critically dependent on the air content of the test sample.

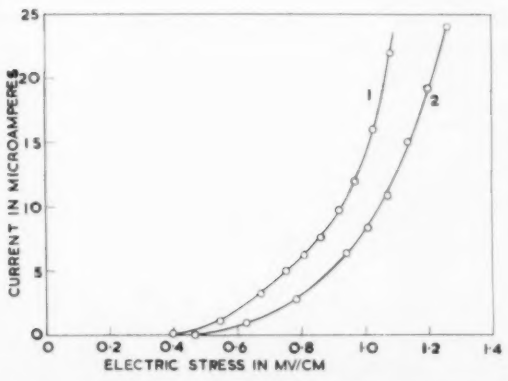

Fig. 1. Conduction current vs. electrical stress; curve 1 for No. 4 filtered oil and curve 2 for No. 5 filtered oil.

The prebreakdown current became noticeable at a stress of about 600 kv/cm, which is somewhat higher than the breakdown strength of less carefully prepared oil. The general shape of the variation of this current with the applied field is shown in Fig. 1 for two samples filtered, respectively, through No. 4 and No. 5 filters. The electrodes were ½ in. diameter stainless steel spheres with a gap setting of 89 μ. The current appeared to depend only on the electric field, and the breakdown of the oil could take place at any value of the current. In the event of a breakdown the subsequent conduction current was higher, but it subsided gradually to the original value.

Prebreakdown Current and Fluorescence

The prebreakdown current was accompanied by light emission from the highly stressed region of the gap. At field strength of 600-700 kv/cm filamentary streamers of constant light intensity could be seen to bridge the gap. The number of these streamers increased with the applied field until the gap was bridged by a diffuse glow which, for field strength of about 1000 kv/cm, had a diameter of 2-3 times the gap spacing. The color and frequency of the emitted light was similar to the blue fluorescence which is observed when the oil is irradiated from an ultraviolet source.

Darveniza (2), who has studied this phenomenon in detail, has shown that it is a fluorescence effect. It is known that traces of polycyclic aromatic compounds are present in the oil, and he suggested that the light emission is due to excitation of molecules of this type. Like the conduction current, the luminosity was found to increase exponentially with the applied field, but no marked change with field could be observed in the spectrum of the emitted light. Removal of most of the fluorescent impurities by fractional distillation reduced the intensity of light emission, and at the same time an increase of the breakdown strength of the oil from 1100 to 1300 kv/cm was obtained.

In support of his suggested explanation Darveniza has shown that fluorescence induced by high electric stress does also occur in n-hexane when small traces of anthracene or p-terphenyl are added to this liquid. The light emitted is characteristic of the added impurities, while for spectroscopic grade of n-hexane no luminosity could be detected for electric fields up to 1100 kv/cm when breakdown occurred. As for oil, the presence of the fluorescent impurities in the hexane increased the conduction current and lowered its breakdown strength.

It might be thought that the light emission of the highly stressed oil was due to micro discharges rather than to excitation of fluorescent impurities. However, subjecting the oil to a negative pressure during the tests did not bring about a change in the intensity of the emitted light, nor did fracture of the oil under tension occur at field strengths as high as 1000 kv/cm.

Variation of Strength with Air Content

The third important observation which was made with degassed oil was the great sensitivity of the breakdown strength to small changes in the air content. For example, a change of air content corresponding to a change in partial pressure from 0.02 to 0.8 mm Hg can result in an increase in the breakdown strength of approximately 20%. Increasing the air content also lowers the conduction current. This is more marked at lower field strengths and more difficult to observe at higher fields near breakdown because of the rapid increase of the current in this region.

There is strong experimental evidence that the increase in breakdown strength is due to the oxygen which is introduced with the air into the oil. This effect of oxygen also has been noticed in the breakdown of compressed gases, and it has an important bearing on the study of the breakdown of other organic liquids. For n-hexane it has been examined fairly extensively in this laboratory by Sletten (3). He found for distilled and carefully degassed hexane that the measurements of the conduction current were very erratic and breakdown occurred at strength values of the order of 890 kv/cm with a coefficient of variation of 10%. Results were the same when nitrogen was dissolved in the hexane after distillation. However, replacing the nitrogen by oxygen or air resulted in a marked improvement, and he was able to obtain consistent and repeatable conduction current characteristics for fields right up to the breakdown of the liquid. With oxygen present, the breakdown strength was 1300 kv/cm and the scatter in the measurements was reduced to 5.8%. It is believed that this effect of oxygen may well explain some of the discrepancies in the published breakdown data for liquids. It has certainly helped us to understand and clarify some of our own experimental results of the past, and any theory for the breakdown mechanism of liquid dielectrics must take account of it.

The variation in breakdown strength for small additions of air to the degassed oil is shown in Fig. 2. The values plotted were obtained with No. 5 filtered oil tested between ½ in. diameter spherical stainless steel electrodes and a gap spacing of 89 μ.

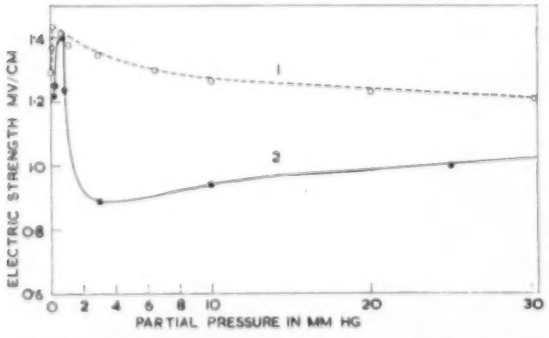

Fig. 2. Electrical strength vs. partial pressure of dissolved air; curve 1 with electrodes conditioned in degassed oil before test, curve 2 with fresh electrodes for each point, i.e., with conditioning in oil of different air content.

The figure reveals the rapid variation of the electric strength which is characteristic of low air content when the dissolved air is changed by small amounts. It is difficult to obtain for this region reliable results for the variation of strength unless the air content of the test sample is controlled carefully and varied by sufficiently small amounts. Without this precaution the changes in breakdown strength are masked, and what is observed is an apparent random fluctuation in the measurements which is appreciable and may be confused with an excessive scatter. It should be noted, however, that the change of breakdown strength resulting from changes in air content is greater than the scatter of the results for one particular air content.

The situation is made more complicated by the fact that the actual breakdown values measured do depend on the measuring technique adopted during the tests. This is illustrated by the two curves No. 1 and 2 in Fig. 2. The points on curve No. 1 were obtained with the same pair of electrodes which were conditioned before the test in degassed oil, while for curve No. 2 fresh electrodes were used for each of the samples of different air content, so that conditioning took place in oil containing various amounts of dissolved air. There is a marked difference between the two cases. In both there is the sharp rise in breakdown strength already referred to as the air content is increased. After this the strength decreases again, but whereas this takes place gradually for curve No. 1, there is a sharp drop to a low value in the case of curve No. 2, after which it rises again.

The subsequent change in electrical strength as the air content exceeds a value corresponding to 30 mm Hg is shown for the two cases in Fig. 3. The general shape of the variation, particularly for curve No. 2, is of the type first reported by Clark in 1933 (4). As far as the author is aware there is no other reference in the literature to this behavior of the breakdown strength, and the above results confirm Clark's observation. However, as can be seen, the observed variation does depend significantly on the test procedure, and the results in Fig. 2 and 3 provide a good illustration of how the latter can affect the results of breakdown measurements.

A similar variation of electric strength with air content was found for No. 4 filtered oil, except that the values were lower, and still lower values were obtained for No. 5 filtered oil when tested with aluminum spheres.

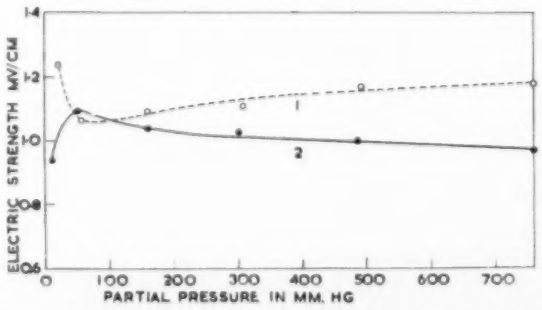

Fig. 3. Continuation of curves 1 and 2 of Fig. 2 for higher partial pressures.

The effect of the filter porosity becomes more pronounced as the air content is increased, and the strength decreases by nearly 30% when oil saturated with air at 760 mm Hg was filtered with a No. 4 filter instead of a No. 5 filter. The strength of the oil saturated with air at atmospheric pressure was still dependent on the electrode metal, and stainless steel electrodes again gave the higher strength. With this metal and No. 4 filtered oil the strength values measured were 15% higher than when aluminum electrodes were used.

Effect of Hydrostatic Pressure

The effect of hydrostatic pressure on the breakdown strength of the oil was examined for pressures in the range of approximately 0.02 mm Hg to atmospheric pressure. No. 4 and No. 5 filtered oil which was degassed was used, as well as oil filtered in this way, but containing varying amounts of air. The results for the No. 5 filtered oil and the No. 4 filtered oil are shown in Fig. 4 and 5, respectively. Each point on the curve represents the average of 10 breakdown measurements.

For No. 5 filtered degassed oil no pressure dependence could be detected when the normal procedure was used, that is to say, when conditioning before the tests was done at atmospheric pressure. However, as can be seen from the figure, there was a marked pressure dependence when the conditioning process was carried out at a reduced pressure. In this case the same breakdown strength was obtained at atmospheric pressure, but at reduced pressure the strength was 15% smaller. This provides another example of how experimental procedure can affect the results.

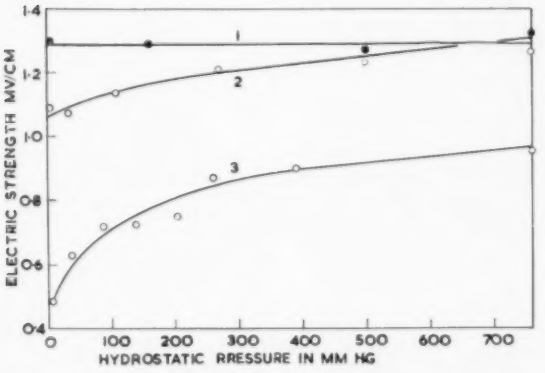

Fig. 4. Electrical strength vs. hydrostatic pressure for No. 5 filtered oil; curves 1 and 2 for degassed oil using two different testing techniques, and curve 3 for oil saturated with air at atmospheric pressure.

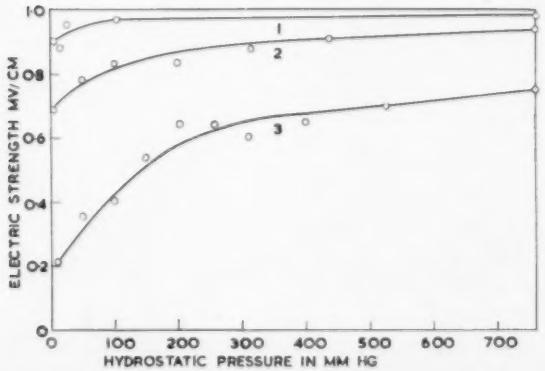

Fig. 5. Electrical strength vs. hydrostatic pressure for No. 4 filtered oil; curve 1 for degassed oil, curve 2 for oil containing air at a partial pressure of 320 mm Hg, and curve 3 for oil saturated with air at atmospheric pressure.

When the degassed oil was filtered through a No. 4 filter and conditioning was done at atmospheric pressure there was again no pressure dependence when the pressure was varied from 760 to about 50 mm Hg, but for smaller pressures the electric strength values decreased, and a more detailed examination of the low pressure region showed the presence of a kind of Paschen minimum, which is not shown in Fig. 5.

As was to be expected, a more pronounced pressure dependence was observed as the air content of the oil increased. For oil saturated with air at atmospheric pressure and No. 5 filtered the strength increased from 500 to 950 kv/cm as the pressure increased from a low value to atmospheric pressure, and for No. 4 filtered oil of the same air content, the increase for the same pressure range was from 200 to 750 kv/cm. For the sake of comparison a test was made with No. 4 filtered oil in equilibrium with air corresponding to a pressure of 320 mm Hg. As can be seen from Fig. 5 the electric strength at atmospheric pressure of this oil is the same as that of the degassed oil, but the pressure dependence is more marked. Over the pressure range considered it shows an increase of 36%, whereas the strength of the degassed oil increases only by about 12%.

During tests at reduced hydrostatic pressures, the evolution of gas bubbles could be observed before breakdown, particularly for No. 4 filtered oil. With oil filtered through a No. 5 filter, several breakdowns could take place before bubbles appeared before breakdown, while with oil filtered with the coarser filter, bubbles appeared before each breakdown. To ensure consistency of test samples the oil, in this case, was changed after each test.

As mentioned already, there was no significant difference in the electrical strength values of the degassed oil when electrodes made of copper, steel, aluminum, and chromium were used, but stainless steel electrodes always gave higher values. With increasing air content stainless steel electrodes still gave higher values, but the difference between the values obtained with electrodes of this metal and those of other metals varied with the air content. As a rule the difference decreased at first as the air content was increased and became more marked again as the air content reached the saturation value.

In all cases the electrical strength remained the same when the gap spacing was varied over a range of about 25-130 μ, but there was a definite electrode area effect. As can be seen from Table I, the electrical strength was nearly 50% higher when ½ in. diameter spherical electrodes were used instead of plate electrodes with an effective area of 3 mm diameter. The results in Table I were chosen to

Table I. Selection of electrical strength values obtained with different electrodes and oil samples; gap spacing 100μ throughout

Electrodes					
Geometry	Metal	Conditions of oil	No. of breakdowns	Electric strength, kv/cm	Coeff. of variation, %
½ in. diam. spheres	Stainless steel	No. 5 filtered, degassed	50	1225	6.0
1 in. diam. hemispheres	Stainless steel	No. 5 filtered, degassed	40	1060	7.8
Plates of 3 mm effective area	Stainless steel	No. 5 filtered, degassed	40	845	4.1
½ in. diam. spheres	Aluminum	No. 5 filtered, degassed	40	950	8.1
½ in. diam. spheres	Stainless steel	No. 4 filtered, degassed	40	1025	6.0
½ in. diam. spheres	Chromium	No. 4 filtered, degassed	50	865	7.9
½ in. diam. spheres	Steel	No. 4 filtered, degassed	40	890	6.0
½ in. diam. spheres	Copper	No. 4 filtered, degassed	60	886	6.1
½ in. diam. spheres	Aluminum	No. 4 filtered, degassed	50	880	7.5
½ in. diam. spheres	Stainless steel	No. 4 filtered, air saturated at 760 mm Hg	30	670	5.9
½ in. diam. spheres	Aluminum	No. 4 filtered, air saturated at 760 mm Hg	30	570	10.5

illustrate that the various factors which affect the strength of the oil (such as electrode metal and size, filter porosity, etc.) do not mask each other when present together but seem to have a cumulative effect.

Influence of Electrode Metal and Polarity

Because of the observed dependence of the electrical strength on the electrode metal, some tests were made using different metals for anode and cathode in order to examine which of the two electrodes played the predominant role in the breakdown. With uniform field configurations it was found, on the whole, that, when the air content of the oil was low, breakdown depended on the metal of the cathode, but the situation changed as more air was dissolved, and for oil saturated with air at 760 mm Hg the metal of the anode seemed to become important.

To establish more definitely the presence of any anode or cathode dependence tests also were made with unsymmetrical field configurations by using a point-plate electrode system. With such a system the electrical field at the two electrodes is different, and tests with different polarities of the applied voltage should, therefore, reveal more readily the presence of any anode or cathode dependence of the breakdown. For degassed oil, and making the plate electrode the cathode, there was a pronounced cathode dependence, and different breakdown voltages were recorded for different cathode metals. When the oil was saturated with air the role of cathode and anode was reversed. In this case the breakdown voltage did not vary for different cathode metals, but reversing the polarity resulted in breakdown values which depended on the metal of the plate electrode which was now the anode.

Conditioning Effect

Many tests were made to study the conditioning process, and it would appear that, for clean oil at any rate, conditioning is an electrode effect. The experiments have shown that, once the electrodes were conditioned in a particular oil sample, they remained conditioned and the same breakdown values were obtained when the electrodes were retained and the sample was replaced by another one of the same kind. The use of new electrodes, however, made fresh conditioning necessary.

The conditioning was more effective when carried out at high hydrostatic pressures. For example, with electrodes conditioned at reduced pressure, subsequent measurements showed a pressure dependence of the breakdown, but this dependence was not so marked, and sometimes even absent (see curve No. 1 of Fig. 4) when the electrodes were previously conditioned at atmospheric pressure. Evacuation of the test cell before filling with oil was important, and short evacuation periods, on the whole, produced low ultimate strength values. All this seems to indicate that the conditioning process is connected with the establishment of equilibrium conditions of adsorbed air on the electrode surface (5). This is further supported by the observation that the presence of air in the oil causes downward conditioning, while for carefully degassed oil upward conditioning, as well as occasional no conditioning, could be observed.

It would appear from the tests that for degassed oil it is the cathode which is responsible for the conditioning. Experiments using nonuniform field configurations seem to confirm this. With a point-plate electrode system conditioning was observed only when the point electrode was positive and it was absent for the negative point breakdown.

Finally, the conditioning process is slower and more gradual, the larger the effective electrode area and the smaller the energy dissipated during breakdown. When a capacitor is connected across the test gap to increase the discharge capacitance, only a few breakdowns are required to complete the process. It is also dependent on the hardness of the electrode metal, and for aluminum, the softest metal used, conditioning was found to be absent, in agreement with previous observations (5).

Discussion

The observed variation of the electrical strength of the oil with air content and its dependence on the hydrostatic pressure suggest strongly that breakdown takes place in the gaseous phase. The experimental results given above provide further evidence in support of the qualitative picture of the break-

down mechanism which was put forward some time ago (6).

According to this, two processes are involved when breakdown takes place. In the first place electrons must be introduced into the gap and it was suggested that this takes place by emission from the cathode, and second, the number of these initial electrons must be adequately multiplied in the bulk of the liquid by some ionization process. As for gas discharges, breakdown will take place when the total electron yield assumes a critical value. Whatever the nature of the second process it will involve the formation of an electron avalanche extending across the electrode gap, and the total electron yield will depend on both the number of initial electrons supplied by the first process and the size of the avalanche which is limited by the electrode spacing.

All the results reported here were obtained from tests using gap settings which were exceedingly small compared with the electrode size, so that the build-up of the avalanches was restricted. Under these conditions, the electron yield necessary for breakdown can be established only if the number of initial electrons fed into the avalanche by the first process is sufficiently large. For these very small gap settings one would expect, therefore, that the breakdown is governed by this process; this was borne out by experiments which showed a marked conditioning effect, a dependence on the electrode metal, and an electrode area effect. The measured breakdown fields of the degassed oil were sufficient for an adequate electron emission from the cathode, and moreover it is very probable that this process was facilitated by an enhanced cathode field due to the presence of positive ions near this electrode and separated from it by an insulating oxide film.

With larger gaps, on the other hand, the size of the avalanche is not so restricted. This will facilitate the electron multiplication process, and adequate electron yield will be possible with a small number of initial electrons, so that the role of the first process will be of minor importance. This was confirmed by Jayasekara (7). Using a large-scale testing technique with gap settings of several millimeters he found that, as the gap setting was increased, the conditioning effect and the dependence of breakdown on the electrode metal became less marked until, for sufficiently large gaps, both were absent. With these larger gaps there was no electrode area effect, but instead a marked gap dependence of the breakdown strength was observed.

The experiments have shown that small additions of air to the degassed oil produce a rapid increase in breakdown strength. Since for small spacings the latter is largely governed by the supply of initial electrons, it would appear reasonable to assume that the additional air must interfere in some way with the first process and render it less effective. This may be accomplished by an electron attachment mechanism, and the trapping of electrons by oxygen molecules is suggested as such a possibility.

The observed fluorescence of the oil may be taken as an indication that electrons with energies of several electron volts were present in the highly stressed region of the oil. Electrons impinging with these high energies may cause chemical dissociation of suitable constituents of the oil, resulting in the formation of H_2 or other substances of low molecular weight. When the local concentration of the gas molecules produced in this way exceeds the solubility of the gas in the oil, gas bubbles will form, and it is suggested that breakdown takes place by the ionization of such gas bubbles. Little or no pressure dependence was found for the breakdown in this region. However it should be realized that, although a pressure dependence may be taken as evidence that the gaseous phase is involved in the breakdown mechanism, the reverse is not necessarily true. It is possible that the field required for gas evolution and bubble formation is so high that, once bubbles are formed, ionization can take place irrespective of the prevailing hydrostatic pressure.

As the air content is increased further the electrical strength falls again, and all the evidence seems to show that the role of the dissolved air in the breakdown process becomes important. It would seem reasonable to suppose that, with increasing air content, less energy will be required for the detachment of the dissolved gas molecules and their subsequent aggregation into micro bubbles so that such bubbles can form in the oil and on the electrode surfaces. Breakdown will be produced by ionization of these air bubbles and will depend on the hydrostatic pressure, as was shown by the experiments. The bubble formation also will depend on particle impurities in the oil since these will offer preferred sites for nucleation. Moreover for oil containing air, the particle impurities themselves may carry micro bubbles which may act as nuclei for further bubble growth. This would explain the higher strength values which were obtained when finer filters were used for the filtration of the oil.

Hence the dissolved air will facilitate the ionization process so that more ions will be introduced into the oil as its air content grows. There will be a tendency, therefore, for space charge formation, aided by the viscosity of the oil. By changing the field distribution in the gap, the space charge will influence the breakdown process, and this will become more pronounced as the air content is increased. The positive space charge which will form in the vicinity of the cathode will enhance the cathode field and weaken the field in the remainder of the gap. The general effect of the space charge will, therefore, be to confine the ionization to the cathode region, and a higher applied voltage will be required to extend it toward the anode. Thus, although the conditions for the establishment of the two processes involved in the breakdown become more favorable as the air content of the oil is increased, it is quite reasonable to expect that, beyond a certain air content, a higher breakdown voltage may be required because of the field constricting effect of the space charge. Thus for aerated oil the observed variation of the electrical strength with air content, which is of the Clark type, may well be explained by the effect of space charges.

Manuscript received Feb. 23, 1960. This paper was prepared for delivery before the Philadelphia Meeting, May 3-7, 1960.

Any discussion of this paper will appear in a Discussion Section to be published in the December 1961 JOURNAL.

REFERENCES

1. A. Khambanonda, Ph.D. Thesis, University of London (1958).
2. M. Darveniza, *Nature*, **183**, 743 (1959).
3. A. M. Sletten, *ibid.*, **183**, 311 (1959).
4. F. M. Clark, *J. Franklin Inst.*, **215**, 39 (1933).
5. R. Hancox and H. Tropper, *Proc. I.E.E.*, Part A, **105**, 250 (1958).
6. M. E. Z. El-Dine and H. Tropper, *ibid., Part C*, **103**, 35 (1956).
7. W. P. Jayasekara, Ph.D. Thesis, University of London (1957).

The Synthesis and Crystallography of Structurally Pure Cubic and Hexagonal Single Crystals of ZnS

Harold Samelson and Vincent A. Brophy

Bayside Laboratories, General Telephone & Electronics Laboratories Inc., Bayside, New York

ABSTRACT

A sealed tube vapor phase method for growing zinc sulfide single crystals of either a structurally pure hexagonal or structurally pure cubic form is described. In the former case, the crystals are of a high degree of chemical purity, but to effect the latter, KCl is employed as an additive and this results in crystals of somewhat uncertain chemical purity. The nature of the faulting commonly found in zinc sulfide is discussed, and the effect of this on the x-ray diagrams is described. The morphology of the structurally pure crsytals is described in some detail.

One of the basic needs of any investigation of the physical properties of zinc sulfide is pure material. Here, the word "pure" refers not only to the chemical residuals but also, and with equal importance, to the deviations from regularity in the crystalline structure. Both of these factors can cause variations in optical, electrical, and crystallographic properties of zinc sulfide. In addition to this, since these properties are directional in some cases, the form of the material for the necessary measurements must be single crystals large enough to be manipulated easily in experiments.

Naturally occurring crystalline zinc sulfide satisfies the requirement of structural purity. It can be found in the cubic (F $\bar{4}$3m) and hexagonal (C 6mc) forms and also as polytypes whose unit cell is larger than that of the cubic or hexagonal crystals. Unfortunately, the natural crystals are highly contaminated, as much as 10%, and one of the common impurities is iron, a luminescence killer. Attempts in this laboratory to leach out these impurities have met with failure since the crystal disintegrated after treatment.

Growing structurally pure crystals synthetically is difficult. Even though one has control over the ingredients and can keep the chemical purity high, the crystals themselves will not be structurally coherent throughout their bulk. Zinc sulfide transforms from cubic to hexagonal above 1020°C (1), and there is evidence to suggest that another transition occurs above about 1240°C[1] where a pseudocubic structure will form. The customary methods (2, 3) for the preparation of zinc sulfide crystals result in crystal growth at a temperature between these transition temperatures and usually produce a structurally impure crystal which may be considered a mixture of the two-layer (hexagonal) and three-layer (cubic) modifications. Another method (4) provides for growth well above 1240°C where the crystals are of the reversed pseudocubic type.

In this paper we shall discuss the nature of the faults commonly found in synthetic zinc sulfide crystals and the means of detecting them as well as the preparation of a chemically and structurally pure hexagonal crystal and structurally pure cubic crystal doped with 1.0 and 0.5 mole % KCl. The latter-type crystal has not been reported in the literature prior to this.

Structural Considerations (5)

Since all zinc sulfide crystals are built up from close-packed layers and can be oriented with respect to a hexagonal set of axes, the reason for the structural impurity can be observed readily by looking at the atoms in the (11.0) plane (Fig. 1). Here, we are looking at the layers edgewise. Each layer, as it adds onto the one below, has a choice of two positions. The cyclic repetition of the layers as they build up determines the space group to which the crystal will belong. An alternation between any two positions leads to the hexagonal form; ABABAB; BCBCBC; CACACA. The face-centered type arises from the sequential repetition of all three positions; ABCABCABC or ACBACBAC. . . If either of these sequences is interrupted during growth by a layer choosing the alternate position, rather than the specific position necessary for maintaining the space group symmetry, a fault is formed. A large number of faults in any crystal is referred to as one-dimensional disorder. Faults repeated in a regular sequence result in the formation of polytypes.

[1] This phase change is suggested from x-ray investigation of crystals grown at varying temperatures. These x-ray results were obtained on crystals from more extensive experiments than are reported here.

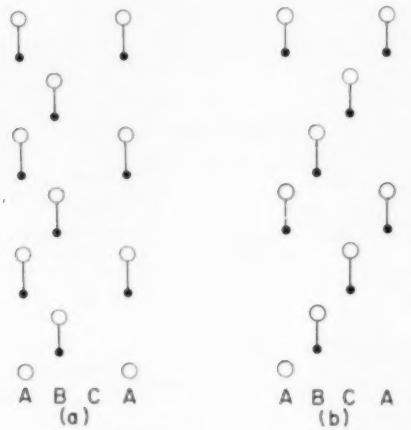

Fig. 1. Stacking of hexagonal (a) and cubic (b) ZnS; • Zn; o, S.

The detection of faults in these crystals is relatively easy. They can be examined between crossed nicols along the general direction [h.k.0] in a polarizing microscope. The appearance of birefringence banding, as illustrated in Fig. 2, indicates the presence of faults. However, the absence of such banding does not prove that there are no faults. The most positive means of detecting them is by single crystal x-ray diffraction, and the technique of the precession camera is advantageous since it eliminates multiplicity effects. Precession films of an unfaulted and a faulted crystal, taken with the x-ray beam perpendicular to (11.0) are illustrated in Fig. 3a and 3b. In one, the vertical rows of spots are sharp while in the other the spots are streaked along the rows. The streaking of spots is caused by faults (6), and only spots corresponding to planes of the type where $h-k \neq 3n$ are streaked.

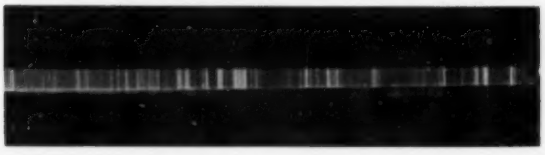

Fig. 2. Crystal of ZnS in polarized light showing banded birefringence.

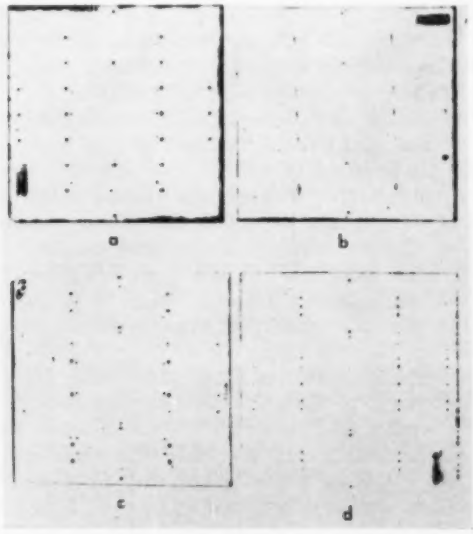

Fig. 3. X-ray precession diagrams of various ZnS crystals: (a) pure hexagonal, 2-layer, sharp spots; (b) disordered hexagonal, smeared spots; (c) reversed cubic; (d) mixed hexagonal and reversed cubic.

In the hexagonal system, the principal type of stacking fault is the intrusion of a three-layer sequence in a dominantly two-layer repeat sequence. This is indicated in Fig. 4a. The limit of detection of this type of fault is about one in a thousand layers. A frequency less than this will probably not lead to a streaking of the x-ray spot which is easily detected. In the cubic system, twinning is the principal fault as is seen in Fig. 4b. This system is unique in that detection of any odd number of faults down to one is possible. This arises from the threefold symmetry about the "c" axis or body diagonal. A single fault twins the two portions it separates, and the reciprocal lattices of the two portions are rotated 60° with respect to one another. As can be seen in Fig. 3c, this causes specific spots of one lattice to occupy lattice positions in the other which normally are absences, and the x-ray pattern, by layer lines, shows a cubic or three-layer identity distance along c^* (reciprocal lattice axis), with a pseudosixfold symmetry about c^*.

These x-ray patterns can be compared with those obtained from crystals whose preparation is described below. Figure 3a illustrates the x-ray pattern of a hexagonal crystal, and it is seen that the spots are sharp and there is no evidence of smearing. Figure 5a is that of a cubic crystal, and it is seen that it is cubic and there is no sixfold symmetry about c^*. This absence of sixfold symmetry is also seen in Fig. 5b which is a Laue pattern. Copper radiation was used in all the x-ray work.

Preparation and Properties of the Crystals

The crystals are prepared by a sealed tube method similar to that used by Tomlinson (2) and Reynolds (3). The furnace used in these experiments and a typical temperature gradient are illustrated in Fig. 6. An experimental run consists of two parts; the

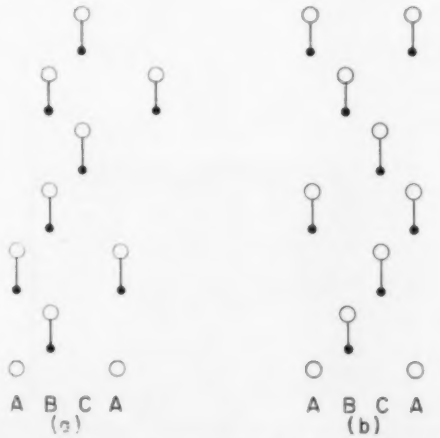

Fig. 4. Stacking sequence of faulted ZnS crystals; • Zn; o, S

outgassing step, and the growth step. The ZnS, either pure or doped with KCl, is put in quartz tubes 8 in. long and 1½ in. in diameter, and these are outgassed. For pure runs, this is done at 825°C and for KCl doped runs it is done at 525°C to avoid excessive loss of additive. The outgassing is continued at the specified temperature until the pressure falls to 10^{-4} mm. In the case of a pure run, the tube is then cooled and 15 cm of H_2S is added. It is then heated to 850°C in the H_2S environment and kept there for 30 min. After this, it is cooled to 825°C and the H_2S pumped out. When the pressure has again fallen to 10^{-4} mm, the outgassing furnace is removed and the tube allowed to cool to room temperature. Hydrogen sulfide is then added to a pressure between 10 and 15 cm, the tube sealed, and put in the furnace for a growth run. In the case of the KCl additive, the second heating step is omitted and, after the first addition of H_2S, the tube is sealed and put in the furnace for a growth run.

The pure runs which result in hexagonal crystals are started at a hot zone temperature of 1100°C. This is increased slowly at about the rate of 10°C per day for fourteen days until the hot zone temperature reaches 1230°C. The linear temperature gradient is adjusted to provide a temperature which varies from 900° to 1020°C in the cold end of the tube. In this type of experiment, a transfer of 15 g of material is effected in the stated time. The crystals, exclusively of the rod type, about 0.5 to 1.0 cm long and about 0.1 mm in diameter, are found about 2 in. from the cold end of the tube. This fixes the maximum growth temperature at 1090°C. The majority of these crystals are of the pure hexagonal structure, have sharp x-ray diagrams as shown in Fig. 3a, and microscopic examination shows a uniform birefringence with no evidence of banding, as seen in Fig. 7. The major impurities in these crystals are copper at 2 ppm, silicon at 7 ppm, and chlorine at 20 ppm. Other cation impurities are not detected which limits their individual concentrations to less than 1 ppm.[2]

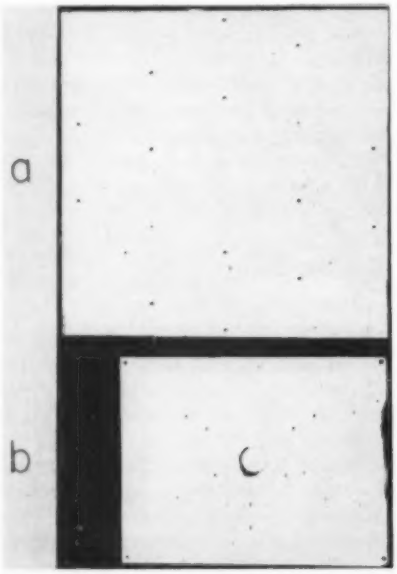

Fig. 5. (a) Precession photograph of true face-centered cubic ZnS crystal; (b) Laue photograph of this crystal showing the three-fold symmetry and absence of sixfold symmetry.

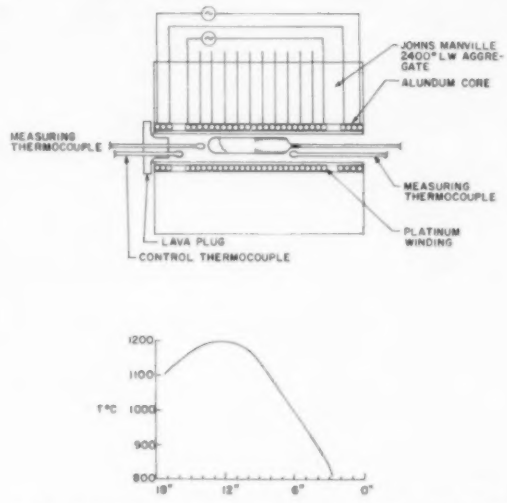

Fig. 6. Furnace used in the experimental work and a typical temperature gradient.

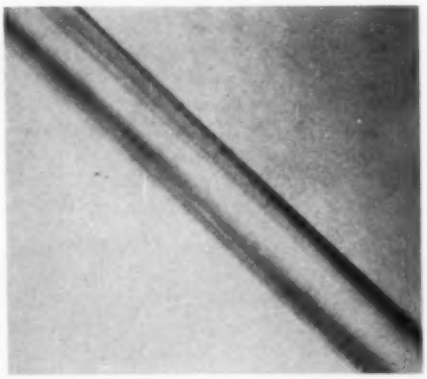

Fig. 7. Photograph of hexagonal crystal in polarized light with a quarter wave compensating plate. The crystal shows no banding of birefringence.

The KCl doped runs require a much steeper gradient. These runs have a duration of 7-10 days. The initial temperature of the hot zone is 1100°C and is increased to 1150°C in a uniform manner for the first half of the run and is kept at the higher temperature for the remaining time. The cold end temperature varies from 550° to 600°C in this time. The crystals are generally found within 2 in. of the cold end so that the maximum growth temperature is 800°C.

The crystals resulting from these runs are thin plates from 10 to 200 μ thick and have an area which varies from 1 mm^2 to 1 cm^2. The flat faces of these crystals are the (111) planes of the cubic system and the bounding edges, when they provide good reflections, are usually found to be the (110) type.

[2] Cation analyses were performed spectrographically using a d-c arc technique and the total energy method described by Slavin (7). The instrument used was an Ebert 1st order grating spectrograph, and the cations analyzed for were: Cu, Ag, Mn, Ni, Pb, Fe. Chlorine was analyzed by a nephelometric method which has a precision of 10%, and potassium was determined by a flame photometer to a precision of 20%.

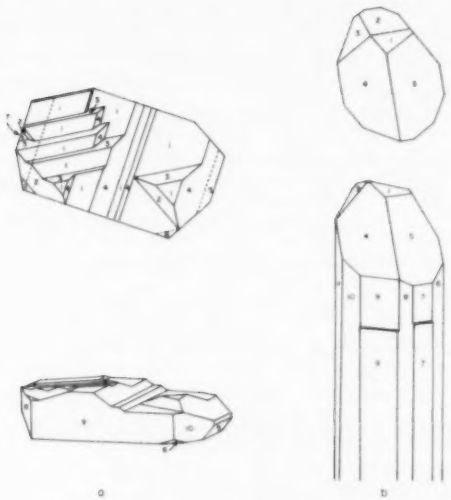

Fig. 8. Drawings of typical hexagonal and cubic crystals indicating the faces which are found.

One surface of the crystal, the flat side facing the hot end, frequently shows triangular geometrical markings. This is illustrated in Fig. 8. The other side, the one facing the cold end, usually shows contour markings. These markings are strongly suggestive of the spiral surface markings reported by Amelinckx (8) and Verma (9) on silicon carbide which grows with the same morphology as these ZnS crystals. We have not, however, seen any individual spirals such as these other workers report. The x-ray patterns of the majority of these crystals indicate a pure cubic structure as shown in Fig. 5a and 5b. Chemically, these crystals show the same impurities in the same amounts as the pure crystals, except that the potassium and chlorine found are generally half the amount that had been added to the original charge. In all these experiments, the tubes were cooled at the rate of 2°C/min to a hot zone temperature of 600°C. After annealing at this temperature for 15 min, the tubes are removed from the furnace.

In Fig. 8 there are slightly idealized drawings of two typical zinc sulfide crystals, both of which are pure structural types, as ascertained by x-ray diffraction. The platelike crystal is cubic face centered and shows large (111) type faces on both sides of the plate. These (111) planes are broken mainly by dodecahedral faces and occasionally by (100) type faces. The angular relations between the observed faces can arise only from a pure cubic structure. The rod-like crystal is hexagonal close packed and shows both (10.0) and (11.0) type faces about its trunk. It is capped by (10.2) and (10.4) type faces. The cap faces when used to calculate the c/a ratio give a value of 1.640 which agrees closely with that for zinc sulfide calculated from x-ray diffraction (1.638). A list of the indices of the observed faces is given in Table I.

Table I. Crystal faces

Face No.	Crystal a		Crystal b
	3-Layer hexagonal index	Cubic index	Hexagonal index
1	00.1	111	10.4
2	10.4	110	$\bar{1}$1.4
3	01.4	101	01.2
4	$\bar{1}$1.4	011	1$\bar{1}$.2
5	$\bar{1}$1.2	$\bar{1}$00	10.2
6	01.4	1$\bar{4}\bar{1}$	11.2
7	$\bar{1}$1.4	4$\bar{1}\bar{1}$	10.0
8	21.0	10$\bar{1}$	21.0
9	11.0	01$\bar{1}$	1$\bar{1}$.0
10	$\bar{1}$2.0	$\bar{1}$10	$\bar{1}$2.0
11	01.0	$\bar{1}$21	01.0

Discussion

In both of these types of experiments the essential factor appears to be the growth temperature of the crystals. Indeed, it appears to be far more critical for the hexagonal than the cubic crystals. In the case of the cubic crystals, the low growth temperature is achieved by a combination of the steep gradient and the KCl additive. Even though the potassium alters the morphology, through using it, the growth temperature can be brought so low that the heat of condensation cannot raise the temperature of the growing crystal above the first transition point. If the gradients used are smaller, so that the cold end temperature and the growth temperature are higher, the resulting crystals are largely of the reversed cubic structure and the pure cubic structure is an infrequent event.

The situation with regard to the hexagonal crystals is, as has been said, more critical. The growth temperature has to be confined to a range of about 200°C. The problem here is made even more complicated because the rod-like morphology is one in which it is more difficult to dissipate the heat of condensation. If one tries to keep the growth temperature low enough to avoid crossing the second transition point at 1240°C, it may cross the lower one at 1020°C. However, if it turns out that these temperature conditions are properly adjusted, structurally pure hexagonal crystals can be obtained.

Summary

In this paper, the types of structure faults commonly encountered in zinc sulfide single crystals have been described and discussed. The temperature conditions for the growth of structurally pure crystals of either type have been presented. These can be achieved in a chemically pure system for hexagonal crystals, but the presence of KCl in a concentration of 0.5-1.0 mole % was helpful in producing the cubic crystals described in this work. Lower concentrations of KCl were not effective. Finally, a model has been presented which helps understand why, even though the temperature conditions may appear to be satisfied, the resulting crystals may be faulted.

Acknowledgment

The authors would like to take this opportunity to express their appreciation to Mr. W. S. Romito for his help in conducting the growth experiments, to Mr. S. R. Kellner for his help in the X-ray work, to Mr. S. Weissberger for the cation analyses, and to Mr. R. Weberling for the chlorine analyses.

Manuscript received July 14, 1960. This paper was prepared for delivery before the Chicago Meeting, May 1-5, 1960.

Any discussion of this paper will appear in a Discussion Section to be published in the December 1961 JOURNAL.

REFERENCES

1. E. T. Allen, J. L. Crenshaw, and H. E. Merwin, *Am. J. Sci.*, **34**, 341 (1912).
2. T. B. Tomlinson, *J. Electronics*, **2**, 293 (1956).
3. D. C. Reynolds and S. J. Czyzak, *Phys. Rev.*, **79**, 543 (1950).
4. D. C. Reynolds, L. C. Greene, S. J. Czyzak, and W. M. Baker, *J. Chem. Phys.*, **29**, 1375 (1958).
5. The existence and nature of stacking faults and one-dimensional disorder in ZnS have been discussed by: (*a*) H. Jagodzinski and F. Laves, *Schweiz Min & Petrogr. Mitteilungen*, **28**, 456 (1948); (*b*) H. Jagodzinski, *Acta Cryst.*, **2**, 201, 208, 298 (1949); (*c*) H. Muller, *Neues Jb. Min. Geol. u. Pal.*, **84**, 43 (1952); (*d*) L. Strock and V. A. Brophy, *Am. Mineral.*, **40**, 94 (1955).

In this section we base our discussion on these previous works and in particular point out the necessity of detecting the rotation twin type of fault in the cubic structure with some special technique as the precession camera.

6. A. J. C. Wilson, *Proc. Roy. Soc. London*, [A] **180**, 277 (1942).
7. M. Slavin, *Ind. and Eng. Chem., Anal. Ed.*, **10**, 407 (1938).
8. S. Amelinckx, *Phil. Mag.*, **43**, 562 (1952).
9. A. R. Verma, "Crystal Growth and Dislocations," Academic Press Inc., New York (1953).

Infrared Enhancement and Quenching of Photoconduction in Single Crystals of ZnS:Cu

F. G. Ullman[1] and J. J. Dropkin

Department of Physics, Polytechnic Institute of Brooklyn, Brooklyn, New York

ABSTRACT

An ohmic infrared photoconductivity peaking at 0.65 and 1.35 μ has been observed at room temperature in synthetic single crystals of ZnS:Cu. The photocurrents are constant with time, not dependent on any previous excitation, and linear with intensity. With simultaneous 3650Å ultraviolet (UV) and infrared (IR) the resultant photocurrents are less than the sum of the separate UV and IR photocurrents as measured independently. The spectral dependence of this so-called "quenching" and also of the IR absorption are similar to that of the IR photoconductivity (as well as to quenching and stimulation spectra reported for ZnS:Cu powder phosphors elsewhere). If each of these is assumed to arise from the same transition, the quenching phenomenon can be interpreted to be an electron-carrier UV photocurrent quenched by a hole-carrier IR photocurrent as in a Schoen-Klasens model. Both the IR photocurrent and the IR quenching decrease sharply at low temperatures and apparently require thermal activation.

Infrared (IR) quenching of photoconduction which has been excited by shorter wave lengths is a well-known phenomenon (*e.g.*, 1-5) that is now commonly attributed to the injection of minority carriers by IR. Most quenching studies have been concentrated on CdS (2-4) except for the recent work of Broser and Warminsky (5) on fluorescent synthetic crystals of ZnS:Cu. The absence of steady photocurrents excited by the quenching radiation alone has been attributed to the small mobility or lifetime of minority carriers in CdS and ZnS (6, 7). [Transient stimulation effects have been observed in CdS (2-4). IR photocurrents have been found in ZnS powder phosphors after previous UV excitation (8, 9).] We have found a steady IR photocurrent in nonluminescent, synthetic crystals of ZnS:Cu that does not depend on previous UV excitation. We have studied the wave-length and temperature dependence of this IR photocurrent, of IR enhancement and quenching of 3650Å photocurrent, and also the room-temperature IR absorption spectrum. These results are described below and are compared with the work of others on IR quenching of fluorescence, and on excitation of IR emission in ZnS:Cu phosphors.

[1] Present address: Physical Research Department, The National Cash Register Company, Dayton, Ohio.

Experimental Results

Description of crystals.—Single crystals of ZnS:Cu were deposited from the vapor phase by sublimation of unactivated ZnS powder in an atmosphere of flowing helium (10, 11). They were approximately rectangular plates (approximate dimensions of 0.2 x 0.5 x 1.5 mm) and were colorless, transparent, and nonluminescent. They were used as grown, except for one larger crystal that was polished into a rectangular plate for optical measurements. The streaking of certain reflections in the x-ray rotation diagram indicated that these crystals have stacking faults in the cubic [111] direction, often found in synthetic ZnS crystals (12). All of the reflections could be indexed on the basis of the cubic cell of ZnS. However, the selective streaking of the reflections and the optical birefringence of these crystals indicated that their true symmetry is probably rhombohedral (12) and not cubic even though the unit cell has three equal sides and all angles 90°.

From conventional spectrographic analysis, crystals from the same batch as those studied were found

to contain of the order of 10-100 ppm of Cu and no other detectable impurity. The ZnS powder from which the crystals were grown contained not more than 1 ppm of Cu. The increase in Cu concentration may have occurred by fractional distillation or by furnace contamination.

Electrical behavior.—All photoconduction measurements were made in vacuum and with silver paste electrodes.

Photocurrents were obtained with excitation by 2537Å, 3650Å, and in two regions of the infrared peaking at about 0.65 and 1.35 μ. For all exciting wave lengths the photocurrent rose slowly, reaching a steady value in about 30 sec and decayed in about the same time when the excitation was removed. The dark current was usually less than 10^{-14} amp even at the maximum applied voltage of 1100 v (about 10^4 v/cm) and could be ignored.

The dependence of these photocurrents on applied voltage was ohmic except for small deviations below about 10 v. To illustrate these deviations, the lower voltage portions of the current-voltage characteristics for three different spectral regions and one polarity are shown in Fig. 1. (The low voltage deviations are not apparent on the compressed scale needed to plot the full characteristic.) The low voltage deviations in the white light curve are typical of the largest deviations from ohmic behavior observed. Most of the measurements were made at 400 v where the behavior was ohmic.

Some space-charge polarization was evidenced by observable reverse currents on illumination of the shorted crystals. However, these were always less than 1% of the forward current, even after one or two hours polarizing time, and decayed to zero in less than 30 sec, leading us to assume that the polarization effects were small.

Dependence of photocurrent on light intensity.—Four different light sources were used in these measurements, a Beckman DU spectrophotometer for studies of wave-length dependence, a General Electric germicidal lamp for 2537Å radiation, a General Electric EH-4 lamp with a 3650Å narrow-band-pass filter, and an American Optical Company Model 370 microscope illuminator for visible and near infrared (white light). The white light source was filtered with a Corning No. 2540 filter to pass only wave lengths longer than 0.9 μ ("far" IR) or with a saturated acid solution of ferrous ammonium sulfate ($Fe(NH_4)_2(SO_4)_2$)—to which a few drops per liter of concentrated H_2SO_4 were added to prevent decomposition—to pass only wave lengths shorter than 0.9 μ ("near" IR). The intensities of the light sources were varied with neutral Wratten gelatin filters, calibrated for the three spectral regions of interest. The intensity of 2537Å radiation was varied by changing the distance between the light source and the crystal.

For all wave lengths longer than the fundamental absorption band[2] only a linear dependence of photocurrent on light intensity was found over about four orders of magnitude, the range of photocurrent that was measurable. Typical photocurrent *vs.* intensity curves for the three spectral regions of interest are shown in Fig. 2 (Measurements were not continuous over the full range so only part of the range is shown in the figure.)

IR photocurrent.—An IR photocurrent that was independent of UV excitation and did not decay with time was found in all the crystals examined. The wave-length dependence of this photocurrent was investigated from 0.5 to 2.0 μ and typical spectra are shown in Fig. 3 (the meaning of the labels "quenched" and "enhanced" are discussed in the next section). These data have been corrected to conditions of isophotonic incident light. The uncorrected spectrum has a peak at about 0.9 μ and a somewhat smaller peak at 1.35 μ. In the corrected spectra the percentage ratio of the 1.35 μ peak to the 0.65 μ peak was not constant from crystal to crystal and varied from 2 to 13%.

[2] From a rough check of the 2537Å photocurrent over an intensity range of about an order of magnitude, a square root dependence on light intensity was found which is consistent with a band gap transition.

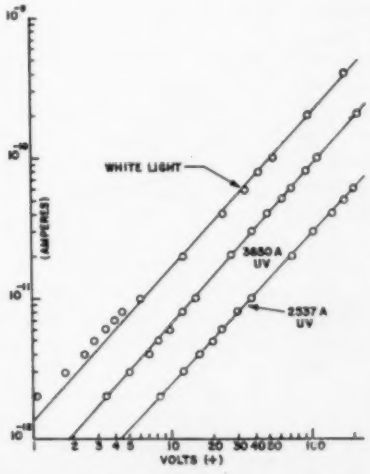

Fig. 1. Current-voltage characteristics for photocurrents excited by various wave lengths.

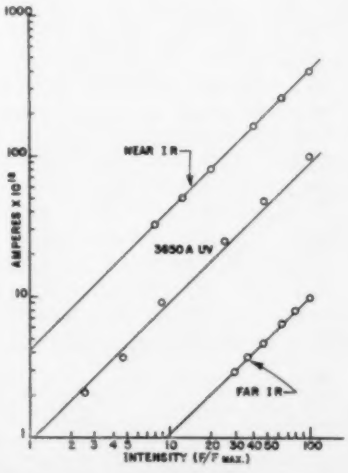

Fig. 2. Dependence of photocurrent on light intensity for various wave lengths.

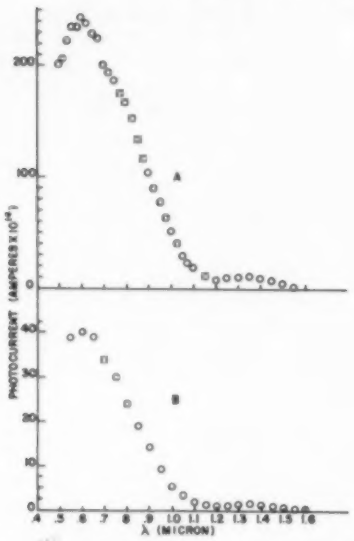

Fig. 3. IR photocurrent spectra: A, "enhanced" crystal; B, "quenched" crystal.

IR absorption.—The relative absorption of several crystals was determined from their measured per cent transmission, and an absorption peak corresponding to the first photocurrent peak was found in all crystals. The changes in absorption in the vicinity of 1.35 μ, however, are very small; hence the second peak was resolved in only one specially selected, thick crystal that was polished into a rectangular plate about 0.6 mm thick. These results are shown in Fig. 4. (The peak at shorter wave lengths is not shown since the transmission was too small to measure below 0.8 μ with this thick sample.) The scatter in the points is indicative of the fact that we were working at the limit of our precision in these measurements. (Since the present authors reported this work at the ECS Meeting in New York in 1958, Halsted, Apple, and Prener (13) have verified these absorption data.)

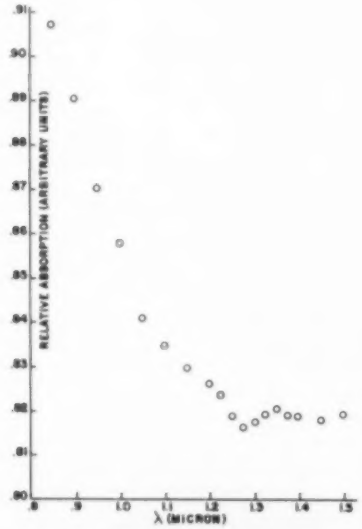

Fig. 4. IR absorption spectrum

Effect of IR on the UV Photocurrent.—In all crystals IR produced the photocurrents described in the previous section. In some crystals the UV photocurrent was quenched by IR and in some enhanced. ("Quenched" crystals also showed enhancement when the UV photocurrent was smaller than the IR photocurrent.) In all crystals, however, the photocurrent excited by simultaneous UV and IR was always less than the sum of the UV and IR photocurrents as measured separately. Since all photocurrents depended linearly on intensity, linear superposition should have occurred unless some recombination quenching was taking place. We concluded that quenching was occurring in all crystals and could be measured in "enhanced" crystals as well as "quenched" crystals by subtracting the contribution of the simultaneously excited IR photocurrent. The per cent IR quenching was defined as

$$\% \text{ quenching} = [I_v - (I_{v,r} - I_r)/I_r] \times 100 \quad [1]$$

where I_v is 3650Å UV photocurrent,[3] I_r is IR photocurrent, and $I_{v,r}$ is photocurrent excited by simultaneous UV and IR. It is readily seen that if I_r is small compared to $I_{v,r}$, Eq. [1] reduces to the usual expression for quenching. Enhancement is defined in the usual way as

$$\% \text{ enhancement} = [(I_{v,r} - I_r)/I_r] \times 100 \quad [2]$$

We studied the wave-length dependence of both IR quenching and enhancement. Typical quenching spectra, one for a "quenched" crystal and one for an "enhanced" crystal, are shown in Fig. 5 and an enhancement spectrum is shown in Fig. 6. The isophotonic correction has been applied to these spectra, also. Special care was taken to restrict the measurements to an intensity range for which $I_{v,r}$ was

[3] IR has the same effect on the 2537A photocurrent as on the 3650Å photocurrent. The former was not studied in detail to avoid the complications introduced by the simultaneous excitation of both electrons and holes by 2537Å radiation.

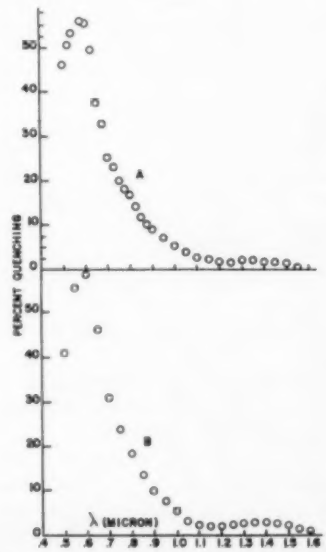

Fig. 5. Spectral dependence of IR quenching of 3650Å UV photocurrent: A, "enhanced" crystal; B, "quenched" crystal.

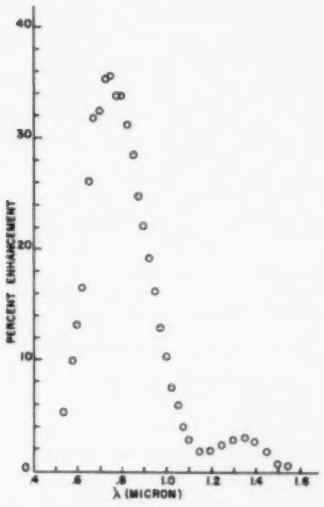

Fig. 6. Spectral dependence of IR enhancement of 3650Å UV photocurrent.

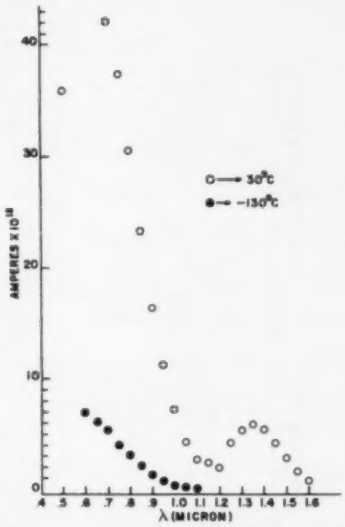

Fig. 7. Spectral dependence of IR photocurrent at −130°C (room temperature spectrum shown for comparison).

linear with intensity (which was not true in general) so that this linear correction could be applied. This was not realizable for wave lengths shorter than about 0.7μ. This nonlinearity at shorter wave lengths had an effect on the shape of the spectra which will be discussed in a later section.

Temperature dependence of IR sensitivity.—Both the IR photocurrent and the IR quenching were found to require thermal activation. Temperature measurements were made with an iron-constantan thermocouple located adjacent to the crystal. (Since the crystals were too small to attach the thermocouple directly to them, the true temperature could have differed somewhat from the measured temperature.) At −160°C I_r was too small to measure ($< 10^{-14}$ amp) and there was no IR quenching of I_r even with the relatively high intensity of the white light source. At −130°C quenching was observable but too small to measure, and I_r could only be observed in the neighborhood of the 0.65μ peak. I_r at −130°C is shown in Fig. 7. For comparison, the room-temperature spectrum for the same crystal is also shown. Since the relative peak heights in the corrected spectra may be misleading, it should be noted that the intensity distribution of the source actually favored the 1.35μ peak. In the actual room temperature measurements the 1.35μ photocurrent was of the same order of magnitude as the 0.65μ photocurrent (measured peak at 0.9μ). At −130°C the 1.35μ photocurrent was four orders of magnitude smaller than at room temperature and barely measurable, whereas the 0.65μ photocurrent was reduced by only a factor of about four. Quenching effects and the 1.35μ photocurrent became measurable at −100°C.

Since the slow rise and decay of photocurrent indicated the possible existence of a high density of shallow traps in these crystals, thermally stimulated current measurements were made to obtain information about such traps, if present. No thermally stimulated current peaks were found even after several hours of UV or IR excitation at low temperatures. In all cases, however, a reproducible, thermally activated, dark current was observed on heating to about 150°C. A rough determination gave an activation energy of 1.3 ev. This current was completely independent of IR or UV excitation at any temperature (even several hours of low temperature excitation had no effect), a result that led us to the tentative conclusion that these were ionic currents. Recent results of others, discussed in a later section, indicate that this conclusion is false.

Discussion of Results

In the nonluminescent ZnS:Cu crystals studied, we have found that IR excites a steady photocurrent, independent of any previous UV or IR excitation, and having the same spectral dependence as the IR quenching and enhancement of 3650Å photocurrent, and as the IR absorption (Fig. 3-7). Similar spectra have been reported for IR quenching of fluorescence (8, 9) and excitation of IR emission (14) in ZnS:Cu phosphors. These results, ours and others, point to the conclusion that all of these phenomena arise from the same IR induced transitions. We propose, as have others, that these transitions are best represented in an energy band model of the Schoen-Klasens type [*e.g.* ref (19)].[4] This implies, in accordance with Kroeger's Hall effect measurements (17)[5] and some recent Russian work (16), that the 3650Å UV photocurrent in ZnS:Cu is electronic in nature and also that the IR photocurrent in the same phosphor is a hole current. The effect of IR on the UV photocurrent will be either enhancement or quenching depending on whether or not the addi-

[4] The Lambe-Klick (15) model cannot be conveniently applied since in that picture fluorescence quenching and photocurrent quenching arise from different transitions, unless two sets of discrete states with coincidentally identical activation energies are postulated.

[5] The fact that Kroeger's measurements were on ZnS:Cl crystals and ours on ZnS:Cu is probably not significant. Many activators produce a long wave-length UV absorption in the neighborhood of 3650Å which has led Klasens (19) to ascribe this absorption to lattice states perturbed in energy by the presence of the activator or by equivalent vacancies produced by a co-activating impurity.

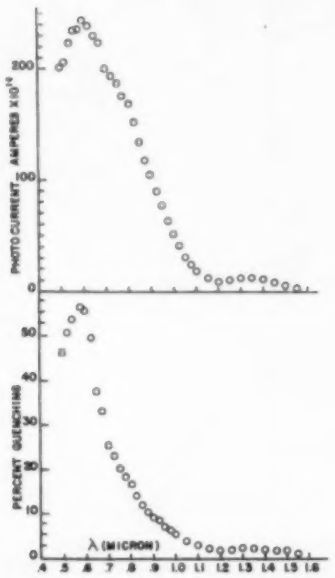

Fig. 8. Comparison of the spectral dependence of IR photocurrent with IR quenching of 3650Å UV photocurrent; upper curve, IR photocurrent; lower curve, IR quenching.

tional hole carriers are of greater or lesser importance than the decrease of electron carriers by recombination with holes.

The model assumed in this paper was suggested by that postulated by Dropkin and Goldstein (9) for IR quenching in the ZnS:Cu:Co:Cl phosphor. In their model IR excites holes from excited Cu luminescent centers to two discrete states lying near the valence band. These holes are then thermally excited into the valence band and recombine with quenching centers or other hole traps.[6]

We have claimed above that the IR photocurrent spectra and the IR quenching or enhancement spectra are identical. However, there are minor differences between these spectra. One spectrum of each type is shown in Fig. 8 for comparison. The bandwidths of the shorter wave-length peaks in the photocurrent spectra are all about 30% greater than the corresponding bandwidths in the quenching spectra. We considered the possibility that this difference was caused by superposed electron currents. If this were so, the enhancement spectrum should be the same as the photocurrent spectrum. This is not the case. The enhancement spectrum shown in Fig. 6 has the same shape as the quenching spectra within experimental error. (There are small differences in the location of the shorter wave-length peak arising from the application of a large isophotonic correction to the small differences between I_0 and I_{0+r} in this region of the spectrum.) This bandwidth difference appears to have resulted from our application of a linear isophotonic correction to the quenching and enhancement spectra which actually had a complex sub-linear dependence on intensity below about 0.7μ. I_r was linear at all wave lengths, and therefore the photocurrent spectra have a different shape from the quenching and enhancement spectra. There is no difference in the bandwidths of the longer wavelength peaks where linearity obtained in all cases.

The temperature dependence we have found is in good agreement with the results of Dropkin and Goldstein. Broser and Warminsky (5), however, find that only the 1.35μ band requires thermal activation. We do not know the reason for this discrepancy, but it is not uncommon to find differences in behavior in the same phosphors prepared in different ways. Their crystals were luminescent and therefore were not the same, chemically, as ours. For example, they find the well known 1.2μ stimulated luminescence at 77°K, and also an accompanying 1.2μ photocurrent (also observed by Dropkin and Goldstein). There was no sign of this 1.2μ sensitivity in our crystals, at any temperature.

The thermally activated dark current that we initially attributed to ionic conductivity had about the same activation energy as the p-type conductivity recently reported by Potter and Aven (20) for ZnS:Cu crystals. Klasens (21) has pointed out that, if the Fermi level in our crystals was low enough, p-type conductivity with this activation energy might be expected and previous excitation would have little or no effect

It is worthwhile at this point to speculate about the nature of the Cu impurity in our crystals which seem to have had some special properties. We would expect from the conditions of preparation that the Cu in our crystals was largely uncompensated. Uncompensated Cu in ZnS should exhibit properties similar to excited Cu centers in luminescent ZnS, such as we have observed. The same IR sensitivity which we have observed has been found by others in ZnS:Cu phosphors (8, 9, 14, 22) but only after UV excitation. [Kastner, Potter, and Aven (23) have found a similar IR reflectance without excitation in phosphors with some uncompensated Cu.] To observe the steady IR photocurrents that we have found, without excitation, it seems clear that the Cu impurity must be largely uncompensated. The 3650Å absorption in our crystals, however, must be associated with some compensated Cu or possibly with accidentally coactivated Zn vacancies.

We have found no satisfactory explanation of the linear intensity dependence of the 3650Å UV and IR photocurrents in these crystals. Strong trapping as a possible hypothesis was investigated, but the only evidence we have found is the slow rise and decay time of the photocurrents.

Finally, our observation of a hole-carrier photocurrent does not necessarily mean that the hole mobility is larger than it has been thought to be in the past; strong trapping could have resulted in a large enough effective lifetime for low mobility hole currents to be observable, if the traps were shallow.

Summary of Results and Conclusions

Nonluminescent single crystals of ZnS:Cu have been shown to exhibit the same IR sensitivity that is normally associated with excited ZnS:Cu phosphors. IR quenching of UV photocurrent, IR absorption, and a steady IR photocurrent that does not

[6] Meijer (18) has proposed a similar model for IR fluorescence of ZnS:Cu phosphors.

require previous UV excitation have been shown to have the same spectral dependence. This IR photocurrent is a new phenomenon in ZnS that has not previously been reported. We have interpreted it to be a hole-carrier photocurrent in accordance with a Schoen-Klasens model.

Acknowledgments

The authors would like to thank Professors I. Fankuchen and B. Post for the use of their x-ray laboratory and the interpretation of the x-ray data. They would also like to thank Professor W. Kiszenick for growing the crystals and for helpful advice and discussion.

Manuscript received June 30, 1960; revised manuscript received Oct. 10, 1960. This paper is part of a dissertation submitted by one of the authors (F.G.U.) in partial fulfillment of requirements for the Ph.D. degree to the Polytechnic Institute of Brooklyn. This paper was prepared for delivery before the New York Meeting, April 27-May 1, 1958. Research was supported by the U. S. Air Force through the Office of Scientific Research of the Air Research and Development Command under Contract AF 18(600)-692.

Any discussion of this paper will appear in a Discussion Section to be published in the December 1961 JOURNAL.

REFERENCES

1. A. E. Hardy, *Trans. Electrochem. Soc.*, **87**, 355 (1945).
2. E. A. Taft and M. H. Hebb, *J. Opt. Soc. Am.*, **42**, 249 (1952).
3. S. H. Liebson, *This Journal*, **102**, 529 (1955).
4. R. H. Bube, *Phys. Rev.*, **99**, 1105 (1955).
5. I. Broser and R. Broser-Warminsky, *J. Phys. Radium*, **17**, 791 (1956).
6. H. S. Sommers, Jr., R. E. Berry, and I. Sochard, *Phys. Rev.*, **101**, 987 (1956).
7. R. E. Halsted, *ibid.*, **99**, 1897 (1955).
8. N. T. Melamed, *This Journal*, **97**, 33 (1950).
9. J. J. Dropkin and B. Goldstein, Polytechnic Institute of Brooklyn Symposium on Electroluminescence and Photoconduction in Inorganic Phosphors, 1955.
10. D. C. Reynolds and S. J. Czyzak, *Phys. Rev.*, **79**, 533 (1950).
11. A. Kremheller, *Sylvania Tech.*, **8**, 11 (1955); *This Journal*, **107**, 422 (1960).
12. L. W. Strock and V. A. Brophy, *Amer. Mineralogist*, **40**, 94 (1955).
13. R. E. Halsted, E. F. Apple, and J. S. Prener, *Phys. Rev. Letters*, **1**, 134 (1958).
14. P. F. Browne, *J. Electronics*, **1**, 95 (1956).
15. J. Lambe and C. C. Klick, *Phys. Rev.*, **98**, 909 (1955).
16. U. Kh. Nymm and L. Ia. Uibo, *Bull. Acad. Sci. USSR*, **21**, 648 (1957).
17. F. A. Kroeger, *Physica*, **22**, 637 (1956).
18. G. Meijer, *J. Phys. Chem. Solids*, **7**, 153 (1958).
19. H. A. Klasens, *This Journal*, **100**, 72 (1953).
20. R. M. Potter and M. Aven, *Bull. Am. Phys. Soc.*, **4**, 227 (1959).
21. H. A. Klasens, Private communication.
22. V. V. Antonov-Romanovskii and I. P. Shukin, *Dokl. Akad. Nauk. SSSR*, **71**, 445 (1950).
23. J. Kastner, R. M. Potter, and M. Aven, Extended Abstracts (#33) of Papers Presented by the Electronics Div., Electrochemical Society Meeting, New York, 1958.

Some Optical Properties of Powder and Crystal Halophosphate Phosphors

P. D. Johnson

Research Laboratory, General Electric Company, Schenectady, New York

ABSTRACT

Diffuse reflectivity and excitation spectra of powder and optical absorption of synthetic single crystal halophosphate phosphors have been determined in the spectral region 1100-3000Å. Intrinsic optical absorption by the host lattice begins at approximately 1500Å in fluoroapatite and 1570Å in chloroapatite. Absorption in bands of manganese in fluoroapatite at 1600, 1750, and 2150Å results in luminescence in the absence of antimony. Absorption due to antimony lies between 1600 and 2900Å. The preparation and some optical properties of synthetic single crystals are described.

Until recently, fundamental investigations of optical and electrical properties of the commercially important oxygen-containing phosphors have been impeded by their chemical and crystallographic complexity, the unavailability of single crystals of many of them, and the general lack of understanding of mechanisms of luminescence in inorganic solids. In recent years the understanding of the optical and electrical properties of ionic and covalent inorganic phosphors such as the alkali halides and the II-VI compounds has progressed to the point where a study of the more complex phosphors promises to be fruitful. For this work we have selected the halophosphate phosphors having the structure and composition of apatite, $3[Ca_3(PO_4)_2] \cdot CaX_2$ where X is F or Cl or a mixture.

Most of the measurements reported here were made on powder phosphors containing manganese and antimony separately and together and on unactivated halophosphates. From diffuse reflectivity and excitation spectra of these powders we have determined the energies at which intrinsic optical absorption of the host crystals takes place, as well as the energies of transitions characteristic of the activators, manganese and antimony. These data have been supplemented by spectral transmission measurements on synthetic crystals whose preparation is described.

Experimental

The powder phosphors were made by usual commercial procedures at the General Electric Chemical Products Plant. Although most of the work has been on fluorophosphates, some data have been obtained on chlorophosphates, on 0.3 chloro-0.7 fluorophosphates, and on fluorophosphates with 90% of the stoichiometric amount of CaF_2. The unactivated powders have luminescent efficiencies less than 1% of the deliberately activated phosphors and thus probably contain of the order of 10 ppm of Sb and Mn.

Activated halophosphates can be fused in air, CO_2, or nitrogen in Pt-Rh alloy crucibles for brief periods with retention of the luminescence characteristics of the original phosphor powder. The melting points of both the chloro- and fluorophosphates are approximately 1650°C. Without seeding, the melts tend to supercool, as much as 300°C below the melting point in the case of the pure fluorophosphate. Crystals can be grown by slow cooling of the melt accompanied by seeding at the appropriate temperatures. In some cases small hexagonal single crystals up to 2 mm long and 0.3 mm across are obtained, slightly larger than crystals made by Hayek and his co-workers (1) by a hydrothermal method. In addition, nearly clear polycrystalline pieces up to 3 x 5 x 8 mm in dimensions are obtained. These latter pieces have been used for optical transmission measurements.

More recently, by using the Kyropoulos method, pulling with a Pt-20% Rh rod from a melt in an induction heated Ir crucible, crystals of fluorophosphate up to 5 cm long and 1 cm in maximum diameter have been made. Some pieces cut from a single boule are shown in Fig. 1. Opalescent inclusions along the center of the boule and straining and cracking of the crystals are minimized by suitable radiation shielding, limiting the diameter of the boule to about 6 mm or less, and using pulling rates of less than 10 mm/hr. Large crystals of chlorophosphate have not been made since considerable loss of $CaCl_2$ occurs at the melting temperature.

Unactivated, nearly stoichiometric, crystals of fluorophosphate are water white. Manganese can be introduced easily by incorporating it into the melt. Antimony is difficult to introduce during growth because of volatilization of the oxide and segregation preferentially into the melt. The luminescence of activated single crystals is polarized, with the electric vector mainly parallel to the crystal optic axis.

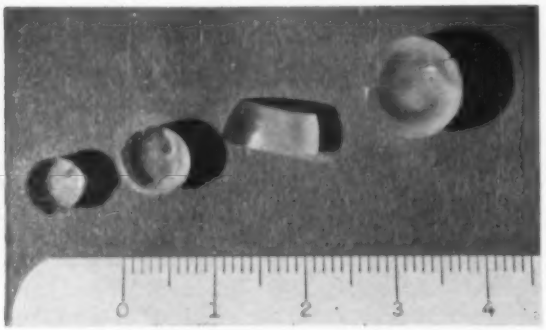

Fig. 1. Photograph of synthetic calcium fluorophosphate single crystals cut from a single crystal boule.

X-ray powder diffraction patterns of synthetic fluorophosphate crystals are identical to that of a natural crystal from Durango, Mexico, and the line positions and intensities agree within the accuracy of observations with the published (2) values for apatite. One cannot be assured that the crystals are stoichiometric since the apatite diffraction pattern is found in nonstoichiometric samples (3). It is possible to detect the strongest diffraction line of α-calcium orthophosphate in the powder diffraction pattern of a polycrystalline boule grown at a rate of greater than 5 cm/hr from a melt of $3[Ca_3(PO_4)_2] \cdot \sim 0.95(CaF_2)$. The difficulty of obtaining perfect stoichiometric crystals is emphasized by the fact that color centers are introduced by x-ray irradiation. The observed color depends on the stoichiometry of the melt. In some cases the x-rayed crystals are dichroic, absorption occurring when the electric vector of the incident radiation is parallel to the optic axis of the crystal.

The optical measurements were made with a 1-m normal incidence grating vacuum monochromator (4). Powder reflectivity and excitation spectra were made using plaques of standardized size, 2/3 mm thick at 45° incidence. The relative output of the monochromator as a function of wave length was determined using as the detecting phosphor sodium salicylate, which has uniform quantum efficiency as a function of wave length in the spectral region under study up to 3000Å. Reflectivity at wave lengths from 2000 to 4000Å was determined relative to MgO. The output of the monochromator was compared to the reflected intensity from 1100 to 3000Å. By matching the curves in the overlapping spectral region from 2000 to 3000Å reflectivity could be determined from 1100 to 4000Å. Suitable filters were placed at the exit slit to eliminate other than first order spectra during the measurements at longer wave lengths.

Results and Discussion

The diffuse reflectivities of fluorophosphate and chlorophosphate powders with no deliberately added impurities show an abrupt decrease with decreasing wave length at about 1500Å in the fluorophosphate and about 1570Å in the chlorophosphate, as shown in Fig. 2. The reflectivities do not change significantly in the wave-length region 1100-1500Å. It can be calculated (5) that the absorption in this region of low reflectivity is greater than 2000 cm^{-1}. Since this absorption intensity cannot be accounted for by the impurities known to be present, it is concluded tentatively that intrinsic optical absorption begins at 7.9 ev in chlorophosphate and at 8.2 ev in the fluorophosphate. A sample with 0.7 CaF_2 and 0.3 $CaCl_2$ has intrinsic absorption beginning at approximately 8.1 ev. Preliminary normal incidence specular reflectance measurements on both synthetic and natural crystals of fluorophosphate show an increase in reflectance in the neighborhood of 1500Å

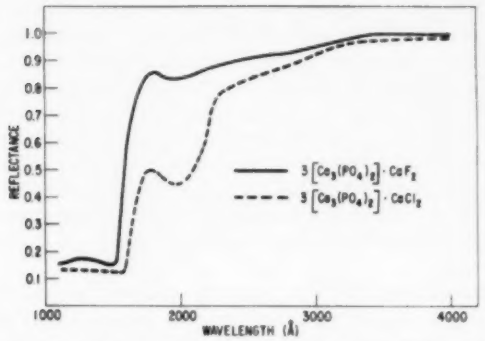

Fig. 2. Diffuse reflectance of choro- and fluorophosphate powders with no deliberately added activators.

rising to a peak at 1320Å and another peak at 1180Å, confirming the conclusion that electronic transitions of the host lattice are responsible for absorption above 8.2 ev.

It is less certain that the absorption bands at 1900Å in the fluorophosphate and 2000Å in the chlorophosphate are intrinsic. The optical absorption of a synthetic fluorophosphate crystal, shown in Fig. 3, reaches 200 cm^{-1} at 1900Å. This value may be accounted for by transition or heavy metal impurities which are present in a molar cation concentration of up to 2×10^{-4}. The absorption is not due to departure from stoichiometry since the reflectivity of $3[Ca_3(PO_4)_2] \cdot 0.9[CaF_2]$ at 1900Å is not significantly different from stoichiometric material.

The effect of adding Mn and Sb, the activators most commonly used in halophosphate lamp phosphors, on the diffuse reflectivity of fluorophosphate is shown in Fig. 4. Manganese alone depresses the reflectivity in three unresolved bands at 1600, 1750, and 2150Å (see also Fig. 6). This absorption is probably due to divalent Mn. Strong absorption in this spectral region by divalent Mn has been found in MnF_2 films (6) and in ZnF_2:Mn crystals (7). Slight depressions of reflectivity in the Mn-activated samples at wave lengths longer than 2500Å and extending into the visible are probably due to Mn in higher valence states. Less than the stoichiometric amount of Ca in the host lattice of samples with Mn as the only activator tends to suppress these longer wavelength bands.

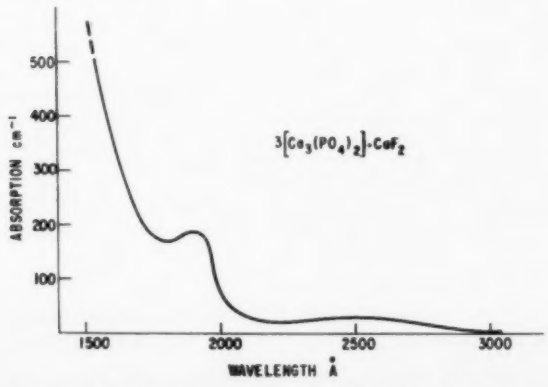

Fig. 3. Optical absorption of synthetic calcium fluorophosphate crystal.

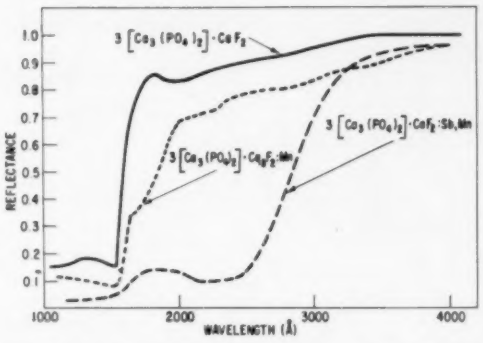

Fig. 4. Diffuse reflectance of calcium fluorophosphate powders with and without added activators.

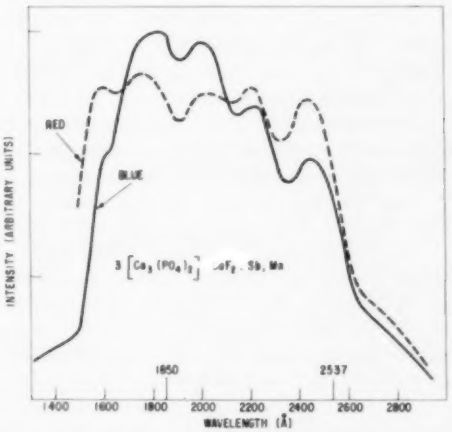

Fig. 5. Excitation spectra of $3[Ca_3(PO_4)_2]\cdot CaF_2$:Sb, Mn powder. Solid line, antimony emission; dashed line, manganese emission.

Trivalent Sb introduces a broad absorption extending from the intrinsic absorption at 1500Å to about 3000Å. The reflectivity of samples containing Sb and no Mn is the same as that shown in Fig. 4 for a sample containing both activators. There is some structure in the depression of reflectivity due to Sb in the spectral region from 1600 to 2600Å which is too small in amplitude to show up in Fig. 4. The differences in reflectivity in the fundamental absorption region result from the larger particle size of the activated powders. The maximum absorption due to Sb is at least 2000 cm^{-1} in samples with approximately 1% Sb. It should be noted that the reflectivity at 2537Å, where the principal excitation in fluorescent lamps takes place, is appreciably higher than at the minimum. The absorption at this wave length is of the order of 1000 cm^{-1}. Reflectivity spectra of chlorophosphates differ very little from those shown for the fluorophosphates either in intensity or wave length.

The excitation spectrum of calcium fluorophosphate containing both Sb and Mn is shown in Fig. 5, where emission intensity divided by excitation intensity is given as a function of wave length of excitation. The solid line is the excitation spectrum for the blue Sb emission, with 3 mm of Pyrex and a Corning 5030 filter between the phosphor and the

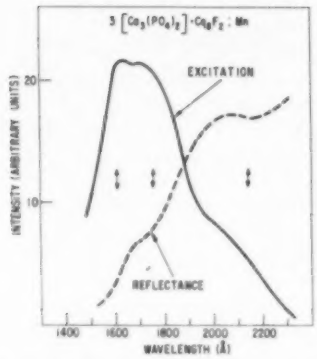

Fig. 6. Excitation and reflectance spectra of calcium fluorophosphate activated by manganese alone.

RCA 5819 photomultiplier, and the dashed line is the excitation spectrum for the red Mn emission, using Pyrex and a Corning No. 3480 filter. The excitation spectrum of fluorophosphate containing Sb and no Mn is the same as that shown for the Sb emission.

The structure mentioned in connection with the reflectivity spectra is clearly in evidence in the excitation spectra. This strongly resembles the structure in the absorption of Sn^{+2} in alkali halides (8). Trivalent Sb and divalent Sn are isoelectronic, and in both phosphors the activator is substituted for a cation of one less positive charge. Thus, except for the difference in crystal symmetry, similar behavior might be expected in the two cases. The principal difference is in the energy range included in the spectra. The excitation peaks of Sb^{+3} in calcium fluorophosphate include energies from 4.6 to 8 ev, whereas the six absorption peaks of Sn^{+2} in KCl range only from 4.3 to 5.5 ev. The separation of the $^1P_1^o$ and $^3P_1^o$ states of the 5s5p configuration differs by less than 15% in the free Sn^{+2} and Sb^{+3} ions. If it is postulated, by analogy with the identification of transitions of Tl^+ in KCl (9) that the excitation and absorption bands of Sn^{+2} and Sb^{+3} result from transitions from the $^1S_0$ to the $^3P^o$ and $^1P^o$ states as modified and split by the crystal interactions, a similar range of transition energies might be expected in the two cases. That the actual ranges differ so much may be due in part to the anisotropy of the crystal field of the fluorophosphate lattice. There is of course some question as to the validity of interpreting spectra in this phosphor on the basis of the tight binding approximation.

Although transfer of energy from Sb to Mn takes place upon excitation in all of the bands of Sb, there is no evidence for the reverse transfer. The fact that excitation of Mn at 1600Å is relatively more effective as compared to some of the other bands may be attributed to direct excitation of the Mn as will be seen subsequently.

As might be expected from the reflectivity spectra, excitation of both emission bands is less effective at 2537 than at 1850Å. Excitation at 1850Å results in more effective excitation of Sb as compared to manganese than excitation by 2537Å in the fluorophosphate. Thus, modification of the 1850/2537 intensity ratio in fluorescent lamps is expected to have at least a minor effect on the color of luminescence.

Excitation in the spectral region of host lattice absorption does not result in efficient luminescence in either the Mn or Sb emission bands. The decrease in efficiency is so abrupt that it cannot be due to the increase in specular reflectivity near the fundamental absorption edge. Energy transfer from host lattice to activator is less efficient than de-excitation at sites other than the activators, possibly surface states.

Manganese emission may be excited in the absence of Sb by radiation in the wave-length region of Mn absorption as shown in Fig. 6. The three unresolved minima in reflectance are at the same wave lengths as the three excitation maxima. Actually it is only in the excitation spectrum that the 1600Å band of Mn^{+2} is observed unobscured by host lattice or antimony absorption.

Conclusions

Absorption and excitation spectra characteristic of calcium halophosphate host lattice and of the activators Mn and Sb have been investigated in the spectral region 1100-3000Å. The host lattices have forbidden energy gaps of approximately 8 ev. Divalent Mn shows strong absorption from 5.5 to 8 ev and trivalent Sb from about 4.5 to 8 ev.

Large single crystals of the halophosphates can be grown from the melt. The study of polarized luminescence, dichroic optical absorption, and other optical and electrical properties of these crystals should make possible the elucidation of the luminescent mechanisms occurring in this important class of phosphors.

Acknowledgments

The author is indebted to G. Lloyd for assistance with some of the reflectivity measurements, to F. C. Mostek for assistance in the optical measurements and crystal growing, and to Dr. John Ross of the General Electric Chemical Products Plant for the specially prepared phosphors.

Manuscript received Aug. 29, 1960. This paper was prepared for delivery before the Chicago Meeting, May 1-5, 1960.

Any discussion of this paper will appear in a Discussion Section to be published in the December 1961 JOURNAL.

REFERENCES

1. Hayek, Böhler, Lechleitner, and Petter, *Z, anorg. u. allgem. Chem.*, **295**, 241 (1958).
2. American Society for Testing Materials, X-Ray Powder Data File (1959).
3. A. S. Posner, Silicium, Schwefel Phosphate Colloq. Sek. Anorg. Chem. Intern. Union Reine U. Angew Chem., Munster 207 (1954).
4. P. D. Johnson, *J. Opt. Soc. Am.*, **42**, 278 (1952); *Rev. Sci. Inst.*, **28**, 833 (1957).
5. P. D. Johnson, *J. Opt. Soc. Am.*, **42**, 978 (1952).
6. W. W. Parkinson and F. E. Williams, *J. Chem. Phys.*, **18**, 534 (1950).
7. P. D. Johnson and F. L. Hughes, *ibid.*, **26**, 612 (1957).
8. M. Hueniger and J. Rudolph, *Z. Physik*, **117**, 81 (1941).
9. P. D. Johnson and F. E. Williams, *Phys. Rev.*, **117**, 964 (1960).

Study of Copper Precipitation Behavior in Silicon Single Crystals

G. H. Schwuttke

General Telephone & Electronics Laboratories Inc., Bayside, New York

ABSTRACT

The precipitation behavior of copper in silicon single crystals containing different amounts of oxygen has been investigated within the temperature range of 900°-1300°C. Precipitation which occurs during the cooling period on structural defects and at random sites throughout the bulk crystal has been detected by infrared transmission microscopy. The shape and crystallographic relationship of the precipitate as related to the silicon matrix was determined. The reliability of the method of copper decoration for the determination of low dislocation densities in the presence of oxygen was investigated by comparing copper decoration pictures with x-ray diffraction photomicrographs.

Dislocations in silicon can be investigated effectively by the copper decoration method as introduced by Dash (1). In applying this method to the study of imperfections in Si we have found that the precipitation behavior of Cu is strongly influenced by the presence of imperfections and impurities. Therefore specific investigations were conducted to clarify: (*a*) influence of impurities on Cu decoration of dislocations; (*b*) reliability of dislocation counts by means of Cu decoration, especially in the presence of impurities; (*c*) shape of the precipitate; and (*d*) crystallographic relationship of the precipitate to the matrix.

The results of these investigations are reported in this paper.

Experimental set-up.—To observe precipitation in Si an infrared microscope was assembled similar to the one described by Deutschbein and Bernard (2). The basic part of our set-up is a Reichert microscope Type Me F. The eyepiece of the microscope was replaced by a snooperscope tube. An infrared-sensitive videcon tube, Type Resistron,[1] was mounted in place of the 35-mm attachment of the microscope. The snooperscope eyepiece was used for low magnification. The videcon was used in connection with a closed circuit TV for higher magnification. The advantage of the TV camera is essentially its high magnification factor which allows the use of a low-power objective for better contrast. Photomicrographs presented in this paper were taken by photographing either the snooperscope or TV screen. This procedure was more convenient than using infrared sensitized plates.

Specimen preparation.—The standard decoration procedure was to place a few tiny drops of copper nitrate solution on the sample surface and to diffuse at temperatures varying from 900° to 1300°C for about 1 hr. Samples were quenched to room temperature either fast within a few seconds by dropping them on a cold surface or slowly up to a few minutes by leaving them in the quartz boat after removal from the furnace. After diffusion the samples were ground to a thickness of 1 mm and highly polished.

[1] Supplied by Physikalische Werkstaetten, Professor Heimann, Wiesbaden-Dotzheim, Germany.

Survey of Precipitation Behavior of Copper

Precipitation is observed after diffusion of Cu into Si crystals at higher temperatures and subsequent cooling to room temperature. The precipitation occurs entirely during the period of cooling. The amount of precipitation depends on diffusion temperature and cooling rate.

To investigate the influence of impurities on the precipitation behavior of Cu, high-purity crystals of approximately 2,000 ohm-cm resistivity grown by the floating zone method were compared with crystals of low resistivity containing different amounts of oxygen.

Figure 1 shows part of a dislocation line as obtained by the decoration of a crystal of high-purity, p-type, 2000 ohm-cm resistivity, grown in the floating zone. Copper was diffused at 900°C for 1 hr

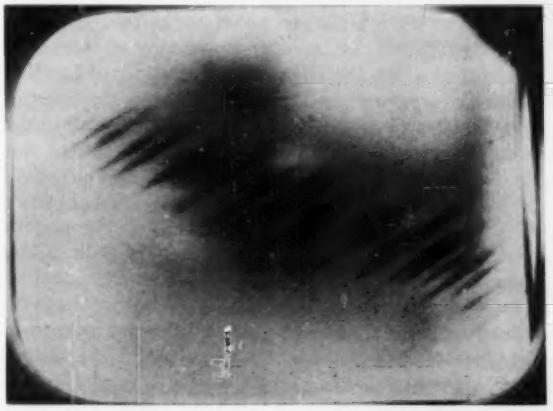

Fig. 1. Part of a decorated dislocation line in a silicon crystal of high purity, p-type, 2000 ohm-cm. Magnification 1500X; all magnifications in this paper are before reduction for publication.

Fig. 2. Part of a decorated dislocation line in a silicon crystal containing oxygen, p-type, 30 ohm-cm. Magnification 1500X.

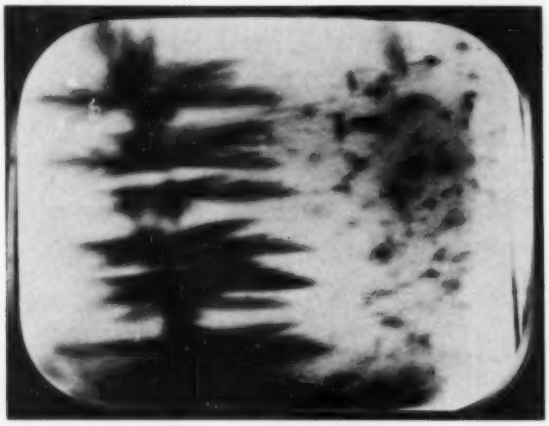

Fig. 3. Part of decorated dislocation line in a silicon crystal containing oxygen, p-type, 30 ohm-cm. Magnification 250X.

after which the crystal was quenched to room temperature within a few seconds. The dislocation density in this crystal, as measured by counting etch pits, was $10^5/cm^2$. The Cu has precipitated in needles, which point in <110> directions. The needle size is approximately 20-30μ. Remarkable for this type of crystal is the well-defined needle shape of the precipitate, their orderly arrangement along the lines, and the fact that no other precipitation is found elsewhere in the crystal. Higher diffusion temperature and slower cooling rates do not produce any marked changes in the precipitation picture for this type of crystal.

In crystals of lower purity, considerable differences can be observed. In addition to decorated dislocation lines, precipitation in isolated spots is found. Changes in diffusion temperature and cooling time have a pronounced influence on the precipitate. The shape of the precipitate along dislocation lines as well as in isolated areas can take a variety of complicated forms. Figure 2 represents part of a decorated dislocation line in a p-type crystal of 30 ohm-cm resistivity containing 4×10^{17} atoms oxygen per cm^3. Copper was diffused at 900°C for 1 hr and the sample was quenched to room temperature within seconds. The line is decorated by a row of composite structures which look like crosses built up of needles. A cloudy structure around and between the crosses, more or less pronounced, can be observed also in the original, which does not show up in the photo due to lack of contrast. In comparison, a heavily decorated dislocation line is shown in Fig. 3 as obtained in a similar crystal of slightly higher oxygen concentration; this time Cu was diffused at 1200°C and the cooling rate was 1 min. Due to the slow cooling rate, the dislocation line is heavily decorated with rather large deposits. The size of the precipitate in this case is approximately 300μ while in Fig. 2 it is approximately 20-30μ.

Broad dislocation lines, approximately 50μ wide, of the type shown in Fig. 4 are also found in these crystals. At lower magnification this type looks like a broad straight line; at higher magnification, as shown in Fig. 4, it appears to have the form of a

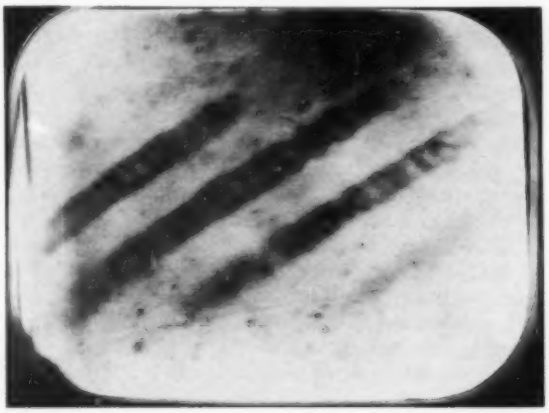

Fig. 4. Decorated dislocation line in silicon containing oxygen. This type was observed only on {111} planes, in <110> directions. Magnification 250X.

hollow cylinder. Since this type is always found on {111} planes in <110> directions, we assume that it is a decorated screw dislocation.

There is also precipitation at random sites throughout the bulk of the crystal. If diffusion is done at lower temperature, 900°-1000°C and the crystal is quenched within seconds to room temperature, the deposits are of the order of 10μ in size and have simple needle shape or structures which look like crosses built from needles. If diffusion is done at high temperature up to 1300°C and the crystals are cooled slowly, within 2 min, the deposits will grow in size. An extreme size of 1 mm is not unusual to observe. Such needle structures are shown in Fig. 5. Copper was diffused at 1300°C and the sample quenched to room temperature within 1 min. The plane of observation is a {100} plane. The needles point in <110> directions.

In addition to these simple forms more complex structures are frequently observed. Figure 6 shows a deposit found quite often in areas of high oxygen concentrations. The striking characteristic of these precipitates is the pronounced structure of spines in various <110> directions. Size and development

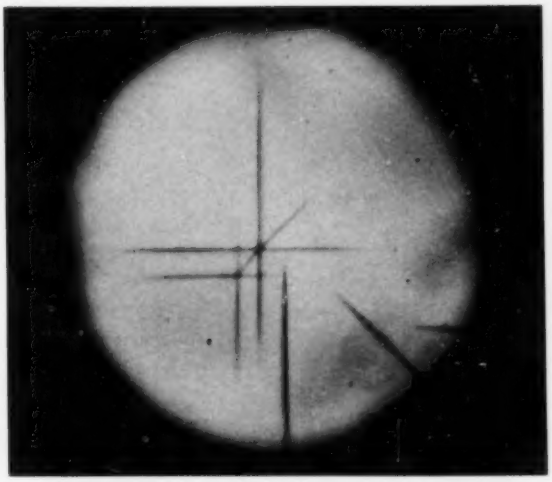

Fig. 5. Composite structure of copper precipitate in Si built up of needles in {100} planes, quenched from 1300°C. Magnification 100X.

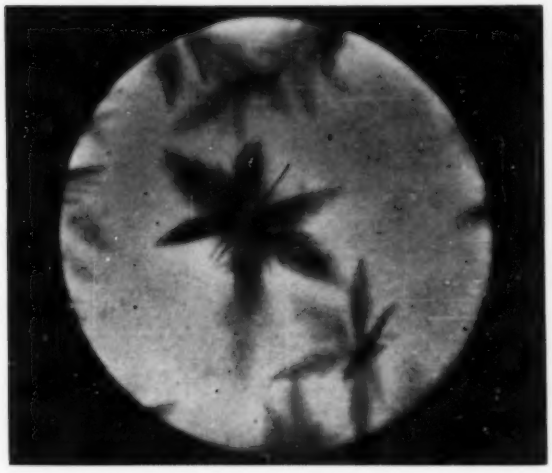

Fig. 6. Close up of a copper precipitate in silicon. Magnification 750X.

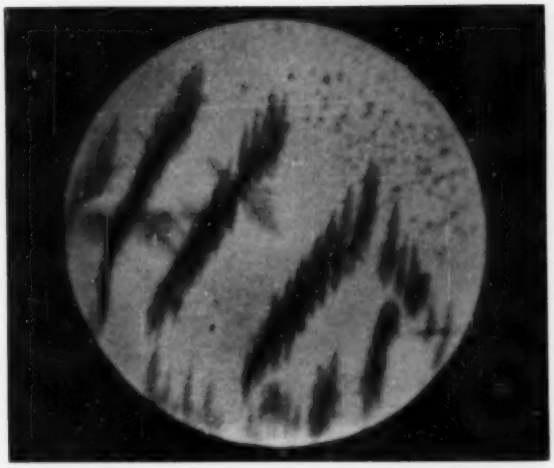

Fig. 7. Rows of decorated dislocations. Area between dislocations is free of precipitates. Magnification 100X.

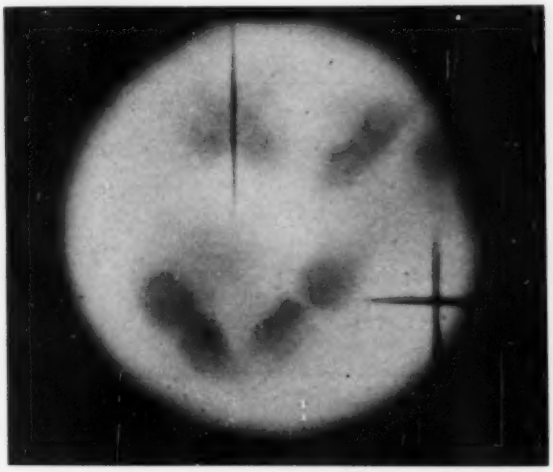

Fig. 8. Plate-like precipitate observed in {100} plane. Magnification 100X.

of these deposits is very much dependent on diffusion temperature and cooling rate; higher temperatures and slower cooling rates produce larger deposits. Decorated dislocations made up of the same structures have also been observed. This is shown in Fig. 7. There tends to be a dearth of precipitation in the direct vicinity of structures shown in Fig. 6 as well as around dislocations like those shown in Fig. 7. Therefore, we assume that these precipitates are nucleated on impurity clusters, in this case probably SiO_2 clusters which have precipitated along dislocations or at random sites during the growth process. The observation that dislocations introduced into the crystal by deformation show simple needle shaped precipitates along dislocations after decoration, which is typical for pure crystals, confirms this assumption. The depletion effect observed around grown-in dislocations has an interesting implication. It suggests a method for the formation of p-n junctions around a crystal defect by precipitating the proper impurity. The feasibility of such a method was demonstrated (3) quite recently by precipitating aluminum in phosphorus doped silicon.

In addition to these needle structures, a plate-like precipitate was also observed in crystals of low resistivity. The plates are very thin and grow only in {100} planes in <100> directions. Figure 8 shows an example. Because the needle form is also developed in the {100} planes in <110> directions composite structures can be observed where the needles bisect the angle between the plates. Since the precipitate can form three-dimensional structures, often only the projection of the real form into the plane of observation is seen. If this plane is chosen to be a {100} plane, a pattern of fourfold symmetry (cross) is seen. If the plane of observation is a {111} plane, the pattern is a projection of the precipitate into this plane and exhibits threefold symmetry as in Fig. 9, which shows a combination of plate-like and needle-like precipitate into a star pattern.

Silicon crystals which are rotation grown in a quartz crucible exhibit microsegregation of oxygen.

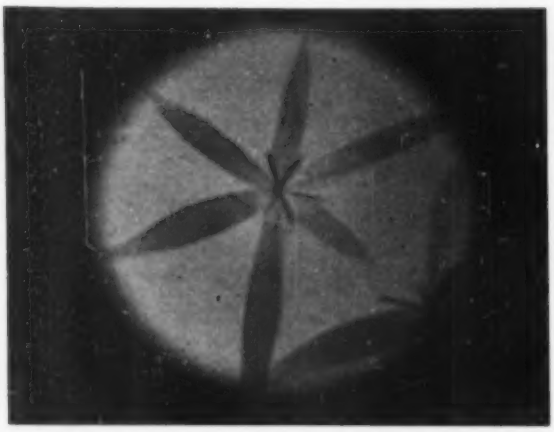

Fig. 9. Composite structure as seen in {111} planes. Plate-like and needle-like precipitate forming star pattern. Magnification 100X.

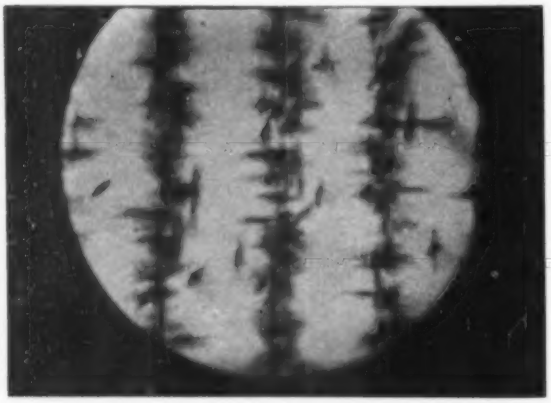

Fig. 10. Copper decorated oxygen layers in a crystal showing microsegregation of oxygen. Magnification 100X.

The oxygen segregates in planes perpendicular to the growth direction. A wafer was cut from such a crystal, parallel to the growth direction, and then copper was diffused at 900°C. Figure 10 is a picture of such a crystal. The oxygen stripes appear heavily decorated with Cu. No decorated dislocation lines are observed in the areas between the growth rings. This could mean that the crystal is dislocation free in these areas, which is improbable if Tiller's model (4) of crystal growth is valid. This model requires a dislocation density of at least $10^5/cm^2$, due to microsegregation of impurities. Alternatively, one might assume that oxygen inhibits the decoration mechanism in these areas.

To clarify this situation we investigated this effect by means of x-ray diffraction microscopy, using the moving crystal-film method described by Lang (5). The investigations were conducted in crystals showing homogeneous distribution of oxygen and in crystals exhibiting microsegregation of oxygen. Figure 11 represents a crystal area containing 5×10^{17} atoms of oxygen/cm^3 decorated by Cu. The lines are decorated dislocation lines. Figure 12 shows an x-ray image of the same crystal area obtained before Cu decoration. The white trails are dislocation lines. A

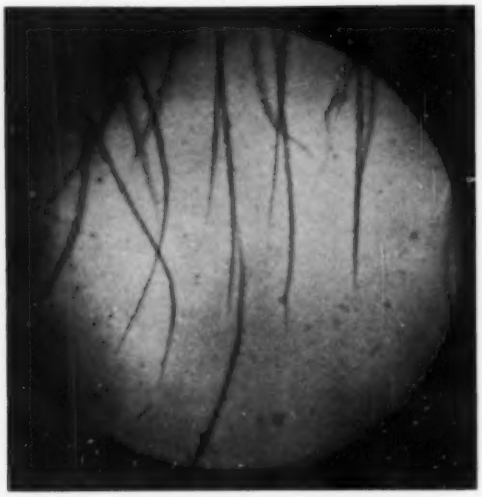

Fig. 11. Decorated dislocations in silicon containing 5×10^{17} atoms oxygen per cm^3. Magnification 28X.

Fig. 12. X-ray image showing dislocation lines in the same crystal as Fig. 11 before copper decoration. Crystal contains 5×10^{17} atoms oxygen/cm^3. Magnification 20X.

1:1 correspondence between the dislocation lines in both figures can be established.

An x-ray image of a crystal area containing oxygen stripes is represented in Fig. 13. Here also good agreement is found with the Cu decorated sample as shown in Fig. 10. No dislocation lines are visible; therefore we have to conclude that the crystal in this area is really dislocation free and that Tiller's model is not valid for this case.

Conclusions

The precipitation behavior of Cu in Si single crystals is influenced by the oxygen content of the crystal. This influence of the oxygen concentration on the shape of the precipitate suggests the formation of a copper-oxygen complex. Two simple types of precipitates have been identified: a needle-like shape and a plate-like shape. The precipitates have definite preferred orientation with respect to the crystal lattice. The particles prefer to segregate on {100} planes. The needles grow in <110> directions while the plates are oriented in such a way that their edges are parallel to the <100> directions. Com-

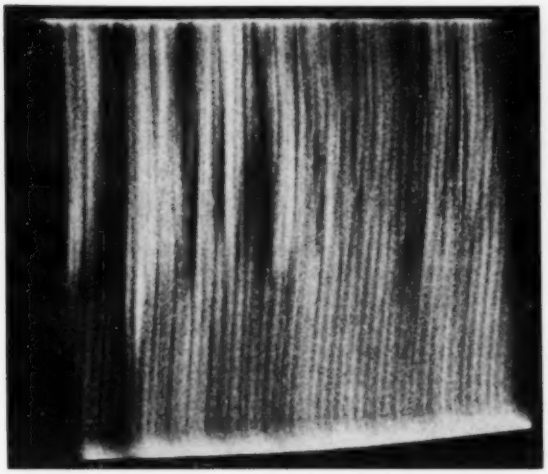

Fig. 13. X-ray diffraction photomicrograph of a silicon crystal showing segregation of oxygen. Magnification 20X.

posite structures built up of needles and plates occur. These structures appear as crosses when observed in the {100} planes. If the plane of observation is a {111} plane, their projection appears as a star pattern. The needles always bisect the angle between the plates.

The method of Cu decoration for the determination of low dislocation densities is an accurate method. Dislocations respond differently to their development by decoration depending on history, impurity cloud, and experimental conditions, but Cu is always able to decorate dislocation lines. In Si containing oxygen, Cu precipitates preferably in the region of high oxygen concentration, thus delineating the areas of high density of oxygen clusters. A comparison of Cu decoration pictures with x-ray diffraction photomicrographs produced evidence that no dislocations are present in areas showing microsegregation of oxygen. Since this would not be expected on the basis of Tiller's model of crystal growth, which calls for a dislocation density of $10^5/cm^2$ due to microsegregation of oxygen, we conclude that Tiller's model is not valid in this case.

Acknowledgments

The author would like to thank Dr. P. H. Keck for many enlightening discussions, Dr. K. M. Arnold who grew most of the crystals used for these experiments, and Mr. Ray Modena for preparing the numerous samples. The research reported in this paper was sponsored by the Electronics Research Directorate of the Air Force Cambridge Research Center, Air Research and Development Command, under Contract No. AF 19(604)3482.

Manuscript received June 3, 1960; revised manuscript received Oct. 7, 1960. This paper was prepared for delivery before the Chicago Meeting, May 1-5, 1960.

Any discussion of this paper will appear in a Discussion Section to be published in the December 1961 JOURNAL.

REFERENCES

1. W. C. Dash, *Phys. Rev.*, **98**, 1536 (A) (1955); *J. Appl. Phys.*, **27**, 1193 (1956); *Phys. Rev. Letters*, **1**, 400 (1958).
2. O. Deutchbein and A. M. Bernard, Intern. Congress on Solid State Physics, Brussels (1958).
3. R. Bullough, R. C. Newman, J. Wakefield, and J. B. Willis, *Nature*, **183**, 34 (1959).
4. W. A. Tiller, *J. Appl. Phys.*, **29**, 611 (1958).
5. A. R. Lang, *ibid.*, **29**, 597 (1958).

Radio-Frequency Carrier and Capacitive Coupling Procedures for Resistivity and Lifetime Measurements on Silicon

I. R. Weingarten[1] and M. Rothberg

Merck Sharp & Dohme Research Laboratories, Division of Merck & Company, Inc., Rahway, New Jersey

ABSTRACT

By use of a radio-frequency carrier and capacitive coupling it has been possible to measure the resistance and lifetime of silicon rods without making direct ohmic contact to the samples. Even with contacts, the use of an RF carrier to observe lifetime by photoconduction decay eliminates the need for insuring solid ohmic contacts as is required with a d-c carrier. With low loss insulation between coupling capacitors and sample, an RF bridge will measure separately both the sample resistance between the coupling capacitors and the value of this coupling capacitance.

In the study of zone refining of silicon, it is often desirable to know the changes in resistivity and lifetime as successive passes or changes in procedure are carried through. Direct current methods of measuring resistivity and lifetime involve handling and operations that are likely to interfere with further purification (1). Henisch and Zucker (2) described a radio-frequency contactless method for estimating resistivity and lifetime of semiconductors using inductive coupling and measuring the coil properties with a Q meter. Since the coil coupling to the sample was not determined readily, a system of arbitrary calibrations was required. The contactless method reported in this paper utilizes a radio-frequency current and capacitive coupling which may be measured readily so that resistivity may be calculated directly. The RF measuring procedures

[1] At present engaged in private consulting.

described also lend themselves to measurement of polycrystalline material by using the capacitive coupling between grains to by-pass the intergranular contact resistances (3). Methods for estimating and measuring lifetime using capacitive coupling with a high-frequency carrier also were developed. At the same time this work was done, Keller developed some similar high-frequency carrier lifetime methods (4).

Principle of the Method

The Si samples studied were cylindrical rods 1.0-1.8 cm in diameter and 10-20 cm in length. Two coupling capacitors, which were cylinders, 1 or 2 cm long, concentric to the rod, were used. Coupling capacitors were Al foil wrapped in thin polyethylene sheet and separated from the Si either by an air gap and polyethylene sheet wrapped around the Si or just by the polyethylene on the Si (Fig. 1). It is essential that any insulating material in the capacitor gap between the electrodes and the Si be low loss at the frequencies used. Lossy insulating material in this space adds to the apparent resistance of the sample. The circuit for the configuration is shown in Fig. 2 and consists essentially of two capacitors, the metal foil cylinders, which were connected by a resistor, the section of Si rod between them. The impedance of this circuit is then simply

$$Z = R_s + 2/jw2C_s = R_s + 1/jwC_s \qquad [1]$$

where w is 2π, f is frequency.

The resistance R_s may vary from 20 to 2000 ohms while the value of the series coupling capacitance, C_s, ranges from 10 to 30 $\mu\mu$f so that direct measurement as a series circuit is not readily accomplished with the standard radio-frequency bridges or Q meters. However, if the impedance Z of the two terminal series circuit of Fig. 2 is treated as a two terminal parallel circuit consisting of a resistor R_p in parallel with a capacitor C_p, then the corresponding admittance Y may be measured on a General Radio Twin T Bridge or a Boonton Q meter, and R_s, the desired series resistance value, can be computed. The calculation of R_s from the measured values, R_p or G, and from C_p is derived from the usual expression for the conversion of an impedance Z to its reciprocal, the equivalent admittance Y.

$$Y = G + jB = \frac{1}{R_p} + jwC_p = \frac{1}{R_s + \dfrac{1}{jwC_s}}$$

$$= \frac{w^2C_s^2R_s + jwC_s}{1 + w^2C_s^2R_s^2} \qquad [2]$$

For resistance values of the order of hundreds to a few thousand ohms, frequencies of 0.5-2 megacycles were used, while for lower resistances of 20-50 ohms, frequencies up to 20 megacycles were necessary. Generally, the frequency may be chosen so that the term $w^2R_s^2C_s^2$ in the denominator is negligible compared to unity and may be dropped. This term wR_sC_s is the dissipation factor D of the capacitor formed by coupling through the Si rod. In the measurement of polycrystalline rods and some high resistance single crystals, the apparent dissipation factor D may be larger than 0.2 and must be retained in order to achieve accuracies of 5-10%. The use of this correction for large D will be discussed in a later section. When it is dropped, however, the denominator of the expression for Y is unity; then the series coupling capacitance C_s and the measured value C_p are essentially equivalent. The rod resistance R_s is given by the expression:

$$R_s = \frac{G}{w^2C_p^2} = \frac{1}{w^2C_p^2R_p} \qquad [3]$$

The Twin T Bridge measures G and C_p so that R_s can be calculated directly from the bridge readings, while use of a Q meter requires additional steps which will be outlined in the latter part of the next section.

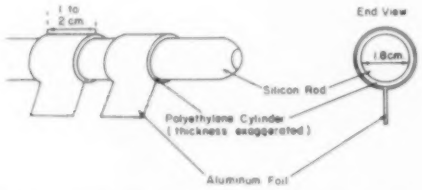

Fig. 1. Diagram of capacitance cell with silicon crystal inserted.

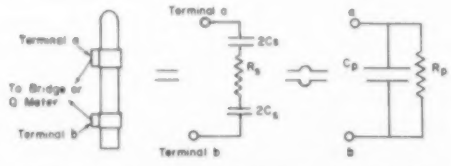

Fig. 2. Circuit equivalent of capacitance cell with silicon crystal.

Measurement Procedure

Using the GR821A Twin T Bridge, C_p readings are taken with empty capacitor cylinders connected to the bridge and spaced for the sample. Then the Si sample is inserted into the coupling capacitor and the bridge rebalanced. The required C_p is the difference in the bridge capacitance reading for the coupling capacitors empty and with sample. The conductance G of the sample is read similarly. While total rod resistances are of interest, it is more usual to determine sectional resistances along the length of a zone refined rod. To do this, an initial separation of the coupling capacitors may be as small as 1 cm. On increasing the spacing, the increase in measured resistance is a measure of the sample section introduced by the increased capacitor separation. This procedure also minimizes any errors that may occur due to special end effects at the coupling capacitors. The increment in conductance ΔG observed when the capacitor spacing is increased is then related to the resistance increment ΔR due to the added included length of Si rod, by the expression

$$\Delta R = \frac{\Delta G}{w^2C_p^2} \qquad [4]$$

The value of C_p used at any position on the rod is the difference between the capacitance reading of

Table I. Sample data and calculation of resistivity of silicon rod using a Twin-T bridge

Sample No. 50EY6-1 cross-sectional area 2.70 cm²

$f = 500$ kc $\quad w = 3.14 \times 10^6 \quad w^2 = 9.88 = 10^{12}$

	C in micro-microfarads	G, micromhos
Balanced bridge alone	255.1	0.0
Connected cable and cell (Cell at 1 cm spacing)	157.1	0.10
With silicon rod, 1 cm spacing	147.5	3.70
2 cm spacing	147.8	4.60
3 cm spacing	147.7	5.55
4 cm spacing	147.7	6.65
5 cm spacing	148.1	7.50

Average $\Delta G = 0.95 \times 10^{-6}$ mho
Average $C_p = 9.3 \times 10^{-12}$ farad

$$\rho = \frac{2.70 \times 0.95 \times 10^{-6}}{9.88 \times 10^{12} \times (9.3 \times 10^{-12})^2} \text{ ohm-cm}$$

$\rho = 3000$ ohm-cm

the Twin T Bridge balanced with the coupling capacitor empty, and the reading of the bridge when balanced at that position. Table I is an example of this measurement procedure.

When using a Q meter, a further step in the calculation is required to relate changes in Q to the changes in apparent conductance. If to a circuit reading Q_t and tuned to resonance by capacitance C_t, a conductance G_1 is added in parallel to the capacitance, the added conductance G_1 is related to the new value Q_1 by the expression:

$$G_1 = wC_t \ (1/Q_1 - 1/Q_t) \qquad [5]$$

G_1 in this case is the conductance derived from the value of R_s for the rod section inserted. At any position where a Q, Q_n is measured, the total resistance between the coupling capacitors is given by

$$R_{sn} = C_t/w(\Delta C_n)^2 \ (1/Q_n - 1/Q_t) \qquad [6]$$

When the separation between the coupling capacitor is increased, a new smaller value of Q,Q_2 is observed, corresponding to a new total resistance R_2 between the coupling capacitors given by the expression:

$$R_2 = C_t/w(\Delta C_2)^2 \ (1/Q_2 - 1/Q_t) \qquad [7]$$

The incremental resistance ΔR is the difference between R_1 and R_2. The incremental resistance ΔR due to the added length of Si rod then is given by the following equation, if variations in ΔC are small

$$\Delta R = C_t/w(\Delta C)^2 \ (1/Q_2 - 1/Q_1) =$$

$$C_t/w(\Delta C)^2 \ \Delta Q/Q_1(Q_1 - \Delta Q) \qquad [8]$$

$\Delta Q = Q_1 - Q_2$; ΔC_n, the value of the coupling capacitance at any position n, is as with the Twin T Bridge, the difference in tuning capacitance setting of the Q meter with the coupling capacitors empty, and the reading of the tuning capacitance when tuned at position n on the rod.

Typical data for contactless readings using the Q meter are given in Table II.

Table II. Sample data and calculation of resistivity of silicon rod using a Q meter

Sample No. 50EX46-2 cross-sectional area = 2.70 cm²

$f = 500$ kc $\quad w = 3.14 \times 10^6 \quad w^2 = 9.88 \times 10^{12}$

	Q	C
Resonated Q meter circuit	166.0	398.3
Connected cable and cell (Cell at 1 cm spacing)	161.0	306.6
Inserted rod (1 cm spacing)	109.5	294.3
$C_t = 3.98 \times 10^{-10}$ farad 2 cm spacing	104.5	294.5
$\Delta C = 12.2 \times 10^{-12}$ farad 3 cm spacing	99.0	293.8
$\Delta Q = 5.25$		
$Q_1Q_2 = 99\ (105)$		

$$\rho = \frac{2.70\ (3.98 \times 10^{-10})}{3.14 \times 10^6\ (12.2 \times 10^{-12})^2} \times \frac{5.25}{99\ (105)}$$

$\rho = 1110$ ohm-cm

Variations in ΔC_n with change of position along the rod may be so great that using an average value of coupling capacitance, as is done in Table II, may be undesirable. In that case the total resistance values R_{sn} at each position should be calculated using Eq. [6]. As a further help to averaging when measuring rods that are short compared to the coupling capacitors, or that vary by more than 10% in diameter along the length, the ground and live connections to the capacitors can be interchanged to provide two readings at each position. The reliability of the measured data may be improved further by varying the coupling capacitance to the rod, at any position. This variation in coupling capacitance can be accomplished by change in the area of the capacitor or by changing the separation between the Si and the cylindrical coupling capacitor. With long uniform rods, it is not usually necessary to use all the variations of procedure outlined, but for short irregular rods or rods with widely varying resistance profiles the extra steps may be desirable. Table III summarizes a comparison of resistivity measurements made by each of the RF instruments and by a 2-point d-c method.

Correction for Large Dissipation Factors When Measuring Whole High Resistance Rods or Polycrystalline Rods

In going to Eq. [3] from Eq. [2] a simplification resulted by dropping the square of the dissipation factor term $D = wR_sC_t$. When applying contactless measurements to whole high resistance rods or to polycrystalline rods, this simplification is not always possible.

When using the Twin T Bridge, the value of D is readily calculated from the conductance G and

Table III. Resistance of entire rod by capacitive coupling method

Sample No.	Resistance by Q meter	Resistance by Twin T bridge	Resistance by two-point probe
50EX46-2	1110	1090	1300
50EX48-1	—	2200	2200
50EY6-1	—	3000	2800
50EX48-2	3300	—	3500
50EX21-1	1000	934	900

equivalent parallel capacitance C_p, which are directly read.

$$D = wR_sC_s = 1/wR_pC_p = G/wC_p = 1/Q \quad [9]$$

If D is larger than 0.2, it is desirable to use the complete expression relating R_s and R_p, namely

$$R_s = \frac{R_pD^2}{1+D^2} = \frac{R_p}{w^2R_p^2C_p^2(1+D^2)} = \frac{G}{w^2C_p^2(1+D^2)} \quad [10]$$

The C_p of Eq. [9] and [10] is read in the same way as the capacitance used in Eq. [3] and is the difference between the setting of the Twin T Bridge balancing capacitor before and after connecting the sample.

Using Q meter readings the dissipation factor of the rod section for capacitors at a position n is given by the following expression obtained by combining Eq. [5] and [9] and noting that $\Delta C = C_p$

$$D_n = G_n/w(\Delta C_n) = C_t/\Delta C_n(1/Q_n - 1/Q_t) \quad [11]$$

With an initial Q_t of 100 or more, a ΔC of 20 $\mu\mu$f and C_t 300 $\mu\mu$f, Q_n would be about 30 with a sample D as large as 0.3. With D values greater than 0.3, the total rod resistance must be calculated at each position and differences between these values taken in order to obtain resistance profiles. With single crystal rods this is not usually necessary, since the carrier frequency can be chosen to provide adequate changes in Q without D exceeding 0.1. In the study of polycrystalline rods, however, data over a wide range of frequencies are necessary and corrections for large D are essential. To correct Q meter calculations for D values greater than 0.3, Eq. [5] and [10] are combined to give

$$R_s\ (\text{corr.}) = C_t/w(\Delta C_n)^2\ (1/Q_n - 1/Q_t)\ (1/1+D_n^2) \quad [12]$$

where as before D_n is calculated using Eq. [11]. ΔC_n as observed is of course the apparent parallel capacitance, C_p, of Eq. [9] and [10].

Use of Data Derived from Polycrystalline Rods

The equivalent circuit shown in Fig. 1 represents the Si rod as a single resistor. While this is an adequate representation of single crystals, polycrystalline material behaves more like a complex resistance, capacitance network. The contacts between crystallites behave as resistors shunted by intergranular capacitance. A representation of this essential circuitry is given in Fig. 3. The measurement of the resistivity of polycrystalline aggregates as a function of frequency has been reported in connection with the study of ferrites, zinc oxide (3), and other materials. The capacitive coupling method is well suited to this type of measurement. As in the case of other polycrystalline materials, the apparent resistance decreases and starts to level off with increase in frequency. Five Si polycrystalline rods were measured at increasing frequencies up to 10 Mc. In Table IV the whole rod resistances at 10 Mc are compared to the values calculated from the net carrier density at room temperature as obtained by Hall measurement (5). Relative values are reasonably consistent and could serve to classify the rods, but the RF resistance values are somewhat greater than those calculated from the carrier density, indicating either a lower mobility than used in the calculation, or the need for measurements at still higher frequencies to by-pass intergranular resistance adequately. An even simpler measurement for classification of polycrystalline rods is a single Q measurement at a fixed capacitor spacing at a frequency where there is sufficient dispersion of Q to provide a basis for classification (6). The data in column 1 of Table IV are Q values measured at 2 Mc with capacitor coupling electrodes fixed 1 cm apart. These Q readings correspond to Q_t or Q_s of Eq. [6] and [7], but relate to an apparent resistance which combines intergranular resistance and crystallite resistance. While these are not ultimate measures of the Si granule resistances, these single Q readings have provided convenient control measurements.

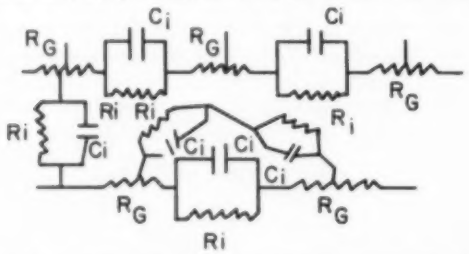

Fig. 3. Circuit equivalent of polycrystalline material. R_G, grain resistance; C_i, intergranular capacitance; R_i, intergranular resistance.

Table IV. Comparison of Q measurement of resistance and Hall measurement calculation of polycrystalline silicon resistance

Sample No.	Q	n Number of carriers/cm³ from Hall data	Apparent resistance of entire rod at 10 Mc	Resistance of entire rod calc. from Hall data (does not include grain boundary resistances)
A 27-28B	37-50	0.6×10^{13}	5650	4125
A 51-1A	118	2×10^{13}	2150	1200
A 57-25A	65	0.6×10^{13}	5600	4125
A 57-8B	35	0.9×10^{13}	4850	2800
A 48-11B	128	3×10^{13}	1080	825

Lifetime Estimation and Measurement

With a sample in the resistivity measuring apparatus, a rapid indication of lifetime may be obtained by illumination of the sample with infrared. This is readily done using the Q meter and a 250-w infrared heat lamp. The change in Q on illumination of the sample by the lamp serves to indicate the general range of lifetime to be expected with more accurate measurement. For a given lifetime, the change in Q on illumination was of course larger for high resistivity rods. With doped low resistivity rods, an increase in carrier frequency beyond that used for resistivity measurement may be necessary to observe a useful change in Q with lifetimes under 50 μ sec.

For photoconductive decay lifetime measurement, with a radio-frequency carrier, the capacitive coupling shown in Fig. 1 was utilized with the detector circuit shown in Fig. 4.

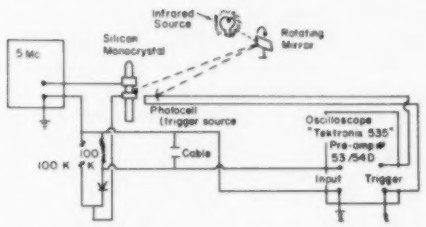

Fig. 4. Diagram for lifetime detection by capacitive coupling (transient) method.

The modulation of resistivity resulting from the production of excess carriers by illumination and their subsequent decay results in the modulation of the amplitude of the radio-frequency carrier passed through the sample. On detection of the carrier and further amplification of the envelope, it was possible to observe a photoconductive decay curve similar to that obtained with direct current. An improved amplifier could be a direct RF or heterodyne amplifier with first stage clipping and then final clipping and detection. There was little difference found between lifetimes measured using d-c and direct contacts and the values obtained with radio frequency carriers over the range of 2-15 Mc/sec. Some typical results are given in Table V. For low resistivity samples direct contact of metallic foil electrodes was sometimes necessary. While this procedure has the disadvantage that the sample surface may be altered, the surface damage is less than that required for d-c ohmic contacts and there is less likelihood of carrier injection.

Table V. Capacitive method of lifetime detection in silicon crystals (Photoconductive decay)

Sample No.	Lifetime using capacitive method, μsec	Lifetime using d-c contact method, μsec
50EX48-2	800-900	800-1000
50EX-2-2	20-25	20-30
50EX38-1	100-200	100-200

Manuscript received April 26, 1960. This paper was prepared for delivery before the Columbus Meeting, Oct. 18-22, 1959.

Any discussion of this paper will appear in a Discussion Section to be published in the December 1961 JOURNAL.

REFERENCES

1. H. C. Theuerer, J. M. Whelan, H. E. Bridgers, and E. Buehler, *This Journal*, **104**, 721 (1957).
2. H. K. Henisch and J. Zucker, *Rev. Sci. Instr.*, **27**, 409 (1956).
3. H. K. Henisch, Editor, "Semiconductor Materials," p. 160, 172, Butterworth Scientific Publications Ltd., London (1951).
4. W. Keller, Private communication.
5. P. J. Olshefski, D. J. Shombert, and I. R. Weingarten, Paper being considered for publication, *This Journal*.
6. P. J. Olshefski, Private communication.

Preparation of Uniform Resistivity n-Type Silicon by Nuclear Transmutation

M. Tanenbaum and A. D. Mills

Bell Telephone Laboratories, Incorporated, Murray Hill, New Jersey

ABSTRACT

By the capture of a thermal neutron, the natural isotope Si^{30} can be transmuted into the unstable isotope Si^{31} which decays by beta emission with a 2.62 hr half-life to the stable isotope P^{31}. By means of this reaction, donors can be produced in a silicon crystal. Because of the uniformity of flux which can be obtained in large nuclear reactors, this technique lends itself to the preparation of uniformly doped n-type silicon. After irradiation the silicon crystal is heavily damaged by the emitted betas, by the recoil of the decaying Si^{31}, and by the high energy neutrons that are unavoidably present in the reactor. However, this damage can be removed by annealing at temperatures near 600°C. The technique has been used to produce n-type silicon with nominal resistivities between 0.1 and 20 ohm-cm. The resistivity of the resulting crystals was uniform over dimensions of 5 cm to within ±5%.

Many experimental and practical uses of semiconductors require single crystals of accurately controlled resistivity. This problem was successfully attacked in germanium by the use of zone leveling techniques (1). It has been possible to produce p-type silicon with the necessary resistivity uniformity by two techniques. Using boron with a distribution coefficient of approximately 0.9, it is possible to pull single crystals of good uniformity (2). Using the floating-zone technique with aluminum whose distribution coefficient is 0.004, it is possible to zone level p-type Si to a high degree of uniformity (3). The preparation of uniform resistivity n-type Si has been a more difficult problem. The less volatile Group V donor impurities such as phosphorus and arsenic have distribution coefficients which are too small to permit their use in normal crystal pulling procedures and too large to permit their use in zone leveling procedures. Antimony and bismuth which have distribution coefficients small enough for zone

leveling are much too volatile and vaporize rapidly from molten Si. Crystal growing procedures have been developed which attempt to compensate for these difficulties. Bradshaw and Mlavsky (4) have pulled Si crystals from phosphorus-doped melts in vacuum where they used the rate of evaporation of phosphorus from the melt to compensate for the increasing phosphorus concentration in the melt caused by segregation. Bridgers (5) has proposed a method for controlling phosphorus concentration in the melt during floating-zone crystal growing by establishing a quasi-equilibrium between the molten zone and a vapor phase containing a volatile phosphorus compound such as phosphorus bromide. Since both of these techniques require the simultaneous control of several kinetic processes including evaporation, segregation, and vapor-liquid reactions, it can be expected that their satisfactory implementation on a routine basis will require considerable ingenuity.

This paper describes a different approach to the problem of the preparation of uniform resistivity n-type Si at any desired resistivity level. The approach is based on a nuclear reaction in which a thermal neutron is captured by the naturally occurring stable isotope Si^{30} to form the unstable isotope Si^{31}. This unstable isotope decays by the emission of a 1.471 Mev β^- with a half-life of 2.62 hr to the stable isotope P^{31}. The cross section for this reaction is known, and thus by determining the total integrated flux of thermal neutrons incident on a Si specimen it should be possible to predict accurately the extent to which this nuclear reaction occurs and thus to determine the total amount of phosphorus that is produced to within a few per cent.[1] Furthermore, if a sample can be placed in a region of a large pile where the flux density is uniform, the doping of the resulting Si crystal should reflect the flux uniformity of the reactor.[2]

In addition to this desired reaction there are other possible nuclear transmutations which can occur in the specimen. Some of these may produce undesirable products and could defeat the purpose of this experiment if they occurred to an appreciable extent. In order to examine the possibility of such interfering reactions it will be assumed that all impurities in the Si crystals before irradiation have been reduced to a level below 10^{13} at./cc. This is a reasonable assumption if floating-zone refined Si crystals are used as the starting material. Thus, it is necessary to consider the possible reactions between neutrons and the stable Si isotopes; Si^{28} (natural abundance 92.27%), Si^{29} (natural abundance 4.68%), Si^{30} (natural abundance 3.05%).[3] Reactions with P^{31} will also be considered.

(n,γ) *Reactions.*—The following reactions may be considered:

$$Si^{28}(n,\gamma)Si^{29} \qquad [1]$$

$$Si^{29}(n,\gamma)Si^{30} \qquad [2]$$

$$Si^{30}(n,\gamma)Si^{31} \rightarrow P^{31} + \beta^- \qquad [3]$$

$$P^{31}(n,\gamma)P^{32} \rightarrow S^{32} + \beta^- \qquad [4]$$

The pertinent cross sections, σ, are listed in Table I. Where an unstable isotope is formed, the decay scheme to the next stable isotope is indicated in the equation and the half-life for decay, τ, is listed in Table I. Reactions [1] and [2] serve only to alter the isotopic ratios. Furthermore, the amount of new Si^{30} produced will be comparable to the amount of P^{31} produced and this increase will generally be negligible. Reaction [3] is the desired reaction to produce donors. Reaction [4] leads to the destruction of the desired donor P^{31} and the creation of S^{32} which is reported to be a donor with ionization levels at 0.18 ev and 0.37 ev from the conduction band (8). However, since the cross section for reaction [4] is only twice that for reaction [3] then

$$\frac{\text{conc. } S^{32}}{\text{conc. } P^{31}} \simeq \frac{\text{conc. } P^{31}}{\text{conc. } Si^{30}} \qquad [5]$$

For a neutron irradiation sufficient to transmute 10^{17} of the Si^{30} into P^{31} the amount of P^{31} destroyed is 5.9×10^{12}. This is obviously insignificant. An equal amount of S^{32} is produced, and it is not expected that

[1] The concentration of P [P^{31}] is given by [P^{31}] = [Si^{30}]σF where [Si^{30}] is the concentration of Si^{30}, σ is the thermal neutron cross section of the reaction, and F is the total thermal neutron flux. Barring any competitive reaction, this could provide accurate means for determining the cross section of the reaction. Lark-Horowitz (6) has discussed this method of doping semiconductors and has compared neutron cross sections in Ge obtained by similar techniques with cross sections obtained by the usual nuclear methods.

[2] Similarly, this could provide a method for probing the flux profile of a reactor.

[3] A study of natural silicates from widely scattered sources has shown that the maximum variation of the ratio Si^{30}/Si^{28} is 3 parts per thousand (7).

Table I. Nuclear data

	n, γ		n, 2n			n, p			n α		
	σ	τ	σ	τ	E (Mev)	σ	τ	E (Mev)	σ	τ	E (Mev)
Si^{28}	0.08 ± 0.03*	—	—	4.92s	17.4**	0.004†f	2.3m	4.0**	—	—	2.7‡
Si^{29}	0.28 ± 0.09*	—	—	—	8.7**	0.10††	6.6m	3.3**	—	—	0.04‡
Si^{30}	0.110 ± 0.010*	2.62h	—	—	10.6‡	—	—	***	~0.00017†f	9.45m	4.2‡
P^{31}	0.20 ± 0.02*	14.3d	—	2.55m	12.6**	0.77††	2.62h	0.97**	0.15††	2.27m	0.91**
O^{16}	—	—	—	126s	17.3**	0.05††	7.38s	10.2**	—	—	2.2‡
O^{17}	—	—	—	—	4.2‡	—	4.14s	8.1‡	0.25±0.15**	5500y	thermal
O^{18}	0.00021*	29s	—	—	8.0‡	—	—	***	—	2.3s	***

* Neutron Cross Sections, D. S. Hughes and R. B. Schwartz, U. S. Gov't Printing Office, Washington, D. C. (1958).
** O. R. Frisch, "The Nuclear Handbook," Chap. 10, D. Van Nostrand, New York (1958).
*** Mass of product nucleus unknown.
† R. H. Smith and H. E. Menker, "Neutron Activation Analysis Calculations," Traceriab, Inc. Report TLW-1051, December 1958.
f = fission spectrum neutrons.
†† 14 Mev neutrons, G. Friedlander and J. W. Kennedy, "Nuclear Radio Chemistry," John Wiley & Sons, New York (1955).
‡ Calculated from mass deficit. Add ~2 Mev for coulomb repulsion for (n, p) reaction and ~4 Mev for (n, α) reaction.

this concentration will effect the electrical properties at the resistivity and lifetime levels usually encountered in devices.

Reaction [4] does have one undesirable effect since it renders the sample radioactive. Because of the relatively long decay half-life of 14.22 days, the sample will remain radioactive for several months. However, an initial concentration of 5.9×10^{12} P^{32}/cc will produce an initial activity of about 0.12 millicuries/cc. Since this activity is a pure beta, it is at a level where it can be handled with minimal shielding. Sanitary precautions such as gloves and adequate ventilation during cutting and shaping would be required. After 2.5 half-lives or 36 days, the activity would be 0.01 millicuries/cc. The total activity will, of course, be proportional to the volume of Si, and the handling of large quantities may require special consideration.

The above reactions are the only expected reactions with thermal neutrons. In available reactors, however, it is not possible to obtain high fluxes of thermal neutrons without also obtaining measurable quantities of high energy neutrons. Unfortunately the flux density and energies of these high energy neutrons are seldom known in any detail. Therefore, it is worthwhile to consider possible high energy neutron reactions and to estimate what possible effect they might have on the irradiated crystals.

(n,2n) *Reactions.*—The following reactions may be considered:

$$Si^{29}(n,2n)Si^{27} \rightarrow Al^{27} + \beta^- \quad [6]$$

$$Si^{29}(n,2n)Si^{28} \quad [7]$$

$$Si^{30}(n,2n)Si^{29} \quad [8]$$

$$P^{31}(n,2n)P^{30} \rightarrow Si^{30} + \beta^- \quad [9]$$

The pertinent cross sections, half-lives, and estimated threshold neutron energies, E, are listed in Table I. None of these reactions are expected to occur with thermal neutrons. Even if they should occur, reactions [7] and [8] would serve only to change the ratio of Si isotopes. Furthermore, these changes would again be negligible. Reaction [6] would be troublesome should it occur to an extent comparable to that of reaction [3] which produces P^{32} for this would result in compensation and could indeed produce a p-type sample instead of the desired n-type. If reaction [6] proceeds to an appreciably smaller extent than reaction [3], its effect would be simply to reduce the apparent efficiency with which the sample is doped with phosphorus and could be easily compensated by a longer bombardment. As we shall see later our results to date indicate that, if reaction [6] occurs, its effect is masked by the other uncertainties in the analysis of our data. If reaction [9] should prove to have a reasonable cross section, we would reduce the amount of P^{32} and increase the amount of Si^{30}. However, the extent of this reaction will be similar to that of reaction [4], and both these effects will be unimportant.

Thus, it is concluded that (n,2n) reactions should not lead to any difficulty.

(n,p) *Reactions.*—The reactions which must be considered are:

$$Si^{28}(n,p)Al^{28} \rightarrow Si^{28} + \beta^- \quad [10]$$

$$Si^{29}(n,p)Al^{29} \rightarrow Si^{29} + \beta^- \quad [11]$$

$$Si^{30}(n,p)Al^{30}\ (\text{unknown}) \rightarrow Si^{30} + \beta^- \quad [12]$$

$$P^{32}(n,p)Si^{32} \rightarrow P^{32} + \beta^- \quad [13]$$

It is evident that reactions [10], [11], and [13] produce no net change and thus can be disregarded. There is no information available on the hypothetical reaction [12]. Al^{30} is an unknown isotope indicating that if this reaction occurs at all the product must have an extremely short half-life. The probable mode of its decay if it is formed is indicated. From these considerations we conclude that (n,p) reactions will not produce undesirable results.

(n,α) *Reactions.*—The reactions that may be considered here are listed in the following equations:

$$Si^{28}(n,\alpha)Mg^{25} \quad [14]$$

$$Si^{29}(n,\alpha)Mg^{26} \quad [15]$$

$$Si^{30}(n,\alpha)Mg^{27} \rightarrow Al^{27} + \beta^- \quad [16]$$

$$P^{31}(n,\alpha)Al^{28} \rightarrow Si^{28} + \beta^- \quad [17]$$

Reaction [17] similar to reaction [9] will result in a negligible change in Si isotope ratio and a negligible decrease in P^{31} concentration. Reaction [16] similar to reaction [6] will be important only if the cross section is high. A very small cross section for fission spectrum neutrons is shown in Table I. This reaction is not expected with thermal neutrons. The data reported below indicate that its occurrence is not detectable within the error of our experiments. Reactions [14] and [15] could conceivably produce amounts of Mg comparable to the amounts of P that are produced. Here again they are not expected to occur with thermal neutrons as indicated by the rough calculations of threshold neutron energy in Table I. However, since exact thresholds and cross sections have not been determined and since the electrical properties of Mg are unknown, it is conceivable that these reactions might lead to difficulties.

In summary, considerations of the nuclear reactions which may occur during the irradiation of natural Si in the thermal column of a nuclear reactor suggest that the principal effect will be the conversion of a small amount of the natural isotope Si^{30} into the stable isotope P^{31}. Very small amounts of sulfur are also produced. The small quantities of high energy neutrons usually unavoidable during such irradiations may produce small amounts of Al and Mg and slightly alter the silicon isotope ratios.

In addition to the chemical changes which will be produced by the neutron irradiation, a large amount of physical damage in the Si crystal will be produced by the neutron and gamma bombardment, by the recoil of the decaying radioactive atoms which are created (9), and by the emitted beta particles. The knowledge of the behavior of Si in a neutron

environment suggests that the crystals immediately after irradiation will be damaged very severely and their electrical properties altered drastically (10). The detailed mechanisms of the annealing of damage in Si produced by neutron bombardment are unknown. Furthermore, there is very little published data on the annealing times and temperatures required to heal neutron damage in silicon. Studies of the electrical changes have shown that the electrical effects of neutron damage shows a gross resemblance to damage produced by high energy electron bombardment (10). It is known that the electron bombardment damage can be removed rapidly by annealing at 400°C (11). The production of semiconducting devices by solid-state diffusion techniques require heating at temperatures much in excess of those usually needed to completely remove radiation damage. Thus one might expect that the irradiated Si could be used directly in the fabrication of devices, the irradiation damage annealing out during the device fabrication process.

Experimental

Six independent irradiation experiments have been performed: three in the graphite moderated reactor of the Brookhaven National Laboratory and three in the light water moderated reactor at Oak Ridge National Laboratory. The pertinent data on these irradiations are given in Table II. The reported fluxes are for thermal neutrons. Information regarding the high energy neutron flux at our sample location was not available for the Brookhaven reactor. The only information available for the Oak Ridge reactor indicated a flux density of 9.5×10^{12} neutrons/cm^2/sec with energies in excess of 2.3 Mev. The Si samples were prepared from floating-zone refined material in the form of either bars 0.2 x 0.2 x 2.0 cm or cylinders approximately 1 cm in diameter and 5 cm long. In the latter case, the cylinders were sectioned into bars 0.2 x 0.2 x 2 cm after bombardment. During bombardment the samples were held in standard Al containers. There was no attempt to cool the samples during bombardment, but in no case did the temperature exceed 200°C. Samples 2, 3, 5, and 6 included monitors of Al-Co alloys from which the thermal neutron flux was determined. The fluxes in samples 1 and 4 were estimated from the bombardment time and expected neutron flux density at the sample location. After receipt of the samples from the reactors a small radioactivity was observed. This activity had the proper energy, half-life, and intensity expected for the decay of P^{32} produced by reaction [4].

Table II. Irradiation experiment data

Sample	Initial resistivity, ohm-cm	Reactor	Total thermal neutron flux	
	p-type			
1	500	Oak Ridge	$1.4 \pm 0.14 \times 10^{20}$	estimated
2	700	Oak Ridge	$5.49 \pm 0.15 \times 10^{19}$	monitored
3	500	Oak Ridge	$4.78 \pm 0.19 \times 10^{20}$	monitored
4	1,200	Brookhaven	$1.4 \pm 0.14 \times 10^{19}$	estimated
5	1,500	Brookhaven	$1.54 \pm 0.04 \times 10^{19}$	monitored
6	15,000	Brookhaven	$1.62 \pm 0.01 \times 10^{19}$	monitored

Resistivities of the samples were measured with a 4-point probe and type K potentiometer when the resistivity level was in excess of 20 ohm-cm. For resistivities less than 20 ohm-cm a 2-point probe with a point spacing of 0.025 or 0.15 cm was employed. With the 2-point arrangement measurements were taken at intervals of 0.013 cm along the bars and recorded on a L&N Speedomax recorder. The smaller spacing was used to obtain a finer profile on some of the specimens. The majority of the measurements were performed with the 0.15 cm spacing. The precision of this measurement is estimated as $\pm 3\%$. For the purpose of the following tables, measurements at intervals of approximately 0.5 cm are quoted from the more detailed data actually obtained.

After the resistivity had been measured following bombardment, the samples were etched in a mixture of 5 parts concentrated HNO_3 to 1 part concentrated HCl, rinsed in deionized water, and then heated in air at varying temperatures and for varying times. The resistivities were measured after each annealing and the samples re-etched before the next annealing. An unbombarded sample was heated with each bombarded sample to control against resistivity changes caused by accidental contamination during the annealing. The resistivity of the control was chosen to approximate the final resistivity expected in the bombarded samples.

Table III contains results from the annealing heat treatments. All the samples were n-type. These results have been selected to be representative and illustrate the general annealing behavior. Data on the controls are not included since they showed no

Table III. Annealing heat treatment results

Sample	1 hr, 600°C	1 hr, 625°C	16 hr, 625°C	1 hr, 800°C
1	6.44			0.334
	6.24			0.334
	6.24			0.334
	6.44			0.326
	6.63			0.334
2	$>10^5$	0.71	0.66	0.65
	$>10^5$	0.71	0.65	0.64
	$>10^5$	0.71	0.65	0.64
	$>10^5$	0.69	0.65	0.64
	$>10^5$	0.71	0.66	0.64
3		0.26	0.110	0.102
		0.28	0.110	0.101
		0.29	0.110	0.101
		0.31	0.110	0.101
		0.34	0.110	0.102
4	3.69			2.51
	3.64			2.54
	3.70			2.54
	3.74			2.51
5		2.08	1.90	1.92
		2.07	1.90	1.90
		2.06	1.90	1.90
		2.06	1.90	1.90
		2.06	1.90	1.92
6		17.8	17.6	15.3
		17.8	17.3	15.1
		18.1	17.3	15.1
		18.1	17.3	15.1
		18.1	17.6	14.8

significant changes during any of the heat treatments reported except in the case of sample 6. In this latter case an unbombarded control showed an increase in donor concentration after heating at 800°C for 1 hr. The original average resistivity of the control was 14.7 ohm-cm. After 1 hr at 800°C, the average resistivity was 13.2 ohm-cm. This compares with the change noted in sample 6 after 1 hr at 800°C and indicates that this decrease from the value after 16 hr at 625°C may be caused by effects independent of the bombardment of the samples. It would be expected that uncontrolled resistivity changes caused by contamination during heating, etc., would be more apparent in high resistivity samples. The source of this change in sample 6 and in the control is not known.

Immediately after bombardment all samples measured greater than 10^5 ohm-cm indicating large concentrations of energy levels near the center of the forbidden energy gap. These defects are due presumably to physical lattice defects. The defects begin to anneal upon heating 1 hr at 400°C as indicated by slight decreases in resistivity. Rapid annealing occurs at 600°C. In general annealing was complete after 16 hr at 625°C. The annealing was considered complete when doubling the total heating time did not produce a significant change in resistivity. Some samples were heated as high as 1200°C for 12 hr to confirm the validity of this procedure.

Table IV summarizes the results and lists the average resistivities and the standard deviation from the average along the length of each bar. Because of the changes after heating at 800°C, the resistivity after 16 hr at 625°C was used for sample 6. In all other cases, the values after 1 hr at 800°C were used. It can be seen that the bombardment was uniform to within ±3% along the length of the 2-cm samples. In addition samples were measured along the 5 cm length of cylindrical bombarded samples and across the diameter of the cylinders. In every case the maximum standard deviation was less than 3% or within the precision of the resistivity measurements.

The lifetime of sample 2 was measured by the van de Graaff technique (12) after heating for 48 hr at 625°C and cooling in the furnace to room temperature. A value of 0.05 μsec was obtained. Mesa-type transistors were made from sample 1, and it was demonstrated that the lifetime was sufficiently high to make this material useful in transistor fabrication (13).

Table IV.

Sample	Resistivity, ohm-cm	Mobility, cm²/v sec	Cross section, barns
1	0.332±0.003	1010*	0.087
2	0.64±0.00	1130*	1.10
3	0.101±0.001	725*	0.12
4	2.53±0.01	1230†	0.092
5	1.91±0.01	1175†	0.11
6	17.4±0.2	1350‡	0.11

* K. Wolfstirn, *J. Phys. Chem. Solids* (in press).
† M. B. Prince, *Phys. Rev.*, **93**, 1204 (1954).
‡ A. W. Ludwig and R. L. Watters, *ibid.*, **101**, 1699 (1956).

Discussion

These experiments indicate that in the high flux thermal columns of both the Brookhaven and Oak Ridge reactors it is possible to obtain neutron fluxes which have been sufficiently thermalized so that thermal neutron capture is the most significant reaction which occurs in high-purity Si.

Table IV also includes the cross sections for reaction [3] using the estimated or monitored neutron flux and a natural abundance of Si^{30} of 3.05%. The cross section obtained by averaging the results of the monitored samples is 0.11 ± 0.01 barns. The literature value reported in Table I is 0.110 ± 0.010 barns. The uncertainties in these experiments are ±3-4% in the flux measurements, ±5% in the absolute resistivity, ±10% in the electron mobility, and ±2% in the natural abundance of Si^{30}. Thus the excellent agreement between the results of these experiments and the literature value is perhaps fortuitous. It also appears that the principal goals of this experiment which were the production of n-type Si with a uniformity of doping of ±5% have been achieved in the samples employed. Furthermore, the reproducibility of the cross section obtained in the two different reactors indicates that an equal accuracy in predicting the level of resistivity can also be obtained.

It is worthwhile to consider the effect of any oxygen that might be dissolved in the Si during the nuclear irradiation. These considerations are not important if floating zone Si is used. However, they would become important if it were desirable to irradiate pulled crystals.

The reactions that must be considered are as follows:

$$O^{18}(n,\gamma)O^{19} \quad [18]$$

$$O^{17}(n,\gamma)O^{18} \quad [19]$$

$$O^{18}(n,\gamma)O^{19} \rightarrow F^{19} + \beta^- \quad [20]$$

$$O^{16}(n,p)N^{16} \rightarrow O^{16} + \beta^- \quad [21]$$

$$O^{17}(n,p)N^{17} \rightarrow O^{17} + \beta^- \quad [22]$$

$$O^{18}(n,p)N^{18}\ (\text{unknown}) \rightarrow O^{18*} + \beta^- \quad [23]$$

$$O^{16}(n,\alpha)C^{13} \quad [24]$$

$$O^{17}(n,\alpha)C^{14} \rightarrow N^{14} + \beta^- \quad [25]$$

$$O^{18}(n,\alpha)C^{15} \rightarrow N^{15} + \beta^- \quad [26]$$

$$O^{18}(n,2n)O^{17} \rightarrow N^{28} + \beta^- \quad [27]$$

$$O^{17}(n,2n)O^{16} \quad [28]$$

$$O^{18}(n,2n)O^{17} \quad [29]$$

* Probable decay product.

It can be seen that reactions [18], [19], [28], and [29] serve merely to alter the oxygen isotope ratio. Reactions [21], [22], and probably [23] produce no net change. Reactions [24], [26], and [27] will probably require neutrons with energies in excess of 5 Mev. Reaction [25] may well occur with thermal neutrons. Because of the very long half-life of the decay of C^{14}, the main effect of this reaction will be to produce carbon. Reaction [20] will also

occur with thermal neutrons but has an extremely small cross section. Furthermore, since the oxygen concentration will probably not exceed 10^{18}/cc, and since the abundances O^{17} and O^{18} are 0.04% and 0.20%, respectively, we would expect the amount of fluorine produced by reaction [20] to be about 10^{-9} of the amount of phosphorus produced, and the amount of carbon produced by reaction [25] to be 10^{-7} of the amount of phosphorus produced. Such quantities of these impurities should be completely negligible. Thus, it would appear that from the chemical viewpoint Si containing up to 10^{18} oxygen atoms per cc could be safely irradiated. On the other hand, it has been reported that oxygen affects the bombardment damage produced by high energy electrons (14). It is possible that similar interactions with high energy neutrons would complicate the physical radiation damage produced in the Si lattice in an undesirable fashion. These questions can be answered most easily by experiment.

Conclusions

It has been shown that the irradiation of Si with thermal neutrons provides a practical method for preparing uniformly doped n-type Si of predictable resistivity level. The method should be practical for doping up to about 5 x 10^{17}/cc. Although it is applicable at higher dopings, the times of irradiation that would be necessary with currently obtainable thermal neutron fluxes become very long. In the low doping or high resistivity region, uniformity is limited only by the purity of the starting material.

Both a study of the possible nuclear reactions and the interpretation of the experimental results indicate that the most important nuclear reaction leading to an electrically active impurity is the capture of a thermal neutron by the natural isotope Si^{30}. Although the experiments have been applied only to floating zone material, it appears that concentrations of dissolved oxygen as high as 10^{18}/cc can be tolerated. The method has the additional advantage that it can be applied equally well to large single crystals, to slices of crystals, or to small wafers which have been preformed to the final dimensions desired in devices.

Acknowledgments

The authors would like to acknowledge the contributions of several of their colleagues. The crystals used in these experiments were supplied by E. Buehler, E. D. Kolb, H. C. Theuerer, and G. H. Edmunds. Lifetime and Hall effect measurements were performed by W. M. Augustyniak and R. A. Logan, respectively. P. Donovan provided some of the estimates of the thresholds for the high energy neutron reactions. The authors are especially indebted to W. Gibson who provided much of the nuclear chemical information required for this study and who, with J. D. Struthers, was instrumental in analyzing the residual radioactivity in the irradiated samples. The monitor alloys were provided and analyzed by W. D. Leddicotte of the Oak Ridge National Laboratories.

Manuscript received July 11, 1960; revised manuscript received Oct. 7, 1960.

Any discussion of this paper will appear in a Discussion Section to be published in the December 1961 JOURNAL.

REFERENCES

1. W. G. Pfann and K. M. Olsen, *Phys. Rev.*, **89**, 322 (1953); D. C. Bennett and B. Sawyer, *Bell Sys. Tech. J.*, **35**, 637 (1956).
2. S. J. Silverman, Private communication.
3. E. D. Kolb and M. Tanenbaum, *This Journal*, **106**, 597 (1959).
4. S. E. Bradshaw and A. I. Mlavsky, *J. Electronics*, **2**, 134 (1956).
5. H. E. Bridgers, Private communication.
6. K. Lark-Horovitz, Semiconducting Materials—Proc. of Conf. at Univ. Reading, p. 47, Butterworths, London (1951).
7. J. H. Reynolds and J. Verhoogen, *Geochimica et Cosmochimica Acta*, **3**, 224 (1953).
8. R. O. Carlson, R. N. Hall, and E. M. Pell, "Advances in Semiconductor Science," p. 81, Pergamon, New York (1959).
9. H. C. Schweinler, *J. Appl. Phys.*, **30**, 1125 (1959).
10. G. K. Wertheim, *Phys. Rev.*, **111**, 1500 (1958).
11. W. L. Brown, W. M. Augustyniak, T. R. Waite, and K. A. Wright, *J. Appl. Phys.*, **30**, 1258 (1959).
12. G. K. Wertheim and W. M. Augustyniak, *Rev. Sci. Instr.*, **27**, 1062 (1956).
13. J. M. Goldey, Private communication.
14. G. K. Wertheim and D. N. E. Buchanan, *J. Appl. Phys.*, **30**, 1232 (1959).

Coatings for Columbium

S. T. Wlodek[1]

Technology Department, Union Carbide Metals Company,
Division of Union Carbide Corporation, Niagara Falls, New York

ABSTRACT

The degree of protection from high-temperature oxidation which can be imparted to columbium by ten different types of coatings was evaluated. The coatings were applied by Plasmarc, detonation gun, or gun-metallizing processes. Although chromium, stainless steel, and Nichrome protected columbium from gross oxidation in the temperature range of 950°-1150°C for hundreds of hours, chromium coatings allowed oxygen contamination of the columbium to occur as low as 950°C. A coating of LM-5 (Mo-Si-Cr-B-Al) prevented all reaction for about 1000 hr at 1150°C and 100 hr at 1500°C. The LM-5 coating behaved well under stress and exhibited some self-healing properties and thermal shock resistance. The latter two properties can be increased even further by introducing an alloy layer of the Cb-Ti-Cr-Al-Ni type between the LM-5 and the columbium article. This duplex coating retained the static exposure resistance and strain-rate insensitivity of the LM-5, while being able to withstand 30 water-quenches from 1150°C before failure. These results indicate that satisfactory protection can be obtained for very simple columbium shapes. The coating of shapes large and complex enough to represent a commercially significant component is still an unsolved problem.

The high melting point (2450°C), medium density (8.6 g/cc), and low thermal neutron cross section (1·1 barns) of pure columbium have served to stimulate research on Cb-base alloys for elevated temperature structural applications. With the exception of nuclear applications, Cb-base alloys are generally being considered for service in the temperature range of 1000°-1400°C, a temperature range within which alloys with adequate mechanical properties can be suggested (1).

Due to the low vapor pressure and high melting point of the oxidation products, the problem of designing a satisfactory coating for Cb appears to be easier than for many of the other refractory metals. Cb_2O_5, the predominant oxide formed on oxidizing pure Cb, melts above 1450°C and possesses a very low vapor pressure below 1400°C. In a coated Cb body, therefore, the problem of interaction with a corrosive liquid oxide will not be encountered below 1450°C, and the low vapor pressure of the oxidation products will not produce the physical disintegration of the coating-metal interface that is observed in the case of molybdenum- and tungsten-base systems. Columbium, however, possesses a large solubility for oxygen and nitrogen, and if the coating should allow the diffusion or penetration of these elements into the columbium body, the resultant embrittlement might prove as disastrous as actual failure by oxidation.

The limited work on coatings for Cb which has appeared in the literature has not been encouraging. Beach (2) evaluated the possibility of electroplating Cb with Fe, Ni, Cr, or Pt. Due to the cathodic charging of hydrogen during plating, only very thin electroplates of Fe were found to adhere well. None of these electrodeposited coatings were oxidation resistant enough to warrant further attention. Hirakis (3) has reported some exploratory results obtained in a program directed at developing a high-temperature coating for columbium. The more promising coatings consisted of Al-Ni-Cr-Fe-Si combinations, but none of them could withstand 1 hr at 1370°C.

[1] Present address: Flight Propulsion Laboratory, General Electric Company, Cincinnati, Ohio.

Experimental

General procedure.—Since the main objective of this study was to determine the degree of high-temperature stability that an oxidation-resistant coating can impart to a Cb article, no experimentation on coating techniques was attempted. Plasmarc (4), detonation-gun (5), and gun-metallizing processes were used to apply the different coatings studied. In all cases, standard operating techniques (6) were employed in applying the coatings. Although this approach allowed the study of a large variety of coatings, the practical application of the resultant data is limited to the simple sample geometries that can be coated by the above processes.

Two main types of coatings were evaluated during this study. The first consisted of generally available oxidation-resistant alloys: $CbAl_3$, NiAl, ZrO_2, unalloyed Cr and 302 stainless steel (18-8), Nichrome V (80% Ni, 20% Cr), LA-4 (70% Nichrome V + 30% Al_2O_3), and, LM-5 (40% Mo, 40% Si, 8% Cr, 2% B, 10% Al).

The second type was duplex coatings consisting of an outside layer of chromium or LM-5 superimposed on an inner layer of an oxidation-resistant Cb-base alloy of the Cb-Ti-Cr-V-Al family. The Cb-Ti-Cr-V-Al alloys were selected on the basis of their good oxidation resistance to act as a transition layer between the outside coating and the colum-

bium article. The composition of these alloys is given in Table I, while the oxidation resistance of one of them (D-947) is compared with Cb and stainless steel in Table II.

The behavior of the different coating materials was studied by applying the coating in question to Cb by either the Plasmarc or detonation-gun techniques and evaluating its protective nature under various test conditions. Throughout this study, cold-swaged Cb with the analysis given in Table III was used.

Five types of tests served to determine the degree of protection afforded by the coating. All coatings were first subjected to exposure in static air at constant temperature until failure. Those coatings which showed promise in this test were re-evaluated on the basis of the amount of oxygen or nitrogen contamination which the base metal suffered. The coating systems which still appeared promising were further evaluated for thermal shock resistance and self-healing properties, as well as behavior under stress. In all the tests, the criterion for failure was the first appearance of Cb_2O_5 as determined by visual examination of the specimen.

Static testing.—The static exposure test consisted of heating the coated body on an alumina holder in an open-end, horizontal tube furnace. The specimen was either a 3/16- or 1/4-in. diameter rod with hemispherical ends. Each coating type was tested at 950°C and, if the results warranted it, at temperatures of 1150°-1500°C. At 1500°C, however, alumina holders were found to react with the LM-5 coating, and pure $MoSi_2$ containers had to be used. To guard against excessive thermal shock, specimens were introduced into the hot zone gradually and not removed until failure had occurred.

Table I. Chemical analyses of coating alloys*

Powder type No.	Columbium Alloys Composition, weight per cent Cb	Ti	Cr	V	Fe	Ni	Al
D-945	44.7	32.3	14.9	4.84	—	—	4.24
D-947	43.6	31.1	10.2	—	0.76**	9.9	3.18
D-948	43.9	30.4	9.76	—	11.5	—	3.10
G-418	42.2	28.7	11.1	—	—	9.2	3.4

	Normal Composition of LM-5 Mo	Si	Cr	B	Al
Usable range (7)	30-60	20-50	5-25	1-5	5-20
Used in this study	40	40	8	2	10

* After grinding to minus 325-mesh powder.
** Picked up during grinding to powder.

Table II. Comparison of the oxidation resistance of D-947

Material	100-Hr weight gain (mg/cm²) for exposure in pure oxygen at 800°C	1000°C	1200°C
Pure columbium	3630	6670	24,000
47% Cb-30% Ti-10% Cr-10% Ni-3% Al (D-947)	5.58	19.3	229
304 Stainless steel	2.13	8.64	839
316 Stainless steel	4.91	41.6	131

Table III. Chemical analysis of columbium used

Element	Wt %
Carbon	0.036
Oxygen	0.05
Nitrogen	0.014
Tantalum	0.12
Iron	<0.01

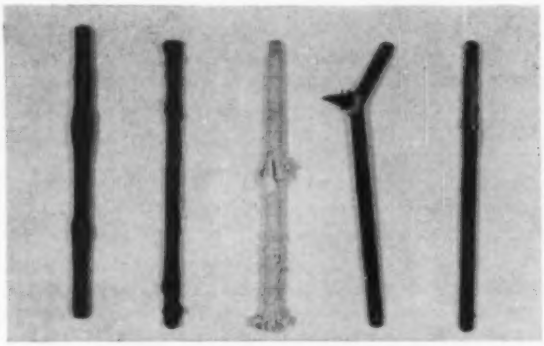

Fig. 1. Appearance of coated specimens after failure. From left to right: Nichrome V coating oxidized through after 104 hr at 1150°C; 302 stainless steel-coated specimen showing signs of fusion (8 hr; 1150°C), failure of $CbAl_3$ coating (22 hr; 950°C) due to porosity, local failure of LM-5 coating (192 hr, 1150°C), and Cr-coated specimen which failed on heating due to poor bonding.

Figure 1 illustrates the visual appearance of characteristic specimens after failure. Most of the static failures which are noted for each sample in Table IV were due to: (*a*) general oxidation of the coating often accentuated by some local weakness; (*b*) porosity through which the Cb oxidized; (*c*) large local weaknesses or thin spots which allowed premature failure; and (*d*) exfoliation due to poor as-coated bond strength.

Coatings such as LA-4, NiAl, some of the Cr coatings, and all the duplex Cr Cb-base alloy specimens failed by exfoliation within 1 hr after reaching temperature. The visual appearance of a Cr-coated sample (Fig. 1) exemplifies this type of failure which originated at the coating-metal interface due to excessive thermal expansion stresses on heating or a poor as-plated bond.

Gross as-plated porosity was the defect principally responsible for the premature failure of the ZrO_2 and $CbAl_3$ coatings. The columbium oxides growing in the pores physically disrupted the coating. The best ZrO_2- and $CbAl_3$-coated specimens lasted only 5 and 22 hr, respectively, at 950°C.

Nichrome V, 302 stainless steel, Cr, LM-5, and the LM-5 plus Cb alloy duplex coatings failed by the general oxidation of the coating until the Cb base became exposed. This process, however, rarely goes to completion, failure usually being accentuated by a crack, thin spot, or other form of local coating discontinuity. In general, Nichrome V, 302 stainless steel, Cr, and various LM-5 combinations provided adequate protection for hundreds of hours at 950°C.

Failure caused by general oxidation is typified in Fig. 1 by a Nichrome V-coated specimen. At 1150°C, failure of stainless steel coatings was accentuated

Table IV. Static exposure testing of coated columbium in air

Coating type	Applied by	Thickness, mils	Test temp, °C	Life, hr	Remarks
LA-4(70% Nichrome 30% Al_2O_3)	D-gun	5.0*	950	<1	All samples failed on heating (3 samples)
NiAl	D-gun	4.0*	950	1	All samples failed on heating (3 samples)
Nichrome V	D-gun	4.5	950	23	Local failure
Nichrome V	D-gun	4.5	950	500	General oxidation
Nichrome V	D-gun	4.5	1150	104	General oxidation
Nichrome V	Metallized	10.0	1150	168	Local failure
Nichrome V	Metallized	10.0	1150	500±10	General oxidation
Nichrome V	Metallized	10.0	1250	25	General oxidation
Nichrome V	Metallized	10.0	1250	25	General oxidation
302 Stainless steel	D-gun	4.5	950	28	Local failure
302 Stainless steel	D-gun	4.5	950	366	General oxidation
302 Stainless steel	D-gun	4.5	1150	8	General oxidation
$CbAl_2$	D-gun	4.5	950	6	Porous coating
$CbAl_2$	D-gun	4.5	950	22	Porous coating
$CbAl_2$	D-gun	2.0	950	>2	Porous coating
ZrO_2	Plasmarc	3.5	950	5	Coating exfoliated, porosity
Chromium	Plasmarc	4.0	950	555	General oxidation
Chromium	Plasmarc	3.5	1150	>0.5	Failed on heating, exfoliated
Chromium	Plasmarc	7.5	1150	165	General oxidation
Chromium	Plasmarc	7.5	1150	40	Local failure
Chromium	Plasmarc	7.5	1150	<1	Failed on heating, exfoliated
Chromium	Plasmarc	7.5	1150	<1	Failed on heating, exfoliated
Chromium	Plasmarc	7.5	1150	18	Coating exfoliated
Chromium	Plasmarc	7.5	1150	18	Coating exfoliated
Chromium + D-945	Plasmarc	4 + 3*	1150	0 to 1	All suffered local failure or failed on heating (7)
LM-5	D-gun	3.0	950	4	Local failure
LM-5	D-gun	3.0	950	<700	General oxidation
LM-5	D-gun	3.0	1150	192	General and local oxidation
LM-5	Plasmarc	7.5	1150	>1008*	No failure some oxidation
LM-5	Plasmarc	8.0	1150	>1050*	No failure some oxidation
LM-5	Plasmarc	4.5	1250	840	General oxidation
LM-5	D-gun	6.5	1250	680	Local failure, general oxidation
LM-5	D-gun	4.5	1250	672	Local failure, general oxidation
LM-5	D-gun	4.0	1500	84	General oxidation
LM-5	D-gun	4.5	1500	108	General oxidation
LM-5	Plasmarc	4.5	1500	>6 to 10	Reacted with holder
LM-5 + D-945	Plasmarc	4.0 + 5.0	1150	>1050**	No failure some oxidation
LM-5 + G-418	D-gun	4.0 + 4.0	1250	672	Cracked on cooling from furnace
LM-5 + G-418	D-gun + Plasmarc	4.0 + 4.0	1500	>6 to 10	Reacted with holder

* Average thickness of all samples tested.
** Drilled for self-healing tests, re-exposed for 138 hr at 1050°C with no further deterioration of undamaged areas.

by local fusion, which probably involved melting of the oxide mixtures of Fe and/or Cr, and Cb.

Data presented in Table IV indicate that same 3- to 4-mil thick coatings of 302 stainless steel, Cr, Nichrome V, and LM-5 can protect Cb under static conditions at 950°C for 350, 500, 550, and 700 hr, respectively. At 1150°C, 302 stainless steel, Cr, Nichrome V, or LM-5 coatings of the same thickness will protect columbium for 8, 100, 165, and in excess of 1050 hr, respectively. LM-5 retains its protective nature to much higher temperatures. A 4.5-mil coating provided 840 hr of protection at 1250°C, and the same thickness sufficed for about 100 hr at 1500°C. The static oxidation behavior of the duplex LM-5 plus Cb alloy combination is governed by the outer LM-5 layer, the life to failure of this two-layer coating being similar to that of the straight LM-5 coating. Thicker coatings are, of course, more protective.

If the life of an adherent and dense coating on Cb depends on the time for which the coating can withstand oxidation at temperature, the results pre-

Table V. Correlation factor for static exposure behavior of some coatings on columbium

Coating type	X coating thickness, mils	T test temp, °C	t, life in hr	K*, in mils²/hr
Pure Cr	4.0	950	555	0.029
Pure Cr	7.5	1150	165	0.34
Nichrome V	4.5	950	500	0.04
Nichrome V	4.5	1150	104	0.19
Nichrome V	10.0	1150	500	0.20
Nichrome V	10.0	1250	25	4.0
Nichrome V	10.0	1250	25	4.0
302 Stainless steel	4.5	950	366	0.55
302 Stainless steel	4.5	1150	8	2.50
LM-5	3.0	950	700	0.013
LM-5	3.0	1150	192	0.047
LM-5	7.5	1150	1008	0.052
LM-5	8.0	1150	1050	0.061
LM-5	4.5	1250	840	0.024
LM-5	6.5	1250	680	0.062
LM-5	4.5	1250	672	0.03
LM-5	4.0	1500	84	0.19
LM-5	4.5	1500	108	0.187

* Calculated from $K = x^2/t$.

sented above can be described by the following *empirical* equation:

$$X^2 = Kt \qquad [1]$$

where X is coating thickness in mils (in. x 10^{-3}), t is life of the coating in hours under static exposure to air, and K is proportionality constant in units of (mils)²/hr.

The validity of this equation in predicting the life to failure can be judged by referring to Table V, which lists the values of the constant K for pure Cr, Nichrome V, 302 stainless steel, and LM-5 over the temperature ranges used in the static evaluation. The constant K in Eq. [1] can be used to estimate roughly the life of a particular coating for any thickness or temperature condition. Using these values for K, it is possible to show that a 1-mil coating of 320 stainless steel, Cr, Nichrome V, and LM-5 will protect Cb for 10 hr at about 700°, 1050°, 1060°, and 1400°C, respectively (Fig. 2).

LM-5 is the only coating which can be used effectively above 1250°C. Both Nichrome V and Cr are effective for long-time service only below 1150°C,

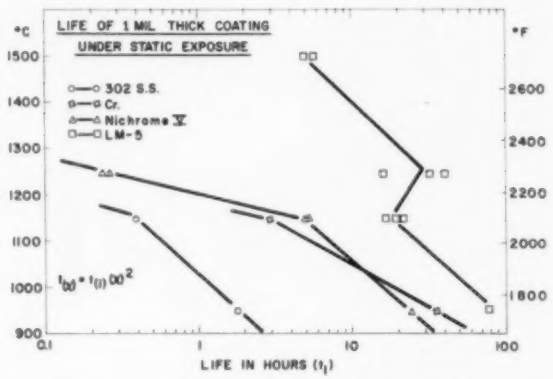

Fig. 2. Correlation of life to failure against test temperature for a number of coating systems as reduced to a 1-mil coating thickness by Eq. [1].

with Nichrome V being slightly preferred above 1050°C, while Cr is superior below 1050°C. The 302 stainless steel is considerably less protective, being, however, extremely useful for long-term service below 1000°C.

Contamination of coated columbium.—The amount of oxygen or nitrogen contamination which occurred during static exposure tests was determined by metallographic and microhardness techniques. The thicknesses and hardnesses of the contamination and interdiffusion bands which developed during static testing of the more promising coatings are given in Table VI. In some cases, the oxygen contamination of the Cb substrate is also reported on the basis of the average vacuum-fusion oxygen analysis of the specimen after removal of the coating. A plot of Vickers microhardness against distance from the coating-metal interface is given for some of the specimens after air exposure at 1150°C in Fig. 3.

The hardness increases noted are due to two sources, the first being the solution of the coating constituents in the Cb during service. This accounts for the 3- to 10-mil thick "interfacial" hardened layers found in all samples coated with LM-5, LM-5 plus D-945, or stainless steel and Nichrome-coated bodies tested at 950°C. Chromium coatings at all temperatures tested and Nichrome V coatings at

Table VI. Hardness traverses of coated columbium

Coating	Test temp, °C	Time at temp, hr	Interfacial hardness band: V.P.H. range	Interfacial hardness band: Band width, mils	Interior hardness band: Max. V.P.H.	Interior hardness band: Band width, mils	Oxygen analysis on Cb after removal of coating
Nichrome V	950	23	205-160	6.0	140*	None	0.07%
Nichrome V	1150	500	225-200	3.0	200	2500**	—
302 S.S.	950	366	172-160	6.0	150*	None	0.08%
Cr	950	555	300-240	7.0	200	1250**	0.49%
Cr	1150	40	250-220	10.0	210	70.0	0.13%
LM-5	950	700	150-140	6.0	125*	None	0.06%
LM-5	1150	1008	150-140	3.0	130*	None	—
LM-5	1150	1050	175-160	6.0	150*	None	—
LM-5	1250	840	300-170	5.0	120*	None	—
LM-5 + D-945	1150	1050	295-160†	4.0†	130*	None	—

* Equivalent to initial hardness, no hardening outside of thin band next to coating interface.
** Whole specimen contaminated to this hardness level.
† Includes width and hardness of D-945.

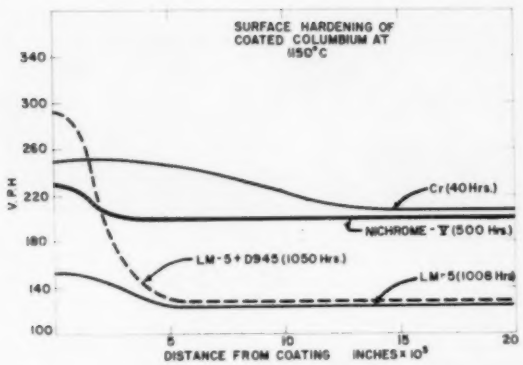

Fig. 3. Microhardness profiles of Cb metal adjacent to the coating interface. All samples exposed at 1150°C for times equivalent to the limit for each type of coating. The hardness increases stem from two sources. The first represents the solution of the coating in the first 2-5 mils of the coated body. The second, as exhibited by the samples coated with Cr or Nichrome V, reflects the contamination of the specimen by atmospheric gasses.

1150°C, however, appear to permit the hardening of the Cb by the introduction of oxygen and/or nitrogen. This contention is borne out by the vacuum-fusion oxygen analyses tabulated in Table VI. It is possible to conclude that stainless steel and Nichrome V at 950°C and LM-5 or LM-5 plus D-945 coatings at all temperatures tested protect Cb from oxygen embrittlement and are insoluble enough in the Cb article to produce only a thin interdiffusion layer.

The mechanism of contamination is believed to be the diffusion of oxygen and nitrogen through the coating or through Kirkendall pores that form readily, especially in the case of Cr coatings. The characteristic Kirkendall porosity and the presence of discrete oxide particles which formed during exposure are clearly visible in the chromium and Nichrome coatings after exposure at 1150°C (Fig. 4a and 4b). Although the LM-5 coating had almost completely oxidized away after 840 hr at 1250°C (Fig. 4c), the remaining material was unaffected, and little or no oxygen contamination took place. All of these observations were made on samples whose as-plated coating was dense and free of porosity.

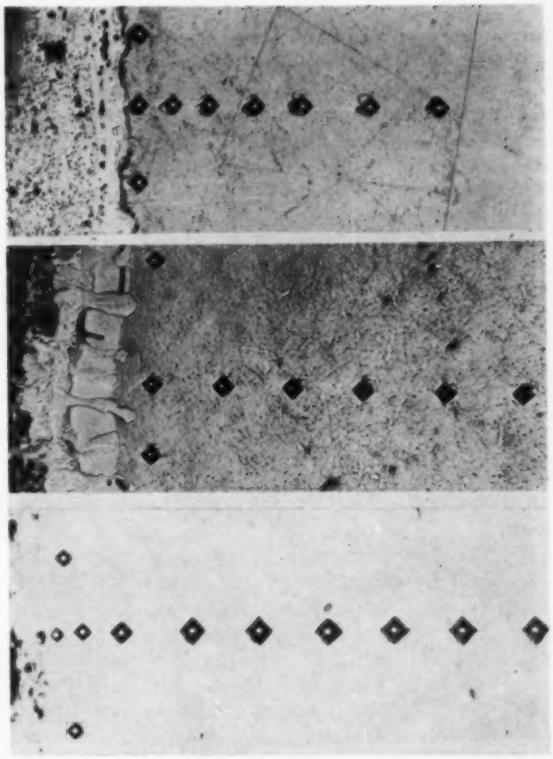

Fig. 4a. (top) 7.5 mils Cr (far left). Sample exposed 40 hr at 1150°C. Note porosity which could act as a source of oxygen contamination. Microhardnesses, center line: 252, 252, 256, 240, 236, 228, 211 V.P.N. (left to right).

Fig. 4b. (center) 10 mils Nichrome V (partially visible at far left). Sample exposed 500 hr at 1150°C. Note wide zone of intermetallic compounds and porosity in Nichrome V. In Fig. 4a and 4b the porosity formed during exposure and was not present in the as-plated condition. Microhardnesses, center line: 225, 202, 208, 214, 205, and 225 V.P.N. (left to right).

Fig. 4c. (bottom) 4.5 mils LM-5 (far left). Sample exposed 840 hr at 1250°C. Microhardnesses, center line: 410, 247, 177, 128, 116, 110, 112, 106, and 110 V.P.N. (left to right). Unetched. Magnification 200X before reduction for publication.

Thermal shock testing.—Since only LM-5 or LM-5 plus the Cb alloy duplex coatings withstood gross oxidation and contamination under static conditions

Table VII. Thermal shock testing of LM-5 and duplex-type coatings from 1150°C

Coating type	Thickness, mils	Type and No. of cycles	Life in hr*	Remarks
LM-5	7.5	31 A.C.	194	No failure
LM-5	7.5	27 A.C.	167	No failure
LM-5	7.5	3 W.Q.	142	W.Q. started after 120 hr previous static exposure
LM-5	7.5	5 W.Q.	154	
LM-5 + D-945	4.0 + 4.0	7 W.Q.	136	Local crack
LM-5 + D-947	4.0 + 3.0	30 W.Q.	267	Local crack
LM-5 + D-947	4.0 + 3.0	24 W.Q.	188	Local crack
LM-5 + D-948	4.0 + 3.0	21 W.Q.	248	Local crack
LM-5 + D-948	4.0 + 3.0	—	1	Local failure

A.C., Specimen removed from furnace and air-cooled three times per 24-hr period to room temperature and immediately replaced.
W.Q., As above only directly quenched in water.
*, Total time at temperature between thermal cycles before failure.

at 1150°C, only these types of coatings were evaluated for thermal shock properties. LM-5 coatings withstood, without failure, in excess of 30 air-cooling cycles from 1150°C (Table VII) but failed after 3-5 water-quenching cycles. The behavior of the duplex coatings was markedly better. In particular, the LM-5 plus D-947 (Cb-Ti-Cr-Al-Ni) or LM-5 plus D-948 (Cb-Ti-Cr-Al-Fe) combinations withstood 21-30 water-quenches before local failure occurred.

The excellent thermal shock resistance of the duplex coatings at 1150°C can be associated with the presence of small amounts of liquid phase in the Cb-Ti-Cr-Al plus Fe or Ni alloy. Although the amount of liquid phase formed at 1200°C in an alloy of this type is some 20-30 volume %, the loss of the low melting point constituent during Plasmarc plating reduces the amount of liquid phase present in the as-plated D-947 composition to about 5%. Figure 5 illustrates the microstructure of such a duplex coating.

Self-healing properties of LM-5 coatings.—The self-healing tendencies of punctured LM-5-type coatings were measured on three samples, two of which had been coated with the straight LM-5 coating, while the third had been coated with a duplex combination of LM-5 plus D-945. All three specimens had withstood in excess of 1000 hr exposure at 1150°C without failure. After this exposure, the three specimens were drilled to produce equally spaced damaged areas, 0.0135, 0.02, 0.031, and 0.04 in. in diameter with a depth slightly in excess of the coating thickness. The specimens were then exposed again in air at 1050°C to determine the amount of oxidation that would occur through the punctured coating.

After 18 hr at 1050°C, appreciable oxidation occurred at each damaged area for specimens covered with the LM-5 coating, producing small protuberances of Cb_2O_5, some 1/32 in. high. The amount of oxidation which occurred in the LM-5 plus D-945 coated specimen after 18 hr at 1050°C was much less. Following this visual examination, the specimens were re-exposed at 1050°C for a further 120 hr. The specimens were then sectioned and examined metallographically to determine the amount of oxygen contamination and metal conversion to oxide that resulted in the areas of coating damage (Fig. 6). The results of these measurements are given in Table VIII.

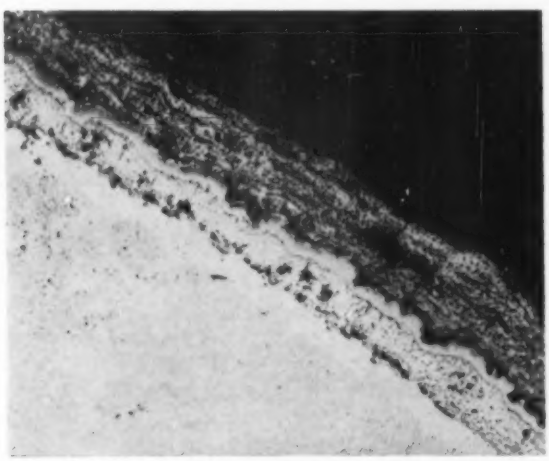

Fig. 5. Duplex coating of LM-5 (top) and D-947 (center) on Cb (bottom). After 188 hr at temperature and 37 water-quenches from 1150°C. Unetched. Magnification 200X before reduction for publication.

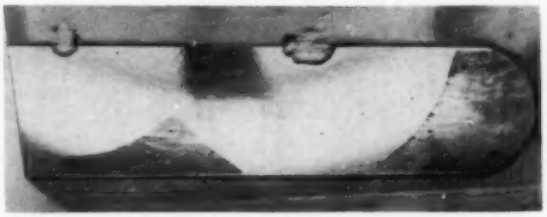

Fig. 6. Resistance of LM-5 coating to oxygen penetration. 7.5 mils LM-5 exposed 1008 hr at 1150°C, then drilled to damage coating and re-exposed for 138 hr at 1050°C. Note arcs of oxygen-contaminated Cb originating at areas of damage. Hardness of contaminated Cb 180 V.P.N.; uncontaminated 140 V.P.N. Etched with 1HF: 1HNO_3: 2 Glycerol. Magnification 7X before reduction for publication.

These data illustrate that the straight LM-5 coating, when damaged by the removal of an area some 40 mils in diameter, allows the oxidation of only 80 mils of Cb to take place in 138 hr at 1050°C. Uncoated Cb under the same conditions would react with air to produce an oxide penetration, or metal loss rate, of some 400-700 mils. The LM-5 coating, therefore, reduces the amount of penetration that occurs by a factor of at least five. The system is thus partially self-healing, or at least not very sensitive to fairly extensive coating damage. The behavior of the LM-5 plus D-945 coating was about the same as the straight LM-5 for holes of 40 mils diameter but appreciably better for pores of smaller diameter. This is shown in Fig. 7 which presents a plot of depth of oxidation below each pore *vs.* diameter of pore for LM-5 and LM-5 plus D-945 coatings exposed at 1050°C for 138 hr. Although the LM-5 plus D-945 combination is much more self-healing for coating discontinuities in the size range of 20-30 mils, the LM-5 and LM-5 plus D-945 coatings behaved much the same with pores produced in the size range above 30-40 mils. The amount of oxygen contamination which occurs through the damaged

Table VIII. Self-healing in LM-5 and LM-5 + D-945 coatings

	A 7.5 mil LM-5; drilled and exposed at 1050°C for 138 hr		B 4.0 mil LM-5 + 5.0 mil D-945; drilled and exposed at 1050°C for 138 hr	
	Depth, mils, of		Depth, mils, of	
Diameter of pore, mils	Oxide* penetration	Oxygen contamination	Oxide* penetration	Oxygen contamination
13.5	32	2000	22	1200
20.0	50	1600	32	1200
31.0	75	2700**	42	1600
40.0	80	2300	75	2000

* Pure, unclad Cb under same conditions would exhibit an oxide penetration or metal loss value of some 400-700 × 10^{-3} in.
** Exceeds 0.25-in. specimen diameter; estimated from contamination arc geometry.

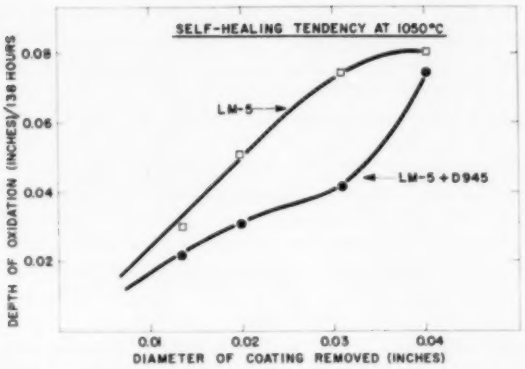

Fig. 7. Relation of depth of metal consumed and diameter of artificially created discontinuity as a measure of the self-healing tendency of LM-5 and the duplex LM-5 + D945 coatings.

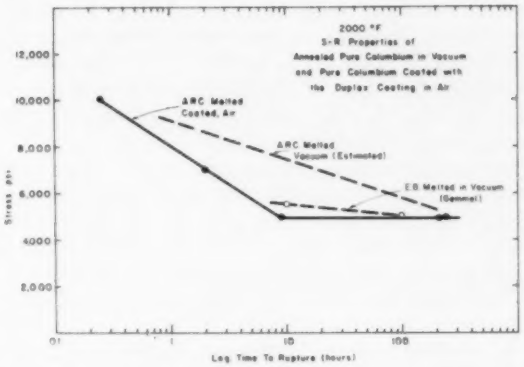

Fig. 8. Stress-rupture properties of unalloyed Cb; uncoated, in vacuum and coated wth the duplex coating, in air.

coating is, however, about the same as might be expected from oxygen diffusion in columbium. The oxygen contamination data given in Table VIII for pores of different diameter indicate that the LM-5 plus D-945 combination is slightly superior to the straight LM-5 coating in preventing oxygen contamination through the damaged area. Although the rate of oxygen contamination through the artificially damaged coating was rapid in both cases, no contamination occurred in areas where the coating was dense, even though most of these coated bodies had been tested in excess of 1000 hr, in air, at 1150°C before the coatings were punctured.

Creep-rupture testing of LM-5-coated columbium.—Conical, creep-rupture specimens of Cb, coated with 6-7 mils of LM-5 or with 4 mils of LM-5 plus 4 mils of G-418 (46% Cb-30% Ti-10% Cr-4% Al-10% Ni alloy), were tested in creep-rupture in air at 1093°C (2000°F). Before testing, the specimens were screened by exposing them at 1150°C for 24 hr. Specimens containing as-plated inhomogeneities or discontinuities in the coating were thus eliminated.

The results obtained are presented in Table IX in terms of the creep rate measured during the first and second stages of creep as well as the time interval of the creep-rupture test during which each stage operated. The results did not permit any differentiation in the behavior between the LM-5 and the LM-5 plus G-418 duplex coating. The time to rupture is plotted in Fig. 8 which compares the stress-rupture properties of the LM-5-coated specimens in air at 1093°C with the stress-rupture properties of electron beam melted high-purity Cb tested in vacuum by Gemmel (8) and an estimated curve for columbium of the purity used in this coating study.

Comparison of the stress-rupture results of LM-5-coated Cb in air with comparable purity Cb tested in vacuum indicates that the 100-hr life in air of the coated Cb is almost identical to that exhibited by Cb in vacuum. At higher stresses, which produce creep rates in excess of that to which the coating can accommodate itself, lower creep-rupture properties are obtained. By referring to creep rates presented in Table IX, it appears that the LM-5 coating or the LM-5 plus G-418 duplex combination is resilient enough to withstand creep rates of the order of 2-3%/hr as experienced during the first stage of creep for time intervals of 3-5 hr. Creep rates of the order of 0.1-0.2%/hr can be withstood for hundreds of hours without reducing the stress-rupture properties inherent in the columbium body.

Discussion

The results of this study indicate that coatings of 302 stainless steel, Cr, Nichrome V, and LM-5 can be used to allow the high-temperature service of coated Cb structures in air. The upper service limit of Type 302 stainless steel, Cr, and Nichrome V was found to be about 1100°C. For prolonged service, 302 stainless steel coatings should not be used in excess of 1000°C, while thick Nichrome coatings could perhaps be used as high as 1150°C. These temperature limits do not allow for the fact that Cr-

Table IX. Creep-rupture testing of coated columbium* in air at 1093°C (2000°F

Coating type	Applied by	Coating thickness, mils	Stress, psi	Creep rate, in./in./hr during First stage	Creep rate, in./in./hr during Second stage (M.C.R.)	Time in hours to end of First stage	Time in hours to end of Second stage	Hours to rupture
LM-5	D-gun	7.0	5,000	2.68	0.166	3.0	120.0	123.0
LM-5	D-gun	6.0	10,000	50.0	21.5	0.1	0.24	0.25
LM-5 + G-418	Plasmarc + D-gun	4.0 + 4.0	5,000	2.33	0.103	5.0	123.0	124.0
LM-5 + G-418	Plasmarc + D-gun	4.0 + 4.0	5,000	8.0	1.17	1.0	7.0	9.4
LM-5 + G-418	Plasmarc + D-gun	4.0 + 4.0	7,000	16.7	7.15	0.2	1.6	2.0

Before testing, the specimens were heated for 24 hr at 1150°C (2100°F). Two specimens failed under this test and were not tested in creep-rupture.

* At 2000°F and in inert atmosphere, the ultimate tensile strength of this lot of Cb is about 12,000 psi, and the stress for 100-hr life in vacuum is about 6000 psi.

coated Cb bodies were found susceptible to oxygen penetration through the coating at temperatures as low as 950°C, while Nichrome V-coated bodies suffered the same type of embrittling contamination at 1150°C. All of these results were obtained with dense and porosity-free coatings.

Of all the coatings tested, the most satisfactory was the LM-5 (Mo-Si-Cr-B-Al alloy) coating or its duplex modifications. Coatings of this type were protective above 1100°C at which temperature a 5-mil thick coating of LM-5 suffices for about 700 hr. Indeed, even at 1500°C, 4.5 mils of LM-5 protected columbium from oxidation for 108 hr.

In addition to static protection, the straight LM-5 coating resists oxygen contamination of the Cb body during service, possesses considerable resilience under stress, and at least some self-healing and thermal shock resistance. In addition, at 1093°C, LM-5-coated Cb exhibits the same stress-rupture properties in air as uncoated Cb would exhibit when tested in high vacuum. The behavior of the LM-5 coating on Cb exceeds, or at least equals, the behavior of the best coatings on Mo. Even further improvements in regard to the self-healing and thermal shock properties of the LM-5 coating can be obtained by precoating the Cb article with an alloy of the Cb-Ti-Cr-Al-(Ni or V) family. Such duplex coatings retain the static exposure, oxygen contamination, and resilience under stress exhibited by the LM-5 coating while improving its self-healing and thermal shock properties. An undercoating of 3.0 mils of D-947 (47% Cb-30% Ti-10%Cr-10% Ni-3% Al), for instance, allowed an LM-5 coated body to withstand 24-30 water-quenches from 1150°C before failure.

Factors affecting coating behavior.—As a result of these tests, a series of generalizations can be made. In the first place, the coating must be oxidation resistant enough to withstand exposure at temperatures where Cb alloys can be economically used. The exploitation of Nichrome, Cr, and stainless steel is primarily limited by their decreasing oxidation resistance above 1100°C. More oxidation-resistant materials such as NiAl, $CbAl_3$, or zirconia were not found satisfactory due primarily to the difficulty of depositing adherent and porosity-free coatings. The LM-5 coating provided the best combination of as-plated adherence and density with excellent oxidation resistance, the latter property stemming directly from its molybdenum disilicide characteristics, a material in which the rate of oxidation between 1100°-1550°C is almost insensitive to temperature. This property stems from the silica film that develops by vaporization of the Mo as molybdenum trioxide and the retention of the Si in a silica film tightly adhering to the body. This mechanism provides a renewable film of a tightly adherent oxide which, however, does not form readily below 1100°C, especially in flowing air, and is not stable above 1550°C, where SiO becomes a volatile species (9). These limitations in the oxidation behavior of pure molybdenum disilicide are partially overcome by the addition of Cr, B, and Al which are present in the LM-5 coating designed by Weatherly and Conant (7). The high-temperature oxidation products on LM-5 consist of a layer of mullite ($3Al_2O_3 \cdot 2SiO_2$) and cristobalite. In addition, the presence of B and Cr aids in the development of oxidation-protective films at a temperature below that needed for the formation of the mullite and cristobalite combination. Although the experimental data and the nature of the oxidation process of LM-5 suggest that this coating could be used to 1550°C or above, such temperatures should be considered only for non-critical components. This limitation is imposed by the melting point of Cb_2O_5(1450°C), and the consideration that liquid oxidation products would produce catastrophic failure whenever a coating discontinuity should occur.

The improved thermal shock resistance and self-healing properties of the duplex LM-5 plus Cb alloy combination are believed to be due to the small amount of liquid phase that forms in the Cb alloy layer. Although the amount of liquid phase present at about 1200°C in the as-plated subcoating is not believed to exceed 5-10 volume %, this amount appears sufficient to absorb and even out the shear stresses that are produced at the coating-metal interface on thermal cycling. In addition, if the LM-5 coating should be damaged, the small amount of liquid phase, rich in the elements Ti, Ni, Cr, V, and Al which improve the oxidation resistance of Cb, can seep into the crack. As there is some experimental evidence to show that the amount of liquid phase that forms in a Cb-Ti-Cr-Ni-Al alloy at 1200°C is decreased by oxygen contamination, it is possible to propose that, once the crack has been partially infiltrated with the Cb-base alloy, oxygen contamination will raise the melting point of the infiltrated material to the point that solidification occurs.

Conclusions

A variety of coatings can be used to protect Cb at elevated temperatures. Type 302 stainless steel, Nichrome V, and Cr can be exploited best below 1100°C with the limitation that Cr coatings allow oxygen contamination of the base metal to occur as low as 950°C. For high-temperature, high-strength applications above 1150°C, the LM-5 or LM-5 duplex coatings appear most promising.

Unalloyed Cb was used in this study to evaluate the coating material under more stringent conditions than those which would have been experienced if an oxidation, or oxygen-contamination-resistant, alloy had been used. However, since the geometry of the specimens used was such as to eliminate sharp radii of curvature from the coated shape, the results obtained cannot be extrapolated directly to structures with sharp surface discontinuities. This limitation, as well as the size and shape limitations, inherent in the Plasmarc and detonation-gun coating processes do not allow the immediate extrapolation of these results to commercial conditions. Indeed, coatings of the quality tested here cannot at present be applied to most actual parts of interest. The results of this work are thus best regarded as the characterization of the behavior of a series of coating systems on Cb.

Acknowledgments

The author is indebted to the staff of the Speedway Laboratories, Linde Company, for the application of the coatings and for Mr. D. R. Hilburger's assistance in the performance of the testing program.

Manuscript received Aug. 8, 1960; revised manuscript received Sept. 20, 1960. This paper was prepared for delivery before the Indianapolis Meeting, April 30-May 4, 1961.

Any discussion of this paper will appear in a Discussion Section to be published in the December 1961 JOURNAL.

REFERENCES

1. D. L. Douglass, Editor, "Columbium Metallurgy Symposium Proceedings," Sagamore, N. Y. (1960).
2. J. G. Beach, "Electroplated Metals on Niobium," in "Technology of Columbium," B. W. Gonser and E. M. Sherwood, Editors, John Wiley & Sons, Inc., New York (1958).
3. E. C. Hirakis, WADC TR 58-545, "Research for Coatings for Protection of Niobium Against Oxidation at Elevated Temperatures," (February 1959).
4. R. M. Gage, (assigned to Union Carbide Corp.) U. S. Pat. 2,862,099 (1958).
5. R. M. Poorman, H. B. Sargent, and H. Lamprey, (assigned to Union Carbide Corp.) U. S. Pat. 2,714,563 (1955).
6. J. W. Lyle, R. G. Rudness, and D. M. Yenni, Private communications.
7. L. A. Conant, S. E. Adair, W. C. McGill, and M. H. Weatherly, Unpublished Results; and M. H. Weatherly and L. A. Conant, (assigned to Union Carbide Corp.) U. S. Pat. 2,939,785 (1960).
8. G. D. Gemmel, *Trans. A.I.M.E.*, **215**, 898, (1959).
9. R. Kieffer and F. Benesovsky, *Metall.*, **6**, 171 (1952).

A Study of Pore Structures on Anodized Aluminum

T. A. Renshaw[1]

Naval Air Material Center, Philadelphia, Pennsylvania

ABSTRACT

It is demonstrated that the presence of surface oxide films on aluminum, prior to anodizing in a pore-forming electrolyte, can reduce the number of surface pores and the surface roughness compared to that normally obtained with fresh aluminum surfaces. Electron micrographs show that, in such a case, porous anodization proceeds by the branching of isolated surface pores and the development of pore colonies beneath the pre-existing films. The colonies are shown to consist of uniform hemispherical arrays of anodization cells which grow by continual branching of the internal pore structure. Pore colonies can be produced at will by anodizing first in an ammonium tartrate solution and then in chromic acid solution. The colonies are not found to be distributed uniformly over the surface. With very pure metal, they are found to develop largely at those sites where stress cracking of the surface oxide may be expected.

In the course of testing the adhesive properties of paints purchased for Naval aircraft, considerable variation was encountered in the qualities of the anodized aluminum test panels. An electron microscope study was made to determine what surface differences could be found on the various panels and why these differences existed.

Initial work indicated that a prime criterion for comparing the adhesive quality of panels was the relative number of surface pores per unit area. Panels to which paint adhered firmly had very rough and porous surfaces, while panels to which paint adhered poorly were found to have only a relatively few, isolated pores. Differences of adhesion were assumed then to be related, in a large part, to the ability of paint to key itself mechanically to the porous surfaces.

Various aspects of anodizing on aluminum then were studied to determine the mechanisms by which size and concentration of surface pores could be varied. One such mechanism is demonstrated and discussed in detail in this report. Quantitative experiments relating controlled or known surface porosities to paint adhesion have not yet been sufficiently sophisticated to provide reliable data; however, the information developed in this study emphasizes the truism that all electrolyte bath parameters as well as other preparation steps should be controlled rigorously when preparing test panels which are to be used to rate the adhesive quality of paints.

The structural features of the usual porous type of anodic oxide formed on clean aluminum surfaces in acidic electrolytes have been defined by others (1). These films consist of arrays of hexagonal columnar oxide cells oriented perpendicular to the aluminum surface. As depicted in Fig. 1, each cell consists of a body of oxide a central pore, and a barrier oxide film between the base of the pore and the underlying aluminum. The size of the cells and the thickness of the nonporous barrier films are effectively direct functions of the voltage employed in anodizing.

Experimental Procedures

Anodizing was carried out on several types of aluminum; Alclad 24ST panels, commercial household foil, (99.5%) and high-purity foils (99.97%). Most of the data presented in this report are, however, based on the high-purity foils because the

[1] Present address: Republic Aviation Corporation, Farmingdale, N. Y.

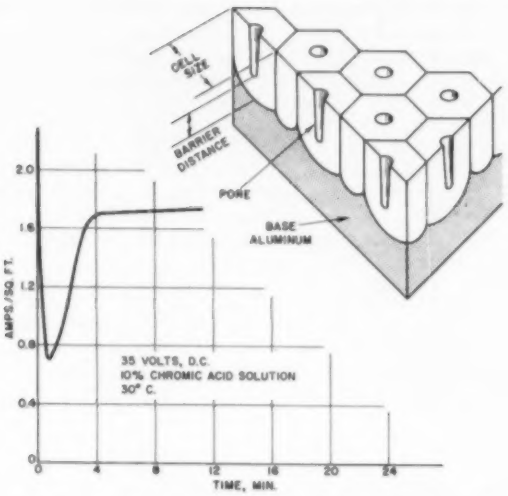

Fig. 1. Structure of a porous anodic oxide film found on a clean Al surface. The graph illustrates the characteristic current variations encountered with time, when anodizing at constant voltage.

structural nature of the anodized films is developed less ambiguously on these.

The electrolyte of principal interest for the formation of porous films was a 10% (by weight) solution of chromic acid. Nonporous barrier-type anodization films were formed in 3% tartaric acid solution (adjusted to pH 5.5 by addition of NH_4OH) as employed by Hass (2). Electrolyte temperatures were held to within 0.1°C.

In most cases the aluminum surfaces were preconditioned by chemical polishing with Alcoa R-5 Bright Dip (94 parts of 85% H_3PO_4 and 6 parts of 70% HNO_3).[2] The voltages employed in these experiments were chosen principally in order to stay within the range of film thicknesses suitable for transmission electron microscopy. For nonporous films lower voltages produce thin films which are difficult to handle and higher voltages produce films which are thick enough to reduce the intensity, contrast, and resolution of the images obtained with 50 kv electrons. Since the thickness of the porous films is influenced by other factors in addition to voltage, such as time and temperature, these also were controlled suitably to obtain adequate images.

When oxide films were required for electron microscope examination, they were stripped from the base metal by the familiar mercuric chloride technique (3) and mounted directly on 200-mesh specimen screens.

In general, a constant voltage power supply was employed which has a high degree of regulation.[3] Overloading of it at the start of a run was avoided by employing small sized panels. Current-time curves were obtained by placing pen or stylus-type current recorders of low time constant in the anodizing circuit.

[2] U. S. Pat. 2,650,157.

[3] Sorenson, Model 560, Nobatron Supply.

Discussion

Anodization at Constant Voltage

While the anodization of aluminum in practice and in the laboratory is carried out more frequently under constant or near constant current conditions so that its progress is followed by observing voltage variations, there is much to recommend the practice of constant voltage anodization in which current variations are studied. For example, constant voltage control leads to greater uniformity in the structural form of the growing oxide film. The current level also directly reflects the rate of formation of the oxide layer at any time. This leads then to a more realistic interpretation of the effects of the peculiar structure of a porous oxide film on the rate of reaction. Thus it is possible to interpret readily the current excursions which are associated with the initial part of an anodization carried out at constant voltage.

Referring to the graph in Fig. 1, the heavy current drain, which decreases rapidly in the first minute, is associated with the formation of a barrier film over the entire surface. This association is based, in part, on the fact that the electrical characteristics of the films formed during this period are nearly identical with those found for anodization in a barrier-type, nonporous oxide-forming electrolyte such as ammonium tartrate solution. Current flow drops to a minimum at 1 min and solution effects then become important as surface oxide sites are attacked and pores begin to form. A dynamical balance develops between oxide growth and solution effects in the pores and, in a short period when the entire panel surface is covered with growing cells, a plateau is reached in current flow (1, 4). This plateau is not entirely flat due to complex effects which develop as the pores deepen and further changes in current flow with time are usually observed. Such current-time curves also can be used to understand and explain more complex anodization situations such as are discussed below.

Formation of Pore Colonies

From the study of electron micrographs of porous anodic oxide films stripped from uncleaned specimens which showed only incipient pore formation (2-3 min anodization periods), it was noted that all areas of the surface are not subject to immediate pore and cell formation as is the case with freshly cleaned aluminum surfaces. To test whether surface oxide films could alter the distribution and concentration of surface pores significantly, anodization runs were carried out on foils which were pretreated in a number of ways.

In the most striking case, panels were treated by pre-anodizing at room temperature in ammonium tartrate electrolyte to form thin, nonporous oxide films prior to anodizing in chromic acid solution also at room temperature. As an example, the normal anodization curve for 35 v in 10% chromic acid solution (curve A, Fig. 2) is compared with that obtained under the same condition for a specimen which had been pre-anodized at 40 v for 5 min in the tartrate solution (curve B). The latter sample was delayed in attaining plateau level current by 26 min. Less

striking delays of 6-12 min were obtained when panels were pretreated by being heated in air at various temperatures or by immersion in boiling water for various time intervals.

The extension of the time period from the minimum current point to the beginning of the plateau can be interpreted as being due to an inhibition of the normal formation of surface pores. The eventual rise to normal plateau level current flow can be attributed to the branching of those pores which do develop below imperfection sites in the surface oxide film. By this branching and spreading beneath the relatively impervious surface oxide films, interface areas and current flows approaching those observed on clean aluminum foils are obtained eventually. These conditions are obtained some distance below the original oxide surface after the branched units have grown together.

To observe this branching effect microscopically and under controlled conditions, clean surface films some 340Å thick were produced by anodizing clean aluminum foil first in the ammonium tartrate electrolyte at 25 v at 30°C for 1 min. The specimens then were anodized at 15 v in 10% chromic acid also at 30°C. The barrier film formed at the base of cells during the chromic acid anodization cannot be greater than about 180-200Å thick. [13.5Å per volt of potential is the limiting oxide thickness obtainable (2) under these conditions and the conditions at the base of a growing pore would indicate that much lower values, ≅ 12Å per volt, are in order (4).] Ideally then, it should be impossible for current to flow until the 340Å surface film has dissolved away to a thickness of the order of 180-200Å. However, the time intervals employed are too short for this to occur, and it is concluded that some low resistance pathways are present which pass far enough through the surface oxide to establish electrical contact with the base aluminum.[4] These paths form the source or mother pore for a colony of pores. Three steps in the process of colony growth are illustrated in the schematic drawing at the top of Fig. 2.

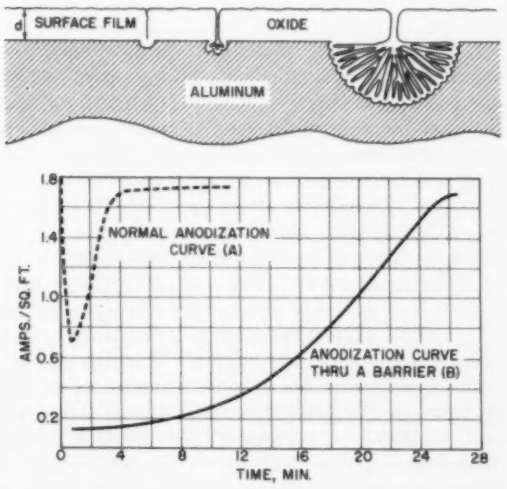

Fig. 2. Formation of pore colonies beneath a surface film of barrier oxide. The manner in which current flows with time, when anodizing at a constant 35 v, through a thick surface oxide film is shown in the graph. The surface film was formed by pre-anodizing the specimen at 40 v in ammonium tartrate solution.

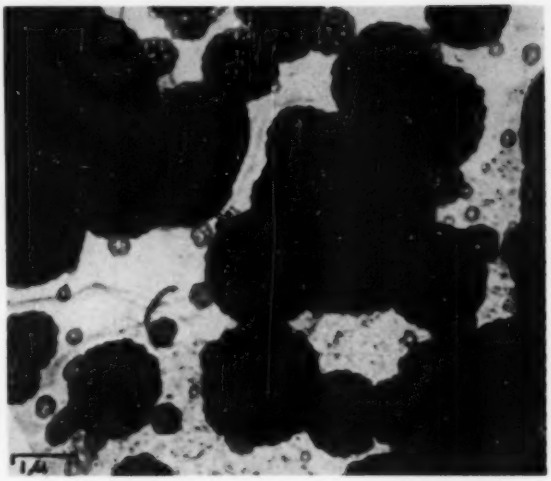

Fig. 3. A transmission electron micrograph of an oxide film containing colonies which was stripped from aluminum. The structure of the internal branching pores may be seen in colonies of various sizes. The clear areas are portions of the thin continuous nonporous oxide film through which the colonies were formed. Preparation: (99.97% Al), a, ammonium tartrate solution for 1 min at 25 v, 30°C; b, 10% chromic acid solution for 30 min at 15 v, 30°C.

This interpretation is further illustrated with the micrograph in Fig. 3 where distinct colonies of cells and pores can be seen to be arranged about the central mother pores. The view is normal to the surface through the nonporous surface oxide film and the attached pore colonies. An area containing a range of colony sizes was selected in order to show various stages in their growth. Single, dual, triple, and multiple pore colonies may be seen in outline. Figure 4 is a carbon replica of the metal-oxide interface of a similar specimen, and it confirms the very uniform manner in which the colony cells grow radially from the central mother pore.[5]

It has been observed as the result of many experiments along these lines that colony formation occurs for all such 2-step anodizing conditions as long as the voltage for nonporous oxide formation is greater than the voltage for pore formation. As the difference in these voltages is increased fewer colonies form and a longer period of time passes before normal plateau level anodization begins. This behavior is explicable in terms of the numbers of low resistance pathways passing far enough through the barrier oxide to establish electrical contact between the electrolyte and base metal. It is assumed that the imperfections in the surface oxide have a distribu-

[4] Unreported studies by the author have shown that anodic Al_2O_3 dissolves in 10% chromic acid solutions at 30°C at a rate of somewhat less than 23 Å/hr.

[5] Very large colony-type growths of porous oxide already have been demonstrated by light microscopy by Edwards and Keller (5). These authors showed that semi-circular porous growths developed by anodizing in sulfuric acid beneath nonporous surface oxide films. The artificial pores at which the growths initiate were created by intentional bending and cracking of the nonporous films.

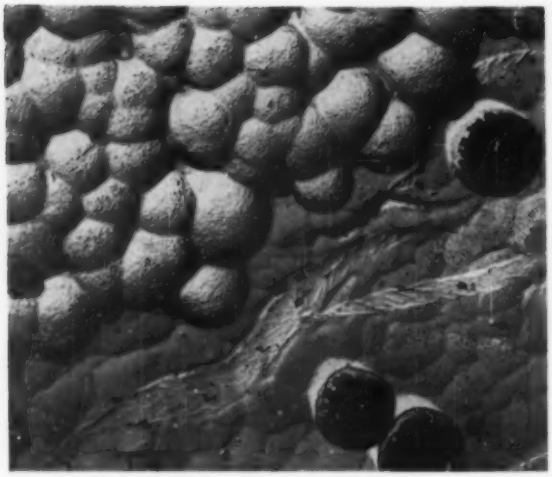

Fig. 4. A shadowed carbon replica of the oxide side of the metal-oxide interface. A grain boundary separates the two regions. In the dark colonies the oxide has been only partially dissolved away from the carbon replica. Preparation: (99.97% Al), a, ammonium tartrate solution for 5 min at 25 v, 30°C; b, 10% chromic acid solution for 128 min at 15 v, 30°C.

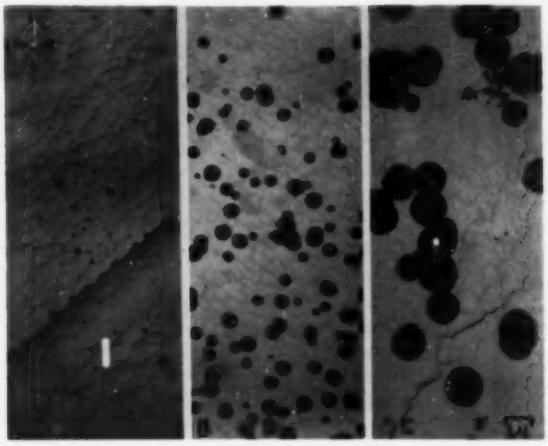

Fig. 5. Transmission electron micrographs of oxide films containing pore colonies after (a) 5, (b) 15, and (c), 30 min of growth. Preparation: (99.97% Al), a, ammonium tartrate solution for 5 min at 25 v, 30°C; b, 10% chromic acid solution for 5, 15, and 30 min at 15 v, 30°C.

tion in depth of penetration through the oxide thickness so that, in conjunction with the reaching distance of the potential (voltage x 13.5Å) applied in the chromic acid anodizing step, only a limited number of the imperfections can become active and pass current. Thus, for a given thickness of barrier oxide, reducing the voltage of the second, pore-forming step will also reduce the number of imperfections brought into circuit.

Curves such as B in Fig. 2 also were obtained readily by manipulating anodizing voltages in a single pore-forming electrolyte such as chromic acid solution. In such cases, after starting to anodize at some voltage level for 1 min to the minimum current point, the voltage was lowered suddenly by 10 v or so. A very slow rate of rise to the plateau level again is experienced since the cell base barrier film produced at the initial voltage necessitates that further anodization proceed by colony formation. In the same way any anodization run proceeding at plateau level can be stopped off effectively by dropping the voltage a suitable increment; the return to normal plateau currents will again develop slowly by the colony mechanism.

The radial growth rate of these colonies may be determined by stripping the oxide films at various times after the chromic acid anodizing has commenced. Figure 5 shows the colonies' size as a function of time.

Having measured the rate of radial growth of the colonies from such a series, it is necessary only to know the time period extending from the low point in the current-time curve to the beginning of the plateau portion in order to calculate the approximate number of colonies present per unit area. The rate of growth times the period of growth leads to the size and hence the area of each colony at the moment when they have grown together or coalesced. Dividing this area into a unit area leads to an approximation of the number of colonies or "surface pores" per unit of surface area. The term surface pores is employed to denote pores which intersect the oxide surface in this special case.

This method of estimating the number of surface pores for adhesion studies was developed because of the large uncertainties involved in counting the colonies directly from micrographs. As may be noted in Fig. 4, these uncertainties arise because the populations of colonies vary greatly from grain to grain on the aluminum metal. The estimation method has a number of drawbacks in that it does not account for colonies which start to grow beyond the low current point, nor does it consider that some grains are much more highly populated with pores than others. The method tends to gloss over, but indirectly account for these factors, and it therefore provides a very averaged value for any large surface. The tendency for colonies to develop only on certain grains is much more striking on the 99.97% pure aluminum samples than on samples of lower purity. If the colony-forming or porous anodization step is prolonged, there is a distinct delineation of the grains on the aluminum surface when observed under low power microscopy (Fig. 6). The effect is that of having two types of grains, one of which is brought into relief by more extensive colony formation (the dark grains in Fig. 6). Along this line it also has been noted in the course of preparing thick barrier oxide films that a similar delineation of the grain structure occurs through the formation of colors of different hues on different grains. Hone and Pearson (6) actually demonstrated a variation of thickness of porous oxide film over differently oriented grains, but in this case the variations were attributable to variations in the angle of pore growth away from the surface normal. Film thickness variations actually have not been demonstrated in pore free oxide coatings over differently oriented grains, although Cabrera and Mott (7) suggest that the dislocation densities of dif-

Fig. 6. A light micrograph of an anodized aluminum surface illustrating the growth of large colonies and the relative activity of certain grains. (Colonies are the small dots spread uniformly throughout the light areas but packed densely in the dark areas.) It may be seen that colony development is also influenced by the residual milling lines. Preparation: (99.97% Al), a, ammonium tartrate solution for 10 min at 25 v, 30°C; b, 10% chromic acid solution for 120 min at 15 v, 30°C.

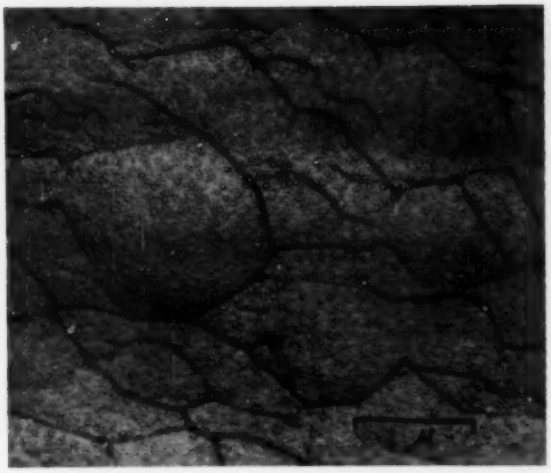

Fig. 7. A transmission electron micrograph through a thin porous anodic oxide film showing the development of minute anodization cells with respect to the surface etch structure. The cells are not clearly defined because of the thinness of the film but they can be discerned as minute ring-like forms. Preparation: (99.97% Al), ammonium tartrate solution for 120 min at 25 v, 30°C.

ferent crystal faces may lead to differences in the effective activation energies required to move the metal atoms from their lattice positions into the oxide. Different activation energies could lead to different film growth rates and thicknesses. As previously indicated, different barrier thicknesses might then account for the differences in colony population.

Sites of Colony Formations

It may be noted in Fig. 5 that the colonies in most cases initiate at the boundaries of the subgrain structure which was developed by the action of the R-5 brightener. Why these boundaries or ridges provide the sites for colony formation is a matter of interest, and a number of explanations have been considered. It is important to consider the origin of this subgrain structure which is revealed by the R-5 brightener's etchant action and by other etches. The subject was reviewed by Philips and Welsh (8) who discussed its possible origins and who provided strong evidence that this etch structure is not due to the misorientation of subgrain blocks, i.e., dislocations, within the crystals. In view of this, it is not reasonable to associate the original presence of dislocations in the aluminum to the development of the colonies on the substructure.

Welsh in an earlier paper (9) suggested that the substructure is caused by the merging of independent shallow etch pits and that the form of the structure (equiaxed or elongated) depends on the angle which the etch pits make with the surface plane. It also has been noted generally in the literature that the size of the structure increases with increasing purity of the metal. While it appears that the ridges or boundaries would be more cathodic than the interior portions of the structure, there has been no evidence that discrete impurity phases are present there. In a more recent paper (10) Cuff and Grant consider the substructure to be the surface manifestation of a 3-dimensional network of impurity atom segregation enclosing volumes of relatively high-purity aluminum. They consider that the impurity atoms probably have a Maxwellian distribution about the ridges such that, by influencing the electrostatic forces on the surface and by causing surface corrosive currents, they cause the observed structure to develop. The question then arises, whether the extent of impurity segregation present in the region of the ridges is sufficient to change the resistive and dielectric properties of the anodic oxide which is formed over them so that pores or pore colonies are initiated more easily and propagated there.

It has been found that, under conditions where porous columnar anodization cells are formed, very few actually develop over the ridges. Figure 7, illustrating this point, is a transmission micrograph of a thin porous oxide film formed by anodizing aluminum in an ammonium tartrate solution for a prolonged period of time.[6] This particular and unusual type of porous oxide film was used here because the very small size of the pore and cell structures permit a clearer resolution of the effects under question than is possible with ordinary porous films.

The small amount of pore formation over the ridges probably can be attributed to a somewhat

[6] There has been a general acceptance of the idea that oxide films formed by anodizing in an ammonium tartrate solution are true nonporous barrier type films. The micrograph in Fig. 7 and others taken under different conditions have established that this is rarely the case. It is found that only on the shortest anodization periods (<1 min) may these films be considered to be effectively nonporous. On any extended soak periods with potential applied, the minute pore and cell systems are found to be present. It is interesting that Plumb (11) already has pointed out that this probably occurs due to the fact that the low buffering capacity of the ammonium tartrate electrolyte may permit the solution in immediate contact with an anodizing surface to become rather acidic. This undoubtedly is the explanation since a relatively low pH is required for an appreciable oxide solution rate to develop. There are several other works (12, 13) which also have shown cellular developments on thick oxide films formed in borate solutions.

thicker barrier oxide which forms initially in these areas because of the higher electrostatic fields present over protuberances. The occasional large cells which are seen scattered about on the ridges probably originate at the same sites which give rise to the colonies. It is indicated therefore, on the basis of these observations, that the impurities which may be present in the vicinity of the ridges have no significant or general influence in promoting porous anodization activity there.

Another explanation has been developed which seems to be more consistent with the observed facts, namely, that the colonies develop at the sites of minute cracks in the oxide film. Young (14) has developed the argument, in the case of anodic tantalum oxides, that the oxide will form over acute protuberances of metal with internal stresses large enough to cause oxide failure and cracking. Because of the similarities of the two cases (both oxides occupy more volume than the equivalent converted metal) one can apply the same arguments to anodic aluminum oxide. Whether the failures are compressive or tensile is determined by whether the oxide film grows near the metal surface or near the electrolyte surface. On an acute protuberance, the former case would lead principally to tensile stresses in the oxide and the latter case would lead principally to compressive stresses in the oxide film.

In the present case, this explanation would indicate that the ridges in the surface structure would have the greatest crack frequency since they are protuberances of metal. In those grains where a minimum of sharp ridges exist it also may be expected that few or no cracks (or colonies) would form. This explanation also would indicate that common points of intersection of three or more subgrain structures would be particularly active since peaks of metal form in these areas. All of these effects have been observed to be true generally although no attempt has been made to provide conclusive evidence because of the experimental problems involved in determining the ridge angles. Most of these effects may be discerned in the micrographs in Fig. 5 and especially in Fig. 5(A) where the colonies are just beginning to grow. Additionally, it may be noted in Fig. 6 that colony formation is influenced by the surface roughnesses that remain from the milling operation.

As a further test of this mechanism, oxide films formed on aluminum, which had been etched in concentrated HCl, also were exposed to colony-forming conditions. It was thought that the many right angles present on the rectangular etch structures would provide a reliable test of the stress crack-colony formation theory. The manner in which the colonies develop may be seen in Fig. 8. Stereoscopic pairs of this region established that the edges marked with arrows were protruding edges of metal. Alternate lines, of course, are those of internal steps. It may be seen that many of the colonies developed as expected; however, there are also a number the origins of which may or may not be related to this mechanism.

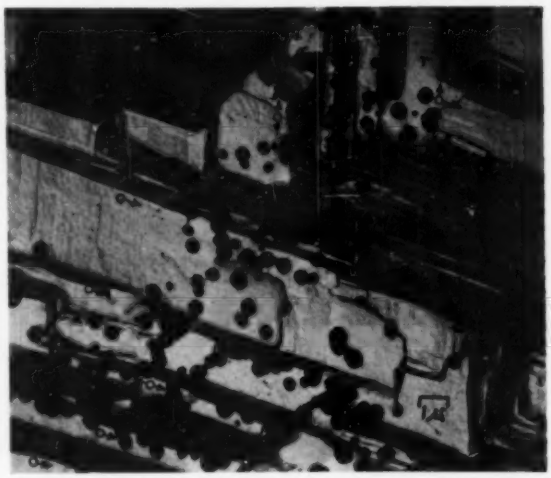

Fig. 8. An electron micrograph of colonies which formed on the rectangular structure produced by etching the aluminum in concentrated HCl solution. There is a definite tendency for the colonies to form on the 90° step edges. It was determined stereoscopically that the marked edges are those which protrude from the surface. Preparation: (99.97% Al), a, ammonium tartrate solution for 1 min at 20 v, 30°C; b, 10% chromic acid solution for 15 min at 12 v, 25°C.

There are several difficulties which prevent more direct proofs of this mechanism. For one, the separated oxide films are so fragile as to prohibit an independent study of the minute cracks which may be present before they are removed from the metal. On the other hand, because of the self-healing properties of nonporous barrier type oxide films, cracks (and colonies) are not always obtained where they would be expected. It also should be pointed out that the above mechanism is not necessarily the sole means by which colonies may initiate. For instance, discrete impurity phases which are present in the aluminum metal can provide pathways through the oxide. Some impurities when converted to oxides are more soluble than aluminum oxide and would lead to voids in the surface films, whereas other impurity phases could provide diffusion paths between the electrolyte and the aluminum. It may be for these reasons that the effect of surface structure in determining local concentrations of colonies can be discerned clearly only when high-purity foils are used. The effect may be masked in low-purity foils by the general development of colonies resulting from gross impurity effects. Associations between colony sites and impurities have, in fact, been observed in micrographs, but this situation has not been explored systematically.

Since it has been suggested that defects take a part in establishing the basic electrical properties of barrier oxide films (15), it may be of some interest to employ the colonies as a decoration technique in studying the quantitative importance of the defects.

Conclusions

It is demonstrated that the surface of anodized aluminum may be made considerably less porous than is normal due to the presence of oxide layers on the surface prior to anodization in a pore form-

ing electrolyte. It is shown that this is accomplished by a mechanism involving the growth of pore colonies beneath the pre-existing surface films. It also is shown that the initial current density-time curves can be related to the growth of the colonies and to the number of colonies present. It is concluded necessarily that colonies initiate at defects or low resistance pathways that are present in the surface barrier films. The location of the defects is dependent both on the grain orientation and the surface roughness.

Evidence is presented to show that many of the low resistance pathways which lead to the formation of pore colonies occur at points where microscopic stress cracks may be expected to have developed.

Manuscript received April 7, 1960; revised manuscript received Sept. 21, 1960. This paper was presented in part before the Santa Monica meeting of the Electron Microscope Society of America, Aug. 8, 1958.

Any discussion of this paper will appear in a Discussion Section to be published in the December 1961 JOURNAL.

REFERENCES

1. F. Keller, M. S. Hunter, and D. L. Robinson, *This Journal*, **100**, 411 (1953).
2. G. Hass, *J. Opt. Soc. Am.*, **39**, 532 (1949).
3. S. Wernick, *J. Electrodepositors Tech. Soc.*, **9**, 153 (1934).
4. M. Hunter and P. Fowle, *This Journal*, **101**, 481 (1954).
5. J. D. Edwards and F. Keller, *Trans. Am. Inst. Mining Met. Engrs., Tech. Publ. 1710* (1944).
6. A. Hone and E. C. Pearson, *Metal Progr.*, **53**, 363 (1948).
7. N. Cabrera and N. F. Mott, *Repts. Progr. Phys.*, **12**, 163 (1948).
8. R. Philips and N. C. Welsh, *Phil. Mag.*, **3**, 801 (1958).
9. N. C. Welsh, *J. Inst. Metals*, **85**, 567 (1956).
10. F. B. Cuff and N. J. Grant, *J. Inst. Metals*, **87**, 248 (1959).
11. R. C. Plumb, *This Journal*, **105**, 498 (1958).
12. R. W. Franklin, *Nature*, **180**, 1470 (1957).
13. D. J. Stirland and R. W. Bicknell, *This Journal*, **106**, 481 (1959).
14. L. Young, *Acta Met.*, **5**, 711 (1957).
15. A. W. Smith, *Can. J. Phys.*, **37**, 591 (1959).

Galvanic Behavior in Fused Electrolytes

III. Potentials of Calcium, Magnesium, and Nickel in LiCl-KCl-K_2CrO_4 and NaCl-KCl-K_2CrO_4

Sidney M. Selis[1] and Laurence P. McGinnis

Diamond Ordnance Fuze Laboratories, Washington, D. C.

ABSTRACT

Referred to Ag/LiCl (or NaCl)-KCl-AgCl (N = 0.100), the oxidation potential of calcium at 700°C is —1.72 v in LiCl-KCl-K_2CrO_4 and —0.41 v in NaCl-KCl-K_2CrO_4. The lesser polarization in the lithium electrolyte is due to the formation *in situ* of a semiliquid electrode surface and is not due to the inherent chemical nature of lithium. The polarization in the sodium electrolyte is ascribed to a film which may be a chromite. Such a film is apparently not adherent in the case of magnesium or nickel for these metals are much less polarized in the sodium electrolyte than is calcium.

In a previous paper, the behavior of the nominal system Mg/LiCl-KCl-K_2CrO_4/Ni at 440°C was discussed, and the cathode half-cell reactions were considered (1). The present work was begun in order to elucidate some aspects of anode half-cell behavior. It was decided to include measurements on calcium electrodes since Goodrich and Evans (2) had implied that calcium anodes are usable in the above-mentioned electrolyte. It was also decided to measure electrode potentials in fused NaCl-KCl-K_2CrO_4 although a much higher cell temperature is needed because of the melting range of this electrolyte. The presumed advantage of the sodium electrolyte is its lower hygroscopicity, which would simplify the experimental procedure.

It should be emphasized that no basic thermodynamic significance can be ascribed to the electrode potentials reported here although the chemical systems and measured values are indeed reproducible. The systems are complicated ones and the potential-determining couples cannot be defined completely. Yet the values are interesting and surprising in nature, and questions are raised as to how the simple substitution of sodium ion for lithium can affect the potential of the calcium electrode so markedly. This paper suggests logical reasons and may introduce an area of special interest in regard to fused salt electrolytes.

[1] Present address: Research Laboratories, General Motors Technical Center, Warren, Michigan.

Experimental

Materials.—The chemicals used in this study were all of reagent grade and not purified further. As far as possible, they were handled in an air atmosphere having a relative humidity of 6% or less. The electrode metals were generally of the highest grade commercially obtainable and are described in Table I.

Procedure.—In this work, the reference electrodes were prepared by melting pure silver chloride in 30-cm lengths of 7-mm Vycor tubing, the lower

Table I. Electrode Materials

Metal	Purity (and major impurities)	Form
Ag	99.95%	Annealed wire, 0.81-mm diameter
Ca	98-99% (Mg)	Ingot
Cu	99.9%	Ingot
Li	99+% (Na)	Wire
Mg	99.8% (Ca, Zn)	Rolled sheet, 0.33-mm thick
Na	99.98%	Ingot
Ni	98-99% (Co, Fe, Zn)	Semiannealed sheet, 0.33-mm thick; annealed wire, 0.81-mm diameter

ends of which were completely closed. A silver lead was inserted in the silver chloride which then was allowed to freeze. At 700°C, a null-balancing potentiometer could be used effectively in measurements with this electrode.

Adjunctive to the use of the Ag, AgCl, glass electrode, compartmented cells of the type Ag/LiCl (or NaCl)-KCl-AgCl//Vycor//AgCl/Ag were prepared, and their potentials were measured as a function of the silver chloride concentration at the negative electrode of these compartmented cells. In this series of experiments, the tubes were open to the atmosphere. Yet, close obedience to the Nernst equation was realized. The results of this work and their implication in the present study are discussed later.

The technique of arranging strip electrodes, the glass-enclosed Ag, AgCl electrode, and a thermocouple tube in a 38-mm glass container has been essentially described before (3). In the present study, side arms were sealed near the tops of the Vycor electrode tubes, and small vents were located further down. Side arms also were located near the upper ends of the Vycor cell containers. Only the reference electrodes were sealed to the caps.

The alloy electrodes, when used in place of solid strip electrodes, were prepared in the following manner. Alloy compositions were so chosen that in the temperature range of 700°-720°C there would be about 90 wt % of the calcium-rich solid phase and 10 wt % of saturated liquid. It was judged that this would yield an electrode which would have a semifluid surface and still be adequately rigid. To select such Ca-Li and Ca-Na alloys, reference was made to the equilibrium diagrams of Wolfson (4) and Rinck (5), respectively; the mole fractions of calcium in the alloys as used in this work were, respectively, 0.85 and 0.98.

The alloy electrodes were prepared by heating and mixing the components in an Armco iron crucible under dry argon to a temperature of 900°C. After cooling in the inert atmosphere, the central portion of the solidified alloy was machined out under dry oil. The turnings were rinsed in dry hexane and tamped into suitable lengths of Vycor tubing. A lead of strip calcium was inserted, and the tube was heated for a short time under dry argon so as to establish a satisfactory electrical connection but not to melt the strip. The alloy electrodes were stored under dry petroleum ether. During cell measurements, only the bottoms of the assemblies were exposed to electrolyte.

The procedure and auxiliary equipment used in making a run were similar to those described before (3). The cell container was charged with the proper electrolyte salts and was placed in the furnace. When the desired temperature was reached, the container was loosely capped and purged with dry argon gas fed through the side arm. With continuing argon flow, the cap was removed and the electrode holder was positioned such that the anode was out of the electrolyte but was being preheated. The anode tube was purged with argon which entered the tube side arm and which vented through the small hole located below. During this time, connections to the cell were completed and the thermocouple was introduced.

To activate the cell, the anode tube was lowered into the electrolyte. Except as specifically noted in the next section, tabulated potentials were the steady-state values developed after a few minutes. As before, steady-state cell and thermocouple potentials were measured with a null-balancing potentiometer and any continuous potential readings were made with an oscillograph having an input impedance of 9 megohms and a full-scale response time of 50 msec (1).

The nominal ratio of lithium chloride or sodium chloride to potassium chloride was such as to produce a mixture having the minimum melting point. For LiCl-KCl, the eutectic composition is 58 mole % LiCl and 42 mole % KCl (6); for NaCl-KCl, it is a solid solution containing 50 mole % NaCl and 50 mole % KCl (7). Potassium chromate additions were in the amount of 4.83 mole %. Because of the higher melting temperature of the sodium-containing electrolyte, a minimum cell temperature of 700°C was used; temperatures of 720°C or slightly higher were used for semiliquid calcium-sodium alloys.

The film conductivity on the calcium electrode in NaCl-KCl-K_2CrO_4 was estimated from measurements made in a U-shaped cell constructed of 20-mm Vycor tubing. After the cell containing the fused salt electrolyte had attained thermal equilibrium, a preheated calcium electrode, having a total immersed area of 3 cm^2, was inserted and mounted in each leg. A 5000-cps sinusoidal signal was impressed, and a reading was obtained with a conventional impedance bridge. No appreciable difference in readings was observed by using frequencies of 10,000 and 20,000 cps.

Prior to measuring the resistance offered by the calcium electrodes, a "cell constant" was obtained. The cell was filled with a copper(II) sulfate solution of established concentration and temperature. The level of solution in the cell was the same as would be occupied by the molten salt electrolyte. Copper electrodes were prepared which had the same geometry and which would be immersed to the same depth as the calcium electrodes. The copper electrodes were "shorted," and it was ascertained that they had a negligible resistance. They were im-

mersed then in the cell filled with copper sulfate solution and an impedance value was obtained for each of the above-noted frequencies. These values did not vary appreciably with frequency. Using the values of specific conductance for copper sulfate solutions as given by Owen and Gurry (8), the "cell constant" was computed.

Using the data and equations published by Van Artsdalen and Yaffe (9), the specific resistance of the molten NaCl-KCl was determined. Then by applying the "cell constant" value, it was found that the resistance offered by the fused salt electrolyte was small compared to that of the whole cell (which included the calcium electrodes). From the cell resistance the electrolyte resistance was subtracted, and the difference was multiplied by the total immersed calcium area (6 cm^2) to yield a "specific resistance" for the calcium electrode. The approximate value for "specific conductance," as given in the next section, is the reciprocal of this "specific resistance."

Results and Discussion

Reference electrodes.—As a matter of convenience, the calcium, magnesium, and nickel electrodes were measured against Ag, AgCl in Vycor. This glass electrode structure (containing *diluted* silver chloride) has already been described by Bockris, *et al.* (10) and by Yang and Hudson (11) who actually included Vycor in their membrane potential studies. However, the discussion of values referred to this electrode would have little meaning because the difference in liquid junction and membrane potentials across the glass would cause the reference to be different in the two electrolytes.

Accordingly a series of measurements was made with special cells of the type Ag/LiCl (or NaCl)-KCl-AgCl//Vycor//AgCl, Ag. Table II lists the potentials of silver in diluted silver chloride as measured against the glass electrode. It will be noted that the mole fraction of silver chloride was varied from 0.0100 to 0.300.

These negative electrodes are apparently reversible within 1 to 4 mv. Furthermore, the observed least squares values of $(dE/d \log N_{AgCl})_T$ for the LiCl-KCl and NaCl-KCl solvents are 0.189 and 0.190 v, respectively, in agreement with the calculated Nernst value of 0.193 v for 700°C. It is presumed that the membrane potential did not vary appreciably due to changes in silver chloride concentration. At least in regard to the LiCl-KCl solvent, Yang and Hudson (11) indicate that membrane potentials do not change appreciably up to silver chloride mole fractions of 0.6.

In this paper the calcium, magnesium, and nickel electrode potentials will be referred to Ag/LiCl (or NaCl)-KCl-AgCl ($N = 0.100$). This is accomplished by subtracting the appropriate value in Table II from a potential measured against the glass electrode. For instance, the calcium potential in LiCl-KCl-K_2CrO_4, measured against the glass electrode, is −2.29 v. This calcium potential will be reported as −1.72 v *vs.* Ag/LiCl-KCl-AgCl ($N = 0.100$). Liquid junction potentials, that would be developed at the interface LiCl (or NaCl)-KCl-K_2CrO_4//LiCl (or NaCl)-KCl-AgCl, can be neglected presumably. The chromate ion is large and is present only to the extent of 2.4 ion %; the silver ion is present to the extent of 5.0 ion %. Probably neither species contributes very much to the electrolyte conductivities. In fact the strict Nernst behavior mentioned above is indirect evidence that silver ion is not an important conductor in its electrolyte; otherwise the membrane potential would change as the silver ion concentration was increased from 0.5 to 15 ion %.

Table II. Potentials of Ag/LiCl (or NaCl)-KCl-AgCl vs. Ag/AgCl in glass at 700°C

N_{AgCl}	Solvent:	Potential (v) LiCl-KCl	NaCl-KCl
0.0100		−0.755	−0.940
0.0300		−0.663	−0.856
0.100		−0.568	−0.753
0.300		−0.474	−0.661

Table III. Electrode potentials vs. Ag/LiCl (or NaCl)-KCl-AgCl ($N = 0.100$)

in LiCl-KCl-K_2CrO_4 Electrode	E, v	in NaCl-KCl-K_2CrO_4 Electrode	E, v
Ca	−1.72	Ca	−0.41
Mg	−1.45	Mg	−1.20
Ni	+0.24	Ni	+0.37

Electrode potentials.—Calcium, magnesium, and nickel electrode potentials are recorded in Table III.

It will be noted that in the sodium-containing electrolyte the magnesium potential is less anodic by 0.25 v, and the nickel potential by 0.13 v, than in the lithium-containing electrolyte. However, of particular interest is the observation that the calcium potential in the sodium electrolyte is less anodic by 1.31 v than it is in the lithium electrolyte. The remainder of this paper is devoted primarily to a consideration of this large and surprising difference in calcium half-cell potentials.

The explanation given here, as to why the calcium potential is more anodic in the lithium electrolyte than in the sodium electrolyte, is based on an earlier observation that calcium metal can displace lithium ion from solution. The lithium metal then would form an alloy with calcium, and the alloy would be at least partially liquid at temperatures above 231°C (4). The formation of a semiliquid calcium-lithium alloy was actually demonstrated in this work by inspection and then by using a qualitative spectroscopic method. (It should be noted here that the formation of a calcium-sodium alloy *in situ* is also thermodynamically favored. The latter alloy should be semiliquid at temperatures above 710°C (5), but no such behavior was noted at temperatures as high as 740°C after a 2-hr wait.)

It is postulated that a fluid surface, continuously renewed by convective flow, would not be subject to the marked change in potential developed by a wholly solid surface. To test this idea, a calcium-lithium alloy electrode was prepared which would be semiliquid at 700°C. Table IV gives its reproducible potential as measured in the sodium-containing electrolyte. It is evident that the semiliquid

Table IV. Electrode potentials of alloys vs. Ag/NaCl-KCl-AgCl ($N = 0.100$)

Electrode	E, v
Ca-Li	−1.52
Ca-Na	−1.51

electrode is much more anodic in this electrolyte than is the solid calcium electrode and the potential of −1.52 v does approach the value of −1.72 v for calcium in LiCl-KCl-K_2CrO_4.

Such a calcium-lithium alloy electrode was immersed in the sodium electrolyte and removed 5 min later. Spectroscopic examination of the electrolyte gave no evidence of lithium ion in amounts greater than 0.01-0.1 mole %, and so the presence of this latter entity can hardly account for the more anodic potential of the alloy electrode.

A semiliquid calcium-sodium electrode then was measured in the sodium electrolyte at 720°C. Table IV shows that this electrode is also relatively anodic and proves that this anodic value is due to a fluid surface rather than to any specific effect of lithium metal.

The high degree of passivation of the calcium electrode in NaCl-KCl-K_2CrO_4 (see Table III) is also manifested by its relative chemical inertness. When the high-temperature cell is opened to the atmosphere, the electrode is not oxidized rapidly by the air. Furthermore, there is no evident reaction with the Vycor electrode tubes. On the other hand, in LiCl-KCl-K_2CrO_4 the electrode is very reactive, undergoing vigorous oxidation when the cell is opened to the air and reacting with the Vycor to give a dark-colored product, presumably elemental silicon formed according to reaction [1] whose standard molar free energy change is −85.5 kcal at 700°C.[2]

$$2Ca(c) + SiO_2(c) \rightarrow 2CaO(c) + Si(c) \qquad [1]$$

The nature of the film on calcium in the sodium electrolyte was studied by recording the potential of the preheated calcium electrode continuously as a function of time from the moment of cell activation. In the sodium electrolyte at 720°C, the initial potential of the calcium electrode was quite anodic, i.e., −1.65 v. Over a 50- to 60-sec period, it became less anodic, nearly linearly with time, to the value −0.41 v previously observed. Similar studies of the potentials of calcium in the lithium electrolyte and calcium-lithium alloy in the sodium electrolyte gave steady values of −1.72 and −1.54 v, respectively, from the moment of cell activation. It is confirmed therefore that the change in the cathodic direction is due to a film which, at the elevated temperatures, requires about 1 min to develop fully.

It was suggested that the difference between −0.41 and −1.72 v might be accounted for in terms of an IR drop across the film. Meters of high effective impedance had been used, but nothing was known of the film conductance. Using a 5000-cps signal, the latter was measured and was found to be 0.05 ohm^{-1} cm^{-2}. This value is sufficiently high such that, with the meters used, no observed difference in potential can possibly be ascribed to an ohmic loss across the film. To account for the observed difference in terms of IR drop, a film conductivity as low as 10^{-4} ohm^{-1} cm^{-2} would be required.

The exact nature of the film remains unknown although the presence of chromate ions in the anolyte is essential for film formation. (Measurements of the potential of calcium in a sodium electrolyte free of chromate ion gave a value of −1.80 v. This strongly negative potential definitely indicates the absence of a film.) In regard to the chemical nature of this film, the present authors suggest a chromite, i.e., a compound of CaO and Cr_2O_3. However, attempts to characterize it by x-ray powder diffraction techniques were unsuccessful.

It is clear that magnesium and nickel are far less passivated in the sodium electrolyte than is the calcium in the same electrolyte. In the case of magnesium, a film formation would be expected, and it would seem that the small passivation of magnesium in either electrolyte results from the poor adherence of this film.

Electrolyte composition.—Nominally the electrolytes include lithium or sodium chloride, potassium chloride, and potassium chromate. However, the presence of other species can be inferred. As discussed by several authors (1, 3, 13, 14), water of hygroscopicity will serve to hydrolyze a portion of the alkali metal halides and to produce some hydroxide and oxide ion. Then equilibria such as reaction [2] [discussed in an earlier paper (1)] will be operative in the

$$SiO_2(c) + 2Li^+(l) + O^=(l) \rightleftharpoons Li_2SiO_3(amorph) \qquad [2]$$

Vycor cell container and will fix the oxide ion activity for a given temperature.

Reaction [3] expresses still another equilibrium pertinent

$$2CrO_4^=(l) \rightleftharpoons O^=(l) + Cr_2O_7^=(l) \qquad [3]$$

in these electrolytes, but the constant is not known. Yet the oxide ion activity will be fixed in a given electrolyte, and since the same quantity of chromate ion has been used in each experiment, the ratio of dichromate ion to chromate ion has been the same for each run with a given electrolyte.

The deposition of lithium metal on the calcium electrode would be accompanied by the introduction of calcium ion in the electrolyte as expressed by reaction [4]. During the time for an

$$Ca(c) + 2Li^+(l) \rightleftharpoons Ca^{++}(l) + 2Li(l) \qquad [4]$$

experiment, equilibrium is probably not attained, and this reaction might proceed to different extents from run to run. This would cause the electrode potential to vary, but within the limits already stated, variations were not observed.

The chemistry of the electrolyte is indeed a complicated matter, and undoubtedly, such species as oxide, hydroxide, dichromate, and calcium ions affect the observed electrode potentials. Yet in the case of the calcium electrode, at least, the large variation in potential is probably due to basic phenomenological

[2] This calculation was made from values listed by Coughlin (12).

differences rather than to more subtle variations in the activities of certain dissolved species.

Summary

Referred to the Ag/LiCl (or NaCl)-KCl-AgCl ($N = 0.100$) electrode the calcium electrode at 700°C yields a potential of −1.72 v in the molten salt electrolyte LiCl-KCl-K_2CrO_4. In the electrolyte NaCl-KCl-K_2CrO_4, the electrode is more cathodic with a potential of −0.41 v. In going from the first to the second electrolyte, the magnesium potential changes from −1.45 to −1.20 v and the nickel potential changes from +0.24 to +0.37 v.

The more negative calcium potential in the lithium-containing electrolyte is attributed to the formation *in situ* of a semiliquid calcium-lithium alloy electrode. The semiliquid characteristic is of importance rather than any specific effect of lithium.

The protective film on the calcium in the sodium electrolyte is of relatively high conductance. It presumably is a calcium chromite.

The lack of severe passivation of magnesium or nickel in either electrolyte is due to poor adherence of any film which might be formed.

Manuscript received Dec. 9, 1959; revised manuscripts received June 22, 1960 and Sept. 16, 1960. This paper was presented before the American Chemical Society, Miami, Florida, April 7-12, 1957.

Any discussion of this paper will appear in a Discussion Section to be published in the December 1961 JOURNAL.

REFERENCES

1. S. M. Selis and L. P. McGinnis, *This Journal*, **106**, 900 (1959).
2. R. B. Goodrich and R. C. Evans, *ibid.*, **99**, 207C (1952).
3. S. M. Selis, G. R. B. Elliott, and L. P. McGinnis, *ibid.*, **106**, 134 (1959).
4. M. R. Wolfson, *Trans. Am. Soc. Metals*, **49**, 794 (1957).
5. E. Rinck, *Compt. rend.*, **192**, 1378 (1931).
6. C. Solomons, J. Goodkin, H. J. Gardner, and G. J. Janz, *J. Phys. Chem.*, **62**, 248 (1958).
7. E. K. Akopov and A. G. Bergman, *Zhur. Obshchei Khim.*, **24**, 1524 (1954).
8. B. B. Owen and R. W. Gurry, *J. Am. Chem. Soc.*, **60**, 3070 (1938).
9. E. R. Van Artsdalen and I. S. Yaffe, *J. Phys. Chem.*, **59**, 118 (1955).
10. J. O'M. Bockris, G. J. Hills, D. Inman, and L. Young, *J. Sci. Instr.*, **33**, 438 (1956).
11. L. Yang and R. G. Hudson, *This Journal*, **106**, 986 (1959).
12. J. P. Coughlin, Bur. Mines Bull. 542, Washington (1954).
13. H. A. Laitinen, W. S. Ferguson, and R. A. Osteryoung, *This Journal*, **104**, 516 (1957).
14. G. Delarue, *J. Electroanalyt. Chem.*, **1**, 13 (1959).

Technical Notes

The Preparation of Fluorescent Germania

J. F. Sarver and F. A. Hummel

Department of Ceramic Technology, The Pennsylvania State University, University Park, Pennsylvania

Germania occurs in three crystalline modifications. The stable low-temperature form has the rutile structure in which the Ge^{4+} ions are octahedrally coordinated by six oxygen ions. The rutile form changes very slowly to the stable high-temperature or β-quartz form at about 1050°C. The inversion is accelerated by the presence of small amounts of mineralizers such as alkali halides. In the quartz modification, the Ge^{4+} ions have tetrahedral oxygen coordination. Upon rapid cooling, with or without mineralizers, the β-quartz form does not revert to the stable rutile form but inverts rapidly and reversibly to a metastable α-quartz modification at about 1000°C (1).

Commercial germania (fluorescent grade) has the metastable α-quartz structure and is nonfluorescent. In order to convert it to the stable rutile form, mineralizers must be added and the assemblage must be heated for a few hours at temperatures between 800° and 1000°C. An alternative method is to subject the GeO_2 as received to hydrostatic or hydrothermal pressures in the range between 200° and 500°C.

Experimental

In experiments carried out to establish the temperature of the stable β-quartz $\rightleftharpoons$ rutile inversion in GeO_2, it was necessary to add mineralizers to the starting material to complete the inversion in a reasonable length of time. A very effective mineralizer consisted of a 1% by weight addition of the eutectic mixture of LiCl-KCl which caused the inversion to go to completion in a few hours at temperatures as low as 800°C. The rutile form of GeO_2 which was produced developed a slight pink coloration, and when examined under cathode ray and germicidal lamp, *i.e.*, principally 2537Å excitation, it showed a yellow fluorescence.

Additions of other mineralizers such as Li_2O, Na_2O, K_2O, and LiF were effective in promoting the conversion of the α-quartz form to the rutile form, and the same yellow fluorescence was characteristic of these preparations.

Starting with a 5-g quantity of the α-quartz form, the rutile form was prepared hydrothermally by heating for 24 hr in a silver-lined Morey bomb with enough distilled water to give a pressure of about

Table I. Effect of various types of mineralizing additions on the emission characteristics of GeO_2

Addition	Peak position, Å	Brightness, ft-L
LiCl-KCl	5380	21.1
Li_2O	5380	15.7
Na_2O	5370	4.5
K_2O	5370	24.6
LiF	5380	13.1

10,000 psi at 550°C. The rutile form of GeO_2 obtained was well crystallized, as indicated by an x-ray diffraction pattern, but was nonfluorescent. Subsequent heat treatment at 950°C for 8 hr was effective in developing a relatively weak yellow fluorescence under cathode-ray excitation, with an accompanying very slight pink coloration.

A sample of very pure transistor grade GeO_2 having an average resistivity of 35 ohm-cm (equivalent to 1.10 ppb impurity) with a 1% by weight addition of the LiCl-KCl eutectic mixture, heated to 900°C for 24 hr, developed the yellow fluorescence when excited by cathode-ray and 2537Å radiation. This preparation also became pink in color.

Spectroradiometer measurements were made on several of the fluorescent samples of the rutile form of GeO_2 prepared by heating at 850°C for 24 hr with additions of 1% by weight of the eutectic mixture of reagent grade LiCl-KCl, Li_2O, Na_2O, K_2O, and C.P. LiF. Li_2O, Na_2O, and K_2O were added as C.P. carbonates. Results of the as-recorded emission characteristics under cathode-ray excitation using 16 kv electrons at 2 $\mu a/cm^2$ on a focused raster are shown in Table I. A National Bureau of Standards sample of Zn_2SiO_4:Mn gave a brightness of 47.1 ft-L with 0.5 $\mu a/cm^2$.

For each preparation, the emission band was contained between approximately 4400 and 7200Å.

2537Å excitation produced similar peak positions (5370-5380Å) and band widths but generally weaker fluorescence. The K_2O preparation was relatively brighter than the LiCl-KCl preparation, etc., the Na_2O preparation being the weakest, as with the cathode-ray excitation.

No measurements were made for the heat-treated hydrothermally prepared sample or the transistor grade GeO_2 sample. Visually, the color of the emission could not be distinguished from that of the previous preparations.

It was observed that the samples did not reach maximum intensity of emission immediately when placed under 2537Å radiation. In contrast to Zn_2SiO_4:Mn, which appears to reach maximum intensity immediately upon exposure to 2537Å excitation, the GeO_2 samples appeared to increase gradually to maximum brightness.

Figure 1 shows the decay characteristics after cathode-ray excitation of the GeO_2 prepared with the eutectic mixture of LiCl-KCl as the mineralizer. Calculations give the rate constant $\alpha = 7.32 \times 10^3$ sec^{-1} and the lifetime of the excited state $\tau = 0.137$ msec, where $L/Lo = e^{-\alpha t}$ and $\alpha = \tau^{-1}$.

Discussion

The similarity in peak position and band width for the various preparations of the rutile form of GeO_2 suggests that the same mechanism may be effective in all cases studied. Chlorides, fluorides, and oxides of the alkali metals produce similar effects.

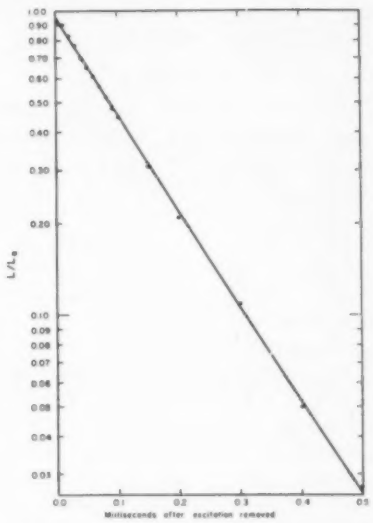

Fig. 1. Decay curve for fluorescent GeO_2

A possible explanation for the fluorescence may be the presence of loosely bound excitable electrons in the GeO_2 lattice due to anion vacancies. TiO_2 develops anion vacancies at elevated temperatures in air, becoming discolored and semiconducting. Defective TiO_2 may be represented by the formula Ti^{4+} O_{2-x}^{2-} $(e^-)_{2x}$ $(A.V.)_x$. Alternatively, it has been represented as Ti_{1-2x}^{4+} Ti_{2x}^{2+} O_{2-x}^{2-} $(A.V.)_x$, but this formula does not imply semiconducting properties so that the first representation is more appropriate to the discussion. A similar condition may develop in the rutile form of GeO_2 in which case the electrons which are not strongly quantized with respect to the Ge^{4+} ions may give rise to fluorescence and account for the pink body color. At any given temperature, at 1 atm in air, there should be an equilibrium number of anion vacancies. The rate of approach to this equilibrium value may be affected by the particular mineralizer added, thus giving rise to different values of brightnesses but similar emission bands.

The fluorescence produced in the preparation from transistor grade GeO_2 suggests that the emission is not due to impurities in the GeO_2.

Acknowledgments

The authors wish to thank the Chemical Products Plant of the General Electric Company, Cleveland, Ohio, for the financial support of this work. They also thank Miss Marjorie Brines for supplying the emission data.

Manuscript received Sept. 8, 1960. Contribution No. 60-5 from the College of Mineral Industries, The Pennsylvania State University, University Park, Pa.

Any discussion of this paper will appear in a Discussion Section to be published in the December 1961 JOURNAL.

REFERENCE

1. J. F. Sarver and F. A. Hummel, *J. Am. Ceram. Soc.*, **43**, 336 (1960).

N- and P-Type Single Crystal Bismuth Telluride

A. C. Yang and F. D. Shepherd

Electronic Material Sciences Laboratory, Electronics Research Directorate,
Air Force Research Division, Bedford, Massachusetts

Both p- and n-type single crystal Bi_2Te_3 have been grown by the Czochralski method. Some of these crystals were "dendritic like," similar to Ge dendrites reported by Billig (1). Starting materials were Bi and Te, both 99.999% pure.[1] The materials, in stoichiometric proportions, were melted together in a hydrogen atmosphere to form Bi_2Te_3. The melt was then cooled and any slag formed during reaction was removed by slicing off the surface. Crystals were grown in a hydrogen atmosphere to minimize the presence of oxide slag. A mixture of argon and hydrogen was not sufficient to prevent the formation of slags during growth. The seed crystal was rotated at rates from 1 to 25 rpm without any effect on the growth parameters. Pulling rates were from 0.2 cm/hr to 20 cm/hr. Seed crystals were oriented with hexagonal basal planes perpendicular to the melt. When other orientations were used, slip occurred, resulting in reorientation into this direction.

From stoichiometric melts only p-type crystals were obtained. Efforts to pull n-type crystals from Te-rich melts were not successful. The addition of 1% Cu^+ ion, in the form of Cu_2Te, to stoichiometric melts yields n-type crystals. In order to grow n-type crystals it was necessary to use pulling rates less than ½ cm/hr.

Crystals grown at rates less than 3 cm/hr were elliptical in cross section as reported by Ainsworth (2); however, at growth rates greater than 3 cm/hr, crystals assumed a dendritic form (see Fig. 1). During fast growth, the melts were undercooled and the resulting crystals had flat mirror-like surfaces and cleaved very easily along basal planes. In all cases, growth took place in the $2\bar{1}\bar{3}0$ direction as evidenced by orientation of etch pits and macroscopic hexagonal steps observed on crystal surfaces. There was no appreciable growth along the C axis, except for discrete step as above (Fig 2). The step growth assumed a definite hexagonal crystallographic shape in contrast with the curvilinear step growth in Ge dendrites (3). This suggests a growth mechanism similar to the activated screw-dislocation mechanism observed in the growth of alpha-SiC from the vapor phase. There was no visible evidence of twin plane formation in these crystals as has been observed in dendritic cubic crystal (4). It is suggested that in a faulted crystal structure, such as found in Bi_2Te_3 and alpha-SiC, twin plane formation is not necessary for dendritic growth.

During growth, there was appreciable Te vapor in the crystal puller resulting from decomposition of the melt. The vapor tends to condense onto the crystal and covers the crystal with Te. At the part of the crystal near the melt where the temperature is higher than the Te melting point, it is condensed as liquid Te and etches the crystal surface. This condensation yields a clear demarcation line between the regions where Te condenses as a liquid and as a solid. If the temperature at this line were assumed to be at the melting point of Te, a rough estimate of the temperature gradient during growth could be taken as approximately 60°C/cm.

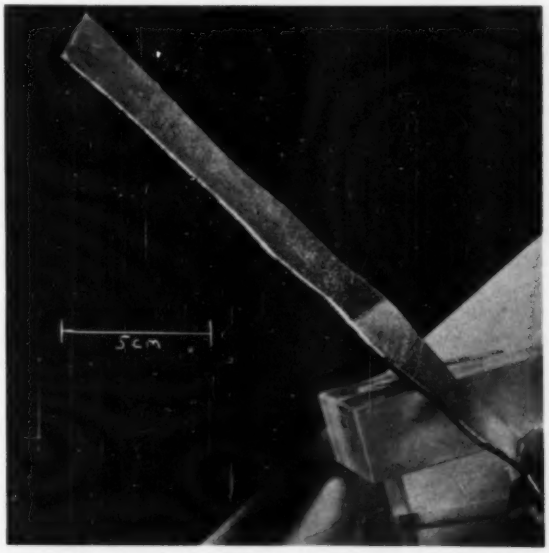

Fig. 1. P-type Bi_2Te_3 crystal grown at 8 cm/hr. Pitted surface is due to etching by gaseous Te above melt surface.

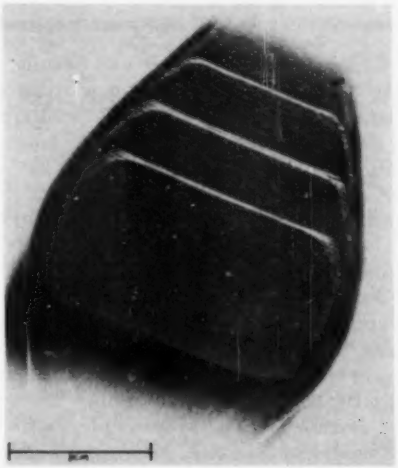

Fig. 2. Growth in discrete steps along the C-axis as observed in crystals grown at rates greater than 3 cm/hr.

[1] Obtained from American Smelting and Refining Co.

X-ray powder diffraction patterns of both p-type and n-type crystals gave identical lines. The diffraction lines observed agreed with those reported by Wyckoff (3) (and the A.S.T.M. index).

Preliminary room temperature thermoelectric measurements indicate Seebeck coefficients of 240 μv/°C and 120 μv/°C for p- and n-type crystals, respectively. Resistivity of the crystals was approximately 2 x 10^{-3} ohm-cm.

Acknowledgment

The authors wish to thank Mr. Joseph R. O'Connor for many helpful discussions with respect to the interpretation of results.

REFERENCES

1. E. Billig, *Proc. Roy. Soc.* (*London*), **A229**, 346 (1955).
2. L. Ainsworth, *ibid.*, **B69**, 606 (1956).
3. A. I. Bennett and R. L. Longini, *J. Appl. Phys.*, **116**, 53 (1959).
4. E. Billig and P. J. Holmes, *Acta Met.*, **5**, 53 (1957).

A Chemical Treatment for Rendering Silicon-Doped Aluminum Solderable

Sheldon L. Matlow[1] and Herbert J. Gould[2]

Hoffman Electronics Corporation, El Monte, California

Although the aluminum-tin system has a eutectic at 228.3°C (97.63 at. % Sn) (1), it is not possible to solder to aluminum directly using any of the lead-tin solders. The cause of the difficulty is usually attributed to the presence of the strongly adhering Al_2O_3 film on the aluminum. A procedure is available for direct soldering by use of ultrasonics (2, 3). In this process the ultrasonic cavitation is used to break up the oxide film under a layer of molten solder. Another method reported in the literature for removing the oxide under molten solder is that of anodic etching in a solder bath (4). An alternate approach is to electroplate a solderable metal onto aluminum (5, 6).

None of these procedures are convenient for the fabrication of semiconductor devices, especially when mass production processing is desired. The ultrasonic or electroplating equipment would not be necessary if a "simple" aqueous dip process were available which would bond a solderable metal directly to the aluminum surface, provided that the metal-aluminum bond obtained is sufficiently strong. The following is a report on such a dip process of the displacement plating type. A discussion of the mechanism of this process has been published (7).

Experimental Procedure and Results

Twenty mil, 99.999% aluminum wire was evaporated and alloyed using standard techniques (8) onto 0.5 ohm-cm n-type silicon wafers, 1 cm x 2 cm x 0.6 mm, to a thickness of about 2.5 x 10^{-3} mm. A methanol solution of a proprietary organic flux was used for the "tinning" operation. The alloyed aluminum was "tinned" by dipping into a 200°C 60/40 Sn-Pb solder bath. Part of the aluminum was masked during surface treatment with a mylar tape.

The exposed aluminum (1 mm x 2 cm along an edge) was then treated with the plating solution. After being rinsed and dried, the treated aluminum was "tinned" using the organic flux. The masking was then removed. Two such samples were placed solder to solder and heated, forming a bonded area approximately 0.1 x 2 cm. In the assembled unit the nonbonded 2 cm edges were approximately 1.8 cm apart. The assembled unit was held parallel to the floor, and the upper wafer was clamped in a padded vise so that the edges of the jaws of the vise were adjacent to the bonded area. A wire hook was placed on the unclamped wafer about 8.5 mm from the bonded area and 1 cm from each of the 1 cm edges of the wafer. Weights were then attached to the hook until either the bond or the silicon broke. Previous studies on solar cells 0.5 mm thick showed that the silicon broke when the weight exceeded 718 g; therefore, 0.6 mm thick wafers were used and no attempt was made to go beyond 718 g. The weight at which the bond broke was recorded as the bond strength. If it did not break, 718 (held) was recorded.

Experimental results.—The greatest bond strength was obtained with $CuSO_4 \cdot 5H_2O$ and concentrated aqueous HF (48%) in deionized water. Most of the time the alloyed specimen was treated shortly after removal from the vacuum. A study was also made on samples plated 20 days after alloying in order to determine the effect of oxidation of the aluminum.

In Table I it is shown that 20 g/100 ml of $CuSO_4$ is the optimum concentration. In Table II the optimum value for HF is shown. The optimum plating time with 20 g/100 ml of $CuSO_4 \cdot 5H_2O$ and 1 ml of HF was 5 min (Table III). Two further studies were made which indicated that the process is reproducible.

Some comment is indicated to account for the optima found. Displacement plating is an etching proc-

Table I. Concentration of $CuSO_4 \cdot 5H_2O$ varied

HF added, 1 ml; plating time, 5 min

Conc. of $CuSO_4 \cdot 5H_2O$ g/100 ml H_2O	15	20	25	30
Bond strength in grams	610	718 (held)	404	Did not solder
	718 (held)	718 (held)	404	
	404	718 (held)	610	
	404	718	290	
Average	534	718	427	—

[1] Present address: Intellux, Inc., Santa Barbara, Calif.
[2] Present address: Giannini Controls Corporation, Pasadena, California.

Table II. HF added—varied

$CuSO_4 \cdot 5H_2O$—20 g/100 ml H_2O; plating time, 5 min

ml of HF added	0.5	1.0	1.5	2.0
Bond strength in grams	Did not solder	718 (held)	404	610
		718 (held)	718 (held)	404
		718 (held)	718 (held)	290
		718	404	404
Average	—	718	561	427

Table III. Plating time—varied

$CuSO_4 \cdot 5H_2O$—20 g/100 ml H_2O; HF added, 1 ml

Plating time in min	4	5	6
Bond strength in grams	Did not solder	718 (held)	404
		718 (held)	404
		718 (held)	404
		718	404
Average	—	718	404

Table IV. $CuSO_4 \cdot 5H_2O$—20 g/100 ml H_2O

HF added, 1 ml; plating time, 15 min

Stored 20 days in	Air	Absolute methanol	Perchloro-ethylene
Bond strength in grams	404	610	404
	114	290	290
	114	290	114
	114	114	114
	610	290	610
	290	718	404
	290	404	290
	290	404	290
		290	
		404	
Average	370 ± 120	444 ± 110	393 ± 108

ess, and the aluminum layer is quite thin. If the etching is rapid or if etching time is great, a large fraction of the aluminum is removed, exposing silicon to which the solder will not adhere.

Three sets of alloyed samples were stored for twenty days: one in air, the second in a closed container of absolute methanol, and the third in a closed container of perchlorethylene. None plated well after 5 min of plating. The study was repeated using a 15-min plating time (see Table IV). From the data it is clear that in no case is the bond strength of the aged samples as great as that of fresh samples. However, if storage is necessary after alloying and before plating, the samples should be stored in absolute methanol.

Manuscript received June 13, 1960. This paper was prepared for delivery before the Columbus Meeting, Oct. 18-22, 1959.

Any discussion of this paper will appear in a Discussion Section to be published in the December 1961 JOURNAL.

REFERENCES

1. L. E. Samuels, *J. Inst. Metals*, **84**, 333 (1955-6); M. Hansen and K. Anderko, "Constitution of Binary Alloys," 2nd ed., p. 135, McGraw-Hill Book Co., New York (1958).
2. Aeroprojects Inc., "The Soldering of Aluminum and Its Alloys: A Comprehensive Review of the Literature," *Research Report No. 54-8*, March 1954 (Contract No. DA 36-034-ORD-1401 with Pitman-Dunn Labs., Frankford Arsenal).
3. J. B. Jones and J. G. Thomas, "Ultrasonic Soldering of Aluminum," ASTM 1956 Preprint 89C.
4. J. R. Williams (to Raytheon Manufacturing Co.), U. S. Pat. 2,857,321, Oct. 21, 1958.
5. J. T. N. Atkinson, *This Journal*, **105**, 24 (1958).
6. R. F. Hafer, in "Metal Finishing Guide Book—Directory," 27th ed., p. 279, Metals and Plastics Publications, Inc., New Jersey (1959).
7. S. L. Matlow, *SPAN*, p. 4, (Nov.-Dec. 1959).
8. J. M. Goldey in "Transistor Technology," F. J. Biondi, Editor, Vol. III, pp. 231 ff, D. Van Nostrand Co., Princeton, N. J. (1958).

Brief Communication

Antimony-Rich Surface Layer on Diffused Germanium

J. E. McNamara

Materials Research Department, Motorola Semiconductor Products Division, Phoenix, Arizona

The objective of this communication is to report the initial results of a study of the properties of an antimony-rich surface layer which we have observed to form during the diffusion of antimony into germanium from a vapor phase.

A well-known method for establishing diffused gradients of antimony in germanium consists of exposing the semiconductor to hydrogen gas containing antimony vapor. This component of the gas phase is usually produced by allowing the carrier gas to pass over hot antimony metal before it enters the diffusion furnace.

Diffused gradients established by the above procedure have been measured in this laboratory. Antimony metal containing the radioactive isotope Sb-124 was used as the source of the diffusant vapor pressure. Precision lapping methods were utilized to remove successive increments of the diffused material. The amount of antimony in the first increment was consistently larger than predicted from the error function distribution of the concentrations in the succeeding increments. When the diffused germanium samples were rinsed in hydrofluoric acid prior to lapping, the concentration of antimony

in the first increment was observed to decrease to a value consistent with the error function distribution. This observation was interpreted as evidence for the presence of an antimony-rich film on the surface of the freshly diffused germanium.

The objective of the experiments reported in this communication was to obtain preliminary information concerning the rate of formation of the film during diffusion, the effect of diffusion temperature on the film concentration, the rate of removal of the film by hydrofluoric acid, and the effect of crystallographic orientation of the germanium surface on the film concentration.

The experimental procedure consisted of measuring the loss of radioactivity by the diffused germanium samples after successive 2-min washes in hydrofluoric acid at room temperature. Sheet resistivity measurements taken after each wash demonstrated that no significant fraction of the loss in radioactivity could be attributed to solution of the germanium by the acid. The relation between the amount of radioactivity and the number of antimony atoms was determined by counting known weights of the antimony source in an environment equivalent to that used in counting the diffused germanium samples. Control experiments showed that less than 1% of the film concentrations reported below could result from antimony condensation on the surfaces of the samples during their movement into and out of the diffusion furnace.

The film concentrations for various diffusion times and temperatures are tabulated in Table I. The film concentration (C_f) appeared to reach a saturated value within 45 min at a diffusion temperature of 648°C. A larger film concentration was measured for the sample diffused at the higher germanium and antimony temperatures. In Fig. 1 are shown the data for the rate of removal of the film by hydrofluoric acid at room temperature. The film formed at the higher diffusion temperature dissolved in the acid at a considerably slower rate. No significant difference in the rate of removal was observed between the etched and mirror-polished samples.

The values of the film concentrations reported are in close agreement with the maximum number (7×10^{14}/cm^2) of unsaturated bonds on a (111) germanium surface. This observation suggested that each antimony atom in the surface film may be covalently bonded with one of the germanium atoms containing an unsaturated bond. According to this model, the two remaining electrons needed to fill the antimony valence shell would be furnished from a sharing of electrons between adjacent antimony

Table I. Film concentrations (C_f) of antimony on diffused germanium (111) surfaces

Diffusion temp, °C	Antimony temp, °C	Diffusion time, hr	C_f, atoms/cm^2
648	409	0.75	0.65×10^{15}
648	409	3.50	0.62×10^{15}
648	409	16.00	0.64×10^{15}
648	409	48.00	0.67×10^{15}
755	484	3.50	0.77×10^{15}

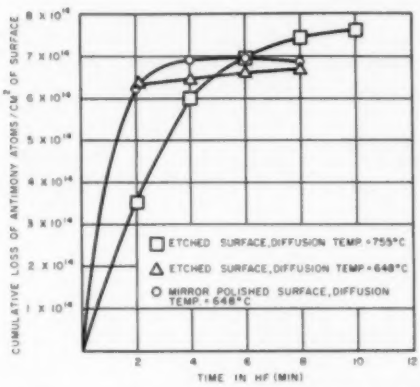

Fig. 1. Removal of antimony surface film from diffused germanium (111) surfaces; HF concentration 48% by weight.

atoms on the surface. This model of the structure of the surface film predicts that the film concentration on a (100) surface should be significantly higher since this plane contains a higher density of free bonds (1.2×10^{15}/cm^2). However, initial measurements on (100) surfaces indicate film concentrations within 10% of those obtained for the (111) surfaces.

An antimony-rich surface layer would be expected to form if the antimony vapor pressure over the germanium during diffusion were in excess of the equilibrium vapor pressure of the saturated solid solution of antimony in germanium. However, previous experiments showed that the surface concentrations of antimony in germanium under the conditions encountered in these experiments were an order of magnitude lower than the solid solubilities reported by Trumbore (1). Furthermore, out-diffusion of antimony from germanium was observed to result in the re-formation of the antimony surface film. This observation is thermodynamically incompatible with the concept of the formation of an alloy phase.

At the diffusion temperatures employed in this work, antimony vapor consists almost entirely of molecules having the composition (Sb_4) (2). During the diffusion anneal this molecule must undergo dissociation on the germanium surface to form atomic antimony. This dissociative reaction would result in some finite steady-state concentration of antimony on the surface. Studies of the film concentration over a wide range of antimony vapor pressures should prove of value in evaluating the extent to which this dissociative process is responsible for the film concentrations reported in this communication.

Manuscript received Aug. 26, 1960.

Any discussion of this paper will appear in a Discussion Section to be published in the December 1961 JOURNAL.

REFERENCES

1. F. A. Trumbore, *Bell System Tech. J.*, **39**, 205 (1960).
2. M. C. Sneed and R. C. Brasted, "Comprehensive Inorganic Chemistry," Vol. 5, p. 111, D. Van Nostrand Co., New York (1960).

Feature Section

Science and Electrode Processes

Second William Blum Lecture[1]

Sigmund Schuldiner[2]

Scientists usually are so involved with their own particular area of investigation that they have little time to think about the philosophy of science. I feel that now and then we should consider seriously the broader and more general aspects of science, especially as applied to one's particular field. I should like to develop here a few thoughts concerning science in general, and then my own particular field of electrode processes. As stated by Bronk,[3] "Science can seldom be developed by scientists who do not have such specialized competence, but more is needed for the development of science. Scientists whose knowledge is narrowly restricted are hampered in their research; they are unfitted to form new facts into conceptual schemes . . . ."

Science, or more specifically the scientific method, was defined by Bridgeman[4] as follows: "The so-called scientific method is merely a special case of the method of intelligence, and any apparently unique characteristics are to be explained by the nature of the subject matter rather than ascribed to the nature of the method itself." Intelligence, a rigorous logic, and objective observations, however, are not enough for the successful development of science. These factors have been applied to other areas of human endeavor but they have not led consistently to an accelerated improvement of our well-being in the same degree as has science. A missing ingredient is, I believe, honesty in reporting data. This factor usually is omitted in discussions concerning the scientific method because scientists naturally assume its implication. But as Delahay[5] so aptly stated, honesty in reporting data is one of the remarkable and necessary traits of the scientist. This, plus the rigorous rules which are applied to the scientist by his fellow scientists in reporting his work, has resulted in an international system of endeavor which indeed has been successful. Honestly reported data and adequately described experimental techniques can be duplicated anywhere. It cannot be stressed too strongly that this scientific attitude is a most essential part of the scientific method. Thus, a really important lesson to be learned from the scientific method is that a rigorous code of moral behavior, which is self-enforced by the scientific community, can be successful on a world-wide scale. The factors involved in this enforcement are: the universal knowledge that the scientific method would be hampered seriously without it, the self-respect of the individual scientists, the respect of one's fellow scientists, and the strict denial of the validity of that much-used attitude that the ends justify the means. The unique system of free communication among scientists is another important factor in maintaining this scientific attitude.

By careful observation, experimentation, and generalization, the scientist has been able to put many of the facts of our physical world in convenient form that can be put to practical use. Mathematics gives him an excellent tool for summarizing his generalizations and for transforming these summaries into forms of the most immediate practical use. The variations and permutations of the physical world are too numerous for their complete observation or experimentation. Scientists must be able to select critical experiments which will give information not only about the particular system under observation, but, much more important, about a large class of systems. In this way, the scientist by relatively few observations can summarize about a large area of the physical world and predict how unknown systems will behave. This, of course, is the area where the theoretician plays his primary role. However, it should be realized that in theorizing one generally must derive relationships which closely satisfy, but are not necessarily exact representations of the true physical world. These relationships can be expressed as idealized models which in themselves cannot be true because the theories only approximate nature, and the truth is not something which can be approximated—it is one of those black and white concepts.

I say this not to depreciate the use of idealized models, because this has been an essential device in science. However, it is important that we do not deceive ourselves in believing that these idealized models represent the ultimate truth. These models may represent perfection in scientific logic, but they are still man made. Sometimes it seems that we scientists are so impressed with this type of perfection in reasoning that we really think that we have the ultimate key to nature. We often hear that the theory represents the facts much better than the experimental results do. In fact, we as scientists are allowed only to approximate the reality in nature—our approximations become better with time, but still the truth about the ultimate aspects of nature will undoubtedly always evade us. This is fortunate since the world would be a dull place, indeed, if we knew all the answers. Many of the nineteenth century scientists believed that it was a matter of just a few years before all the important knowledge about our physical world would be known. In the late nineteenth and in the twentieth century, however, new concepts forced us to realize that there may be limitations to our knowledge of nature. The ultimate truth about nature probably belongs in the realm of religion anyway, not science. A

[1] Delivered at an award dinner held November 17, 1960 (see p. 32C of this issue.)

[2] U.S. Naval Research Laboratory, Washington, D. C.

[3] D. W. Bronk, "The Unity of the Sciences and the Humanities," p. 11, Fourth Annual A. D. Little Memorial Lecture at the Massachusetts Institute of Technology, Cambridge, Mass., 1949.

[4] P. W. Bridgeman, "Physical Science and Human Values," p. 145, Princeton University Press, Princeton, N. J. (1947).

[5] P. Delahay, *American Scientist*, 48, 28 (1960).

primary purpose of science is to find rules in nature and to apply this knowledge to our benefit.

The investigation of the mechanisms of electrochemical reactions is in many respects a most frustrating field of science. From its very nature, we must be burdened with a negative approach. One is limited to proposing various models which represent particular mechanisms, and experimental kinetic studies can prove only the impossibility of certain of these models, but cannot furnish the sufficient condition which uniquely defines a particular mechanism. This does not mean that the kinetic approach is not useful or is hopeless; it only means that much more work is needed, plus a real breakthrough in our thinking, before kinetics approximates the exactness of thermodynamics. Much progress has been made in recent years, but the basic concepts still are not well defined in many cases and, indeed, the physical meaning of some of the fundamental parameters is still in doubt. Anyone who has worked in the field of electrokinetics for any length of time realizes the inadequacies in this respect. This is especially brought home when a student or newcomer in the field asks you to recommend a textbook or references which will give him an adequate and understandable introduction into the field.

Undoubtedly one of the major difficulties in the study of electrode mechanisms is our lack of understanding of the surface states of electrodes. Surface chemistry has not yet advanced to the point where a surface has been defined adequately and this is necessary before electrochemical measurements of many irreversible electrode phenomena really can be meaningful. The fact that we can obtain reproducible data for an electrode reaction which can then adequately be applied to an over-all mechanism does not necessarily give us any details about the reaction. For example, when we say that a reaction is controlled by a slow discharge step, does this mean that the actual electron transfer is slow? Or does it mean that we have not divided this step into detailed-enough steps to determine precisely what the slow step is?

In spite of the many shortcomings in the study of electrode processes, many advances have been made in recent years. A realization of the importance of the cleanliness of electrode surfaces has led to rigorous purification techniques. These methods have yielded many consistent experimental results which are independent of the investigator. This has been an important step in obtaining meaningful data. Largely because of the pioneering work of Grahame, a great deal now is known about the structure of the double layer on an ideally polarized mercury surface. Adsorption phenomena on electrode surfaces have been investigated in great detail and much is known about these effects. The work of Frumkin and his school in this area is well known. Many new, highly complex experimental techniques have been developed to aid us in determining the necessary parameters of electrokinetics. These are to a large extent alternating- and direct-current transient methods, and today the electrochemist spends a great deal of his time developing and adapting electronic techniques. These methods also have required an extensive study of the interpretation of electrical measurements in terms of the reactions occurring on the electrode surface. Transient methods now are in use that can determine potential-current changes on an electrode surface in a fraction of a microsecond. We can observe and quantitatively measure changes in the order of the relaxation times of ions at the electrode/solution interface. With these transient techniques, we can separate processes occurring at different rates at the electrode/solution interface.

In many electrode reactions using so-called inert electrodes, the electrodes are not mere electron sources or sinks, but play an intimate part in the electrode mechanisms. When chemisorbed reactants or products influence the reaction rate, the sites on the electrode surface are part of the electrode process. Here the electrode surface can catalyze or retard the reaction rate. In these cases, the heat of adsorption of the adsorbed species will influence the catalytic activity. In this area of research, some work has been done relating the bulk properties of the electrode material with the bonding energies on its surface. Thus, relationships between the electronic configuration of transition metals and their alloys have shown some interesting correlations to the heat of adsorption of adsorbed species. Even though this approach has led to spectacular confirmations of this hypothesis in some cases, there also have been some serious letdowns. It appears that we now are reaching the point in many of these areas where new concepts are needed in order to evolve theories which better fit the facts.

Outside of solution transport effects, electrode processes involve many complex phenomena occurring within a very narrow region at the electrode/solution interface. We have the advantage in electrochemistry that the over-all reaction rates can be controlled easily and measured by means of electric currents. We also easily can control the energetics of the surface by controlling its potential. We have the advantage, too, that electronic measuring equipment has been developed to an extremely advanced state so that we have a great variety of very accurate and sophisticated tools. In fact, the rate of advance in electronics is so fast that it is impossible for the electrochemist to keep up with it. The really difficult problem is to translate our precise measurements with these tools into meaningful electrochemical processes—in this, we have a long way to go. The tools are available; we need only a great deal of hard work and critical thinking to understand what we are measuring.

FUTURE MEETINGS OF
The Electrochemical Society

Indianapolis, Ind., April 30, May 1, 2, and 3, 1961
Headquarters at the Claypool Hotel
Sessions will be scheduled on
Electric Insulation, Electronics (including Luminescence and Semiconductors), Electrothermics and Metallurgy, Industrial Electrolytics (including a Symposium on Fuel Cells), and Theoretical Electrochemistry (including a Symposium on Instrumentation)

★ ★ ★

Detroit, Mich., October 1, 2, 3, 4, and 5, 1961
Headquarters at the Statler Hotel
Sessions probably will be scheduled on
Batteries, Corrosion, Electrodeposition (including symposia on Addition Agents and on Electrodeposited Magnetic Films), Electronics (Semiconductors), Electro-Organics, and Electrothermics and Metallurgy

★ ★ ★

Los Angeles, Calif., May 6, 7, 8, 9, and 10, 1962
Headquarters at the Statler Hilton Hotel

★ ★ ★

Boston, Mass., September 16, 17, 18, 19, and 20, 1962
Headquarters at the Statler Hilton Hotel

Papers are now being solicited for the meeting to be held in Detroit, Mich., October 1-5, 1961. Triplicate copies of each abstract (*not exceeding 75 words in length*) are due at Society Headquarters, 1860 Broadway, New York 23, N. Y., *not later than May 15, 1961* in order to be included in the program. *Please indicate on abstract for which Division's symposium the paper is to be scheduled, and underline the name of the author who will present the paper.* No paper will be placed on the program unless one of the authors, or a qualified person designated by the authors, has agreed to present it in person. An author who wishes his paper considered for publication in the JOURNAL should send triplicate copies of the manuscript to the Managing Editor of the JOURNAL, 1860 Broadway, New York 23, N.Y.

Presentation of a paper at a technical meeting of the Society does not guarantee publication in the JOURNAL. However, all papers so presented become the property of The Electrochemical Society, and may not be published elsewhere, either in whole or in part, unless permission for release is requested of and granted by the Editor. Papers already published elsewhere, or submitted for publication elsewhere, are not acceptable for oral presentation except on invitation by a Divisional program Chairman.

Current Affairs

Sigmund Schuldiner Receives William Blum Award of Washington-Baltimore Section

Sigmund Schuldiner of the Naval Research Laboratory, Washington, D. C., was presented the second William Blum Award of the Washington-Baltimore Section of The Electrochemical Society at a dinner at Brook Farm Restaurant on November 17, 1960. (Mr. Schuldiner's award address appears on pp. 29C-30C of this issue.)

The Blum Award, consisting of $100.00 and a certificate, is presented biennially to a member of the Local Section of The Electrochemical Society for outstanding contributions to electrochemistry. The award is named for Dr. William Blum, retired head of the Electrodeposition Section at the National Bureau of Standards, in honor of his distinguished contributions to the theories and techniques of electrodeposition.

Jerome Kruger, Chairman of the Washington-Baltimore Section, made the presentation citing the recipient for his contributions to the science of electrochemistry, with special reference to the hydrogen-producing reactions on noble metals.

Sigmund Schuldiner receives the second William Blum Award of the Washington-Baltimore Section from Jerome Kruger, Chairman of the Section.

J. C. White, chief of the Electrochemical Branch of the Chemistry Division of the Naval Research Laboratory, presented a brief résumé of the personal and professional achievements of the award recipient.

During the past ten years, Mr. Schuldiner has developed techniques for studying electrode mechanisms using highly purified solutions in Teflon cells and using an electronic current interrupter to separate the various components of the over-all polarization potential. Using these techniques, he was able to determine mechanisms and kinetics of hydrogen reaction on platinum, palladium, and a number of other metals. In addition, mechanisms of transport of hydrogen and deuterium through platinum, palladium, and palladium-clad metals were determined.

Mr. Schuldiner was born in Chicago in 1913, and received his A.B. degree from New York University in 1938 and his A.M. degree from Columbia in 1939. He worked briefly at the National Bureau of Standards, then at the Norfolk Naval Shipyard during the war. In 1946, he transferred to the Naval Research Laboratory where he worked in the Corrosion and Electrochemical Branches of the Chemistry Division. He now is head of the Electrode Mechanisms Section of the Electrochemistry Branch.

Section News

News from India

ISI and Batteries.—The Indian Standards Institution (ISI) has two committees to prepare Indian Standards covering the field of batteries: Primary Cells and Batteries Sectional Committee ETDC 10 and Secondary Cells and Batteries Sectional Committee ETDC 11. The first committee has published the following standards: (*a*) IS: 203-1958, Leclanché type dry batteries for flashlights (revised); (*b*) IS: 267-1958, Leclanché type inert cells (revised); (*c*) IS: 268-1959, Leclanché type sack cells (revised); (*d*) IS: 556-1960, Leclanché type radio batteries (revised); (*e*) IS: 586-1959, Leclanché type dry batteries for telecommunication, signaling, and general purposes (revised); (*f*) IS: 1025-1957, Glossary of terms for primary cells and batteries. The subjects under study are: flashlight torches, batteries for photoflash lamps, batteries for hearing aids, batteries for transistorized equipment, terminals and connectors for primary batteries, and carbon rods for primary cells.

The standards published by the Secondary Cells and Batteries Sectional Committee are: (*a*) IS: 395-1959, Lead-acid storage batteries (light duty) for motor vehicles (revised); (*b*) IS: 541-1954, Stationary accumulators (to be superseded); (*c*) IS: 985-1958, Lead-acid storage batteries (heavy duty) for motor vehicles; (*d*) IS: 1145-1957, Lead-acid storage batteries for motor cycles; (*e*) IS: 1147-1957, Glossary of terms for secondary cells and batteries. The following standards have been finalized and are to be published shortly: (*a*) lead-acid storage batteries (24 v, 40 AH) for aircraft (aerobatic and nonaerobatic); (*b*) Hard rubber containers for storage batteries; (*c*) Stationary cells and batteries, lead-acid type (with tubular positive plates); (*d*) Stationary cells and batteries, lead-acid type (with Plante positive plates). Batteries for miners' cap lamps are under study.

Potassium Chlorate Plant at Mettur.—The potassium chlorate plant of the Mettur Chemical and Industrial Corp. Ltd., Mettur Dam R.S., was formally opened on August 30, 1960 by the Chief Minister of Madras. It was completely designed, fabricated, and erected by the technicians of the company. The chlorate is produced by the electrolysis of potassium chloride between graphite

anodes and iron cathodes. The 6000-ampere "Mettur Cell" incorporates several special design features in respect of placement of electrodes, cathode construction, cooling arrangement, etc. Twenty-four cells have been installed with a capacity of 624 tons per year. The setting up of this plant goes a long way in meeting the shortage of this chemical in India and also in saving foreign exchange. The current annual production of chlorate in India is about 4300 tons, but the estimated demand after five years is 8000 to 10,000 tons. The Mettur plant is the first of its kind to be installed in Madras State and the third in India.

Expansion Program of Mettur Chemicals.—The Mettur Cemical and Industrial Corp. Ltd. has in hand a big program of expansion of caustic soda production. The existing capacity of 20 tons per day is proposed to be doubled during 1961. This will be achieved by the installation of additional 10,000-ampere Hooker S diaphragm cells, and a new triple effect caustic soda evaporation plant with a capacity of 50 tons per day. The direct current for the electrolytic cells will be obtained from the latest type semiconductor silicon rectifiers. There also will be a new synthetic hydrochloric acid plant adequate to handle 18 tons of chlorine a day.

Corrosion Refresher Course.—A five-week refresher course on "Corrosion and Its Prevention" was held at the Central Electrochemical Research Institute, Karaikudi, beginning November 7, 1960. It was open to persons sponsored by industrial organizations or government departments. The topics for the course covered corrosion processes and economics, and preventive measures, supplemented with extension lectures and practical work.

Aluminum Industry in India.—A license has been granted to the Madras Aluminium Co. for installing a 10,000-ton-per-year plant at Mettur, Madras. The State Government will participate financially, and the Italian firm Montecatini will be collaborating financially and technically. Another plant of 20,000 tons capacity in Maharashtra State is expected to be licensed. This project will be in collaboration with Aluminum Corp. of America.

India's First Heavy-Electrical Plant.—The Heavy Electricals Factory at Bhopal, the first of its kind in India and claimed to be the biggest in Asia, started production in July 1960 according to schedule. It will produce switch-gears, control panels, power transformers, capacitors, traction motors, equipment for electric locomotives, industrial motors, and generators. The plant will be in full stride in about seven years. The annual output is expected to be Rs.25 crores.

New Patrons—India Section.—The following industries have become Patrons of the India Section: 1. Phoenix Chemical Works, Bombay; 2. Navyug Industries, Bombay.

T. L. Rama Char,
India Correspondent

Indianapolis Section

The Indianapolis Local Section held its initial technical meeting of the current season on Tuesday, November 22, 1960, at Butler University in Indianapolis. Two speakers were featured. This proved to be a well-received departure from our previous programming activities.

Our first speaker was John J. Lander, director of electrochemical research, Delco-Remy Division, General Motors Corp. His presentation, entitled "Partial Plated Monolayers of Silver on Gold," dealt with a differing and most interesting interpretation of the data in the papers of Byrne, Rogers, and Griese.

Our second speaker was Dr. Thomas Murrell from the Computer Laboratory of the University of Illinois, Urbana, Ill. His subject was "Recent Trends in Semiconductor Research." Dr. Murrell spent several months in Europe last summer. During this time, he visited a number of the foremost European organizations in this field. His personal observations contrasting current developments and trends in Europe with those he observed during his last visit four years ago and with those prevalent in this country proved to be quite interesting.

T. C. O'Nan, *Sec.-Treas.*

New York Metropolitan Section

A meeting of the Section was held at Victor's Restaurant in New York City on November 16, 1960. Speaker of the evening was J. O'M. Bockris, professor of chemistry, University of Pennsylvania. Dr. Bockris reviewed some recent work that has been done in the electrochemical laboratories of the university.

In his discussion of the mechanism of deposition and dissolution of metals, he mentioned that the investigation has permitted the application of the dislocation theory to electrochemistry for the first time. (When anions come into contact with an edge dislocation, the dislocation will grow if its length is greater than a critical value. The

Manuscripts and Abstracts for Fall 1961 Meeting

Papers are now being solicited for the Fall Meeting of the Society, to be held at the Statler Hotel in Detroit, Mich., October 1, 2, 3, 4, and 5, 1961. Technical sessions probably will be scheduled on Batteries, Corrosion, Electrodeposition (including symposia on Addition Agents and on Electrodeposited Magnetic Films), Electronics (Semiconductors), Electro-Organics, and Electrothermics and Metallurgy.

To be considered for this meeting, triplicate copies of abstracts (*not exceeding 75 words in length*) must be received at Society Headquarters, 1860 Broadway, New York 23, N. Y., *not later than May 15, 1961. Please indicate on abstract for which Division's symposium the paper is to be scheduled and underline the name of the author who will present the paper.* No paper will be placed on the program unless one of the authors, or a qualified person designated by the authors, has agreed to present it in person. An author who wishes his paper considered for publication in the JOURNAL should send triplicate copies of the manuscript to the Managing Editor of the JOURNAL, 1860 Broadway, New York 23, N. Y.

Presentation of a paper at a technical meeting of the Society does not guarantee publication in the JOURNAL. However, all papers so presented become the property of The Electrochemical Society, and may not be published elsewhere, either in whole or in part, unless permission for release is requested of and granted by the Editor. Papers already published elsewhere, or submitted for publication elsewhere, are not acceptable for oral presentation except on invitation by a Divisional program Chairman.

critical length decreases with increase in potential.)

The adsorption of organic compounds at metal-solution interfaces depends on the type of compound. Working with liquid mercury, Dr. Bockris found that aliphatic and aromatic compounds had quite different adsorption properties. The laboratory is developing methods of studying adsorption of compounds on solids under potential control.

A method has been developed for the detection of the concentration of sub-monolayer deposition of hydrogen (of the order of 10^{-10} mols/sq cm). Work performed on silver, copper, and iron indicates that results of practical value can be obtained.

J. L. Everhart

Ontario-Quebec Section

On November 1, 1960, the Ontario-Quebec Section held a Joint Dinner Meeting with the Toronto Section of the National Association of Corrosion Engineers. The program consisted of a paper entitled "New Light on Fuel Cells" by Norman Hollefriend of Canadian Allis-Chalmers, followed by a showing of the film "Corrosion in Action."

Mr. Hollefriend outlined briefly the basic reactions of fuel cell operation, then went on to describe the progress which the Allis-Chalmers organization has made in the development of a practical operating cell. The cell chosen by this company is one which operates at low pressure and normal temperatures, using hydrogen as fuel. A standard-sized tractor has been operated successfully from a bank of these cells.

The film "Corrosion in Action," a sound and color movie which explains how corrosion occurs and tells what can be done to control it, was introduced and commented on by Mr. R. J. Law of the International Nickel Co.

R. A. Campbell, *Sec.-Treas.*

San Francisco Section

The second meeting of the 1960-1961 season was held November 16, 1960 at the University of California Men's Faculty Club.

A panel discussion of "Micro Circuit Systems" being developed at the Missiles and Space Division of Lockheed Aircraft Corp. was initiated by W. Dale Fuller, manager of their Microsystems Electronics Dept. He sketched the development from etched wiring circuitry through micromodule to integrated solid-state circuit units. This represents a shift in thinking from component to circuit orientation. This development permits a significant improvement in the reliability of operation, and gives the added advantages of smaller size and less power.

Merle E. Sibert presented comparative data on some electrical properties of a wide variety of refractory materials. Titanium and its oxide were selected as a suitable pair for circuit elements, and various experimental procedures for their formation were tried.

Ross A. Quinn discussed the particularly successful techniques now used in the formation of circuit blocks whereby titanium is thermally deposited on alumina for conductive elements, then oxidized in selected areas to produce resistive and capacitive elements.

Dale Fuller finished the panel presentation with a discussion of the "transfer function" approach. This goes even beyond the circuit concept, and designs hardware to perform according to in-out black box transfer functions. Some useful new circuit elements have been invented in this approach.

The meeting ended after a lively discussion.

Worden Waring, *Vice-Chairman*

Notice to Members

According to the Constitution of the Society, Article III, Section 9, "Any member delinquent in dues after April 1 of each year shall no longer receive the Society's publications. . . ." Such delinquents will not receive the May issue of the JOURNAL. A reminder notice will be mailed to delinquents about the middle of February and a final notice about the first week in April.

New Members

In January 1961, the following were elected to membership in The Electrochemical Society by the Admissions Committee:

Active Sustaining Members

T. F. Olt, Research Center, Armco Steel Corp., Middletown, Ohio (Electrothermics & Metallurgy)

G. J. Wilson, National Cash Register Co., Main & K Sts., Dayton 9, Ohio (Electronics)

Active Members

R. F. Amlie, Electric Storage Battery Co.; Mail add: 11 Olivia Dr., Yardley, Pa. (Battery)

W. T. Biedler, III, Research Labs., United Aircraft Corp., Silver Lane, East Hartford 8, Conn. (Industrial Electrolytic, Theoretical Electrochemistry)

M. S. Chao, Dow Chemical Co.; Mail add: 415 E. Larkin St., Midland, Mich. (Industrial Electrolytic, Theoretical Electrochemistry)

R. J. Cox, Pennsalt Chemicals Corp., Biddle Ave., Wyandotte, Mich. (Industrial Electrolytic)

W. P. Cox, Rheem Semiconductor Corp.; Mail add: 3544 Constance Dr., San Jose 28, Calif. (Electronics)

S. N. Dermatis, Westinghouse Electric Corp.; Mail add: 115 N. 4 St., Youngwood, Pa. (Electronics-Semiconductors)

G. T. Croft, Pitney-Bowes Inc.; Mail add: 38 Dulan Dr., Stamford, Conn. (Battery)

T. H. Dexter, Hooker Chemical Corp.; Mail add: Elliott Dr., Lewiston, N. Y. (Corrosion)

G. A. Di Pietro, Vacuum Specialties Co.; Mail add: 22 Country Club Rd., Arlington 74, Mass. (Electrothermics & Metallurgy)

R. A. Eppler, Fundamental Chemistry Research Dept., Corning Glass Works, Corning, N. Y. (Electric Insulation, Electronics-Luminescence)

L. A. Friedrich, Pratt & Whitney Aircraft (Canel); Mail add: 202 Washington St., Hartford 6, Conn. (Electrodeposition, Electrothermics & Metallurgy)

T. M. Gladstein, Technion-Israel Institute of Technology, Library, P. O. Box 4910, Haifa, Israel

R. E. Gonzalez, General Electric Co.; Mail add: 101 Jewell Dr., Liverpool, N. Y. (Electronics-Semiconductors)

Ludwik Gutnajer, Budd Electronics Inc.; Mail add: 79 Barrow St., New York 14, N. Y. (Electronics)

S. J. Guttman, Patterson-Moos Research Div. of Leesonia; Mail add: 7004 Perry Terrace, Brooklyn 9, N. Y. (Battery)

R. V. L. Hall, Bridgeport Brass Co., 30 Grant St., Bridgeport 2, Conn. (Corrosion)

R. P. Hamlen, General Engineering Lab., General Electric Co., One River Rd., Schenectady, N. Y.

By action of the Board of Directors of the Society, all prospective members must include first year's dues with their applications for membership.

Also, please note that, if sponsors sign the application form itself, processing can be expedited considerably.

(Battery, Corrosion, Theoretical Electrochemistry)

G. R. Hoey, Central Research Labs., Canadian Industries Ltd., McMasterville, Que., Canada (Industrial Electrolytic)

M. L. Hollander, American Smelting & Refining Co.; Mail add: 1338 E. 7 St., Plainfield, N. J. (Electrodeposition, Industrial Electrolytic)

C. E. Ingersoll, Williams Gold Refining Co., Inc., 2978 Main St., Buffalo 14, N. Y. (Electrodeposition)

V. J. Jennings, Semiconductor Div., Westinghouse Electric Corp., Youngwood, Pa. (Electrodeposition, Electronics–Semiconductors and Luminescence, Theoretical Electrochemistry)

C. H. Layer, Battelle Memorial Institute; Mail add: 581 Harley Dr., Columbus, Ohio (Electrodeposition)

Bela Lombos, Northern Electric Co. Ltd.; Mail add: 3280 Linton Ave., Montreal, Que., Canada (Electronics-Semiconductors)

R. L. Luce, Philco Corp., Lansdale Div.; Mail add: 5225 N. Front St., Philadelphia 20, Pa. (Electronics-Semiconductors)

R. R. McWilliams, Semiconductor Div., Minneapolis-Honeywell, 1177 Blue Heron Blvd., Riviera Beach, Fla. (Electronics-Semiconductors)

D. A. Marino, Western Electric Co.; Mail add: 29 Winsor Place, Glen Ridge, N. J. (Electrodeposition)

I. F. Matthysse, Burndy Corp., Norwalk, Conn. (Industrial Electrolytic)

H. S. Miller, Lummus Co.; Mail add: 310 Lexington Ave., New York 16, N. Y. (Battery, Corrosion, Electrodeposition, Industrial Electrolytic, Theoretical Electrochemistry)

R. L. Myers, Borg-Warner Corp., Ingersoll Research Center; Mail add: 1114 Merril St., Winetka, Ill. (Theoretical Electrochemistry)

A. G. Ostroff, Socony Mobil Oil Co.; Mail add: 619 Misty Glen Lane, Dallas 32, Texas (Corrosion)

ECS Membership Statistics

The following three tables give breakdown of membership as of Jan. 1, 1961. The Secretary's Office feels that a regular accounting of membership will be very stimulating to membership committee activities. In Table I it should be noted that the totals appearing in the right-hand column are *not* the sums of the figures in that line since members belong to more than one Division and, also, because Sustaining Members are not assigned to Divisions. But the totals listed are the total membership in each Section. In Table I, Sustaining Members have been credited to the various Sections.

Table I. *ECS Membership by Sections and Divisions*

Section	Division: Battery	Corrosion	Electric Insulation	Electro-deposition	Electronics	Electro-Organic	Electrothermics & Met.	Industrial Electrolytic	Theoretical Electrochem.	No Division	Total as of 1/1/60	Total as of 1/1/61	Net Change
Boston	18	37	14	37	86	5	25	10	28	5	168	177	+ 9
Chicago	25	33	10	38	29	16	19	14	35	7	134	148	+ 14
Cleveland	54	28	1	47	42	8	30	30	38	6	198	192	— 6
Columbus, Ohio	5	14	2	13	13	2	30	5	11	2	62	60	— 2
Detroit	21	21	4	51	17	8	9	7	38	6	97	104	+ 7
India	11	10	2	24	9	6	8	10	17	3	35	42	+ 7
Indianapolis	30	10	11	13	24	7	14	6	14	2	53	69	+ 16
Midland	10	16	1	5	3	3	10	15	9	—	43	43	0
Mohawk-Hudson	7	24	17	8	19	1	13	1	20	5	70	76	+ 6
New York	107	113	31	174	186	42	103	73	128	34	575	618	+ 43
Niagara Falls	13	19	2	25	27	6	72	59	13	11	180	168	— 12
Ontario-Quebec	8	20	2	13	8	2	42	29	14	4	93	92	— 1
Pacific Northwest	5	9	1	8	1	—	9	11	12	3	43	38	+ 5
Philadelphia	39	23	7	39	77	9	29	24	44	16	205	210	+ 5
Pittsburgh	4	46	5	30	36	6	37	23	36	1	136	133	— 3
San Francisco	14	14	1	28	34	3	16	21	24	3	78	98	+ 20
S. Calif.-Nevada	23	25	5	38	70	4	31	22	39	4	135	150	+ 15
Texas	4	23	2	14	41	3	9	24	31	1	0	103	+103
Washington-Baltimore	38	39	9	38	27	5	14	7	25	2	140	144	+ 4
U. S. Non-Section	61	70	11	76	68	32	64	51	84	25	452	349	—103
Foreign Non-Section	61	66	15	71	38	29	49	64	83	80	285	302	+ 17
Total as of Jan 1, 1960	479	658	117	755	748	198	569	502	718	331	3182		
Total as of Jan. 1, 1961	558	660	153	790	855	197	633	506	743	220		3316	+134
Net Change	+79	+2	+36	+35	+107	—1	+64	+4	+25	—111	+134		

Table II. *ECS Membership by Grade*

	Total as of 1/1/60	Total as of 1/1/61	Net Change
Active	2761	2895	+134
Faraday (Active)	32	33	+ 1
Deutsche Bunsen Gesellschaft (Active)	18	17	— 1
Delinquent	88	84	— 4
Active Representative Patron Members	10	10	0
Active Representative Sustaining Members	111	107	— 4
Total Active Members	3020	3132	+112
Life	17	16	— 1
Emeritus	48	65	+ 17
Associate	33	39	+ 6
Student	57	43	— 14
Honorary	7	7	0
Total	3182	3316	+134

The figures pertaining to Patron and Sustaining Member Representatives, and Faraday and Deutsche Bunsen Gesellschaft members subscribing to the JOURNAL, have been added to reflect reclassifications and changes in membership status.

Table III. *ECS Patron and Sustaining Membership*

	Total as of 1/1/60	Total as of 1/1/61	Net Change
Patron Member Companies	5	5	0
Sustaining Member Companies	160	157	— 3

Stanley Pessok, General Instrument Corp., Semiconductor Div.; Mail add: 44 S. Munn Ave., East Orange, N. J. (Electronics-Semiconductors)

R. W. Pickering, Electrolytic Zinc Co., G.P.O. Box 377D, Hobart, Tasmania, Australia (Electrothermics & Metallurgy, Industrial Electrolytic)

M. E. Richardson, Central Research Labs., Daystrom Inc., 620 Passaic Ave., West Caldwell, N. J. (Electronics)

W. W. Robertson Aluminum Co. of Canada, Arvida, Que., Canada (Industrial Electrolytic)

Nathan Sclar, Nuclear Corp. of America, 2 Richwood Pl., Denville, N. J. (Electronics–Semiconductors)

L. E. Sharif, Texas Instruments Inc.; Mail add: 5023 Gaston Ave., Dallas, Texas (Electronics)

I. L. Smith, General Electric Co.; Mail add: 2344 Belvoir Blvd., Cleveland 21, Ohio (Electronics)

D. F. Stahr, Syntron Co., Homer City, Pa. (Electronics-Semiconductors, Theoretical Electrochemistry)

W. B. Stephenson, Jr., General Electric Co., Flight Propulsion Div.; Mail add: 2434 St. Albans Ave., Cincinnati 13, Ohio (Electrodeposition)

C. G. Thornton, Lansdale Div., Philco Corp., Lansdale, Pa. (Electronics-Semiconductors)

Atsuyuki Ueno, Applied Chemistry Div., Nihon University, 5-1 Kanda Surugadai Chiyoda-Ku, Tokyo, Japan (Electrodeposition, Electro-Organic, Industrial Electrolytic)

Jay Utken, P. R. Mallory & Co., Inc.; Mail add: 2130 Cord St., Indianapolis 24, Ind. (Electric Insulation, Electronics, Electrothermics & Metallurgy)

Banyat Viryasiri, Battery Organization; Mail add: 463 Rama IV Rd., Bangkok, Thailand (Battery)

Jaroslav Vnuk, Bateria Slany, Netovicka 875, Slany, Czechoslovakia (Battery)

P. R. Voyentzie, Sonotone Corp.; Mail add: Shadowy Lane, West Milford, N. J. (Battery, Theoretical Electrochemistry)

H. L. Watkins, National Cash Register Co.; Mail add: 1512 W. 96 St., Los Angeles 47, Calif. (Electrodeposition)

B. J. Welch, Reduction Research Lab., Reynolds Metals Co.; Mail add: 233 Bayless Ave., Florence, Ala. (Electrothermics & Metallurgy, Industrial Electrolytic, Theoretical Electrochemistry)

T. A. Whatley, Lockheed Aircraft Corp., Space & Missiles Div.; Mail add: 686 Cypress St., Sunnyvale, Calif. (Battery)

A. J. Whitney, U. S. Industrial Chemicals Co., State Rd., Ashtabula, Ohio (Industrial Electrolytic)

C. R. Wilson, United Gas Corp., P. O. Box 1407, Shreveport, La. (Battery)

Associate Members

N. P. Cerniglia, Sylvania Electric Products Inc., 100 Sylvan Rd., Woburn, Mass. (Electronics-Semiconductors)

E. T.-K. Chow, National Cash Register Co., Electronics Div.; Mail add: 4932 Imlay Ave., Culver City, Calif. (Electrodeposition, Electronics - Semiconductors, Theoretical Electrochemistry)

L. J. Douglas, National Cash Register Co., Electronics Div.; Mail add: 1864 S. Virginia Rd., Los Angeles, Calif. (Electrodeposition, Electronics – Semiconductors, Theoretical Electrochemistry)

W. R. Johnson, U. S. Steel Research Center, Monroeville, Pa. (Electrodeposition)

C. A. Rivera, R.C.A.; Mail add: 16 Willet St., Bloomfield, N. J. (Electronics-Semiconductors)

Student Member

G. E. Smith, Dept. of Chemistry, Michigan State University, East Lansing, Mich. (Battery, Electronics-Semiconductors and Luminescence, Theoretical Electrochemistry)

Notice to Members and Subscribers
(Re Changes of Address)

To insure receipt of each issue of the JOURNAL, please be sure to give us your old address, as well as your new one, when you move. Our records are filed by states and cities, not by individual names. The Post Office does not forward magazines.

Reinstatement to Active Membership

A. W. Dimond, Canadian Carborundum Co. Ltd.; Mail add: 78 St. Peter Ave., Niagara Falls, Ont., Canada (Electrothermics & Metallurgy)

Deceased

C. S. Taylor, Chinook, Wash.
Harry Hey, Melbourne, Australia

Personals

V. Aravamuthan has been promoted to assistant director, Central Electrochemical Research Institute, Karaikudi, India.

Lawrence G. Bockstie, Jr., previously with the Research Div. of the Philco Corp. in Philadelphia, Pa., recently took a position as senior product development engineer at the Electronic Components Div. of Corning Glass Works, Bradford, Pa.

A. R. Lytle, formerly director of research of the Metals Research Labs. of the Electro Metallurgical Co., Div. of Union Carbide Corp., New York City, now is senior consultant of the Electric Welding Dept. of the Linde Co., Div. of Union Carbide, New York City.

Clarence K. Morehouse recently joined the Globe Battery Co., Div. of Globe Union Inc., Milwaukee, Wis., as vice-president of engineering. He had been affiliated with the Semiconductor and Materials Div. of the Radio Corp. of America, Somerville, N. J.

T. L. Rama Char and K. S. G. Doss, both of India, have become Fellows of the Physical Society, London, with the amalgamation of the Institute of Physics and the Physical Society

M. S. Thacker, New Delhi, India, has been elected chairman of the Commonwealth Scientific Committee for the term beginning 1961.

News Items

1960 Annual Index

The Annual Index for Vol. 107 (1960) of the JOURNAL appears on pp. i-x of this issue. Reprints of the Index may be obtained about the middle of March by writing to The Electrochemical Society, 1860 Broadway, New York 23, N. Y.

New ECS Sustaining Member

Armco Steel Corporation, Middletown, Ohio, recently became a Sustaining Member of The Electrochemical Society.

Gallium Alloys for Low-Temperature Bonding

The National Bureau of Standards, in a project sponsored by the Air Force, has developed gallium alloys for the low-temperature bonding of wires to heat-sensitive electronic devices, such as transistors. These alloys, which are soft when mixed at room temperature, resist temperatures up to 900°C after hardening. It also has been found that they can be used to "cold solder" certain ceramic and metallic surfaces.

To form gallium-based alloys, weighed portions of liquid gallium (mp 29.9°C) and a finely powdered metal thoroughly are mixed in a Teflon beaker. After several minutes' mixing, during which the gallium "wets" the other metal, the alloy is ready for use.

Various combinations of gallium with copper, gold, nickel, and silver were prepared and tested in the program. Tin was added to several of the gallium-copper alloys, and acted to delay the initial set. Practical batches as small as 0.1 g were prepared, which was sufficient to attach several electrodes to a surface. It was found that unused portions of gallium-gold alloys could be preserved for later use if refrigerated before hardening had occurred.

Expansion tests on various gallium alloys indicated that as much as 10% expansion may occur during hardening. This expansion is not of critical importance, however, as the soft-packed metal will generally compress itself rather than damage the material in which it is imbedded. The addition of aluminum oxide to gallium-gold alloys resulted in better bonding in cavities of barium titanate, perhaps by reducing the thermal expansion of the mixture.

G. E. Combination Thermionic-Thermoelectric Energy Converter

General Electric engineers have operated a combination thermionic-thermoelectric energy converter which, without additional heat input, produced twice as much power as a thermionic converter alone.

Using "waste" heat rejected by the thermionic converter, a thermoelectric generator (essentially a thermocouple) produced significant boosts in both power output and efficiency. The work was done by I. T. Saldi, of the company's Power Tube Dept., as part of a study to prove the feasibility of the cascaded device.

The new device takes advantage of the fact that thermionic conversion is most efficient at higher temperatures while a thermoelectric generator works best at relatively lower temperatures.

In the developmental work, a General Electric production-type vacuum thermionic converter (Z-5386) was "sandwiched" with a zinc-antimonide constantan thermoelectric generator, designed by W. J. van der Grinten, of the company's Electronics Lab., Syracuse, N. Y.

The thermionic converter, running at a cathode temperature of 875°C (well below its normal operating temperature) produced 0.2 w. At the same time, the thermoelectric generator produced 0.34 w at a hot-junction temperature of 350° and a heat sink temperature of 100°C. This increase in system power output without more heat input indicates that the system efficiency also was doubled. The heat source was propane gas.

When operated at a cathode temperature of 1150°C, the thermionic converter produces 1 w with about 2.5% efficiency. If the waste heat from a Z-5386, operated at this cathode temperature, were to be used to power a lead-telluride thermoelectric generator, the power output of the cascaded system would be expected to be about 2 w and efficiency about 5-6%, the company's engineers said. Ultimate efficiencies as high as 16% are possible.

1961 Temperature Symposium

The technical program now is complete for the most comprehensive meeting ever held on the subject of temperature measurement. About 200 papers will cover temperature measurements from absolute zero to 10,000,000°K with interests ranging from the temperature of the human body to the temperature of the sun. Almost every area of the physical, biological, and medical sciences will be represented at the 1961 Symposium on "Temperature, Its Measurement and Control in Science and Industry," to be held in Columbus, Ohio, March 27-31, 1961. The conference is sponsored by the American Institute of Physics, the Instrument Society of America, and the National Bureau of Standards.

Temperature ranks as one of the most important of the physical quantities, and its measurement and understanding have provided some of the most difficult and challenging problems in experimental and theoretical physics. The 200 papers scheduled for presentation come from universities, government and military research laboratories, and industrial research laboratories in this country, as well as from research centers in Australia, Germany, Netherlands, Canada, Soviet Russia, and Great Britain.

The symposium is organized into 16 sessions, devoted to such topics as: Basic Concepts of Temperature, Temperature Scales, Thermocouples, Resistance Thermometers, Gas Thermometers, Spectroscopic Methods, Pyrometry, Miscellaneous Methods, Automatic Methods for Measurement and Control, Measurement in Dynamic Systems, Special Sources of Temperature, Cryogenics, Plasmas, Temperature Measurement in Geophysics, Temperature Measurement in Astrophysics, and Temperature

ECS Indianapolis Meeting, April 30-May 3, 1961

The Spring Meeting of The Electrochemical Society will be held in Indianapolis, Ind., from April 30 through May 3, 1961. Headquarters will be at the Claypool Hotel. The General Chairman of the meeting is A. M. Max.

Technical sessions will be held on: Electric Insulation (Thin Dielectric Films; Epoxy Resins); Electronics-Luminescence; Electronics-Semiconductors (Crystal Growth and Structure; Semiconductor Surfaces; Compound Semiconductors; Device Processing and Characterization; Diffusion-Oxidation; Etching); Electrothermics and Metallurgy (High-Temperature Materials; Extractive Metallurgy; Ultrafine Particles—Production; Properties; Particle Size Measurement and Surface Effects); Industrial Electrolytic—General; Industrial Electrolytic — Theoretical Electrochemistry — Battery Joint Symposium on Fuel Cells; Industrial Electrolytic—Battery Joint Symposium on Fuel Cells; Theoretical Electrochemistry (General Session and Symposium on Modern Instrumentation and Techniques of Electrochemical Measurements).

The complete program, including general information and 75-word abstracts of papers to be presented, will appear in the March JOURNAL.

Measurement in Biophysics and Medicine.

Some of the most recent advances in high-temperature and low-temperature measurements will be described in the papers delivered at the symposium. Interest in the higher regions is sparked by the great efforts being made in plasma physics. At the lower end of the scale, there is great interest in extending the International Practical Temperature Scale down to the region of 1°K.

Persons interested in the symposium can obtain further information by writing to V. W. Sikora, Instrument Society of America, 313 Sixth Ave., Pittsburgh 22, Pa.

Clevite-Shockley Transistor Building Under Construction

Maurice Hanafin, general manager of the Shockley Transistor unit of Clevite Transistor, recently announced that construction had begun on the new Shockley Transistor facility in Palo Alto, Calif.

The new building, the first of four to be built in the new center, will consolidate the administration, research, production, and marketing operations that have grown into three separate buildings in Palo Alto and nearby Mountain View. The first unit will be a one-million-dollar building located on the ten-acre site at the corner of Page Mill Rd. and Junipero Serra Blvd. in Stanford Industrial Park, Palo Alto. Approximately 250 employees will occupy the building on completion this spring. Plans provide for a four-building complex which will ultimately provide over 200,000 square feet of working area.

Because of the precise manufacturing procedures required in the production of Shockley four-layer diodes, the building will be completely air-conditioned with additional special control of temperature, humidity, and dust in critical manufacturing areas. Even during construction, unusual precautions will be necessary. Particular care will be taken not to "build dust" into the building. Dirt and dust will be throughly eliminated as each phase of the construction is completed.

The company was founded in 1955 by Dr. William Shockley, co-winner of the Nobel Prize in Physics, as the Shockley Semiconductor Laboratory of Beckman Instruments. From an exclusively research and development organization, the company has become a quantity producer of a unique semiconductor device.

The Shockley organization recently became a part of Clevite Transistor of Waltham, Mass., which is in turn a division of Clevite Corp. in Cleveland, Ohio.

Literature from Industry

MACro Brite 2, a new single-immersion, clear chromate conversion coating for zinc plate, may be used in applications requiring a low-cost, blue-bright finish with improved corrosion protection. Parts may be processed on racks, in barrels, or in bulk.

Technical Data Sheet No. 58 is available from MacDermid Inc., Waterbury, Conn.

MACro Brite L-6, a new leach-type, clear chromate conversion coating, produces clear white bright, clear blue bright, or iridescent bronze chromate coatings on zinc or cadmium plate or zinc die castings. These coatings have a higher corrosion resistance than clear coatings and provide an excellent base for organic coatings.

Technical Data Sheet No. 61 is available from MacDermid Inc., Waterbury, Conn.

MACro Brite C-9, a new single-dip, clear chromate conversion coating for cadmium offers protection against fingerprinting, staining, and the formation of white corrosion products. No liquid acid is required to make up the solution, so carboys are eliminated and controls are simplified.

Technical Data Sheet No. 73 is available from MacDermid Inc., Waterbury, Conn.

Employment Situations

Positions Available

Glass-Ceramics—Ph.D. or perhaps M.S. for advanced work with glasses and ceramics for special applications in semiconductor devices. Professional level in Research and Development Department. Basic research is desired as well as some applications to particular devices. Please send detailed résumé including salary requirements to Mr. Don Palmer, Fairchild Semiconductor Corporation, 844 Charleston Road, Palo Alto, California. Interviews for qualified applicants will be arranged from anywhere in the United States. All inquiries strictly confidential and acknowledged.

Surface Physics—Ph.D. or possibly M.S. for research on surface physics of semiconductors. Some experience is advantageous but not essential. Professional level in Research and Development Department. Well-equipped laboratory near major universities. Please send detailed résumé including salary requirements to Mr. Don Palmer, Fairchild Semiconductor Corporation, 844 Charleston Road, Palo Alto, California. Interviews for qualified applicants will be arranged from anywhere in the United States. All inquiries strictly confidential and acknowledged.

Four challenging research positions for experienced surface chemists, in fully-equipped laboratory devoted to research and development on aluminum and copper alloys, involving: A. Electrochemical kinetics, adsorption, and oxide film structure investigations related to finishing processes. B. Studies of interfacial surface reactions between polymeric resins and metal oxide surfaces relating to strength and permanence of joints in the adhesive bonding of metals. C. Mechanisms relating to surface phenomena, associated with liquid metal-solid metal inter-action as applied to soldering and brazing. D. Surface and electrochemical reactions effecting the kinetics of general, localized, and stress corrosion processes. Pleasant living, with access to major university. Send reply to R. H. Endriss, Personnel Manager, Olin Mathieson Chemical Corp., 125 Munson St., New Haven, Conn.

Position Wanted

Chemical Engineer—B.S., registered professional engineer, 17 years of electrolytic background including development and production of tantalum capacitors, development in electrodeposition processes, corrosion. Desires responsible position in development or production work. *Reply to Box No. 371, c/o The Electrochemical Society, 1860 Broadway, New York 23, N. Y.*

Advertiser's Index

Great Lakes Carbon Corp., Electrode Division ..... Cover 2

E. H. Sargent & Company 28C

Stackpole Carbon Company 27C

The Electrochemical Society

Patron Members

Aluminum Co. of Canada, Ltd., Montreal, Que., Canada

International Nickel Co., Inc., New York, N. Y.

Olin Mathieson Chemical Corp., Chemicals Div., Industrial Chemicals Development Dept., Niagara Falls, N. Y.

Union Carbide Corp.
Divisions:
Union Carbide Metals Co., New York, N. Y.
National Carbon Co., New York, N. Y.

Westinghouse Electric Corp., Pittsburgh, Pa.

Sustaining Members

Air Reduction Co., Inc., New York, N. Y.

Ajax Electro Metallurgical Corp., Philadelphia, Pa.

Allen-Bradley Co., Milwaukee, Wis.

Allied Chemical & Dye Corp.
General Chemical Div., Morristown, N. J.
Solvay Process Div., Syracuse, N. Y. (3 memberships)

Allied Research Products, Inc., Detroit, Mich.

Alloy Steel Products Co., Inc., Linden, N. J.

Aluminum Co. of America, New Kensington, Pa.

American Metal Climax, Inc., New York, N. Y.

American Potash & Chemical Corp., Los Angeles, Calif. (2 memberships)

American Smelting and Refining Co., South Plainfield, N. J.

American Zinc Co. of Illinois, East St. Louis, Ill.

American Zinc, Lead & Smelting Co., St. Louis, Mo.

American Zinc Oxide Co., Columbus, Ohio

M. Ames Chemical Works, Inc., Glens Falls, N. Y.

Armco Steel Corp., Middletown, Ohio

Basic Inc., Maple Grove, Ohio

Bell Telephone Laboratories, Inc., New York, N. Y. (2 memberships)

Bethlehem Steel Co., Bethlehem, Pa. (2 memberships)

Boeing Airplane Co., Seattle, Wash.

Burgess Battery Co., Freeport, Ill. (4 memberships)

Canadian Industries Ltd., Montreal, Que., Canada

Carborundum Co., Niagara Falls, N. Y.

Catalyst Research Corp., Baltimore, Md.

Ciba Pharmaceutical Products, Inc., Summit, N. J.

Columbian Carbon Co., New York, N. Y.

Columbia-Southern Chemical Corp., Pittsburgh, Pa.

Consolidated Mining & Smelting Co. of Canada, Ltd., Trail, B. C., Canada (2 memberships)

Continental Can Co., Inc., Chicago, Ill.

Cooper Metallurgical Associates, Cleveland, Ohio

Corning Glass Works, Corning, N. Y.

Diamond Alkali Co., Painesville, Ohio (2 memberships)

Dow Chemical Co., Midland, Mich.

Wilbur B. Driver Co., Newark, N. J. (2 memberships)

E. I. du Pont de Nemours & Co., Inc., Wilmington, Del.

Eagle-Picher Co., Chemical Div., Joplin, Mo.

Eastman Kodak Co., Rochester, N. Y.

Thomas A. Edison Research Laboratory, Div. of McGraw-Edison Co., West Orange, N. J.

Electric Auto-Lite Co., Toledo, Ohio
C & D Division, Conshohocken, Pa.

Electric Storage Battery Co., Yardley, Pa.

Englehard Industries, Inc., Newark, N. J. (2 memberships)

The Eppley Laboratory, Inc., Newport, R. I. (2 memberships)

Erie Resistor Corp., Erie, Pa.

Exmet Corp., Tuckahoe, N. Y.

Fairchild Semiconductor Corp., Palo Alto, Calif.

Food Machinery & Chemical Corp.
Becco Chemical Div., Buffalo, N. Y.
Westvaco Chlor-Alkali Div., South Charleston, W. Va.

Foote Mineral Co., Paoli, Pa.

Ford Motor Co., Dearborn, Mich.

General Electric Co., Schenectady, N. Y.
Chemistry & Chemical Engineering Component, General Engineering Laboratory
Chemistry Research Dept.
General Physics Research Dept.
Metallurgy & Ceramics Research Dept.
Aircraft Accessory Turbine Dept., West Lynn, Mass.

General Instrument Corp., Newark, N. J.

(Sustaining Members cont'd)

General Motors Corp.
Delco-Remy Div., Anderson, Ind.
Guide Lamp Div., Anderson, Ind.
Research Laboratories Div., Detroit, Mich.
General Transistor Corp., Jamaica, N. Y.
Gillette Safety Razor Co., Boston, Mass.
Globe-Union, Inc., Milwaukee, Wis.
Gould-National Batteries, Inc., Minneapolis, Minn.
Grace Electronic Chemicals, Inc., Baltimore, Md.
Great Lakes Carbon Corp., New York, N. Y.
Hanson-Van Winkle-Munning Co., Matawan, N. J. (2 memberships)
Harshaw Chemical Co., Cleveland, Ohio (2 memberships)
Hercules Powder Co., Wilmington, Del.
Hill Cross Co., Inc., West New York, N. J.
Hoffman Electronics Corp., El Monte, Calif.
Hooker Chemical Corp., Niagara Falls, N. Y. (3 memberships)
Hughes Aircraft Co., Culver City, Calif.
Industro Transistor Corp., Long Island City, N. Y.
International Business Machines Corp., Poughkeepsie, N. Y.
International Minerals & Chemical Corp., Skokie, Ill.
ITT Federal Laboratories, Div. of International Telephone & Telegraph Corp., Nutley, N. J.
Jones & Laughlin Steel Corp., Pittsburgh, Pa.
K. W. Battery Co., Skokie, Ill.
Kaiser Aluminum & Chemical Corp.
Div. of Chemical Research, Permanente, Calif.
Div. of Metallurgical Research, Spokane, Wash.
Kawecki Chemical Co., Boyertown, Pa.
Kennecott Copper Corp., New York, N. Y.
Keokuk Electro-Metals Co., Keokuk, Iowa
Libbey-Owens-Ford Glass Co., Toledo, Ohio
M. & C. Nuclear, Inc., Attleboro, Mass.
Mallinckrodt Chemical Works, St. Louis, Mo.
P. R. Mallory & Co., Indianapolis, Ind.
McGean Chemical Co., Cleveland, Ohio
Merck & Co., Inc., Rahway, N. J.
Metal & Thermit Corp., Detroit, Mich.
Minnesota Mining & Manufacturing Co., St. Paul, Minn.
Monsanto Chemical Co., St. Louis, Mo.
Motorola, Inc., Chicago, Ill.
National Cash Register Co., Dayton, Ohio
National Lead Co., New York, N. Y.
National Research Corp., Cambridge, Mass.
National Steel Corp., Weirton, W. Va.
New York Air Brake Co., Kinney Vacuum Div., Boston, Mass.
Northern Electric Co., Montreal, Que., Canada
Norton Co., Worcester, Mass.
Olin Mathieson Chemical Corp., Research & Engineering Operations, Energy Div., New Haven, Conn.
Ovitron Corp., Long Island City, N. Y.
Peerless Roll Leaf Co., Inc., Union City, N. J.
Pennsalt Chemicals Corp., Philadelphia, Pa.
Phelps Dodge Refining Corp., Maspeth, N. Y.
Philco Corp., Philadelphia, Pa.
Philips Laboratories, Inc., Irvington-on-Hudson, N. Y.
Pittsburgh Metallurgical Co., Inc., Niagara Falls, N. Y.
Poor & Co., Promat Div., Waukegan, Ill.
Potash Co. of America, Carlsbad, N. Mex.
Radio Corp. of America
Tube Div., Harrison, N. J.
RCA Victor Record Div., Indianapolis, Ind.
Ray-O-Vac Co., Madison, Wis.
Raytheon Manufacturing Co., Waltham, Mass.
Reynolds Metals Co., Richmond, Va.
Rheem Semiconductor Corp., Mountain View, Calif.
Schering Corporation, Bloomfield, N. J.
Shawinigan Chemicals Ltd., Montreal, Que., Canada
Speer Carbon Co.
International Graphite & Electrode Div., St. Marys, Pa. (2 memberships)
Sprague Electric Co., North Adams, Mass.
Stackpole Carbon Co., St. Marys, Pa.
Stauffer Chemical Co., New York, N. Y.
Sumner Chemical Co., Div. of Miles Laboratories, Inc., Elkhart, Ind.
Sylvania Electric Products Inc., Bayside, N. Y. (2 memberships)
Tennessee Products & Chemical Corp., Nashville, Tenn.
Texas Instruments, Inc., Dallas, Texas
Three Point Four Corp., Yonkers, N. Y.
Titanium Metals Corp. of America, Henderson, Nev.
Tung-Sol Electric Inc., Newark, N. J.
Udylite Corp., Detroit, Mich. (4 memberships)
Universal-Cyclops Steel Corp., Bridgeville, Pa.
Upjohn Co., Kalamazoo, Mich.
Victor Chemical Works, Chicago, Ill.
Western Electric Co., Inc., Chicago, Ill.
Wyandotte Chemicals Corp., Wyandotte, Mich.
Yardney Electric Corp., New York, N. Y.